Untersuchungen zur Metabolisierung therapeutisch aktiver D-Peptide

Inaugural-Dissertation

zur Erlangung des Doktorgrades
der Mathematisch-Naturwissenschaftlichen Fakultät
der Heinrich-Heine-Universität Düsseldorf

vorgelegt von
Anne Elfgen
aus Bad Honnef

Düsseldorf, Februar 2018

aus dem Institut für Physikalische Biologie
der Heinrich-Heine-Universität Düsseldorf

Gedruckt mit der Genehmigung der
Mathematisch-Naturwissenschaftlichen Fakultät der
Heinrich-Heine-Universität Düsseldorf

Berichterstatter:

1. Prof. Dr. Dieter Willbold
2. Prof. Dr. Henrike Heise

Tag der mündlichen Prüfung: 16.01.2018

Inhaltsverzeichnis

Abbildungsverzeichnis

Tabellenverzeichnis

Abkürzungsverzeichnis

Abb.	Abbildung
AD	Alzheimer-Demenz
ANOVA	Varianzanalyse (engl. *analysis of variance*)
apoE4	Apolipoprotein E4
APP	Amyloid-Vorläuferprotein (engl. *amyloid precursor protein*)
Aβ	Amyloid-β-Peptid
CO_2	Kohlenstoffdioxid
CSF	Zerebrospinalflüssigkeit (engl. *cerebrospinal fluid*)
CYP	Cytochrom P450
DAAO	D-Aminosäureoxidase (engl. *D-amino acid oxidase*)
DAspO	D-Aspartatoxidase
DMEM	*Dulbecco's Modified Eagle Medium*
EDTA	Ethylendiamintetraacetat
EOAD	Früh manifestierende Alzheimer-Demenz (engl. *early-onset Alzheimer's disease*)
ESI	Elektrospray-Ionisation (engl. *electrospray ionization*)
FDA	Amerikanische Lebens- und Arzneimittelbehörde (engl. *U.S. Food and Drug Administration*)
FRα	Folat-Rezeptor α
G-RD2	RD2 mit Glycin-Linker
HFBA	Heptafluorbuttersäure (engl. *heptafluorobutyric acid*)
HSM	Human-spezifischer Metabolit
i.v.	Intravenös
IDE	Insulin-abbauendes Enzym (engl. *insulin-degrading enzyme*)
Konz.	Konzentration
LC-MS	Flüssigchromatographie-Massenspektrometrie (engl. *liquid chromatography – mass spectrometry*)
LOAD	Spät manifestierende Alzheimer-Demenz (engl. *late-onset Alzheimer's disease*)
LRP	*Low-density lipoprotein receptor-related protein*
MTT	3-(4,5-Dimethylthiazol-2-yl)-2,5-diphenyltetrazoliumbromid
NADPH	Nicotinamidadenindinukleotidphosphat
NEP	Neprilysin
NFT	Neurofibrilläre Bündel (engl. *neurofibrillary tangles*)
NMDA	N-Methyl-D-Aspartat

NRS	NADPH-regenerierendes System
PC12	Phäochromozytom-Zellen
PCFT	Protonengekoppelter Folattransporter (engl. *proton-coupled folate transporter*)
pEAβ	Pyroglutamat-Amyloid-β
PepT1	Peptidtransporter 1
Ph. Eur.	Europäisches Arzneibuch
PSEN	Gene der Präsenilin-Proteine
QTOF-MS	Quadrupol-Flugzeitmassenspektrometrie (engl. *quadrupole time-of-flight mass spectrometry*)
RAGE	*Receptor for advanced glycation endproducts*
RFC	Folattransporter 1 (engl. *reduced folate carrier*)
RP-HPLC	Umkehrphasen-Hochleistungsflüssigkeitschromatographie (engl. *reversed-phase high-performance liquid chromatography*)
SGF	Künstlicher Magensaft (engl. *simulated gastric fluid*)
SIF	Künstlicher Darmsaft (engl. *simulated intestinal fluid*)
TCA	Trichloressigsäure (engl. *trichloroacetic acid*)
UHPLC	Ultra-Hochleistungsflüssigkeitschromatographie (engl. *ultra high-performance liquid chromatography*)
v/v	Volumen pro Volumen
w/v	Gewicht pro Volumen (engl. *weight per volume*)

Einbuchstabencode natürlich vorkommender Aminosäuren:

F	Phenylalanin
H	Histidin
K	Lysin
L	Leucin
N	Asparagin
P	Prolin
R	Arginin
T	Threonin
V	Valin

Zusammenfassung

Die Alzheimer-Demenz (AD) ist eine neurodegenerative Erkrankung und die häufigste Form der Demenz. Die Zahl der an AD erkrankten Menschen wird aktuell weltweit auf mehr als 20 Millionen geschätzt. Da derzeit lediglich palliativ wirkende Medikamente zugelassen sind, die die Progression der Krankheit aber nur kurzzeitig verlangsamen können, ist die Nachfrage nach krankheitsmodulierenden und kausalen Therapieansätzen sehr hoch. Für die Entstehung und Progression der Krankheit wird nach vorherrschender Meinung das Amyloid-β-Peptid (Aβ) verantwortlich gemacht, dessen nicht-toxische Monomere zu neurotoxischen Oligomeren aggregieren können, die letztendlich zur Neurodegeneration führen. Ein vielversprechender Therapieansatz ist daher die Stabilisierung der Aβ-Monomere und die gezielte Eliminierung bereits bestehender Aβ-Oligomere. Auf dieser Strategie basiert der Wirkmechanismus des D-enantiomeren Peptids D3, das mittels Spiegelbild-Phagendisplay gegen Aβ-Monomere selektiert wurde. Die Wirksamkeit von D3 konnte bereits *in vitro* und *in vivo* bestätigt werden. Durch rationale Umstrukturierung dieser Leitstruktur wurde das D-Peptid RD2 entwickelt, das *in vitro* eine verbesserte Interaktion mit Aβ im Vergleich zu D3 zeigte und *in vivo* kognitive Defizite transgener AD-Mäuse verbesserte. Für die *in vitro*-Charakterisierung wurde u.a. ein Nukleationsassay zur Untersuchung des Einflusses von RD2 auf die Nukleus-induzierte, beschleunigte Aggregation entwickelt. Es zeigte sich, dass RD2 den katalytischen Effekt der Aβ-Nuklei auf die Aβ-Aggregation signifikant verringert.

Sollen diese Wirkstoffe oral appliziert werden, muss sichergestellt werden, dass sie eine hohe Resistenz gegenüber metabolischen Prozessen aufweisen. Für D3 und RD2 konnte gezeigt werden, dass sie aufgrund ihrer D-enantiomeren Struktur einen entscheidenden Vorteil gegenüber häufig verwendeten L-Peptiden bieten: Sie wiesen eine außerordentlich hohe Stabilität gegenüber Proteasen und CYP-Enzymen auf, die im Gastrointestinaltrakt, im Blut und in der Leber u.a. für die Wirkstoff-Metabolisierung verantwortlich sind. Obwohl bei der Leberpassage viele Wirkstoffe für eine Begünstigung des Abbaus und der Ausschleusung modifiziert werden, wurden bei RD2 nur wenige Metaboliten *in vitro* in Lebermikrosomen gebildet. Der am häufigsten gebildete Metabolit wurde identifiziert und stellte sich als nicht toxisches und reversibles Produkt Formaldehyd-kontaminierter Lebermikrosomen heraus. Darüber hinaus konnte gezeigt werden, dass RD2 kein Substrat für die humane D-Aminosäureoxidase (DAAO) darstellt, obwohl diese auf die Metabolisierung D-enantiomerer Aminosäurereste spezialisiert ist. RD2 nahm außerdem keinen Einfluss auf die Aktivität der DAAO und der Enzyme, die an der Peptid-Metabolisierung in den zuvor genannten Medien beteiligt sind.

Zur Verbesserung der oralen Bioverfügbarkeit von RD2 wurden zwei Folsäure-RD2-Konjugate entwickelt, durch die die RD2-Aufnahme über das Darmepithel begünstigt werden soll. Die Metabolisierung zum unkonjugierten Wirkstoff RD2 wurde *in vitro* und *in vivo* untersucht. Eines der beiden Folsäure-RD2-Konjugate stellte sich dabei als potentiell geeignetes Prodrug heraus, das bei oraler Applikation im Gastrointestinaltrakt voraussichtlich stabil bleiben und erst nach systemischer Aufnahme im Blut und in der Leber gespalten werden wird.

Des Weiteren wurde eine sensitive und schnelle bioanalytische Methode entwickelt und validiert, um unmarkiertes RD2 in Maus-Plasma zu quantifizieren. Die Herausforderungen bestanden u.a. darin, eine geeignete Extraktionsmethode und ein chromatographisches Trennverfahren mit Massenspektrometrie-Kopplung für das äußerst hydrophile Peptid zu entwickeln. Mithilfe der validierten Methode wurden Plasmaproben RD2- und Placebo-behandelter Mäuse analysiert.

Abstract

Alzheimer's disease (AD) is a neurodegenerative disorder and the most common form of dementia. The number of people with AD is currently estimated at more than 20 million worldwide. Since only palliative drugs, which can only slow down the progression of the disease temporarily, have been approved so far, the demand for disease modulating and causal therapeutic approaches is very high. The development and progression of the disease is commonly believed to be caused by the amyloid-β peptide (Aβ), whose non-toxic monomers can aggregate into neurotoxic oligomers that ultimately lead to neurodegeneration. Hence, a promising therapeutic approach is the stabilization of Aβ monomers and the targeted elimination of existing Aβ oligomers. The mechanism of action of the D-enantiomeric peptide D3, which was selected by means of mirror image phage display against Aβ monomers, is based on this strategy. The efficacy of D3 has already been confirmed *in vitro* and *in vivo*. By rational rearrangement of this lead compound, the D-peptide RD2 has been developed, which showed a superior interaction with Aβ *in vitro* compared to D3 and improved cognitive deficits of transgenic AD mice *in vivo*. Amongst others, a nucleation assay to investigate the influence of RD2 on nucleus-induced, accelerated aggregation was developed for *in vitro* characterization. It was shown that RD2 significantly reduces the catalytic effect of Aβ nuclei on Aβ aggregation.

To orally administer these drugs, it must be ensured that they have a high resistance against metabolic processes. D3 and RD2 have been shown to offer a decisive advantage over commonly used L-peptides due to their D-enantiomeric structure: They exhibited an extremely high stability towards proteases and CYP enzymes, which are, amongst others, responsible for drug metabolization in the gastrointestinal tract, the blood and the liver. Although many drugs are modified during liver passage to facilitate degradation and clearance, only a few RD2 metabolites were generated *in vitro* in liver microsomes. The most abundant RD2 metabolite was identified and found to be a non-toxic and reversible product of formaldehyde-contaminated liver microsomes. Additionally, it was shown that RD2 is not a substrate for the human D-amino acid oxidase (DAAO) although it is specialized in metabolizing D-enantiomeric amino acid residues. Moreover, RD2 did not have any effect on the activity of the DAAO and the enzymes involved in peptide metabolization in the aforementioned media.

For improved oral bioavailability of RD2, two folic acid-RD2-conjugates were developed to promote RD2 uptake across the intestinal epithelium. The metabolization to the unconjugated drug RD2 was investigated *in vitro* as well as *in vivo*. One of the two folic acid-RD2-conjugates was found to be a potentially suitable prodrug that is expected to remain

stable in the gastrointestinal tract and to be cleaved in the blood and the liver after systemic uptake when administered orally.

Furthermore, a sensitive and rapid bioanalytical method was developed and validated in order to quantify unlabeled RD2 in mouse plasma. The main challenges were to develop a suitable extraction method and a chromatographic separation method with mass spectrometry coupling for the highly hydrophilic peptide. Using the validated method, plasma samples of RD2 and placebo treated mice were analyzed.

1 Einleitung

1.1 Alzheimer-Demenz – ein Überblick

Die Alzheimer-Demenz (AD) ist eine neurodegenerative Erkrankung, die erstmals 1906 von dem deutschen Psychiater und Neuropathologen Alois Alzheimer beschrieben wurde (Alzheimer 1907, Hippius and Neundörfer 2003). AD zeichnet sich symptomatisch durch eine progressive Abnahme der kognitiven Funktionen, zunehmende Verwirrtheit, Veränderungen der Persönlichkeit sowie, im fortgeschrittenen Stadium, eine Einschränkung des Bewegungsapparates aus (Alzheimer's Association 2016). Symptome und Dauer der Krankheit können individuell variieren.

Die Ursachen der AD sind bis heute noch nicht eindeutig geklärt und je nach AD-Form unterschiedlich. Die sich spät, meist nach dem 65. Lebensjahr, manifestierende Form der AD (LOAD; engl. *late-onset Alzheimer's disease*) tritt in den meisten Fällen sporadisch auf. Ursachen für die LOAD konnten bislang noch nicht eindeutig definiert werden. Zu den größten Risikofaktoren zählen jedoch die Bildung des Apolipoproteins E4 (apoE4) (Corder et al. 1993, Saunders et al. 1993, Bekris et al. 2010) und ein hohes Alter (Hebert et al. 2010, Hebert et al. 2013, Weuve et al. 2014). Darüber hinaus stehen verschiedene Faktoren, wie kardiovaskuläre Erkrankungen, geringer Bildungsstand und Schädel-Hirn-Traumata im Verdacht, das Risiko für LOAD zu erhöhen (Baumgart et al. 2015, Institute of Medicine 2015). Verschiedene Mechanismen führen dabei zu einem verringerten Abbau des AD-assoziierten Amyloid-β-Peptids (Aβ) und einer gestörten Aβ-Ausschleusung aus dem Gehirn, infolgedessen es zu einer neurotoxischen Aβ-Aggregation und Aβ-Akkumulation kommt (Selkoe and Hardy 2016). Bei der sich früh, meist vor dem 65. Lebensjahr, manifestierenden Form der AD (EOAD; engl. *early-onset Alzheimer's disease*) handelt es sich in der Regel um eine erbliche, „familiäre" Form. Hier spielen Mutationen im Gen für das Amyloid-Vorläuferprotein (APP; engl. *amyloid precursor protein*) sowie der Gene der Präsenilin-Proteine 1 und 2 (PSEN) eine zentrale Rolle. Diese Mutationen führen zu einer veränderten APP-Prozessierung, die zu einer erhöhten Aβ-Bildung und einer damit verbundenen Aggregation und Akkumulation beitragen (Bekris et al. 2010). Die EOAD tritt wesentlich seltener (5 %) als die LOAD (95 %) auf (Harman 2006, Avramopoulos 2009, Bekris et al. 2010).

Neuropathologisch sind beide Formen der AD gekennzeichnet durch zerebrale extrazelluläre amyloide Plaques und intrazelluläre neurofibrilläre Bündel (NFT; engl. *neurofibrillary tangles*). Damit geht ein Verlust der Neurone und infolgedessen eine Atrophie des Gehirns einher (Alzheimer 1907, Terry et al. 1964, Perl 2010).

Während die AD *post mortem* zweifelsfrei anhand der typischen Pathologie des Gehirns des Patienten diagnostiziert werden kann, ist es zumindest bei der sporadischen AD *pre mortem* bislang noch nicht möglich, eine eindeutige Diagnose anhand klinischer Untersuchungen (z.B. kognitive, neuropsychologische und genetische Tests), bildgebender Verfahren (Positronenemissions-, Magnetresonanz- oder Computertomographie) oder Bestimmung molekularer Biomarker (in der Zerebrospinalflüssigkeit (CSF; engl. *cerebrospinal fluid*) oder im Blut) mit hundertprozentiger Genauigkeit und Zuverlässigkeit zu geben (Ballard et al. 2011).

Die Zahl der Demenzkranken wurde 2016 weltweit auf etwa 47 Millionen geschätzt. AD stellt dabei mit 60 bis 80 % die häufigste Form der Demenz dar (Alzheimer's Association 2016). Weitere Demenzformen sind beispielsweise die vaskuläre, die frontotemporale und die Lewy-Körper-Demenz (Alzheimer's Association 2017b). Im Jahre 2050 wird sich die Zahl der Demenzkranken auf über 100 Millionen erhöht haben (Ferri et al. 2005, Prince et al. 2016). Die Ursache für den rapiden Anstieg der Patientenzahlen liegt in einer zunehmend älter werdenden Gesellschaft. Mit den ansteigenden Patientenzahlen geht auch ein erhöhter Pflegebedarf und eine enorme finanzielle Belastung des Gesundheitssystems einher (Alzheimer's Association 2016, Prince et al. 2016). Über den humanitären Aspekt hinaus wird es auch aus diesem Grund immer wichtiger, Therapien gegen die AD zu entwickeln.

Trotz intensiver Forschung gibt es bis dato weder präventive noch kurative Medikamente gegen die AD. Derzeit können durch palliative Therapien lediglich die Symptome gelindert werden (Huang and Mucke 2012, Folch et al. 2016).

1.2 Neuropathologie der AD

1.2.1 Neuropathologische Kennzeichen

Die auffälligsten neuropathologischen Kennzeichen in Gehirnen von AD-Patienten sind extrazelluläre amyloide Plaques und intrazelluläre NFTs (Abb. 1.1 A) (Alzheimer 1907, Terry et al. 1964, Perl 2010). Bei extrazellulären amyloiden Plaques handelt es sich um unlösliche Ablagerungen aggregierter Aβ-Peptide (Perl 2010, Serrano-Pozo et al. 2011). Die intrazellulären NFTs zeichnen sich hingegen durch Ablagerung des Mikrotubuli-bindenden Proteins Tau infolge einer pathologischen Hyperphosphorylierung aus (Grundke-Iqbal et al. 1986, Perl 2010). Nach aktuellem Kenntnisstand wird vermutet, dass die NFT-Bildung durch bestimmte Aβ-Spezies induziert wird (Hardy et al. 1998, King et al.

2006, Oddo et al. 2006, De Felice et al. 2008). Weiterhin konnte gezeigt werden, dass diese Aβ-Spezies und die NFTs die physiologische Funktion von Neuronen und Synapsen stören und infolgedessen zu deren Degeneration führen (Selkoe and Hardy 2016). Daraus resultiert eine Atrophie des Gehirns, vor allem in der weißen Substanz und den Hirnregionen Kortex und Hippocampus (de la Monte 1989, Kril et al. 2004) (Abb. 1.1 B), die unter anderem für Lern- und Erinnerungsprozesse sowie für motorische und sensorische Informationsverarbeitung zuständig sind (Vanderah and Gould 2015). Gleichzeitig kommt es zu einer Vergrößerung der Hirnventrikel.

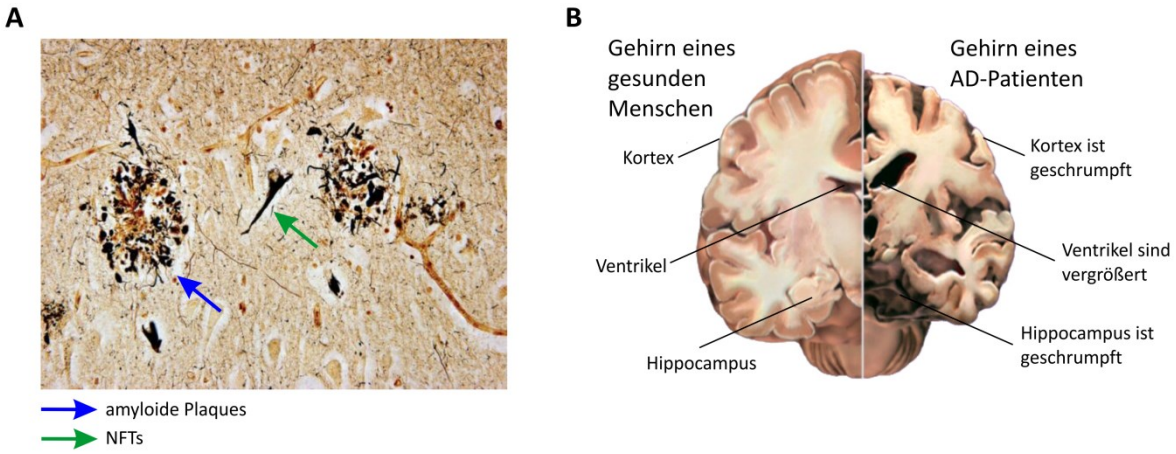

Abbildung 1.1: Charakteristische Merkmale der AD.
A) Aufnahme eines postmortalen Gehirnschnitts, bei dem amyloide Plaques und NFTs gefärbt wurden. Quelle: Modifiziert nach Perl et al. (2010). **B)** Schematische Darstellung des Gehirns eines gesunden Menschen (links) und eines AD-Patienten (rechts). Bei Letzterem ist das Gehirnvolumen infolge einer Atrophie der weißen Substanz, des Kortex und des Hippocampus reduziert sowie die Hirnventrikel vergrößert. Quelle: Modifiziert nach Alzheimer's Association (2017a).

1.2.2 Amyloid-β

Aβ-Synthese

Aβ besteht je nach Isoform aus 36 bis 43 Aminosäuren mit einer Masse von ca. 4,5 kDa (Glenner and Wong 1984, Hamley 2012) und entsteht durch proteolytische Spaltung des APPs, einem ubiquitär exprimierten Transmembranprotein (Kang et al. 1987, LaFerla et al. 2007). Die APP-Prozessierung lässt sich in den nicht-amyloidogenen und den amyloidogenen Weg unterteilen (Abb. 1.2). Bei dem nicht-amyloidogenen Weg wird das APP durch α-Sekretasen innerhalb der Aβ-Region geschnitten. Dabei entsteht N-terminal ein extrazelluläres, lösliches Fragment und C-terminal ein in der Membran verbleibendes Fragment, welches seinerseits weiter prozessiert wird. Bei dem amyloidogenen Weg

hingegen wird das APP durch eine β- und γ-Sekretase so geschnitten, dass neben C- und N-terminalen Fragmenten auch Aβ entsteht (O'Brien and Wong 2011). Da die Spaltung durch die Sekretasen nicht immer an der gleichen Stelle erfolgt, entstehen Aβ-Isoformen unterschiedlicher Längen. Die am häufigsten vorkommende Isoform ist $A\beta_{1-40}$ (80-90 %), seltener wird $A\beta_{1-42}$ gebildet (5-10 %) (Murphy and LeVine 2010). Darüber hinaus werden weitere Isoformen mit versetzten C- und N-terminalen Schnittstellen gebildet, die allerdings nur einen geringen Anteil ausmachen. Bei den N-terminal verkürzten Isoformen ist insbesondere das sogenannte Pyroglutamat-Aβ (pEAβ) zu nennen, das aufgrund posttranslationaler Modifikationen um die ersten zwei Aminosäuren verkürzt ist und mit einem Pyroglutamat an Position 3 beginnt (Saido et al. 1995, Gunn et al. 2010, Jawhar et al. 2011).

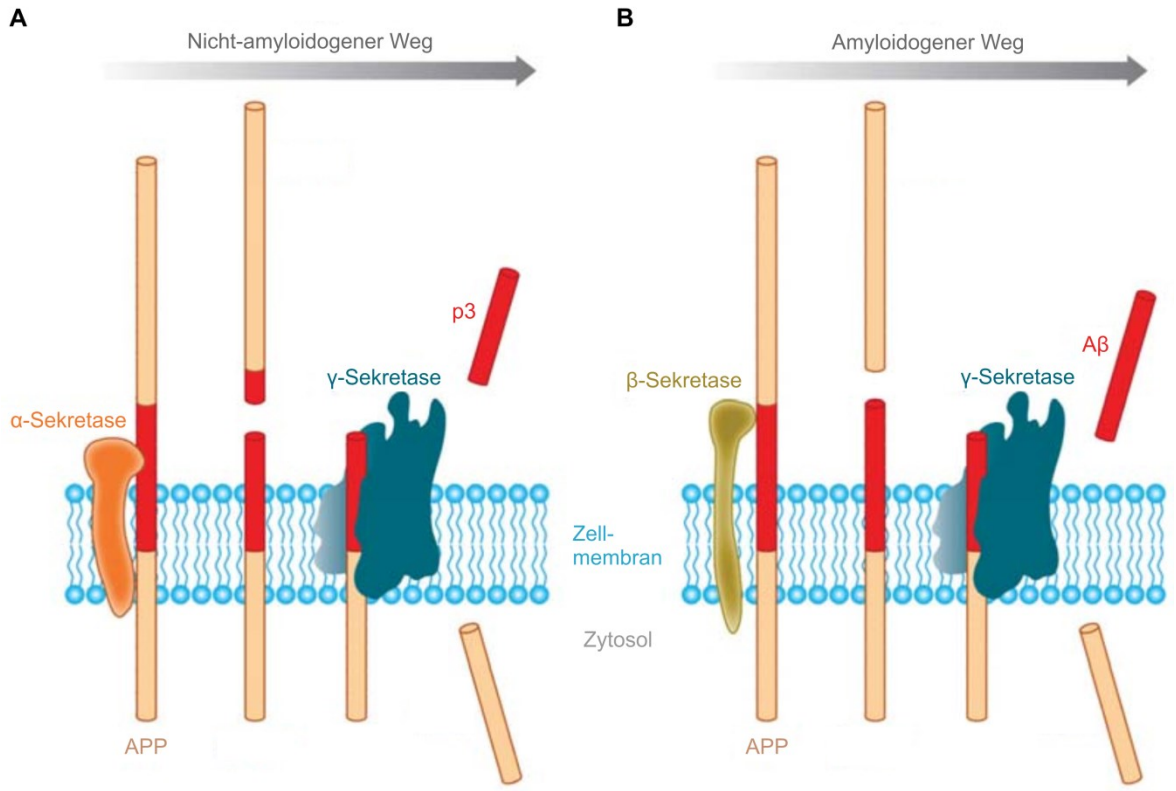

Abbildung 1.2: Prozessierung des Amyloid-Vorläuferproteins (APP).
A) Bei der nicht-amyloidogenen Prozessierung wird APP durch α-Sekretasen innerhalb der Aβ-Region (rot) gespalten. Es entstehen ein lösliches, extrazelluläres und ein membranständiges Fragment, welches seinerseits wiederum durch die γ-Sekretase in das extrazelluläre Fragment p3 und ein intrazelluläres Fragment gespalten wird. **B)** Beim amyloidogenen Weg wird APP zunächst durch die β-Sekretase zu einem extrazellulären und einem membranständigen Fragment prozessiert, welches anschließend durch die γ-Sekretase zu einem intrazellulären Fragment und extrazellulärem Aβ gespalten wird. Abbildung modifiziert nach O'Brien und Wong (2011).

Aβ-Abbau und Aβ-Ausschleusung aus dem Gehirn

Im Gehirn eines gesunden Menschen liegen die Aβ-Akkumulation und der -Abbau im Gleichgewicht, wohingegen dieses im Gehirn eines AD-Patienten gestört ist. Zerebrales Aβ wird prinzipiell durch zwei Mechanismen, proteolytische Spaltung und Rezeptor-vermittelter Transport aus dem Gehirn, reduziert (Tanzi et al. 2004). Die beiden hauptsächlich am proteolytischen Aβ-Abbau beteiligten Endopeptidasen sind das Insulin-abbauende Enzym (IDE; engl. *insulin-degrading enzyme*), auch Insulysin genannt, und das Neprilysin (NEP) (Selkoe 2001, Tanzi et al. 2004). Der Rezeptor-vermittelte Aβ-Transport über die Blut-Hirn-Schranke wird durch die Multiligand-Membranrezeptoren *low-density lipoprotein receptor-related protein* (LRP) und den *receptor for advanced glycation endproducts* (RAGE) reguliert (Yan et al. 2000, Zlokovic 2004). Dabei vermittelt LRP den Aβ-Ausstrom aus der CSF in die Peripherie (Deane et al. 2004), sodass Aβ in der Leber und Niere abgebaut werden kann. RAGE hingegen steuert den Aβ-Einstrom aus der Peripherie zurück in die CSF (Deane et al. 2003). Bei AD-Patienten konnte gezeigt werden, dass die LRP-Aktivität durch einen Aβ-induzierten Proteasom-abhängigen LRP-Abbau reduziert ist. Dies geht mit einem verringerten Aβ-Ausstrom einher (Deane et al. 2004).

Aβ-Aggregation

Aβ-Peptide werden im normalen Stoffwechsel kontinuierlich gebildet. Ihnen werden in monomerer Form unter anderem antimikrobielle (Soscia et al. 2010) und neuroprotektive Funktionen (Giuffrida et al. 2009) sowie Beteiligung an Transkriptions- (Bailey et al. 2011) und Transportvorgängen (Peters et al. 2009) zugesprochen. Erst durch eine Änderung der Konformation und eine damit verbundene Aggregation entwickeln sich die Aβ-Peptide zu toxischen Spezies (nach heutigem Kenntnisstand Aβ-Oligomere) und schließlich zu den charakteristischen amyloiden Plaques. Vom Aβ-Monomer bis hin zum amyloiden Plaque liegt Aβ in verschiedenen Aggregationszuständen vor. Dabei handelt es sich aber keinesfalls um eine fortwährende Polymerisation in Richtung der Plaques, sondern vielmehr um ein dynamisches Verhältnis zwischen Aggregation und Disaggregation (Finder and Glockshuber 2007, Cohen et al. 2013).

Die kleinste Form stellen lösliche Aβ-Monomere dar, die in einer normalen helikalen und in einer abnormalen β-Faltblatt-Konformation vorliegen können (Barrow and Zagorski 1991, Zhang et al. 2000). Die β-Faltblatt-Konformation stellt dabei die Form dar, die die Anlagerung weiterer Aβ-Monomere begünstigt (Barrow and Zagorski 1991). Die Wahrscheinlichkeit einer Fehlfaltung wird durch genetisch bedingte APP- oder Sekretase-

Mutationen (EOAD) bzw. die Anreicherung der löslichen Aβ-Peptide im Laufe des Lebens erhöht (LOAD).

In den vergangenen Jahren wurden verschiedene Modelle zum Aggregationsmechanismus diskutiert (Derreumaux 2013, Arosio et al. 2015). Ein vielseitig favorisiertes Modell ist die Aggregation durch primäre und sekundäre Nukleation (Abb. 1.3). Demnach aggregieren Aβ-Monomere in β-Faltblatt-Konformation zu kleinen, löslichen Aβ-Oligomeren (primäre Nukleation) (Kuo et al. 1996, Walsh et al. 2002), die als Aggregationskeime (Nuklei) dienen und die Bildung unlöslicher Fibrillen mit sogenannter Cross-β-Struktur fördern (Jarrett and Lansbury 1993, Sunde et al. 1997, Walsh et al. 1997). Durch die Anlagerung weiterer Aβ-Monomere an die Oberfläche der Fibrillen entstehen verzweigte Strukturen, wodurch die Bildung neuer Fibrillen katalysiert wird (sekundäre Nukleation). Sowohl die unverzweigten als auch die verzweigten Fibrillen können brechen und somit eine Abspaltung oligomerer Aβ-Fragmente und fibrillärer Bruchstücke mit sich ziehen (Cohen et al. 2013), welche wiederum als Nuklei für die Anlagerung weiterer Aβ-Monomere dienen (Arosio et al. 2015). Als Folge dieser Vorgänge wird einerseits die Aggregation beschleunigt und andererseits die Bildung toxischer Aβ-Oligomere gefördert, auf die im Folgenden noch genauer eingegangen wird. Der Zusammenschluss vieler Fibrillen führt letztendlich zur Bildung extrazellulärer amyloider Plaques (Muller-Hill and Beyreuther 1989).

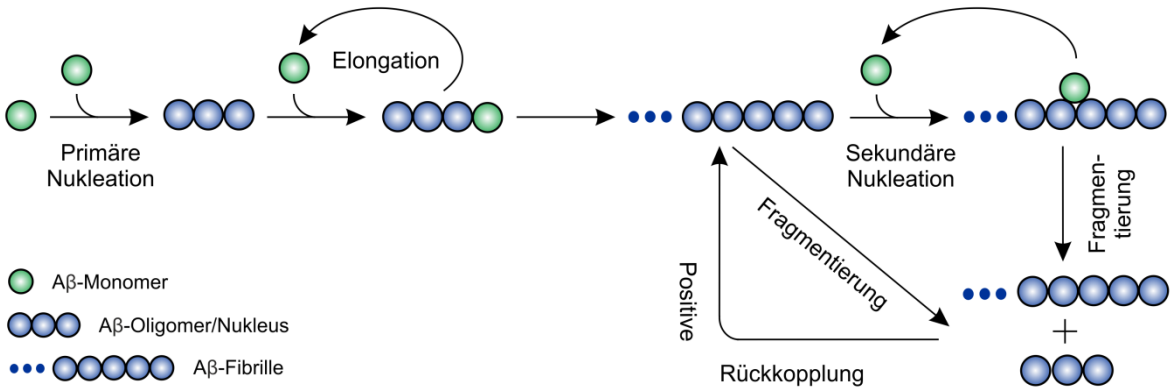

Abbildung 1.3: Aβ-Aggregationsmechanismus.
Fehlgefaltete Aβ-Monomere werden durch primäre Nukleation zu Aβ-Oligomeren, die als Aggregationskeime (Nuklei) dienen und die Fibrillenbildung durch Anlagerung weiterer Aβ-Monomere an ihren Enden (Elongation) katalysieren. An die Oberfläche der Fibrillen lagern sich weitere Aβ-Monomere an, sodass neue Stränge gebildet werden (sekundäre Nukleation). Da die Fibrillen brechen können (Fragmentierung), entstehen neue Aβ-Oligomere und fibrilläre Bruchstücke, die wiederum als Aggregationskeime dienen (positive Rückkopplung). Abbildung erstellt nach Cohen et al. (2013) und De Genst et al. (2014).

Das Aggregationsverhalten der oben genannten Aβ-Isoformen ist sehr unterschiedlich. Die Isoform $Aβ_{1-42}$ wird zwar seltener gebildet als die Isoform $Aβ_{1-40}$ (Murphy and LeVine 2010), zeigt allerdings toxischere Eigenschaften und neigt stärker zur Aggregation als die C-terminal kürzeren Isoformen (El-Agnaf et al. 2000). Die N-terminal modifizierte Isoform $pEAβ_{3-42}$ neigt wiederum noch stärker zur Aggregation als $Aβ_{1-42}$ (Harigaya et al. 2000) und ist dementsprechend toxischer (Tekirian et al. 1999, Youssef et al. 2008).

1.2.3 Amyloid-Kaskaden-Hypothese und Aβ-Neurotoxizität

Die Amyloid-Kaskaden-Hypothese fasst den aktuellen Kenntnisstand zur Entstehung der AD zusammen (Abb. 1.4). Sie wurde 1992 erstmals von Hardy und Higgins formuliert und wird seitdem durch Gewinnung neuer Erkenntnisse fortwährend modifiziert (Hardy and Higgins 1992, Hardy and Selkoe 2002, Selkoe and Hardy 2016). Am Anfang der Kaskade stehen die lebenslange Steigerung der Aβ-Produktion bedingt durch genetische Faktoren (familiäre AD) und die Störung der Aβ-Ausschleusung und des Aβ-Abbaus (sporadische AD), die zu einer Erhöhung der Aβ-Level im Gehirn führen. Infolgedessen kommt es unweigerlich zur Aggregation und Bildung von Aβ-Oligomeren, die letztendlich zu einer Störung der synaptischen Funktionen, neuronalen Degeneration und somit zur Demenz führen. Die These, dass Fibrillen und amyloide Plaques eine toxische Wirkung auf die Nervenzellen haben und den Grund für ihre Degeneration darstellen, gilt als überholt. Nach heutigem Kenntnisstand gelten die Oligomere als toxische Aβ-Spezies (Lue et al. 1999, McLean et al. 1999, Ferreira and Klein 2011, Benilova et al. 2012, Larson and Lesne 2012).

Aβ-Oligomere nehmen auf eine Reihe von Zellfunktionen Einfluss. Beispielsweise werden inflammatorische Signalwege aktiviert, die zu neuronalen Dysfunktionen führen (Itagaki et al. 1989, Meraz-Rios et al. 2013). Des Weiteren können ringförmige Oligomere Ionenkanal-ähnliche Strukturen in Membranen ausbilden, die vermutlich die Homöostase der Zelle stören und zu deren Degeneration führen (Quist et al. 2005). Oligomere beeinträchtigen außerdem Signalübertragungen durch Induktion von oxidativem Stress (Butterfield 2002) und verringern vermutlich den axonalen Transport durch verstärkte Tau-Phosphorylierung (Jin et al. 2011). Darüber hinaus nehmen Oligomere Einfluss auf vaskuläre Funktionen. Dies kann zum einen zu einer Nährstoffunterversorgung der Neurone und zum anderen zu einer reduzierten Aβ-Ausschleusung aus dem Gehirn führen (Iadecola 2004). Außerdem aktivieren sie den N-Methyl-D-Aspartat (NMDA)-Rezeptor, wodurch letztendlich die Langzeitpotenzierung gestört wird (Alberdi et al. 2010,

Texido et al. 2011, Danysz and Parsons 2012). Durch das Zusammenspiel dieser Faktoren wird dann schließlich die Kognition beeinträchtigt.

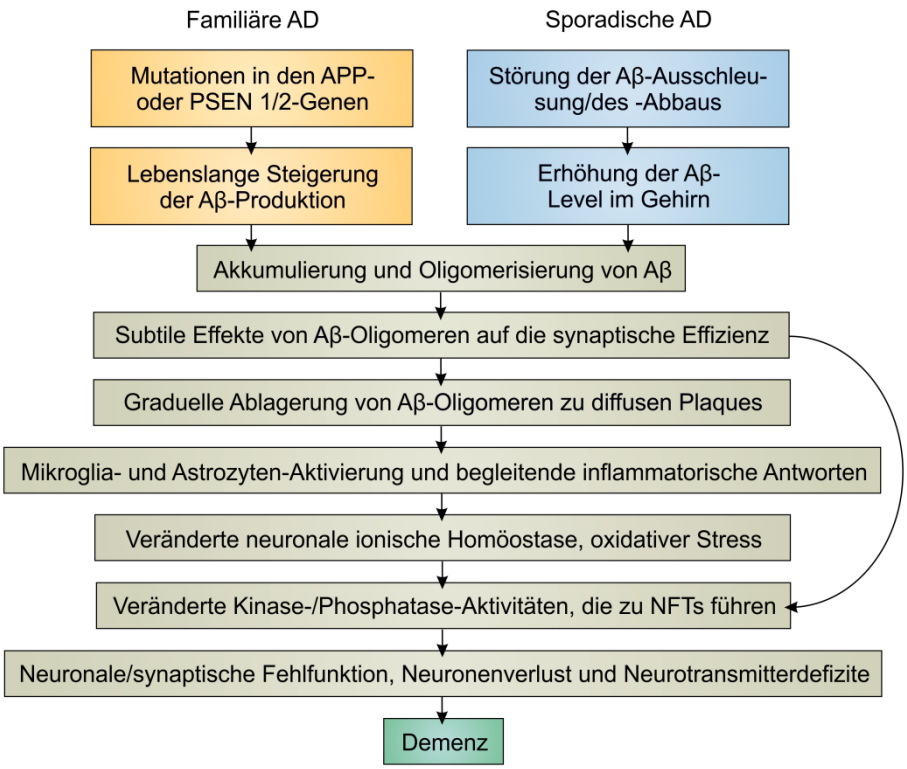

Abbildung 1.4: Amyloid-Kaskaden-Hypothese zur Entstehung der AD.
Die Amyloid-Kaskaden-Hypothese besagt, dass durch ein Ungleichgewicht zwischen Aβ-Produktion und Aβ-Abbau bzw. -Ausschleusung die Aβ-Konzentration ansteigt, Aβ-Monomere zu Oligomeren aggregieren, was letztendlich zu neuronaler Degeneration und somit kognitiven Beeinträchtigungen führt. Eine zentrale Rolle spielen dabei die Aβ-Oligomere, die direkt und indirekt u.a. zu neuronalen und synaptischen Fehlfunktionen, Bildung von NFTs, einer inflammatorischen Zellantwort und oxidativem Stress beitragen. Abbildung modifiziert nach Selkoe und Hardy (2016).

1.3 Therapeutische Ansätze zur Behandlung der AD

1.3.1 Zugelassene palliative Therapien

Derzeit sind ausschließlich palliativ wirkende Medikamente zur Behandlung der AD in Deutschland zugelassen. Zu den palliativen Wirkstoffen, die die Gedächtnisleitung kurzzeitig verbessern können, zählen Acetylcholinesterase-Inhibitioren (Rivastigmin, Galantamin und Donepezil) (Birks 2006) und ein NMDA-Rezeptor-Antagonist (Memantin) (McShane et al. 2006).

Studien zeigten, dass die Degeneration des cholinergen Systems mit der kognitiven Beeinträchtigung bei AD-Patienten korreliert („cholinerge Hypothese“) (Bartus et al. 1982, Perry 1986, Bartus 2000). Auf Grundlage dieser Hypothese wurden verschiedene Behandlungsstrategien entwickelt. Die vielversprechendste Strategie ist die Inhibition der Acetylcholin-abbauenden Acetylcholinesterase, infolge derer die Verfügbarkeit des Neurotransmitters Acetylcholin erhöht wird (Birks 2006).

Bei AD-Patienten ist außerdem die Aufnahme und Freisetzung des Neurotransmitters Glutamat dauerhaft erhöht. Glutamat ist für die NMDA-Rezeptor-vermittelte Neurotransmission verantwortlich, wodurch Lernprozesse ermöglicht werden. Durch eine dauerhafte Glutamat-Freisetzung kommt es zu einer permanenten Aktivierung des NMDA-Rezeptors im Ruhezustand, wodurch die Signalwahrnehmungsschwelle erhöht wird und somit Lernprozesse erschwert werden. Darüber hinaus führt dies zu Exzitotoxizität (Hynd et al. 2004). Durch Antagonisierung des NMDA-Rezeptors wird diesen Vorgängen entgegengewirkt (McShane et al. 2006).

1.3.2 Krankheitsmodulierende Therapien mit Aβ als Zielstruktur

Durch palliative Medikamente kann allerdings lediglich die krankheitsbedingte Symptomatik gelindert, die Progression der Krankheit aber nicht verlangsamt oder aufgehalten werden (Wolfe 2002, Huang and Mucke 2012, Ghezzi et al. 2013, Godyn et al. 2016). Daher ist die Nachfrage nach krankheitsmodulierenden und kausalen Therapieansätzen sehr hoch. Eine Reihe solcher Wirkstoffkandidaten wurde zwar in der Vergangenheit bereits klinisch getestet, bis dato scheiterten sie jedoch alle aus verschiedensten Gründen (Citron 2010, Lukiw 2012, Sun et al. 2012, Jia et al. 2014, Folch et al. 2016, Godyn et al. 2016).

Viele krankheitsmodulierende therapeutische Ansätze orientieren sich an der Amyloid-Kaskaden-Hypothese und sind somit gegen Aβ gerichtet, wobei dessen Produktion reduziert und Aggregation inhibiert werden soll sowie Aggregate abgebaut bzw. aus dem Gehirn ausgeschleust werden sollen (Folch et al. 2016, Godyn et al. 2016). Der Fokus liegt dabei momentan auf der Entwicklung von Immuntherapeutika, der Modulation der Sekretaseaktivitäten sowie der Beeinflussung der Aβ-Aggregation, des Aβ-Abbaus und der Aβ-Ausschleusung (Abb. 1.5).

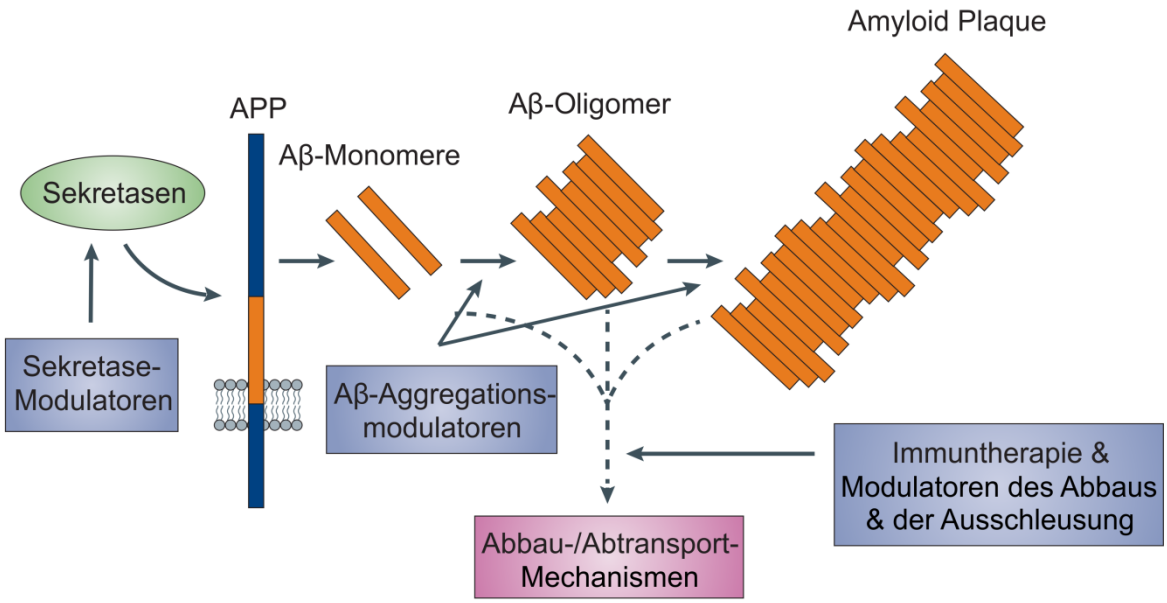

Abbildung 1.5: Mögliche Ansätze für die AD-Therapie mit Aβ als Zielstruktur.
Schematische Darstellung möglicher therapeutischer Ansätze mit Aβ als Zielstruktur. Durch Modulation der Sekretasen, die an der APP-Prozessierung beteiligt sind, kann die Aβ-Produktion reduziert werden. Aβ-Aggregationsmodulatoren verhindern die Aggregation von Aβ-Monomeren zu Oligomeren oder größeren Spezies oder verschieben Aggregationszustände. Bei der Immuntherapie wird eine Immunantwort durch Antikörper ausgelöst, die zum Aβ-Abbau führt. Der Aβ-Abbau und die Aβ-Ausschleusung aus dem Gehirn können darüber hinaus durch Modulatoren gefördert werden, die die Aktivität von Proteasen steigern oder Aβ-Transporter aktivieren bzw. inhibieren. Abbildung modifiziert nach Mullard (2012).

Sekretase-Modulatoren

Die Inhibierung der β- oder γ-Sekretase, die das APP zu Aβ prozessieren, hat sich in der Vergangenheit als durchaus wirksam gegen die übermäßige Aβ-Bildung erwiesen (Imbimbo 2008, Golde et al. 2013, Vassar 2014, Yan and Vassar 2014, Tan et al. 2016). Darüber hinaus gibt es auch Ansätze zur Aktivierung der α-Sekretasen, die APP innerhalb der Aβ-Region spalten und somit dessen Bildung verhindern (Postina 2012). Allerdings besitzen die Sekretasen weitere Substrate (Savonenko et al. 2008, De Strooper 2010, Haapasalo and Kovacs 2011), deren natürliche Funktionen durch Inhibierung oder Aktivierung so beeinflusst werden, dass es zu teilweise starken unerwünschten Arzneimittelwirkungen kommen kann (Postina 2012, Folch et al. 2016, Godyn et al. 2016).

Immuntherapie

Ein weiterer möglicher Ansatz zur präventiven bzw. kurativen Therapie der AD ist die Immuntherapie (Impfung) gegen Aβ. Dabei wird durch aktive oder passive Immunisierung eine Immunantwort durch Antikörper ausgelöst, die den Aβ-Abbau anregen (Folch et al.

2016, Godyn et al. 2016). Bei der aktiven Immunisierung werden Aβ oder Aβ-Fragmente verabreicht, wodurch die Antikörperproduktion gegen Aβ angeregt wird. Bei der passiven Immunisierung werden humanisierte Anti-Aβ-Antikörper direkt verabreicht und somit eine immunologische Reaktion ausgelöst. Ein Vorteil der passiven gegenüber der aktiven Immunisierung ist, dass proinflammatorische T-Zell-vermittelte Immunreaktionen vermieden werden (Folch et al. 2016).

Modulatoren des Aβ-Abbaus und der Aβ-Ausschleusung

Des Weiteren gibt es therapeutische Ansätze, bei denen der Aβ-Abbau und die Aβ-Ausschleusung aus dem Gehirn gefördert werden. Bei AD-Patienten ist die Aktivität bzw. der Gehalt der Aβ-Aggregate-abbauenden Proteasen NEP und IDE reduziert, was zur Aβ-Bildung und -Akkumulation beiträgt (Wang et al. 2003, Caccamo et al. 2005, Higuchi et al. 2005). Daher wurden Wirkstoffe entwickelt, die die Aktivität dieser Proteasen steigern (Nalivaeva et al. 2012, Pivovarova et al. 2016). Des Weiteren werden auch Modulatoren für den Aβ-Transport aus dem Gehirn in die Peripherie entwickelt. Dabei soll der Aβ-Ausstrom von der CSF in die Peripherie über den LRP gefördert und der Aβ-Einstrom aus der Peripherie zurück in die CSF über den RAGE inhibiert werden (Sagare et al. 2007, Panza et al. 2016).

Aβ-Aggregationsmodulatoren

Eine weitere krankheitsmodulierende Therapiestrategie stellen die Aβ-Aggregationsmodulatoren dar. Hierbei wird das Ziel verfolgt, die Konzentration von Aβ-Aggregaten, vor allem von toxischen Aβ-Oligomeren, zu reduzieren, indem z.B. die Aβ-Aggregation verhindert bzw. Aggregationszustände verändert werden. Bei den kleinen Molekülen, die als Aggregationsinhibitoren bzw. als Fibrillen-Destabilisatoren dienen können, handelt es sich um natürlich vorkommende bioaktive Wirkstoffe (da Rocha et al. 2011) wie Polyphenole (Porat et al. 2006), Metallchelatoren (Bush 2002) und sulfonierte Farbstoffe (Pollack et al. 1995). Des Weiteren wurden kurze synthetische Peptide als Aggregationsmodulatoren entwickelt, von denen die meisten Homologien zur Aβ-Sequenz aufweisen und auf die Selbsterkennungssequenz KLVFF ($Abeta_{16-20}$) abzielen (Re et al. 2010, Funke and Willbold 2012), die für die Aβ-Polymerisierung verantwortlich ist (Krysmann et al. 2008). Die häufigste Form der Peptid-basierten Aggregationsinhibitoren sind sogenannte β-Faltblattbrecher mit einem Aβ-Erkennungs- oder -Bindungsmotiv für eine hohe Spezifität, kombiniert mit einem Aβ-Oligomer oder Fibrillen-brechenden Motiv (Soto and Estrada 2005, Funke and Willbold 2012). Darüber hinaus wurden auch Peptide mithilfe kombinatorischer Peptidbibliotheken selektiert, durch die die Bindung einer

Vielzahl von Peptiden an Aβ in verschiedenen Aggregationszuständen überprüft werden kann (Funke and Willbold 2012).

D-enantiomere Peptide D3 und RD2

Das D-enantiomere Peptid D3 wurde mithilfe einer solchen kombinatorischen Peptidbibliothek mittels Spiegelbild-Phagendisplay gegen Aβ-Monomere selektiert (Schumacher et al. 1996, Wiesehan and Willbold 2003, Funke and Willbold 2009). D3 besteht aus 12 D-enantiomeren Aminosäureresten (Sequenz: rprtrlhthrnr) und kann in die Kategorie der Aβ-Aggregationsmodulatoren eingegliedert werden.

D3 bindet an Aβ-Monomere über elektrostatische Wechselwirkungen zwischen den positiv geladenen Argininresten des D3s und den negativ geladenen Gruppen des Aβs (Funke et al. 2010, Olubiyi and Strodel 2012, Olubiyi et al. 2014). Es wird angenommen, dass Aβ-Monomere durch die Bindung von D3 in einer aggregationsinkompetenten Form stabilisiert werden, sodass dadurch das Gleichgewicht zwischen Aβ-Monomeren und Aβ-Oligomeren in Richtung der Aβ-Monomere verschoben wird. *In vitro* konnte gezeigt werden, dass D3 toxische Aβ-Oligomere eliminiert (Funke et al. 2012, Brener et al. 2015) und gleichzeitig hochmolekulare, nicht-toxische, nicht-amyloidogene, amorphe Aggregate ohne Fibrillenstruktur entstehen (Funke et al. 2010). Dadurch wird nicht nur die Aβ-induzierte Zytotoxizität verringert, sondern auch die Aβ-Fibrillisierung reduziert. Weitere *in vitro* Aggregationstests zeigten, dass durch D3 Aβ-Aggregate aufgelöst werden (van Groen et al. 2008) und der katalytische Effekt von Aβ-Nuklei auf die Aβ-Aggregation inhibiert wird (Funke et al. 2010, Klein et al. 2017). Des Weiteren wirkt D3 nicht toxisch auf Zellen, sondern verringert sogar eine Aβ-induzierte Zytotoxizität (van Groen et al. 2008).

In einem AD-Mausmodell konnte gezeigt werden, dass eine D3-Therapie die Plaque-Menge und die Aβ-induzierten inflammatorischen Prozesse im Gehirn reduziert sowie zu einer Verbesserung kognitiver Defizite (van Groen et al. 2008, van Groen et al. 2012, van Groen et al. 2013), sogar nach oraler Applikation (Funke et al. 2010), führt.

Pharmakokinetische Studien mit radioaktiv markiertem D3 zeigten, dass D3 eine hohe orale Bioverfügbarkeit von fast 60 %, eine lange terminale Halbwertszeit von über 40 h im Blut (Jiang et al. 2015) und eine effiziente Blut-Hirn-Schranken-Permeabilität (Liu et al. 2010, Jiang et al. 2016) aufweist.

Auf Grundlage dieser Leitstruktur wurden verschiedene D3-Derivate entwickelt, darunter das D-Peptid RD2, das aus einer rational umstrukturierten Aminosäuresequenz des D3 besteht (Sequenz: ptlhthnrrrrr). RD2 besitzt gegenüber D3 eine höhere orale

Bioverfügbarkeit von 80 % sowie eine längere terminale Halbwertszeit von 60 h im Blut (Leithold et al. 2016). In Studien mit Nagetieren und Nicht-Nagetieren konnte außerdem gezeigt werden, dass durch RD2 in hohen Konzentrationen keine unerwünschten Arzneimittelwirkungen auftreten (unveröffentlichte Daten).

1.4 Orale Applikation, Metabolismus und Bioverfügbarkeit therapeutischer Wirkstoffe

Therapeutische Wirkstoffe können über verschiedene Applikationsformen verabreicht werden. Beim Menschen werden Wirkstoffe bevorzugt oral verabreicht, da diese Applikationsform bei Patienten die höchste Therapietreue (Compliance) mit sich bringt, geringfügig invasiv ist und somit auch ein geringes Risiko mikrobieller Kontamination aufweist. Zusätzlich ist sie kosteneffektiv und flexibel im Design der Dosierungsform (Gomez-Orellana 2005). Vor allem bei Alzheimer-Patienten ist es wichtig, eine praktikable Applikationsform für eine Langzeitanwendung zu haben. Nachteile der oralen Applikation sind allerdings ein hohes Metabolisierungspotential und eine potentiell geringe gastrointestinale Absorption des Wirkstoffs, die sich in einer geringen oralen Bioverfügbarkeit äußern können.

Als Wirkstoff-Metabolismus wird die biochemische Modifizierung von Wirkstoffen in Lebewesen bezeichnet, die meist Enzym-katalysiert ist und zum Abbau oder einer Begünstigung der Ausschleusung des Wirkstoffs führt. Dabei werden Wirkstoffe über Zwischenprodukte, sogenannte Metaboliten, in Endprodukte ab- bzw. umgebaut (Coleman 2010).

Die orale Bioverfügbarkeit gibt an, wieviel eines peroral verabreichten Wirkstoffs unverändert im systemischen Kreislauf zur Verfügung steht (El-Kattan and Varma 2012). Dabei wird die orale Bioverfügbarkeit relativ zur Wirkstoff-Menge nach intravenöser Applikation angegeben.

Bei oraler Verabreichung muss der Wirkstoff den Gastrointestinaltrakt passieren und über den Darm ins Blut aufgenommen werden. Anschließend gelangt der Wirkstoff über die Pfortader zur Leber, wo er metabolisiert werden kann (First-Pass-Effekt). Je nach Wirkstoff kann dieser dann mehrfach zwischen Darm und Leber zirkulieren (enterohepatischer Kreislauf) (Benet 1978). Viele Wirkstoffe besitzen eine geringe orale Bioverfügbarkeit (Gomez-Orellana 2005), die durch das Zusammenspiel einer geringen Aufnahme über das Darmepithel und einer daraus resultierenden hohen

Ausscheidungsrate sowie einer geringen Stabilität im Gastrointestinaltrakt, Blut und in der Leber bedingt ist (Benet 1978, El-Kattan and Varma 2012). Die Aufnahme über das Darmepithel kann über passive Diffusion oder aktiven Transport erfolgen und hängt von den biochemischen Eigenschaften des Wirkstoffs sowie dessen möglicher Affinität zu Transportern ab (El-Kattan and Varma 2012). Der Abbau des Wirkstoffs ist zum einen durch die im Gastrointestinaltrakt und Blut enthaltenen Enzyme bedingt (El-Kattan and Varma 2012). Zum anderen unterliegen Wirkstoffe in der Leber metabolischen Biotransformationsprozessen der Phase I und II. Während der Phase I werden meist durch Proteine der Familie des Cytochrom P450 (CYP-Enzyme) reaktive und polare Gruppen eingeführt (Lu 1976, Guengerich 2001). In der darauffolgenden Phase II wird der Wirkstoff für eine Begünstigung der Ausscheidung und Inaktivierung konjugiert (Jancova et al. 2010, Jančová and Šiller 2012). Beide Prozesse führen zu einer Veränderung der biochemischen Eigenschaften des Wirkstoffs, sodass dessen Wirkung und Aufnahme in die Zielorgane verändert werden können. Manche Wirkstoffe erlangen sogar erst durch diese Prozesse ihre Wirksamkeit (Prodrugs). Die meisten Wirkstoffe sind jedoch nur in ihrer ursprünglich verabreichten Struktur wirksam und könnten nach besagten Transformationsprozessen toxisch auf den Organismus wirken. Daher ist es z.T. unerlässlich, die Stabilität dieser Wirkstoffe zu verbessern.

1.4.1 Metabolismus und orale Bioverfügbarkeit von Peptiden

Peptide, die natürlicherweise hauptsächlich aus L-enantiomeren Aminosäureresten bestehen (Mahalakshmi and Balaram 2006), stellen heutzutage aufgrund ihrer hohen Spezifität, biologischen Aktivität, Diversität und geringen Toxizität vielversprechende Alternativen zu niedermolekularen Verbindungen dar (Lien and Lowman 2003, Danho et al. 2009, Sun et al. 2012). Allerdings besitzen sie eine geringe Halbwertszeit und geringe orale Bioverfügbarkeit, die durch eine hohe proteolytische Instabilität und eine erschwerte Aufnahme über das Darmepithel bedingt sind (Adessi and Soto 2002, Gomez-Orellana 2005, Hamman et al. 2005, Sato et al. 2006, Smart et al. 2014). Beispielsweise sind die im Gastrointestinaltrakt und Blut vorkommenden Proteasen Pepsin, Trypsin, Chymotrypsin und verschiedene Carboxypeptidasen spezifisch für Proteine und Peptide, die aus L-enantiomeren Aminosäureresten bestehen (Keil 1992, Burrell 1993, Van Regenmortel and Muller 1998). Des Weiteren wird die Aufnahme über das Darmepithel dadurch erschwert, dass die meisten Peptide hydrophil und relativ groß sind, wodurch eine para- und transzelluläre passive Diffusion und der Transport über den Peptidtransporter 1 (PepT1), der nur kleine Di- und Tri-Peptide transportiert,

ausgeschlossen ist (Rubas et al. 1996, Camenisch et al. 1998, Rubio-Aliaga and Daniel 2008, El-Kattan and Varma 2012).

1.4.2 Strategien zur Verbesserung der oralen Bioverfügbarkeit und Stabilität von Peptiden

In der Vergangenheit wurden viele Strategien entwickelt, um die geringe orale Bioverfügbarkeit und Stabilität der L-Peptide zu verbessern. Beispielsweise wurden verschiedene Absorptionsverstärker, Enzyminhibitoren und Formulierungen, wie mukoadhesive und Lipid-basierte Systeme, Nano- und Mikropartikel, Hydrogele und Cyclodextrine, entwickelt. Diese verändern zeitweilig die Eigenschaften der Zellmembran bzw. Mukosa, verlängern die Verweildauer an der Mukosa, verhindern den enzymatischen Peptid-Abbau bzw. fördern die Aufnahme ins Zytoplasma durch Integration in die Zellmembran oder Internalisierung (Morishita and Peppas 2006, Renukuntla et al. 2013).

Die orale Bioverfügbarkeit kann außerdem durch Veränderung der physikochemischen Eigenschaften erhöht werden. Eine weit verbreitete Strategie ist dabei die Erhöhung der Lipophilie (Morishita and Peppas 2006, Renukuntla et al. 2013), wodurch die Peptide Membranen leichter transzellulär passieren können (El-Kattan and Varma 2012). Dabei können Peptide z.B. mit hydrophoben Substanzen, wie Lipiden, konjugiert werden (Zhang and Bulaj 2012). In verschiedenen Studien konnte die orale Bioverfügbarkeit von Peptiden dabei erfolgreich durch Palmitoylierung verbessert werden (Hashimoto et al. 1989, Hashizume et al. 1992, Wang et al. 2003).

Des Weiteren können Peptide funktionell modifiziert werden, um die orale Bioverfügbarkeit zu verbessern. Dabei werden Substanzen konjugiert, die Substrate für Membrantransporter oder Rezeptoren sind, die eine Endozytose des Wirkstoffs bewirken (Morishita and Peppas 2006, Renukuntla et al. 2013). Beispielsweise können Liganden für Peptid-Transporter konjugiert werden, die die Peptidaufnahme in die Zelle fördern (Pauletti et al. 1997, Han and Amidon 2000). Membrantransporter sind jedoch auf kleinere Moleküle begrenzt, wohingegen die Größe bei der Rezeptor-vermittelten Endozytose keinen limitierenden Faktor darstellt. Liganden für Rezeptoren, die eine Internalisierung induzieren, sind z.B. Lektine, Toxine, virale Hämagglutinine, Invasine, Transferrin und Vitamine, wie beispielsweise Vitamin B12 und Vitamin B9 (Swaan 1998, Russell-Jones 2004). Vitamin B9 wird synonym auch als Folat (Überbegriff für natürlich vorkommende, reduzierte Formen) oder Folsäure (synthetische, oxidierte Form) bezeichnet (Food and Agriculture Organization of the United Nations and World Health Organization 2001). In

den vergangenen Jahren wurden mehrere Studien zur Endozytose Folsäure-konjugierter Wirkstoffe in verschiedene Gewebe- und Tumorzellen durchgeführt (Hilgenbrink and Low 2005, Leamon 2008), darunter auch Studien zur Erhöhung der oralen Bioverfügbarkeit (Anderson et al. 2001, Roger et al. 2012). Im Darmepithel werden verschiedene Folsäure-Rezeptoren, wie der protonengekoppelte Folattransporter (PCFT; engl. *proton-coupled folate transporter*), der Folattransporter 1 (RFC; engl. *reduced folate carrier*) und der Folat-Rezeptor α (FRα), exprimiert (Parker et al. 2005, Zhao et al. 2009), von denen aber nur der FRα die Aufnahme des Liganden in die Zelle mittels Endozytose vermittelt (Kamen and Capdevila 1986, Leamon and Low 1991, Zhao et al. 2011). Der FRα wird speziell im Dickdarm (Colon) und Mastdarm (Rektum) exprimiert (Holm et al. 1994, Parker et al. 2005) und könnte dort somit die systemische Aufnahme begünstigen.

Für eine Erhöhung der proteolytischen Stabilität können neben den oben genannten Formulierungen auch Modifizierungen am Peptid-Rückgrat oder das Einfügen konformationell veränderter Aminosäuren vorgenommen werden. Beispielsweise können die Enden der Peptide durch Amidierung oder Carboxylierung geschützt (Hetenyi et al. 2002, Sadowski et al. 2004, Szegedi et al. 2005) oder bestimmte Strukturen methyliert werden (Adessi et al. 2003). Eine sehr vielversprechende Strategie zur Erhöhung der proteolytischen Stabilität ist der Einbau D-enantiomerer Aminosäurereste in die Peptidsequenz, da Proteasen i.d.R. stereospezifisch für die L-enantiomere Form sind (Miller et al. 1995, Soto et al. 1996, Poduslo et al. 1998, Findeis et al. 1999, Elmquist and Langel 2003, Tugyi et al. 2005, Werle and Bernkop-Schnurch 2006, Wang et al. 2015).

Im menschlichen Organismus existieren jedoch auch Enzyme, die spezifisch für den Abbau D-enantiomerer Aminosäurereste sind - die D-Aminosäureoxidase (DAAO; engl. *D-amino acid oxidase*) und die D-Aspartatoxidase (DAspO). Sie katalysieren die oxidative Desaminierung D-enantiomerer Aminosäurereste (neutrale und basische D-Aminosäurereste: DAAO; saure D-Aminosäurereste: DAspO) und werden im Menschen hauptsächlich in der Niere, Leber und im Gehirn exprimiert (D'Aniello et al. 1993, Ohide et al. 2011, Yamanaka et al. 2012). Ob die DAAO und die DAspO nicht nur spezifisch für einzelne D-Aminosäurereste sind, sondern auch für D-Peptide, wurde bislang noch nicht untersucht.

Die Strategie D-enantiomere Aminosäurereste zur Erhöhung der Stabilität in die Sequenz Peptid-basierter Wirkstoffe einzubauen, wird auch bei der Entwicklung von Therapien für die Behandlung der AD angewandt (Funke and Willbold 2012, Kumar and Sim 2014). In mehreren Studien konnten Peptid-basierte Aβ-Aggregationsmodulatoren durch D-Aminosäure-Substitutionen modifiziert werden, ohne ihre Wirksamkeit dabei zu

beeinträchtigen (Soto et al. 1996, Poduslo et al. 1998, Findeis et al. 1999, Chalifour et al. 2003, Matharu et al. 2010, Taylor et al. 2010). Im Gegensatz dazu wurde das D-Peptid D3, auf das zuvor bereits detailliert eingegangen wurde, mithilfe eines Spiegelbild-Phagendisplays direkt in D-enantiomerer Konfiguration selektiert, sodass diese Form von vornherein die aktive Form darstellt.

2 Zielsetzung

In der Arbeitsgruppe von Prof. Willbold wurden die beiden Wirkstoffkandidaten D3 und RD2 entwickelt, die Aβ-Monomere in einer aggregationsinkompetenten Form stabilisieren, sodass dadurch das Gleichgewicht zwischen Aβ-Monomeren und Aβ-Oligomeren in Richtung der Aβ-Monomere verschoben wird und bestehende Aβ-Oligomere eliminiert werden. Hierbei handelt es sich um einen vielversprechenden Therapieansatz, da neurotoxische Aβ-Oligomere derzeit als Ursache der AD gelten. Neue Therapieansätze sind von besonderer Bedeutung, da es trotz intensiver Bemühungen bislang noch keine ursächliche AD-Therapie gibt.

Für D3 konnte bereits in mehreren Studien gezeigt werden, dass es *in vitro* Aβ-Oligomere eliminiert und in den Aβ-Aggregationsprozess eingreift sowie *in vivo* die kognitiven Defizite transgener AD-Mäuse verbessert. Die *in vitro*- und *in vivo*-Effizienz von RD2 wurde erst kürzlich von van Groen et al. (2017) publiziert. Im Rahmen der vorliegenden Arbeit sollte ein Aβ-Nukleationsassay zur Untersuchung des Einflusses von RD2 auf die Nukleus-induzierte, beschleunigte Aggregation entwickelt werden. Dieser ist in der oben genannten Publikation veröffentlicht.

Weiterhin sollten *in vitro* Untersuchungen zur D3- und RD2-Metabolisierung durchgeführt werden. Dabei sollte zum einen untersucht werden, ob D3 und RD2 aufgrund ihrer D-enantiomeren Struktur eine hohe Stabilität gegenüber Enzymen des Gastrointestinaltrakts, des Bluts und der Leber aufweisen und somit für eine orale Applikation geeignet sind. Zum anderen sollte untersucht werden, ob RD2 ein Substrat für ein auf die Metabolisierung von D-Aminosäureresten spezialisiertes Enzym, die D-Aminosäureoxidase, darstellt. Umgekehrt sollten mögliche Peptid-induzierte, inhibitorische Effekte auf die zuvor genannten Enzyme untersucht werden, da dies zu einer toxischen Akkumulation anderer Substanzen führen könnte. Des Weiteren sollte *in vitro* überprüft werden, ob human-spezifische Metaboliten in Lebermikrosomen gebildet werden, die potentiell toxisch auf den Organismus wirken könnten. Gebildete Metaboliten sollten identifiziert und auf mögliche Zytotoxizität untersucht werden.

Im Rahmen dieser Arbeit sollte außerdem eine Strategie entwickelt werden, die orale Bioverfügbarkeit von RD2 zu erhöhen. Ein vielversprechender Ansatz ist dabei die Konjugation des Wirkstoffs mit einem Ligand, der spezifisch für Rezeptoren ist, die zu einer Internalisierung des Ligand-Wirkstoff-Konjugats in die Zellen des Darmepithels führen. Die Konjugate sollten als sogenannte Prodrugs entworfen werden, die im Gastrointestinaltrakt stabil sind und nach Aufnahme über den Darm zum unkonjugierten

Wirkstoff metabolisiert werden. Die Abspaltung des Wirkstoffs vom zur Aufnahmebegünstigung verwendeten Liganden sollte *in vitro* und *in vivo* überprüft werden. Außerdem sollte gezeigt werden, dass die Konjugate keine Zytotoxizität aufweisen und weiterhin die $A\beta_{1-42}$-induzierte Zytotoxizität reduzieren, wie es bereits für unkonjugiertes RD2 gezeigt werden konnte.

Ein weiteres Ziel war die Entwicklung und Validierung einer bioanalytischen Methode, unmarkiertes RD2 aus Plasmaproben von beispielsweise therapeutischen oder pharmakokinetischen Studien mit Mäusen zu extrahieren und mittels LC-MS zu quantifizieren. Unter Verwendung dieser Methode sollten Plasmaproben RD2- oder Placebo-behandelter Mäuse analysiert werden.

3 Publikationen

The Aβ oligomer eliminating D-enantiomeric peptide RD2 improves cognition without changing plaque pathology

van Groen T, Schemmert S, Brener O, Gremer L, Ziehm T, Tusche M, Nagel-Steger L, Kadish I, Schartmann E, Elfgen A, Jürgens D, Willuweit A, Kutzsche J and Willbold D

Journal: Scientific Reports

Impact Factor: 4,259 (2015/2016)

Eigener Anteil: 5 % (Entwicklung, Durchführung und Auswertung des Nukleationsassays, Mitwirkung am Verfassen des Manuskripts)

Surprisingly high stability of the Aβ oligomer eliminating all-D-enantiomeric peptide D3 in media simulating the route of orally administered drugs

Elfgen A, Santiago-Schubel B, Gremer L, Kutzsche J and Willbold D

Journal: European Journal of Pharmaceutical Sciences

Impact Factor: 4,159 (2016)

Eigener Anteil: 85 % (Studiendesign, Entwicklung, Durchführung und Auswertung aller Versuche außer LC-MS-Messungen, Verfassen des Manuskripts)

Enzymatic resistance and investigation of potential human-specific metabolites of the amyloid-β oligomer eliminating all-D-enantiomeric peptide RD2

Elfgen A, Hupert M, Bochinsky K, Tusche M, González de San Román Martin E, Gering I, Sacchi S, Pollegioni L, Huesgen PF, Hartmann R, Santiago-Schübel B, Kutzsche J and Willbold D

Journal: Chemical Science

Impact Factor: 8,668 (2016)

Eigener Anteil: 55 % (Studiendesign, Entwicklung, Durchführung und Auswertung der HPLC-Studien, Probenvorbereitung (Zellviabilitätsassay, NMR-Spektroskopie, Massenspektroskopie), Verfassen eines Großteils des Manuskripts)

Development and validation of an UHPLC-ESI-QTOF-MS method for quantification of the highly hydrophilic amyloid-β oligomer eliminating all-D-enantiomeric peptide RD2 in mouse plasma

Hupert M*, Elfgen A*, Schartmann E, Schemmert S, Buscher B, Kutzsche J, Willbold D and Santiago-Schübel B (*Geteilte Erstautorenschaft)

Journal: Journal of Chromatography B

Impact Factor: 2,603 (2016)

Eigener Anteil: 35 % (Probenvorbereitung, Mitwirkung am Verfassen des Manuskripts)

3.1 The Aβ oligomer eliminating D-enantiomeric peptide RD2 improves cognition without changing plaque pathology

van Groen T, Schemmert S, Brener O, Gremer L, Ziehm T, Tusche M, Nagel-Steger L, Kadish I, Schartmann E, Elfgen A, Jürgens D, Willuweit A, Kutzsche J and Willbold D

Scientific Reports 2017, 7(1): 16275

DOI: 10.1038/s41598-017-16565-1

https://www.nature.com/articles/s41598-017-16565-1

SCIENTIFIC REPORTS

OPEN

The Aβ oligomer eliminating D-enantiomeric peptide RD2 improves cognition without changing plaque pathology

Received: 18 July 2017
Accepted: 15 November 2017
Published online: 24 November 2017

Thomas van Groen[1], Sarah Schemmert[2], Oleksandr Brener[2,3], Lothar Gremer[2,3], Tamar Ziehm[2], Markus Tusche[2], Luitgard Nagel-Steger[2,3], Inga Kadish[1], Elena Schartmann[2], Anne Elfgen[2], Dagmar Jürgens[2], Antje Willuweit[4], Janine Kutzsche[2] & Dieter Willbold[2,3]

While amyloid-β protein (Aβ) aggregation into insoluble plaques is one of the pathological hallmarks of Alzheimer's disease (AD), soluble oligomeric Aβ has been hypothesized to be responsible for synapse damage, neurodegeneration, learning, and memory deficits in AD. Here, we investigate the *in vitro* and *in vivo* efficacy of the D-enantiomeric peptide RD2, a rationally designed derivative of the previously described lead compound D3, which has been developed to efficiently eliminate toxic Aβ42 oligomers as a promising treatment strategy for AD. Besides the detailed *in vitro* characterization of RD2, we also report the results of a treatment study of APP/PS1 mice with RD2. After 28 days of treatment we observed enhancement of cognition and learning behaviour. Analysis on brain plaque load did not reveal significant changes, but a significant reduction of insoluble Aβ42. Our findings demonstrate that RD2 was significantly more efficient in Aβ oligomer elimination *in vitro* compared to D3. Enhanced cognition without reduction of plaque pathology in parallel suggests that synaptic malfunction due to Aβ oligomers rather than plaque pathology is decisive for disease development and progression. Thus, Aβ oligomer elimination by RD2 treatment may be also beneficial for AD patients.

Alzheimer's disease (AD) is the most common form of dementia in the elderly[1]. The main characteristic pathological hallmarks of AD are neurodegeneration, neurofibrillary tangles (NFTs), and neuritic plaques in the brain[2]. Intracellular neurofibrillary tangles consist of hyperphosphorylated, twisted filaments of the cytoskeletal protein tau, whereas extracellular plaques are primarily made up of amyloid-β (Aβ)[3], a 39 to 43 amino acid long peptide derived from the proteolytic processing of the amyloid protein precursor (APP)[4]. When APP is cleaved by β- and γ-secretases, the resulting breakdown product is Aβ[5].

Most cases of AD are sporadic, while a small percentage of AD cases are familial[6,7]. These cases are related to mutations in the genes coding for APP, presenilin 1 and 2 (PS1 and PS2)[7]. In general, the mutations influence APP metabolism such that the ratio of Aβ42/Aβ40 is often shifted to higher values[8,9]. Further, it has been shown that duplication of the APP gene[10,11] also results in early AD. Finally, a recent study has demonstrated that a novel mutation in the APP gene protects against the development of AD[12]. Together, these findings imply a central role for APP and its processing for the pathological changes occurring during AD[13,14].

The original amyloid cascade hypothesis[15] postulated that overproduction of Aβ would lead to Aβ deposition in neuritic plaques, which were supposed to be the cause of cognitive deficits. Nowadays, it is thought that soluble Aβ oligomers are the main etiologic agent for pathology and cognitive decline in AD[16–18]. The Aβ oligomers are hypothesized to cause a series of molecular events centring on disrupting the maintenance of synapse structure and function and thus leading to dysfunctional synapses, which are associated with memory loss[19,20].

[1]Department of Cell, Developmental and Integrative Biology, University of Alabama at Birmingham, Birmingham, AL, 35294, USA. [2]Institute of Complex Systems (ICS-6), Structural Biochemistry, Forschungszentrum Jülich GmbH, 52425, Jülich, Germany. [3]Institut für Physikalische Biologie, Heinrich-Heine-Universität Düsseldorf, 40225, Düsseldorf, Germany. [4]Institute of Neuroscience and Medicine (INM-4), Medical Imaging Physics, Forschungszentrum Jülich GmbH, 52425, Jülich, Germany. Correspondence and requests for materials should be addressed to T.G. (email: vangroen@uab.edu) or D.W. (email: d.willbold@fz-juelich.de)

Nowadays, the inhibition of the formation of Aβ oligomers and the elimination of already present Aβ oligomers is thought to be one of the most promising strategies to modify disease progression according to the modified amyloid cascade hypothesis. Currently registered drugs can only ameliorate symptoms and cannot slow down disease progression. Previously, we have reported about a D-enantiomeric peptide, named "D3", which was identified by mirror image phage display and solely consists of D-enantiomeric amino acid residues[21,22]. D3 inhibits the formation of regular Aβ fibrils, eliminates directly and specifically Aβ oligomers and reduces Aβ cytotoxicity *in vitro*[23,24]. *In vivo*, D3 binds to amyloid plaques[25], reduces Aβ plaque load, decreases inflammation and enhances cognition in various transgenic AD mouse models even after oral administration[24,26–28]. In order to enhance D3's potential to remove Aβ oligomers, we have used systematic approaches to identify derivatives with increased Aβ monomer binding activity and increased Aβ oligomer elimination properties[23,29–31]. In parallel, we also tried an additional rational approach to identify more efficient derivatives of D3 and learn more about important sequence motifs. We have identified a compound within this rational design series by the rearrangement of the amino acid residue sequence that showed very promising properties, termed "RD2" (abbreviation for "rational design 2"). In previous studies, we examined the pharmacokinetic characteristics of D3 and RD2[32,33]. These analyses have revealed a higher bioavailability of RD2 compared to D3, indicating improved pharmacokinetic characteristics.

In this study, we examined the *in vitro* profile of RD2 by various analyses to prove our hypothesis whether the rational design enhances the potential of our compound to remove Aβ oligomers. Moreover, we intraperitoneally treated APP/PS1 transgenic mice for only 28 days with RD2 compared to placebo and examined the treatment's influence on cognitive deficits at the end of the treatment period.

Material and Methods

Ethics statement. All experiments were carried out in compliance with the USPHS Guide for Care and Use of Laboratory Animals and approved by the Institutional Animal Care and Use Committee (IACUC; approval number 09457).

Peptides. The compounds D3 (rprtrlhthrnr) and RD2 (ptlhthnrrrrr) with amidated C-termini were purchased as lyophilized powder with >95% purity from JPT Peptide Technologies (JPT, Germany) and Cambridge peptides (Cambridge peptides, United Kingdom), respectively.

Synthetic and recombinant Aβ(1-42) with >95% purity was purchased as lyophilized powder from Bachem (Germany) and Isoloid (Germany), respectively. Biotinylated Aβ(1-42) was also purchased from Bachem (Germany).

Preparation of Aβ(1-42) stock solutions. Lyophilized Aβ(1-42) was dissolved overnight in HFIP (1,1,1,3,3,3-hexafluoro-2-propanol, Sigma-Aldrich, Germany). Aliquots were stored at −20 °C until further processing. Before usage, Aβ(1-42) was lyophilized and dissolved in 10 mM sodium phosphate buffer, pH 7.4.

Surface plasmon resonance measurements. The dissociation constants (K_D) of the compounds binding to Aβ(1-42) were determined by surface plasmon resonance (SPR) measurements using a T200 device (Biacore, GE Healthcare, Sweden). Because of the aggregation tendency of Aβ, especially under the binding assay conditions at neutral pH, Aβ was used solely as a ligand rather than as an analyte. Also, in order to avoid blockage of the microfluidic channels of the SPR device, we have refrained from using larger Aβ assemblies or fibrils as ligands or analytes. Immobilization was performed as described by Frenzel *et al.*[34] with minor modifications. 8 µM N-terminally biotinylated Aβ(1-42) was dissolved in 10 mM sodium phosphate buffer and monomers were separated via density gradient centrifugation as described in the QIAD section. The gradient was fractionated into 14 fractions à 140 µl. Aβ(1-42) monomers from fraction 1 were directly immobilized onto a series S sensor chip SA (Biacore, GE Healthcare, Sweden) by biotin-streptavidin coupling to a final level of 600 RU. The ligand flow cell and a reference flow cell were quenched with 10 µg/ml biotin for 7 min. For affinity determination of RD2 and D3, single cycle kinetic experiments were applied at 25 °C and 30 µl/min flow rate. 0.6 µM, 1.9 µM, 5.6 µM, 16.7 µM, and 50 µM of RD2 or D3 were diluted in 20 mM sodium phosphate buffer including 50 mM sodium chloride, pH 7.4 and injected over the flow cells for 180 s. The reference flow cell and buffer cycles were used for double referencing of the sensorgrams. For evaluation, the sensorgrams were fitted applying the steady state Langmuir 1:1 fit model of the Biacore T200 Evaluation Software 2.0 and the offset was constantly set to zero.

Quantitative determination of interference with Aβ aggregate size distribution (QIAD). For the evaluation of Aβ oligomer elimination of RD2, a QIAD assay (quantitative determination of interference with Aβ aggregate size distribution) was performed according to Brener *et al.*[23]. Briefly, 80 µM Aβ(1-42) was pre-incubated for 4.5 h to enrich Aβ oligomers. Then either RD2 or D3 were added to the pre-incubated solution with the resulting concentration of 20 µM RD2 or D3 and co-incubated for further 40 min. The samples were loaded on top of a density gradient containing 5 to 50% (w/v) iodixanol (OptiPrep, Axis-Shield, Norway) and centrifuged for 3 h at 4 °C and 259.000 × g (Optima TL-100, Beckman Coulter, USA). After centrifugation, 14 fractions à 140 µl were harvested by upward displacement. Fraction 1 from the top of the gradient was the least dense fraction while fraction 14 from just above the bottom was the densest fraction. The pellet of each tube was mixed with 60 µl of a 6 M guanidine hydrochloride solution and boiled for 10 min. The resulting solution represents fraction 15. All fractions were analysed with respect to their Aβ(1-42) content by analytical RP-HPLC (reversed phase-high performance liquid chromatography) and UV absorbance detection at 214 nm. The data for the D3 values and the Aβ(1-42) controls without compounds were already previously used in Brener *et al.*[23]. Analyses were done at least in quadruplicates (D3 and RD2 n = 4, Aβ(1-42) n = 11).

In a second experiment we investigated, whether RD2 eliminates Aβ(1-42) oligomers in a dose-dependent manner. Therefore, the QIAD assay was performed with minor modifications. Instead of 15 single fractions the

fractions 1 to 3, 4 to 6, 7 to 9, 10 to 11 and 12 to 14 have been pooled resulting in a total of six fractions. RD2 was added to 80 µM Aβ(1-42) after the 4.5 h incubation step at 1 µM, 5 µM, 10 µM, 20 µM, 30 µM, and 40 µM final concentrations. As described already above for the QIAD, the resulting mixtures were incubated for further 40 min before being applied to density gradient centrifugation. The half-maximal inhibitory concentration (IC_{50}) resulted from the compound concentration at the inflection point obtained by a logistic fit of the data (OriginPro 8.5 G, OriginLab, USA) obtained for fraction 2 (pooled fractions 4 to 6 of the above described QIAD), which contains the pooled oligomers of interest. The experiment has been performed in triplicate (n = 3).

Thioflavin T assay. The Thioflavin T (ThT) assay is a commonly used assay to visualize and quantify the fibrilisation of Aβ, since this dye binds to amyloidogenic cross-β-sheet structures. While Aβ aggregates into fibrils, the ThT fluorescence intensities increase until a saturation level is accomplished. Within this test, we analysed the inhibitory function of RD2 on the Aβ(1-42) fibril formation. 20 µM Aβ(1-42) was incubated with 5 µM ThT and different concentrations of RD2 (serial dilution from 80 µM till 1.25 µM) for IC_{50} calculation. ThT fluorescence was monitored over 21 h every 5 min at $\lambda_{ex} = 440$ nm and $\lambda_{em} = 490$ nm in a fluorescence plate reader (Polarstar Optima, Germany) at 37 °C. Correction was done using all supplements without Aβ. For data evaluation, the fibril masses were determined by subtracting the baseline fluorescence intensities from the top and normalised to the Aβ control to calculate the inhibition in percent. The IC_{50} resulted from the compound concentration at the inflection point obtained by a logistic fit of the data (OriginPro 8.5 G, OriginLab, USA).

Seeding assay. A seeding assay with RD2 was performed to investigate whether RD2 can inhibit the potential of preformed Aβ(1-42) seeds to accelerate the aggregation of monomeric Aβ(1-42). The seeds were prepared by incubating 200 µM monomeric Aβ(1-42) in 10 mM sodium phosphate buffer, pH 7.4, for three days at 37 °C with slight shaking. Afterwards, the sample was centrifuged at 14,000 × g at 4 °C for 45 min. The supernatant was discarded and the loose pellet, which contained the insoluble fibrils, was resuspended in buffer. The sample was sonicated for 2 min in an ultrasonic bath to disperse large Aβ aggregates. The concentration of Aβ seeds according to the monomers was determined by RP-HPLC[23]. The seeds were incubated with or without RD2 in a molar ratio of 1:1 for 24 h at 37 °C with slight shaking. The samples were sonicated again for 2 min. Lyophyllised monomeric Aβ(1-42) was dissolved at a concentration of 15 µM in buffer immediately before the measurement and was mixed with 1.9 µM seeds (molar ratio of 8:1 monomers:seeds) or 1.9 µM seed-RD2-mix (molar ratio of 8:1:1 of monomers:seeds:RD2). As a control, monomeric Aβ without seeds was used. Every sample was mixed with 20 µM ThT to monitor Aβ aggregation. The ThT fluorescence was monitored for 24 h at 24 °C. Samples were measured in triplicate. The resulting ThT fluorescence intensities were fitted with 5-parametrical logistic fits and the amplitude as well as the half-life was calculated in each case. The amplitude of the fluorescence intensities of the Aβ aggregation alone was set to 100% and the amplitude of the seeded Aβ aggregation with and without RD2 was normalised to it. The measurements were performed in three independent experiments (n = 9).

Cell viability assay (MTT test). MTT (3-(4,5-Dimethylthiazol-2-yl)-2,5-diphenyl-tetrazolium bromide) based cell viability assays were accomplished to examine the cytotoxicity of Aβ(1-42) in the presence of RD2 on two different cell lines, PC-12 (rat pheochromocytoma cell line), and SH-SY5Y (human neuroblastoma cell line) cells[35].

PC-12 cells (DSMZ, Germany) were cultured in DMEM medium supplemented with 10% fetal calf serum, 1% antibiotics (Penicillin/Streptomycin) (all Sigma-Aldrich, USA), and 5% horse serum (PAA Laboratories GmbH, Germany) on collagen A-coated (Biochrom GmbH, Germany) tissue culture flasks (SPL Life Sciences Co., Korea). SH-SY5Y cells (DSMZ, Germany) were cultured in DMEM medium supplemented with 20% fetal calf serum and 1% antibiotics (Penicillin/Streptomycin) (all Sigma-Aldrich, USA) on tissue culture flasks (SPL Life Sciences Co., Korea). Cells were allowed to grow in a humidified incubator with 5% CO_2 at 37 °C and a maximum of 12 (PC-12 cells) or 21 (SH-SY5Y cells) passages. Medium was changed every two days and cells were passaged every three to five days, according to their confluence.

MTT test was performed according to the manufacturer's protocol (CellProliferation Kit I; Roche, Switzerland). PC-12 or SHSY-5Y cells were seeded in clear, collagen-coated 96-well flat bottom microwell plates (Life Technologies Inc., USA) at a density of 1×10^4 cells in a volume of 100 µl per well and incubated for 24 h. For both cell lines, compounds were prepared in the following way as a fivefold determination in three independent experiments. 51 µM Aβ(1-42) was incubated for 4.5 h at 37 °C shaking at 600 rpm. Afterwards, 255 µM RD2 was added and incubated for another 40 min. Throughout the test, cells were exposed to 1 µM Aβ with or without 5 µM RD2. The arithmetic mean of all measurements per approach was calculated. Results are represented as the percentage of MTT reduction, assuming that the absorbance of control cells was 100%.

Animals. For this study, 21 APP/PS1 double transgenic mice (APPSwedish/PS1ΔE9)[36] were used. The very well characterized APP/PS1 mouse model develops cognition deficits and abundant Aβ deposits already at early age. The original mice were purchased from JAX (The Jackson Laboratory, USA) and maintained in our own colony at the University of Alabama in Birmingham. Before treatment, the mice were housed in a controlled environment (humidity 50–60%, temperature 22 °C, light from 06:00 a.m. to 6:00 p.m.) with 4 animals per cage in our facility with food and water available *ad libitum*. After the implantation of the Alzet minipumps the mice were housed individually.

Treatment of APP/PS1 mice. In this study, we treated seven months old female APP/PS1 mice intraperitoneally by use of Alzet osmotic minipumps (Alzet osmotic mini pumps, model #1004, Alzet, USA). Mice were either treated with 5.3 mg/kg/day RD2 (n = 11) or placebo (0.9% sodium chloride solution) (n = 10) as control group. The Alzet minipumps were soaked in sterile 0.9% sodium chloride solution for 24 h before implantation. The next day, the pumps were filled with the appropriate solution and implanted intraperitoneally. In short, mice

were anesthetised with isoflurane, the skin and the muscle layer below were cut in the midline and the pump was inserted in the abdominal cavity. Following placement of the pump, the wound was sutured. Three weeks after the implantations, the mice were tested in different behavioural set ups. 28 days after the implantations, the mice were sacrificed for histopathological analysis. All mice of both groups were included in the experiments described below.

Behavioural tests. The mice were tested at the end of the treatment period in different behavioural tests.

Open field test. The open field test was performed to evaluate the activity and anxiety behaviour of the mice. The arena (42 cm × 42 cm surrounded with clear Plexiglass sides (20 cm high)) was subdivided into two areas: border and centre. The mice were observed with a camera driven tracker system (Ethovision XT10, Noldus, The Netherlands) for 4 min. Time spent in both areas was analysed. After each testing day and in between the mice, the apparatus was wiped out with chlorhexidine and 70% ethanol and allowed to air-dry.

Zero maze. Similar to the open field test, the zero maze was used to assess the anxiety behaviour of the mice. The maze consisted of a circular arena (65 cm diameter) that is raised 40 cm above the table. The maze was separated into four equal parts, with two parts with 15 cm high walls of opaque material and two only 0.5 cm high walls. Therefore, it consisted of two open and two closed areas. The mice were put into the circle and observed for 4 min with a camera driven tracker system (Ethovision XT10, Noldus, The Netherlands). Analysed was the time mice spent in the open and closed arms. After each testing day and in between mice, the apparatus was wiped out with chlorhexidine solution and 70% ethanol and allowed to air-dry.

Morris water maze (MWM). The mice were tested daily for one week in a water maze. Our version of the Morris water maze consists of a blue circular tank (120 cm diameter) filled with clear water (22 °C ± 1 °C). In short, the mice were placed into the water at the edge of the pool and allowed to swim in order to find a hidden but fixed escape platform (0.5 cm below the water surface) by orientating themselves with the help of extramaze cues. The mice were allowed to swim freely for a maximum of 60 s to re-find the hidden platform (or until they climbed onto the hidden platform). If they had not found it, they were placed on the platform for 20 s. Each mouse was tested for three trials per day with inter-trial intervals of 60 s and varying starting positions in a pseudo random order. The platform was placed in the middle of one of the quadrants (south-east) of the pool approximately 30 cm from the edge of the pool. The task of the mice throughout the experiment was to find and escape on the hidden platform. Once the mouse had learned the task (day 6, trial 18), a probe trial was performed immediately following the last trial of acquisition on day 6. In the probe trial (i.e. trial 19), the platform was removed from the pool and animals were allowed to swim for 60 s. Mice were recorded with a camera driven tracker system (Ethovision XT10, Noldus, The Netherlands). It was analysed the time the mice needed to escape to the hidden platform (escape latency) and the time they spent in the target quadrant (probe trial).

Histopathology. In short, mice were anesthetized, transcardially perfused with ice-cold saline and the brains were removed. The brain was cut in half through the midline. One hemisphere was frozen for biochemical analysis and the other half was fixed overnight in 4% paraformaldehyde. Following overnight postfixation and cryoprotection in 30% sucrose, six series (1 in 6) of coronal sections were cut through the brain. One half of the first series of sections was mounted unstained, the other half was stained for Aβ using the W0-2 antibody (mouse anti-human Aβ4-10, Merck, Germany), as described in detail below. The second series was stained immunohistochemically according to published protocols[37]. One half of the second series was stained for GFAP (mouse anti-GFAP; Sigma-Aldrich, USA), a marker for astrocytes, whereas the other half was stained for Iba-1 (rabbit anti-Iba-1; WAKO, USA), a marker for microglia. Some of the stained sections were double stained with either Congo red, Thioflavin S or Thiazine red. The other three series were stored at −20 °C in antifreeze for future analyses.

The sections from the first series which had been destined for Aβ staining were pre-treated for 30 min with hot citrate buffer (85 °C). The series of sections was transferred into a tris-buffered saline (TBS) solution containing 0.5% Triton X-100 (TBS-T) and the primary antibody. 18 h after incubation in this solution at room temperature (20 °C) on a shaker table in the dark, the sections were rinsed three times with TBS-T and transferred into a solution with the secondary antibody (goat anti-mouse*biotin (Sigma-Aldrich, Germany), or sheep anti-rat Ig*biotin (Biorad, USA)) and incubated for two hours. Then, the sections were rinsed three times with TBS-T and transferred into a solution with mouse ExtrAvidin (Sigma-Aldrich, Germany). Following rinsing, the sections were incubated for approximately 3 min with a 3,3′-Diaminobenzidine (DAB) solution enhanced with a saturated nickel ammonium sulphate solution. All stained sections were mounted on slides and coverslipped.

Plaque quantification. The plaque load of the appropriate areas (dorsal hippocampus and parietal cortex) of the brains was determined as described previously[28].

Biochemistry. Diluted brain samples were assayed for Aβ(x-40) and Aβ(x-42) as described previously[24,26,28].

Statistics. All statistical calculations were performed using GraphPad Prism 5 (GraphPad Software, Inc., USA) or SigmaPlot Version 11 (Systat Software, Germany). Data is represented as mean ± SD (SPR, QIAD, ThT assay, seeding assay, MTT test) or SEM (behavioural tests, histochemical and biochemical analysis), $p > 0.05$ was considered as not significant (n.s.). Normal distribution of data was either tested by use of Shapiro-Wilk normality test or by use of a normal probability plot (InVivoStat, Version 3.4.0.0, UK)[38]. Normal distributed data was analysed with one-way ANOVA with Bonferroni post hoc analysis (QIAD assay, seeding assay, MTT test). Two-way ANOVA with Bonferroni post hoc analysis was used to analyse the results of the *in vivo* study (open

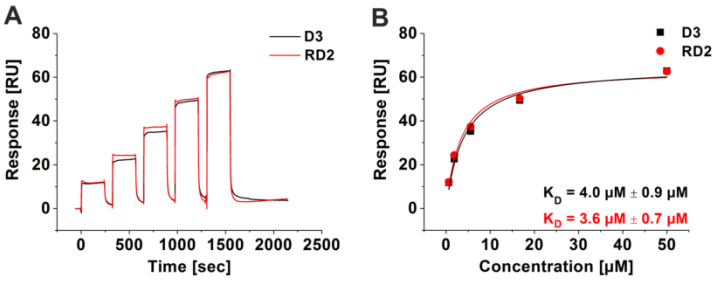

Figure 1. Affinity determination of D3 and RD2 by SPR. N-terminally biotinylated Aβ(1-42) was immobilised on a streptavidin sensor chip and the binding of different D3 (black) and RD2 (red) concentrations was analysed in a single cycle (**A**). For evaluation, the steady-state binding signals were plotted over the concentrations and fitted using a Langmuir 1:1 binding model (**B**). Data is represented as values ± errors of the fit.

field test, zero maze, probe trial Morris water maze, ELISA). Escape latency to the platform within the Morris water maze was considered as not normally distributed and therefore analysed by Friedman Repeated Measures ANOVA on Ranks with Dunn's post hoc analysis.

Results

RD2 and D3 bound to Aβ(1-42) with similar affinities. Binding affinities of D3 and RD2 were determined using surface plasmon resonance (SPR). Monomeric N-terminally biotinylated Aβ(1-42) was immobilized on the surface and concentration dependent series with the respective compound were injected (Fig. 1A). Steady-state analysis of the data revealed similar dissociation constants (K_D) for both peptides which were 4.0 µM ± 0.9 µM for D3 and 3.6 µM ± 0.7 µM for RD2 (Fig. 1B).

RD2 eliminated Aβ oligomers. *In vitro*, the influence of RD2 and D3 on the Aβ aggregate size distribution was tested by the assay for quantitative determination of interference with Aβ aggregate size distribution (Aβ QIAD)[23] (Fig. 2A). Aβ species located in fractions 4 to 6 of the density gradient were efficiently eliminated by RD2 and D3 (Fig. 2B). Aβ species located in these fractions are Aβ oligomers, which were previously characterised in detail[23]. They have a molecular weight of about 100 kDa, corresponding to about 23 monomeric units. Both, RD2 and D3 significantly reduced the amount of Aβ oligomers in fractions 4 to 6 by 71% and 51%, respectively (Fig. 2B, one-way ANOVA, $p \leq 0.001$, Bonferroni post hoc analysis, Aβ(1-42) vs. D3 or RD2 in fractions 4–6, $p \leq 0.001$, fraction 4 D3 vs RD2, $p = 0.019$, fraction 5 D3 vs RD2, $p = 0.025$, fraction 6 D3 vs RD2, $p = 0.045$) without causing a significant change of the Aβ monomer amount in the first fractions of the density gradient (one-way ANOVA, $p = 0.19$). Although RD2 and D3 have the same qualitative effect on Aβ oligomers, RD2 was found to be significantly more efficient in Aβ oligomer elimination (Fig. 2B). Furthermore, a QIAD assay for Aβ(1-42) size distributions was performed in dependence of different RD2 concentration (Fig. 2C). Based on the results of the performed assay it could be shown that RD2 eliminates Aβ(1-42) oligomers in a dose-dependent manner with a resulting half-maximal inhibition concentration (IC_{50}) of 8.4 µM (Fig. 2D).

Aβ fibril formation was inhibited by RD2 in a dose-dependent manner. Investigation of the functional effect of RD2 on Aβ(1-42) fibril formation was accomplished by Thioflavin T (ThT). As demonstrated in Fig. 3A, RD2 inhibited the formation of Aβ(1-42) fibrils in a dose-dependent manner and a half-maximal inhibition concentration (IC_{50}) of 7.7 µM was determined (Fig. 3B). Thus, the IC_{50} value is in very good agreement with the K_D value obtained by SPR, indicating that the binding event is responsible for the inhibitory function of RD2.

RD2 reduced the catalytic effect of preformed seeds on Aβ aggregation. To investigate whether RD2 can inhibit the seeding potential of Aβ, a seeding assay was performed. The aggregation of monomeric Aβ(1-42) alone or together with preformed Aβ(1-42) seeds incubated with and without RD2 was monitored. The resulting intensities were fitted and the amplitude and the half-life ($t_{1/2}$) were calculated. For monomeric Aβ(1-42) without seeds $t_{1/2}$ was 11.6 h, whereas the aggregation of seeded monomeric Aβ(1-42) was significantly ($p \leq 0.001$) accelerated to a half-life of 1 h (one-way ANOVA with Bonferroni post hoc analysis) (Fig. 4A). 24 h incubation of RD2 with seeds decelerated the aggregation of monomeric Aβ significantly ($p \leq 0.001$) by factor of 5 (4.6 h) compared to seeded Aβ without RD2. This indicates that RD2 lowers the catalytic effect of the seeds on Aβ aggregation *in vitro*. The amplitude of seeded Aβ was not affected by the pre-treatment of the seeds with RD2 (Fig. 4B). This observation supports the hypothesis that the observed effect in Fig. 4A was indeed due to the potential of RD2 to reduce the seeding potential of the seeds during the pre-treatment rather than due to any remaining free RD2, which would reduce also the overall fibril formation as shown in Fig. 3A.

Increased cell viability after pre-incubation of Aβ(1-42) assemblies with RD2. The MTT cell viability test was performed to survey the effects of RD2 co-incubated with Aβ(1-42) on PC-12 and SH-SY5Y cells. PC-12 cells are extensively used to study Aβ induced neurotoxicity, because this cell type is vulnerable to Aβ. Additionally, we have used SH-SY5Y cells in addition to study the effects on a more appropriate neuronal cell

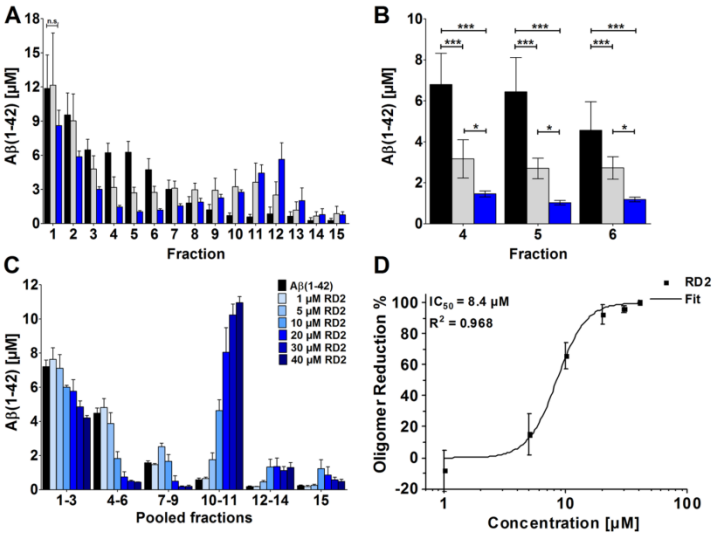

Figure 2. RD2 eliminated Aβ(1-42) oligomers in a concentration dependent manner. Aβ(1-42) size distributions without D-peptide (black in **A**–**C**) and in the presence of compounds were analysed by density gradient centrifugation. Aβ(1-42) concentrations for each fraction were determined by UV absorption during RP-HPLC. Aβ(1-42) oligomers of interest are located in fractions 4 to 6 (**A**–**C**). Comparison of 20 µM D3 (grey) and 20 µM RD2 (blue) (**A**,**B**) revealed the superior oligomer elimination efficacy of RD2. In (**C**) the QIAD assay for Aβ(1-42) size distributions in dependence of different RD2 concentrations (0 µM black, 1 µM till 40 µM, from light to dark blue) are shown. Graphical representation of the measured decrease in oligomer concentration in % of the amount of oligomers found in the control with 0 µM RD2 in dependence of the different RD2 concentration. The curve was fitted according to a logistic fit function yielding an IC_{50} value (**D**). In each experiment, data is represented as mean ± SD; A: one-way ANOVA, with Bonferroni post hoc analysis, Aβ(1-42) vs. D3 or RD2 in fractions 4–6, ***$p \leq 0.001$, fraction 4 D3 vs RD2, *$p = 0.019$, fraction 5 D3 vs RD2, *$p = 0.025$, fraction 6 D3 vs RD2, *$p = 0.045$. Data of Aβ(1-42) and D3 were taken from Brener *et al.*[23].

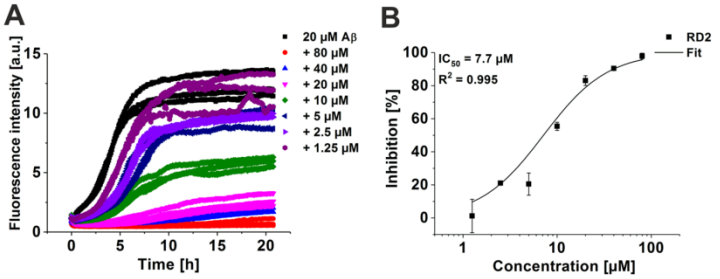

Figure 3. Inhibitory function of RD2 for Aβ(1-42) fibril formation. Aβ(1-42) fibril formation was monitored by Thioflavin T (ThT) in the absence or presence of different RD2 concentrations (0 µM black, 80 µM red, 40 µM light blue, 20 µM pink, 10 µM green, 5 µM blue, 2.5 µM lilac, 1.25 µM purple) (**A**). Fibril mass was normalised to the Aβ control and the inhibition in % was calculated. The curve was fitted according to a logistic fit function yielding an IC_{50} value (**B**). The data represent three replicates.

type. We incubated Aβ(1-42), at a final concentration of 1 µM, with and without 5 µM RD2 on PC-12 or SH-SY5Y cells. We found a significant increase of cell viability of PC-12 and SH-SY5Y cells after pre-incubation of Aβ with RD2 from 25% to 76% (Fig. 5A) and 65% to 94% (Fig. 5B), respectively (both: one-way ANOVA, $p \leq 0.001$ with

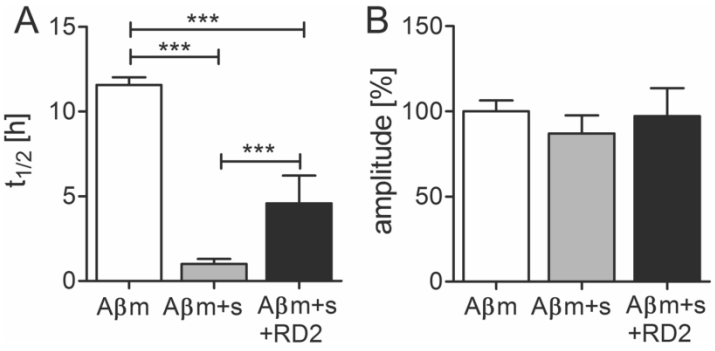

Figure 4. Influence of RD2 on the seeded Aβ(1-42) aggregation. The aggregation of monomeric Aβ without (m, white), and with preformed seeds (s, grey) incubated with or without RD2 (black) was monitored and the half-life ($t_{1/2}$) (**A**) as well as the amplitude (**B**) of the aggregation was determined. In (**B**) the amplitude of monomeric Aβ without seeds was set to be 100% and the amplitudes of the other samples were normalized accordingly. Data is represented as mean ± SD, one-way ANOVA with Bonferroni post hoc analysis, ***$p \leq 0.001$.

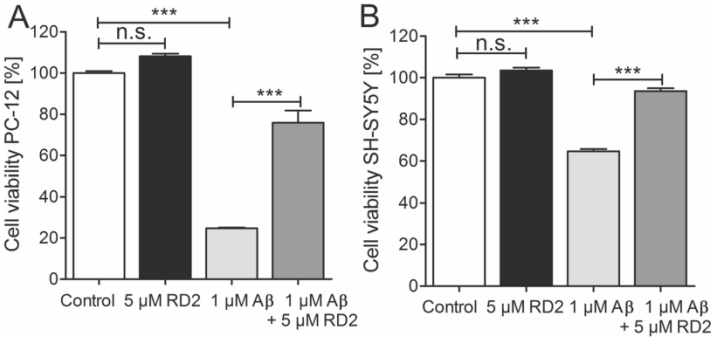

Figure 5. RD2 reduced the negative impact of Aβ(1-42) on cell viability in PC-12 and SH-SY5Y cells. Cell viability was assessed by MTT after incubation of PC-12 (**A**) or SH-SY5Y (**B**) cells with 1 µM Aβ(1-42) (light grey) or 1 µM Aβ(1-42) co-incubated with 5 µM RD2 (grey), respectively. Data confirms the efficacy of RD2 to significantly increase the cell viability after co-incubation with Aβ(1-42) on both cell lines compared to Aβ(1-42) alone. Data is represented as mean ± SD, one-way ANOVA with Bonferroni post hoc analysis, ***$p \leq 0.001$.

Bonferroni post hoc analysis: $p \leq 0.001$). In order to demonstrate that RD2 alone did not influence cell viability, 5 µM RD2 were incubated with both cells lines, which did not result in any change of cell viability compared to buffer control (one-way ANOVA: n.s., $p = 0.4$, Fig. 5A and B).

Treatment with RD2 improved cognition without showing any influence on activity or anxiety. Implantation of Alzet osmotic minipumps filled with RD2 solution or saline (placebo) into APP/PS1 mice neither changed any obvious physiological parameters (e.g. growth as measured by body weight (placebo: 25.7 ± 0.9 g vs RD2: 26.8 ± 0.8 g) or general health, i.e. look of fur, posture, and motor activity) in the implanted mice, nor caused any noticeable discomfort. None of the mice developed any health or motor problems.

After three weeks of placebo or RD2 treatment of APP/PS1 mice, both groups were tested in the open field and zero maze tests. As demonstrated in Fig. 6, there were no significant differences in activity or anxiety levels between the two groups of mice (Fig. 6A; total distance moved in the open field: 2143 ± 217 cm vs 2121 ± 163 cm, respectively, both two-way ANOVA with Bonferroni post hoc analysis, $p = 1$). Speeds in the open field was 8.9 ± 0.9 cm/s vs 8.8 ± 0.7 cm/s, respectively, while in the zero maze the average speed of movement was 5.0 ± 0.6 vs 4.8 ± 0.4 cm/s, respectively (Fig. 6A and B). In the following week, the mice were tested in the Morris water maze. There was no difference in the swimming speed between the groups of mice (placebo: 19.0 ± 1 cm/s and RD2: 18.8 ± 1 cm/s). RD2 treated mice did significantly improve their performance during the week of training

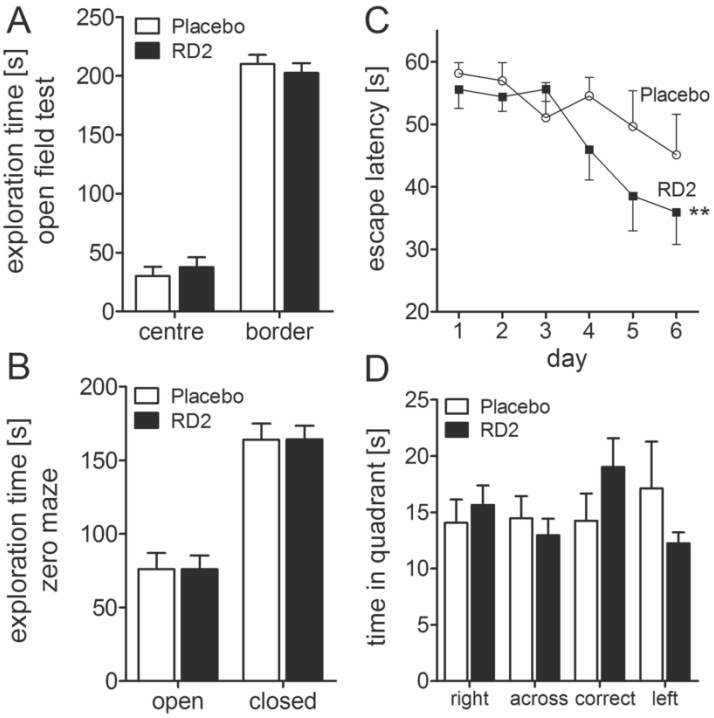

Figure 6. Effects of RD2 on cognition and evaluation of activity and anxiety. Four graphs showing the behaviour of placebo and RD2 treated mice. Assessment of the open field test (**A**) and zero maze (**B**) exhibits no difference of activity or anxiety of RD2 and placebo treated mice. Performance in the water maze showed a significantly improved cognition of RD2 treated mice in contrast to the performance of placebo treated mice (**C**). The RD2 treated group showed a preference for the correct quadrant in the probe trial which followed the last training trial (**D**). Data is represented as mean ± SEM, Friedman Repeated Measures ANOVA on Ranks, (**C**) $^{**}p = 0.003$.

in the Morris water maze compared to the placebo treated mice (escape latency, Friedman RM ANOVA, RD2 treated mice $p = 0.003$, Dunn's post hoc analysis $p \leq 0.05$, placebo treated mice $p = 0.13$, Fig. 6C). Furthermore, the RD2 group showed a preference for the correct quadrant in the probe trial, which followed the last training trial (Fig. 6D). After completion of the behavioural testing, the animals were sacrificed and the brains were removed for further analysis.

The Aβ load was measured in the dorsal hippocampus and parietal cortex by immunohistochemical staining for human Aβ(4-10) (W0-2 antibody). Treatment with RD2 did not reveal any reduction of the Aβ plaque load in the hippocampus or in the cortex compared to the placebo treated mice (% area covered, Fig. 7A–F). Furthermore, analysis of the sections that were stained for activated astrocytes (GFAP) or microglia (Iba-1) revealed that the magnitude of inflammation surrounding Aβ deposits did not differ between the two treatment groups of mice. Neither did RD2 treatment significantly reduce the amount of plaque related microglial inflammation (Iba-1; average density 40.5 ± 2.0 vs 40.7 ± 1.5, respectively; Fig. 7G–I) compared to the placebo treated mice. Nor did treatment with RD2 significantly change the amount of plaque-related activated astrocytes (GFAP; average density 34.6 ± 1.4 vs 36.7 ± 1.7, Fig. 7J–L) compared to the placebo treated mice within the hippocampus. Double staining for microglia and astrocytes confirmed that in the surroundings of all labelled plaques both glial cell types were activated.

The biochemical analysis by ELISA measurements demonstrated that Aβ(x-40) levels did not differ significantly between RD2 and placebo treated mice (insoluble Aβ(x-40): 142.5 ± 3.9 pg/g vs 148.1 ± 3.0 pg/g; soluble Aβ(x-40): 38.9 ± 5.2 pg/g vs 47.8 ± 7.4 pg/g, respectively, Fig. 8A). However, a significant decrease of insoluble Aβ(x-42) levels was detected in the hippocampus of RD2 treated mice in contrast to the placebo treated mice (insoluble Aβ(x-42): 168.8 ± 19.2 pg/g vs 219.4 ± 15.3 pg/g; soluble Aβ(x-42): 15.5 ± 2.6 pg/g vs 23.5 ± 5.1 pg/g respectively, two-way ANOVA, $p = 0.027$ with Bonferroni post hoc analysis, $p = 0.048$, Fig. 8B). Furthermore,

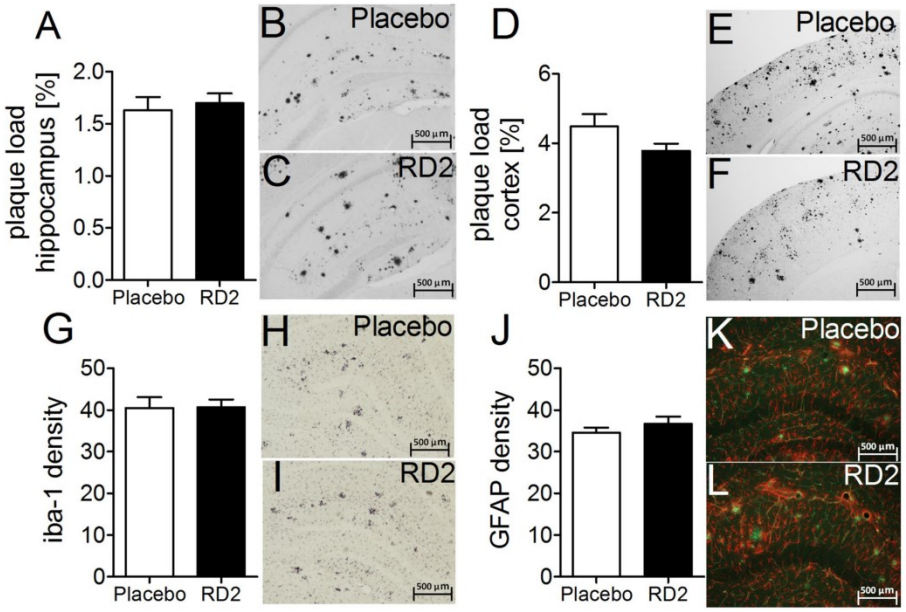

Figure 7. Histopathological analysis of AD pathology in hippocampus revealed no change after intraperitoneal treatment with RD2. Aβ load measured in hippocampus and parietal cortex (**A**–**F**), microglia (**G**–**I**) and activated astrocytes (**J**,**K**) were analysed after the behavioural tests. Data indicates that there is no change in AD typical pathology after 28 days of intraperitoneal treatment with RD2 compared to the pathology of placebo treated mice. Data is represented as mean ± SEM.

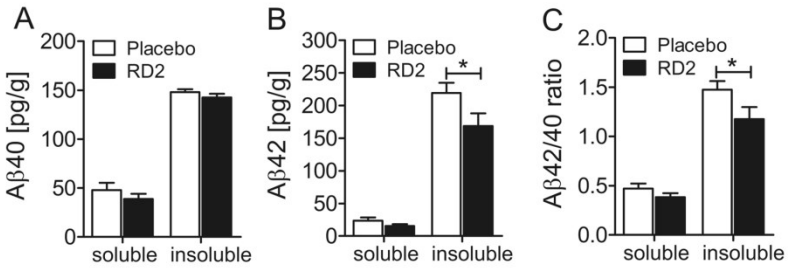

Figure 8. Treatment with RD2 significantly reduced the level of insoluble Aβ(x-42). Levels of Aβ(x-40) (**A**) and Aβ(x-42) (**B**) were analysed in soluble and insoluble fractions of hippocampus by ELISA. Treatment with RD2 exhibited a significant decrease of insoluble Aβ(x-42) level in the hippocampus and significantly lowered the Aβ42/40 ratio (**C**). Data is represented as mean ± SEM, two-way ANOVA with Bonferroni post hoc analysis, (**B**) *p = 0.027, (**C**) *p = 0.026.

treatment with RD2 lowered significantly the ratio of insoluble Aβ42/40 (insoluble Aβ42/40: RD2 1.2 ± 0.1 vs placebo 1.5 ± 0.1; soluble Aβ42/40: RD2 0.4 ± 0.1 vs placebo 0.5 ± 0.1, respectively: two-way ANOVA, p = 0.026 with Bonferroni post hoc analysis, p = 0.047, Fig. 8C).

Discussion

Finding a curative and disease modifying treatment for AD is one of the major challenges of the 21st century. Despite the fact of increasing prevalence of AD, current treatment options are only symptomatic[39], a situation that is considered inacceptable. Today, soluble Aβ oligomers are postulated to be the disease causing

agent and consequently, their elimination is a promising target for therapy. Within the last years, we developed D-enantiomeric peptides, solely consisting of D-enantiomeric amino acid residues, for stabilisation of Aβ monomers in an aggregation incompetent conformation, leading to the specific and direct elimination of Aβ oligomers[23,26].

Here, we characterised our all-D-enantiomeric amino acid residue compound RD2. RD2 is a derivative of the lead compound D3, which was characterised before[24,27,40]. Based on steady state analysis, both compounds, D3 and RD2, showed similar binding affinities to Aβ(1-42) monomers with an equilibrium dissociation constant in the micromolar range, which was shown previously and validated within this study[41]. However, the potential of RD2 to eliminate Aβ oligomers is significantly increased in comparison to D3. Moreover, RD2 eliminates Aβ(1-42) oligomers in a dose-dependent manner with an IC_{50} of 8.4 µM. Additionally, RD2 significantly reduced the cytotoxic potential of Aβ(1-42), shown by the enhanced cell viability in PC-12 and SHSY-5Y cells after co-incubation of Aβ(1-42) with RD2 and inhibited the Aβ(1-42) fibril formation with an IC_{50} of 7.7 µM. This is in very good agreement with the results of the QIAD assay. In accordance with the Aβ oligomer eliminating properties of RD2, RD2 also inhibited the seeding potential of Aβ aggregates.

Investigation of the *in vivo* efficacy of RD2 was carried out in an intraperitoneal treatment study with APP/PS1 transgenic mice. Thereby we could prove our hypothesis that RD2 showed a similar or increased efficacy compared to D3. Short term treatment with RD2 improved cognitive performance significantly after three weeks compared to the placebo control group. Treatment with RD2 did not lead to a significant reduction in the amount of Aβ deposits in the hippocampus. As it is expected that there is an equilibrium between soluble and plaque Aβ, longer treatment periods could have possibly led to a significant reduction of Aβ pathology. Furthermore, analysis of the microglia and astrocytes did not show significant reduction in activated microglia and astrocytes in RD2 treated mice compared to the placebo treated mice. Consequently, improved cognitive performance was not related to a decrease in plaque pathology. Since RD2 significantly reduced the amount of Aβ oligomers *in vitro*, a more likely explanation is that RD2 decreases synaptic toxicity and pathology by reducing the amount of Aβ oligomers *in vivo*, even without significantly changing the Aβ plaque load.

RD2 significantly reduced levels of insoluble Aβ(x-42) in the hippocampus, but did not show any significant reduction of Aβ(x-40) levels. This ultimately led to a decrease of the Aβ42/Aβ40 ratio, without affecting total Aβ levels. What that actually means remains to be elucidated. We hypothesize that the Aβ oligomer eliminating activity of RD2 is based on its binding to Aβ monomers and their stabilisation in an aggregation-incompetent conformation, thereby shifting the equilibrium between monomeric and oligomeric Aβ away from Aβ oligomers, ultimately leading to the elimination of Aβ oligomers. It certainly increases the need to further investigate the underlying mechanism of RD2 based on the improvement of cognitive performance. Irrespective of that, these observations strengthen the potential role of RD2 as a disease-modifying agent for AD treatment. Besides that, the outcome of this study supports the finding that there is not a necessarily dependence between plaque pathology and cognition. Compared with other drugs targeting Aβ oligomers (e.g. antibodies) our compound RD2 does not only interact with Aβ oligomers but directly destroys them without relying on the contribution of components of the immune system. Future treatment studies with RD2 in other transgenic AD mouse models will further elucidate the compound's mechanism of action and its future potential.

Conclusion

Summarised, the identified derivative of the lead compound D3, named RD2, was significantly more efficient in elimination of Aβ oligomers than D3. RD2 improved cognitive performance of APP/PS1 mice already after a short, three weeks, treatment and reduced insoluble Aβ(x-42) levels in the brain without a negative impact on activity or anxiety. Based on this, RD2 is a promising compound to be further developed as a drug candidate for therapy of AD.

References

1. Hirtz, D. *et al.* How common are the "common" neurologic disorders? *Neurology* **68**, 326–337, https://doi.org/10.1212/01.wnl.0000252807.38124.a3 (2007).
2. Montine, T. J. *et al.* National Institute on Aging-Alzheimer's Association guidelines for the neuropathologic assessment of Alzheimer's disease: a practical approach. *Acta neuropathologica* **123**, 1–11, https://doi.org/10.1007/s00401-011-0910-3 (2012).
3. Ballard, C. *et al.* Alzheimer's disease. *Lancet* **377**, 1019–1031, https://doi.org/10.1016/S0140-6736(10)61349-9 (2011).
4. O'Brien, R. J. & Wong, P. C. Amyloid precursor protein processing and Alzheimer's disease. *Annual review of neuroscience* **34**, 185–204, https://doi.org/10.1146/annurev-neuro-061010-113613 (2011).
5. Selkoe, D. J. & Hardy, J. The amyloid hypothesis of Alzheimer's disease at 25 years. *EMBO molecular medicine* **8**, 595–608, https://doi.org/10.15252/emmm.201606210 (2016).
6. Bertram, L. & Tanzi, R. E. Alzheimer's disease: one disorder, too many genes? *Human molecular genetics* **13**(Spec No 1), R135–141, https://doi.org/10.1093/hmg/ddh077 (2004).
7. Bertram, L., Lill, C. M. & Tanzi, R. E. The genetics of Alzheimer disease: back to the future. *Neuron* **68**, 270–281, https://doi.org/10.1016/j.neuron.2010.10.013 (2010).
8. Van Broeck, B., Van Broeckhoven, C. & Kumar-Singh, S. Current insights into molecular mechanisms of Alzheimer disease and their implications for therapeutic approaches. *Neurodegenerative Diseases.* **4**, 349–365 (2007).
9. Pauwels, K. *et al.* Structural basis for increased toxicity of pathologicalabeta42: abeta40 ratios in Alzheimer disease. *The Journal of biological chemistry* **287**, 5650–5660, https://doi.org/10.1074/jbc.M111.264473 (2012).
10. Rovelet-Lecrux, A. *et al.* APP locus duplication causes autosomal dominant early-onset Alzheimer disease with cerebral amyloid angiopathy. *Nature genetics* **38**, 24–26, https://doi.org/10.1038/ng1718 (2006).
11. Sleegers, K. *et al.* APP duplication is sufficient to cause early onset Alzheimer's dementia with cerebral amyloid angiopathy. *Brain: a journal of neurology* **129**, 2977–2983, https://doi.org/10.1093/brain/awl203 (2006).
12. Jonsson, T. *et al.* A mutation in APP protects against Alzheimer's disease and age-related cognitive decline. *Nature* **488**, 96–99, https://doi.org/10.1038/nature11283 (2012).
13. Braak, H. & Braak, E. Neuropathological stageing of Alzheimer-related changes. *Acta neuropathologica* **82**, 239–259 (1991).

14. Braak, H. & Braak, E. Staging of Alzheimer's disease-related neurofibrillary changes. *Neurobiology of aging* **16**, 271–278; discussion 278–284 (1995).
15. Hardy, J. A. 'anatomical cascade hypothesis' for Alzheimer's disease. *Trends in Neurosciences* **15**, 200–201 (1992).
16. Crews, L. & Masliah, E. Molecular mechanisms of neurodegeneration in Alzheimer's disease. *Human molecular genetics* **19**, R12–20, https://doi.org/10.1093/hmg/ddq160 (2010).
17. Larson, M. E. & Lesne, S. E. Soluble Abeta oligomer production and toxicity. *Journal of neurochemistry* **120**(Suppl 1), 125–139, https://doi.org/10.1111/j.1471-4159.2011.07478.x (2012).
18. Ferreira, S. T., Lourenco, M. V., Oliveira, M. M. & De Felice, F. G. Soluble amyloid-beta oligomers as synaptotoxins leading to cognitive impairment in Alzheimer's disease. *Frontiers in cellular neuroscience* **9**, 191, https://doi.org/10.3389/fncel.2015.00191 (2015).
19. Ferreira, S. T. & Klein, W. L. The Abeta oligomer hypothesis for synapse failure and memory loss in Alzheimer's disease. *Neurobiology of learning and memory* **96**, 529–543, https://doi.org/10.1016/j.nlm.2011.08.003 (2011).
20. Wilcox, K. C., Lacor, P. N., Pitt, J. & Klein, W. L. Abeta oligomer-induced synapse degeneration in Alzheimer's disease. *Cellular and molecular neurobiology* **31**, 939–948, https://doi.org/10.1007/s10571-011-9691-4 (2011).
21. Schumacher, T. N. *et al.* Identification of D-peptide ligands through mirror-image phage display. *Science* **271**, 1854–1857 (1996).
22. Wiesehan, K. *et al.* Selection of D-amino-acid peptides that bind to Alzheimer's disease amyloid peptide abeta1-42 by mirror image phage display. *Chembiochem: a European journal of chemical biology* **4**, 748–753, https://doi.org/10.1002/cbic.200300631 (2003).
23. Brener, O. *et al.* QIAD assay for quantitating a compound's efficacy in elimination of toxic Abeta oligomers. *Scientific reports* **5**, 13222, https://doi.org/10.1038/srep13222 (2015).
24. van Groen, T. *et al.* Reduction of Alzheimer's disease amyloid plaque load in transgenic mice by D3, A D-enantiomeric peptide identified by mirror image phage display. *ChemMedChem* **3**, 1848–1852, https://doi.org/10.1002/cmdc.200800273 (2008).
25. van Groen, T., Kadish, I., Wiesehan, K., Funke, S. A. & Willbold, D. *In vitro* and *in vivo* staining characteristics of small, fluorescent, Abeta42-binding D-enantiomeric peptides in transgenic AD mouse models. *ChemMedChem* **4**, 276–282, https://doi.org/10.1002/cmdc.200800289 (2009).
26. Funke, S. A. *et al.* Oral Treatment with the d-Enantiomeric Peptide D3 Improves the Pathology and Behavior of Alzheimer's Disease Transgenic Mice. *ACS chemical neuroscience* **1**, 639–648, https://doi.org/10.1021/cn100057j (2010).
27. van Groen, T., Kadish, I., Funke, A. S., Bartnik, D. & Willbold, D. Treatment with Aβ42 Binding d-Amino Acid Peptides Reduce Amyloid Deposition and Inflammation in APP/PS1 Double Transgenic Mice. *Advances in Protein Chemistry and Structural Biology* **88**, 133–152 (2012).
28. van Groen, T., Kadish, I., Funke, S. A., Bartnik, D. & Willbold, D. Treatment with D3 removes amyloid deposits, reduces inflammation, and improves cognition in aged AbetaPP/PS1 double transgenic mice. *Journal of Alzheimer's disease: JAD* **34**, 609–620, https://doi.org/10.3233/JAD-121792 (2013).
29. Klein, A. N. *et al.* Optimization of the All-D Peptide D3 for Abeta Oligomer Elimination. *PloS one* **11**, e0153035, https://doi.org/10.1371/journal.pone.0153035 (2016).
30. Ziehm, T. *et al.* Increase of Positive Net Charge and Conformational Rigidity Enhances the Efficacy of d-Enantiomeric Peptides Designed to Eliminate Cytotoxic Abeta Species. *ACS chemical neuroscience*, https://doi.org/10.1021/acschemneuro.6b00047 (2016).
31. Klein, A. N. *et al.* Optimization of D-peptides for Abeta monomer binding specificity enhances their potential to eliminate toxic Abeta oligomers. *ACS chemical neuroscience*, https://doi.org/10.1021/acschemneuro.7b00045 (2017).
32. Jiang, N. *et al.* Preclinical Pharmacokinetic Studies of the Tritium Labelled D-Enantiomeric Peptide D3 Developed for the Treatment of Alzheimer s Disease. *PloS one* **10**, e0128553, https://doi.org/10.1371/journal.pone.0128553 (2015).
33. Leithold, L. H. *et al.* Pharmacokinetic Properties of a Novel D-Peptide Developed to be Therapeutically Active Against Toxic beta-Amyloid Oligomers. *Pharmaceutical research* **33**, 328–336, https://doi.org/10.1007/s11095-015-1791-2 (2016).
34. Frenzel, D. *et al.* Immobilization of homogeneous monomeric, oligomeric and fibrillar Abeta species for reliable SPR measurements. *PloS one* **9**, e89490, https://doi.org/10.1371/journal.pone.0089490 (2014).
35. Biedler, J. L., Roffler-Tarlov, S., Schachner, M. & Freedman, L. S. Multiple neurotransmitter synthesis by human neuroblastoma cell lines and clones. *Cancer research* **38**, 3751–3757 (1978).
36. Jankowsky, J. L. *et al.* Co-expression of multiple transgenes in mouse CNS: a comparison of strategies. *Biomolecular engineering* **17**, 157–165 (2001).
37. van Groen, T., Kiliaan, A. J. & Kadish, I. Deposition of mouse amyloid beta in human APP/PS1 double and single AD model transgenic mice. *Neurobiology of disease* **23**, 653–662, https://doi.org/10.1016/j.nbd.2006.05.010 (2006).
38. Clark, R. A., Shoaib, M., Hewitt, K. N., Stanford, S. C. & Bate, S. T. A comparison of *InVivo*Stat with other statistical software packages for analysis of data generated from animal experiments. *Journal of psychopharmacology* **26**, 1136–1142, https://doi.org/10.1177/0269881111420313 (2012).
39. Briggs, R., Kennelly, S. P. & O'Neill, D. Drug treatments in Alzheimer's disease. *Clinical Medicine* **16**, 247–253 (2016).
40. Funke, A. S. *et al.* Oral treatment with the d-enantiomeric peptide D3 improves the pathology and behavior of Alzheimer's Disease transgenic mice. *ACS chemical neuroscience* **1**, 639–648, https://doi.org/10.1021/cn100057j (2010).
41. Olubiyi, O. O. *et al.* Amyloid aggregation inhibitory mechanism of arginine-rich D-peptides. *Current medicinal chemistry* **21**, 1448–1457 (2014).

Acknowledgements

Financial support of D.W. was provided by "Portfolio Technology and Medicine", the Helmholtz-Validierungsfonds of the Impuls and Vernetzungs-Fonds der Helmholtzgemeinschaft. D.W. was supported by the "Portfolio Drug Research" of the Impuls and Vernetzungs-Fonds der Helmholtzgemeinschaft. T.V.G. was partially supported by P30 NS47466.

Author Contributions

D.W., T.v.G., and I.K. designed and planned the study. SPR and ThT experiments were performed by T.Z. O.B. and L.G. designed the QIAD assay, O.B. and L.N.-S. performed the QIAD assays. M.T. conducted the MTT tests and A.E. the seeding assay. The *in vivo* study and all associated experiments were performed by T.V.G. and I.K. Statistical analysis was largely done by S.S. T.V.G., S.S. and D.W. wrote the manuscript, whereas all other authors (E.S., D.J., A.W., J.K.) reviewed and contributed to the manuscript.

Additional Information

Competing Interests: The authors declare that they have no competing interests.

Publisher's note: Springer Nature remains neutral with regard to jurisdictional claims in published maps and institutional affiliations.

3.2 Surprisingly high stability of the Aβ oligomer eliminating all-D-enantiomeric peptide D3 in media simulating the route of orally administered drugs

Elfgen A, Santiago-Schubel B, Gremer L, Kutzsche J and Willbold D

European Journal of Pharmaceutical Sciences 2017, 107: 203-207

DOI: 10.1016/j.ejps.2017.07.015

http://www.sciencedirect.com/science/article/pii/S0928098717304141?via%3Dihub

European Journal of Pharmaceutical Sciences 107 (2017) 203–207

Contents lists available at ScienceDirect

European Journal of Pharmaceutical Sciences

journal homepage: www.elsevier.com/locate/ejps

Surprisingly high stability of the Aβ oligomer eliminating all-D-enantiomeric peptide D3 in media simulating the route of orally administered drugs

Anne Elfgen[a], Beatrix Santiago-Schübel[b], Lothar Gremer[a,c], Janine Kutzsche[a], Dieter Willbold[a,c,*]

[a] Institute of Complex Systems, Structural Biochemistry (ICS-6), Research Center Jülich, 52428 Jülich, Germany
[b] Central Institute for Engineering, Electronics and Analytics (ZEA-3), Research Center Jülich, 52428 Jülich, Germany
[c] Institut für Physikalische Biologie, Heinrich-Heine-Universität Düsseldorf, 40225 Düsseldorf, Germany

ARTICLE INFO

Keywords:
Alzheimer's disease
Amyloid beta protein
All-D-enantiomeric peptide
Oral administration
Oral stability
Metabolism

ABSTRACT

The aggregation of the amyloid β protein (Aβ) plays an important role in the pathology of Alzheimer's disease. Previously, we have developed the all-D-enantiomeric peptide D3, which is able to eliminate neurotoxic Aβ oligomers *in vitro* and improve cognition in a transgenic Alzheimer's disease mouse model *in vivo* even after oral administration. D-Peptides are expected to be more resistant against enzymatic proteolysis compared to their L-enantiomeric equivalents, and indeed, a pharmacokinetic study with tritiated D3 revealed the oral bioavailability to be about 58%. To further investigate the underlying properties, we examined the stability of D3 in comparison to its corresponding all-L-enantiomeric mirror image L-D3 in media simulating the gastrointestinal tract, blood and liver. Potential metabolization was followed by reversed-phase high-performance liquid chromatography. In simulated gastric fluid, D3 remained almost completely stable (89%) within 24 h, while 70% of L-D3 was degraded within the same time period. Notably, in simulated intestinal fluid, D3 also remained stable (96%) for 24 h, whereas L-D3 was completely metabolized within seconds. In human plasma and human liver microsomes, L-D3 was metabolized several hundred times faster than D3. The remarkably high stability may explain the high oral bioavailability seen in previous studies allowing oral administration of the drug candidate. Thus, all-D-enantiomeric peptides may represent a promising new compound class for drug development.

1. Introduction

Alzheimer's disease (AD) is a progressive neurodegenerative disorder and represents 60 to 80% (Alzheimer's Association, 2016) of the currently 47 million dementia cases worldwide with continuously increasing numbers of patients (Prince et al., 2016). The aggregation of the neurotoxic amyloid β peptide (Aβ) is thought to initiate AD pathology leading to characteristic neuritic extracellular amyloid plaques, tau aggregates and loss of neurons in the brain (Hardy and Higgins, 1992; Selkoe and Hardy, 2016).

Despite intensive efforts in drug development, no preventive or curative treatment has been achieved yet (Huang and Mucke, 2012). Besides low molecular weight chemical entities, peptides consisting of L-enantiomeric amino acid residues gain increasing interest (Funke and Willbold, 2012; Sun et al., 2012). Although they offer a variety of favorable qualities like high biological activity and specificity as well as low toxicity (Lien and Lowman, 2003; Sun et al., 2012), they also have disadvantages, like almost no oral bioavailability and rapid proteolytic degradation and clearance (Adessi and Soto, 2002; Gomez-Orellana, 2005; Hamman et al., 2005; Sato et al., 2006). To overcome these disadvantages, several promising strategies were developed. One of these is the replacement of L- against D-enantiomeric amino acid residues. Previously, it has been shown that D-peptides are proteolytically more stable than L-peptides (Elmquist and Langel, 2003; Findeis et al., 1999; Miller et al., 1995; Poduslo et al., 1998; Soto et al., 1996; Tugyi et al., 2005; Wang et al., 2015; Werle and Bernkop-Schnurch, 2006) because proteases are stereoselective for L-amino acid residues (Van Regenmortel and Muller, 1998).

We have identified the all-D-enantiomeric peptide D3 by mirror image phage display against monomeric and small oligomeric Aβ(1-42) (Funke and Willbold, 2009; Schumacher et al., 1996; Wiesehan and Willbold, 2003). This lead compound consists of 12 amino acid residues each in D-enantiomeric configuration. *In vitro* assays revealed that D3 specifically eliminates Aβ oligomers (Brener et al., 2015; Funke and Willbold, 2012), which are supposed to be the most toxic Aβ species (Benilova et al., 2012; DaRocha-Souto et al., 2011; Lambert et al., 1998; Walsh et al., 2002). In studies with AD transgenic mice, D3 reduced the Aβ plaque load as well as cerebral inflammation and showed an improvement in cognition (van Groen et al., 2012; van Groen et al., 2013; van Groen et al., 2008) even after oral administration (Funke et al.,

* Corresponding author at: Institute of Complex Systems, Structural Biochemistry (ICS-6), Research Center Jülich, 52428 Jülich, Germany.
E-mail addresses: d.willbold@fz-juelich.de, dieter.willbold@hhu.de (D. Willbold).

http://dx.doi.org/10.1016/j.ejps.2017.07.015
Received 22 April 2017; Received in revised form 10 July 2017; Accepted 11 July 2017
Available online 12 July 2017

2010). A pharmacokinetic study with the tritiated peptide revealed that D3 is characterized by high oral bioavailability, long blood circulation (Jiang et al., 2015) and efficient blood brain barrier permeability (Liu et al., 2010). The high oral bioavailability is based on an efficient intestinal absorption and probably also on a high resistance against metabolization during the gastrointestinal passage.

In the current study, we investigated the resistance of the all-D-enantiomeric peptide D3 against metabolization *in vitro* in media simulating the route of orally administered drugs, like the gastrointestinal tract, blood and liver, in comparison with the corresponding all-L-enantiomeric mirror image L-D3. We followed metabolization by reversed-phase high-performance liquid chromatography (RP-HPLC).

2. Material & methods

2.1. Peptides

The D-peptide D3 (sequence: rprtrlhthrnr) consists of 12 amino acid residues each in D-configuration with its C-terminus being amidated. The mirror image of D3, L-D3, has the same amino acid sequence but with all amino acid residues in L-configuration. D3 and L-D3 have a molecular weight of approximately 1.6 kDa. The peptides were obtained from Peptides & Elephants (Potsdam, Germany).

2.2. Media simulating the gastrointestinal tract, blood and liver

Preparation of simulated gastric and intestinal fluid was performed according to the European Pharmacopoeia 7.0. Simulated gastric fluid (SGF) was prepared by acidifying distillated water with 80 mM hydrochloric acid and adding 3.2 mg/ml pepsin from porcine stomach (EC 3.4.23.1; Carl Roth, Karlsruhe, Germany; CAS: 9001-75-6, 0230.1, ≥ 0.5 units/mg Ph. Eur.). The final pH was 1. Simulated intestinal fluid (SIF) was prepared by dissolving 0.2 M potassium dihydrogen phosphate in distilled water, adjusting the pH to 6.8 with 15.4 mM sodium hydroxide and adding 10 mg/ml pancreas powder from porcine pancreas (Sigma-Aldrich, St. Louis, USA, CAS: 8049-47-6, P7545, 8 × USP). SGF sine pepsin (SGFsp) and SIF sine pancreatin (SIFsp) were prepared like SGF and SIF but without enzymes.

Plasma samples were obtained from human blood of a volunteer female donor. Blood was taken *via* a venous cannula. K_3-EDTA served as anti-coagulant. The blood sample was centrifuged at 3000*g* at 4 °C for 10 min to obtain the cell free plasma.

Pooled human liver microsomes were purchased from Sigma-Aldrich (St. Louis, USA; M0567, Lot: SLBN7300V). The liver microsomes were diluted in a NADPH regenerating system (NRS) to a final concentration of 4.8 mg/ml (20-fold excess regarding peptide concentration in mg/ml). NADPH serves as reducing agent for the enzyme family cytochrome P450 (CYP) and is therefore an essential factor for their activity. The NRS consisted of 1.3 mM $NADP^+$, 3.3 mM glucose-6-phosphate, 0.4 U/ml glucose-6-phosphate dehydrogenase and 3.3 mM magnesium chloride in 100 mM potassium phosphate buffer (pH 7.4).

2.3. Incubation of D3 and L-D3 in SGF, SIF, human blood plasma and human liver microsomes

150 µM D3 or L-D3 was incubated in SGF, SIF, human plasma and human liver microsomes in triplicate at 37 °C with slight shaking for different time periods. To prevent microbial contaminations in long-term plasma incubations, 0.1% sodium azide was added to the solutions. The incubation was stopped after different periods of time by precipitating the proteins with 3% trichloroacetic acid (*w/v*) under vortexing. The peptides were extracted from the media by centrifugation at 14,000*g* at 4 °C for 5 min. The supernatant containing the peptides was snap-frozen in liquid nitrogen immediately and stored at − 80 °C for further analysis. As reference for quantification, the peptides were transferred into the media and the incubation was stopped immediately by precipitating the proteins. Precipitated media without peptides served as controls.

2.4. Quantification of unmetabolized D3 and L-D3 by reversed-phase high-performance liquid chromatography (RP-HPLC)

Potential peptide metabolization was followed by RP-HPLC. The samples were injected on a C18 column (Agilent Technologies, Santa Clara, USA; ZORBAX 300SB-C18 5 µm, 4.6 × 250 mm). Mobile phases were acetonitrile with 0.15% trifluoroacetic acid (TFA) (*v/v*) (solvent A) and water with 0.15% TFA (*v/v*) (solvent B). The samples were measured isocratically at 10% solvent A at 25 °C with a flow rate of 1 ml/min. This run conditions allowed us to detect the smallest chemical changes and differentiate even between amidated and deamidated peptide forms, which usually elute simultaneously. Namely, D3 and L-D3 can possibly be deamidated at two sites, the C-terminus and the asparagine at position seven. Chromatograms were recorded and analyzed with the Agilent software ChemStation (G2175BA; B03.01). The peptides' peak area after direct extraction from the media was set to 100%. Peak areas of the unmetabolized peptides after different incubation times were normalized to this. Normalized peak areas of each measurement in triplicate were averaged. Data are presented as mean ± SD.

2.5. Confirmation of peptide deamidation by electrospray ionization quadrupole time-of-flight mass spectrometry (ESI-QTOF-MS)

To confirm the identity of a one-fold deamidated D3 or L-D3 metabolite observed during RP-HPLC measurements mentioned above, we collected the respective substance peak during the run. The sample was freeze-dried and subsequently dissolved and diluted in a solution composed of 85% water, 15% acetonitrile and 0.1% formic acid (*v/v/v*). ESI-QTOF-MS infusion experiments of the samples were performed on an Agilent 6250 Accurate QTOF-MS (Agilent Technologies, Santa Clara, USA) in the positive mode. For the calibration of the MS the G1969-8500 QTOF standard calibration mix from Agilent was used. While the amidated peptide has a monoisotopic mass of 1597.914 Da and would be detected in the charge of 3 with *m/z* of 533.64 Da, the one-fold deamidated peptide has a monoisotopic mass of 1598.898 Da and was detected in the charge of 3 with *m/z* of 533.98 Da.

2.6. Recording of a chromatographic metabolite profile of L-D3 in SIF

Additionally, a chromatographic metabolite profile of L-D3 in SIF was recorded by RP-HPLC. The samples were injected on a C18 column (Agilent Technologies, Santa Clara, USA; ZORBAX 300SB-C18 5 µm, 4.6 × 250 mm). Mobile phases were acetonitrile with 0.15% trifluoroacetic acid (TFA) (*v/v*) (solvent A) and water with 0.15% TFA (*v/v*) (solvent B). The samples were measured with a gradient from 0 to 30% solvent A in 30 min at 25 °C with a flow rate of 1 ml/min. Chromatograms were recorded and analyzed with the Agilent software ChemStation (G2175BA; B03.01).

3. Results

To determine whether the D-peptide D3 is more resistant against metabolization in the gastrointestinal tract, blood and liver than its mirror image L-D3, both peptides were incubated in simulated gastric and intestinal fluid (SGF and SIF) as well as in human plasma and human liver microsomes. The resistance against metabolization was quantified by RP-HPLC.

3.1. Simulated gastric fluid

In SGF, the resistance of D3 and L-D3 against degradation was monitored for up to 24 h. While the D-peptide remained almost

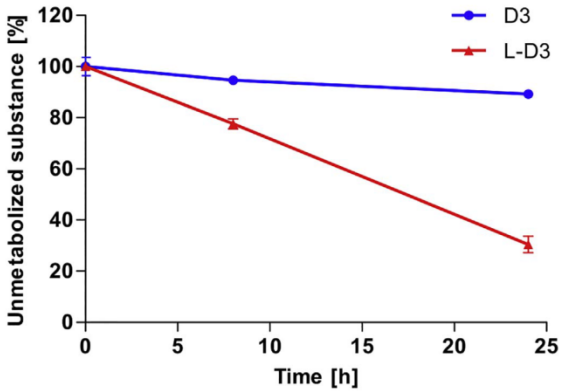

Fig. 1. Stability of D3 and L-D3 in simulated gastric fluid. D3 and L-D3 were incubated in simulated gastric fluid. D3 remained almost completely stable (89 ± 1%) for 24 h, whereas 70 ± 3% of L-D3 was metabolized within the same time. Peak areas of the unmetabolized peptides after different incubation times were normalized to the peptides' peak areas after direct extraction from SGF. Data are presented as mean ± SD (n = 3).

completely stable (89 ± 1%) within 24 h (Fig. 1), 70 ± 3% of L-D3 was metabolized during this time. A proportion of the metabolization of L-D3 accounts for deamidation at one of the two possible deamidation sites within the peptide. Up to 23 ± 2% regarding the initial L-D3 amount was one-fold deamidated within 24 h. Deamidation of L-D3 at one site, which results in a mass shift of + 0.98 Da regarding D3's mass, was additionally confirmed by ESI-QTOF-MS (data not shown). In contrast, D3 was not deamidated in SGF.

3.2. Simulated intestinal fluid

The resistance of D3 and L-D3 against metabolization was also investigated in SIF for up to 24 h. D3 remained stable during this time (96 ± 4%) (Fig. 2A). In contrast, L-D3 was completely metabolized within a few seconds. To confirm the immediate metabolization of L-D3, a chromatographic metabolite profile of L-D3's metabolites after incubation in SIF for a few seconds was recorded and compared to the profile of L-D3 incubated in SIF sine pancreatin (SIFsp) (Fig. 2B). No L-D3 but several metabolites could be detected.

3.3. Human plasma

In human plasma, the stability of D3 was monitored over a time period of 20 days, whereas the degradation of L-D3 was followed for 2 h only due to faster degradation. L-D3 was metabolized > 500 times faster than D3 (Fig. 3). In detail, 74 ± 4% of D3 was degraded within 20 days, whereas 81 ± 1% of L-D3 was already degraded within 1 h.

3.4. Human liver microsomes

Furthermore, metabolization of D3 and L-D3 was examined in human liver microsomes for 24 h and 30 min, respectively. L-D3 was almost completely degraded within 30 min (96 ± 0.3%), whereas only 30 ± 3% of D3 was metabolized within 24 h (Fig. 4A). To prove microsomal long-term activity, we incubated microsomes without peptides for up to 24 h and examined their activity by their ability to degrade L-D3, which was added after 8 and 24 h. The results show that the microsomes remained active during the whole experiment (Fig. 4B).

4. Discussion

Oral application is in general the preferred administration route of drugs because of low invasiveness, low risk of microbial contamination,

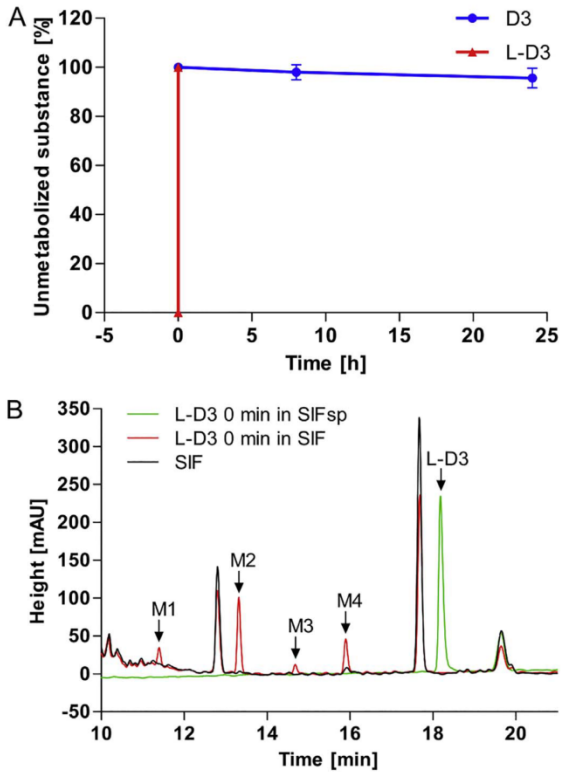

Fig. 2. Stability of D3 and L-D3 in simulated intestinal fluid. D3 and L-D3 were incubated in simulated intestinal fluid (SIF). (A) D3 remained stable for 24 h (96 ± 4%), whereas L-D3 could not be detected already after a few seconds of incubation. Peak areas of the unmetabolized peptides after different incubation times were normalized to the peptides' peak areas after direct extraction from SIF. Data are presented as mean ± SD (n = 3). (B) A chromatographic metabolite profile of L-D3 was recorded after incubation in SIF for a few seconds and was compared to the profile of L-D3 in SIF sine pancreas powder (SIFsp). L-D3 could not be detected, but several metabolites occurred (M1–4).

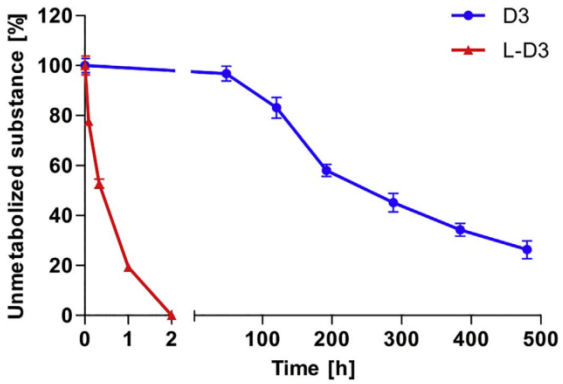

Fig. 3. Stability of D3 and L-D3 in human plasma. D3 and L-D3 were incubated in human plasma. 74 ± 4% of D3 was degraded within 20 days, whereas 81 ± 1% of L-D3 was already degraded within 1 h. Peak areas of the unmetabolized peptides after different incubation times were normalized to the peptides' peak areas after direct extraction from plasma. Data are presented as mean ± SD (n = 3).

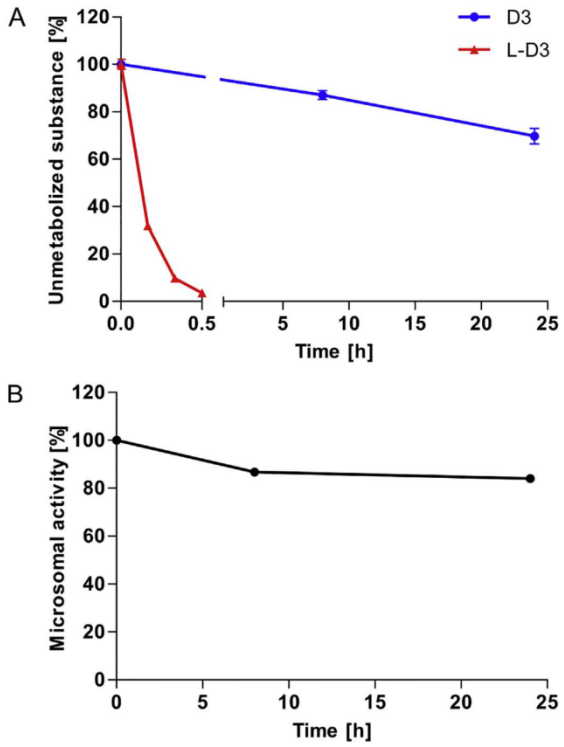

Fig. 4. Stability of D3 and L-D3 in human liver microsomes. D3 and L-D3 were incubated in human liver microsomes. (A) While 30 ± 3% of the D-peptide was metabolized within 24 h, the L-peptide was almost completely degraded within 30 min (96 ± 0.3%). (B) Microsomal activity with the NADPH regenerating system was examined for 24 h. The microsomes remained active during the whole experiment. Peak areas of the unmetabolized peptides after different incubation times were normalized to the peptides' peak areas after direct extraction from microsomes. Data are presented as mean ± SD (n = 3).

good patient compliance, cost-effectiveness and flexibility in the design of the dosage form. Especially for patients with Alzheimer's disease, it is important to have a feasible administration form for long-term application. Peptide-based drugs gain considerable interest due to their high biological activity and specificity as well as low toxicity (Lien and Lowman, 2003; Sun et al., 2012). However, a critical drawback of orally administered pharmaceuticals, especially in the case of peptide-based drugs, is their instability in the gastrointestinal tract, blood and liver (Adessi and Soto, 2002; Gomez-Orellana, 2005; Hamman et al., 2005; Sato et al., 2006). Thus, it is not surprising that it has been tried to increase the stability of peptides by the conversion of single or all L-amino acid residues against D-amino acid residues to promote a distinct enhancement of the metabolic stability in several different body fluids and tissues (Elmquist and Langel, 2003; Miller et al., 1995; Tugyi et al., 2005; Wang et al., 2015; Werle and Bernkop-Schnurch, 2006). This strategy was also applied for some D-peptides targeting Aβ (Findeis et al., 1999; Kumar and Sim, 2014; Poduslo et al., 1998; Soto et al., 1996).

Previously, we have developed the all-D-enantiomeric peptide D3, which specifically eliminates neurotoxic Aβ oligomers *in vitro* (Brener et al., 2015; Funke and Willbold, 2012), has a high oral bioavailability (Jiang et al., 2015) and is therapeutically active *in vivo* (van Groen et al., 2012; van Groen et al., 2013; van Groen et al., 2008) even after oral administration (Funke et al., 2010).

In the present study, we have analyzed the stability of D3 in comparison to its mirror image L-D3 *in vitro* in media simulating the route of orally administered drugs, like the gastrointestinal tract, blood and liver. To our knowledge, this is the first time such a rigorous comparison between two enantiomers of one amino acid sequence has been done. Especially in the gastrointestinal tract it has not been published in that detail yet.

In our study, D3 was incubated in simulated gastric and intestinal fluid for 24 h. The typical residence time of particles in the stomach is 15 min to 13 h, and in the small intestine it is 1 to 3 h depending on the particle size and if the organ is in a fasted or fed state (Dressman et al., 1998). Hence, monitoring the degradation for 24 h was more than sufficient to get an impression of D3's stability in the gastrointestinal tract. The terminal half-life of orally administered D3 in plasma has been shown to be > 24 h in a pharmacokinetic study (Jiang et al., 2015). We incubated D3 in plasma even for 20 days. The actual residence time in the liver cannot be predicted because the peptide may pass through the liver several times during the enterohepatic circulation. We decided to perform our experiments for a maximum of 24 h under monitoring of the activity of the NADPH regenerating system.

Here, we demonstrate that D3 is substantially more resistant against metabolization in simulated gastric and intestinal fluid, human plasma and human liver microsomes than its L-enantiomeric mirror image L-D3. In SGF, D3 remained almost completely stable for 24 h, whereas 70% of L-D3 was degraded within the same time. In SIF, D3 also remained stable for 24 h, while L-D3 was degraded entirely after a few seconds. In blood plasma and liver microsomes, the L-peptide was metabolized several hundred times faster than the D-peptide.

L-D3 has several potential cleavage sites for proteases contained in the gastrointestinal fluid and blood like pepsin, trypsin, chymotrypsin (Keil, 1992) and different carboxypeptidases (Christianson and Lipscomb, 1989; Folk, 1956; Lipscomb, 1970). These cleavage sites are obviously less recognized by proteases within the D-peptide. The proteases seem to be very specific for L-amino acid peptide bonds. Thus, it was not surprising that the L-peptide was degraded many times faster than the D-peptide.

The liver plays a major role in drug metabolism, especially on the first-pass metabolism after oral drug administration. Drugs entering the liver undergo phase I and phase II metabolic biotransformation. During phase I metabolism reactive and polar groups are introduced into the substrate (Guengerich, 2001). During subsequent phase II metabolism the substrate is conjugated, which favors the compound's excretion and inactivation (Jancova et al., 2010). Metabolites modified by phase I reactions are generally more pharmacologically active than phase II metabolites (U.S. Food and Drug Administration, 2008). To this end, it is crucial to investigate the drug's phase I metabolism. In this study, we used liver microsomes containing phase I enzymes, which contain the protein family cytochrome P450 (CYP) (Lu, 1976). CYP enzymes are mainly monooxygenases, which catalyze the substrate's hydroxylation (Guengerich, 2001; Lu, 1976). D3 clearly showed higher resistance against enzymatic modifications in the liver microsomes than its L-enantiomeric mirror image.

In conclusion, the high resistance against metabolization in the gastrointestinal tract guarantees high availability for absorption by the intestine and lets us assume that D3's high oral bioavailability can be explained based on its ability to pass through the gastrointestinal tract upon oral administration entirely and unmodified without protective formulation. Additionally, the high resistance against metabolization in the blood and liver may contribute to the high bioavailability and long terminal half-life of D3 in the blood as observed previously (Jiang et al., 2015). D3 has been shown to improve cognition in AD mice after oral treatment for eight weeks with roughly 30 mg/kg per day (Funke et al., 2010), which is, according to the hereby presented results, certainly attributed to its ability to pass through the gastrointestinal tract unmetabolized as well as to its high blood brain barrier permeability with a brain-plasma distribution ratio of about 0.8 (Jiang et al., 2015). Thus, all-D-enantiomeric peptides may represent a promising new class of

compounds for drug development.

Declaration of interest

The authors declare no competing financial interests.

Submission declaration and verification

The authors guarantee that the manuscript describes original work, is not under consideration for publication concurrently and has not been published elsewhere in any medium including electronic journals and computer databases of a public nature. All authors approved the manuscript and this submission.

Acknowledgment

This work was funded by the Portfolio Technology and Medicine, the Portfolio Drug Research and the “Helmholtz-Validierungsfond” of the “Impuls- und Vernetzungsfond der Helmholtzgemeinschaft” and by the Technology Transfer Department of the Forschungszentrum Jülich. The authors also acknowledge the entire research group for helpful discussions relating to this project.

References

Adessi, C., Soto, C., 2002. Converting a peptide into a drug: strategies to improve stability and bioavailability. Curr. Med. Chem. 9, 963–978.
Alzheimer's Association, 2016. 2016 Alzheimer's disease facts and figures. Alzheimers Dement. 12.
Benilova, I., Karran, E., De Strooper, B., 2012. The toxic Abeta oligomer and Alzheimer's disease: an emperor in need of clothes. Nat. Neurosci. 15, 349–357.
Brener, O., Dunkelmann, T., Gremer, L., van Groen, T., Mirecka, E.A., Kadish, I., Willuweit, A., Kutzsche, J., Jurgens, D., Rudolph, S., Tusche, M., Bongen, P., Pietruszka, J., Oesterhelt, F., Langen, K.J., Demuth, H.U., Janssen, A., Hoyer, W., Funke, S.A., Nagel-Steger, L., Willbold, D., 2015. QIAD assay for quantitating a compound's efficacy in elimination of toxic Abeta oligomers. Sci Rep 5, 13222.
Christianson, D.W., Lipscomb, W.N., 1989. Carboxypeptidase A. Acc. Chem. Res. 22, 62–69.
DaRocha-Souto, B., Scotton, T.C., Coma, M., Serrano-Pozo, A., Hashimoto, T., Sereno, L., Rodriguez, M., Sanchez, B., Hyman, B.T., Gomez-Isla, T., 2011. Brain oligomeric beta-amyloid but not total amyloid plaque burden correlates with neuronal loss and astrocyte inflammatory response in amyloid precursor protein/tau transgenic mice. J. Neuropathol. Exp. Neurol. 70, 360–376.
Dressman, J.B., Amidon, G.L., Reppas, C., Shah, V.P., 1998. Dissolution testing as a prognostic tool for oral drug absorption: immediate release dosage forms. Pharm. Res. 15, 11–22.
Elmquist, A., Langel, U., 2003. In vitro uptake and stability study of pVEC and its all-D analog. Biol. Chem. 384, 387–393.
Findeis, M.A., Musso, G.M., Arico-Muendel, C.C., Benjamin, H.W., Hundal, A.M., Lee, J.J., Chin, J., Kelley, M., Wakefield, J., Hayward, N.J., Molineaux, S.M., 1999. Modified-peptide inhibitors of amyloid beta-peptide polymerization. Biochemistry 38, 6791–6800.
Folk, J.E., 1956. A new pancreatic carboxypeptidase. J. Am. Chem. Soc. 78, 3541–3542.
Funke, A., Willbold, D., 2012. Peptides for therapy and diagnosis of Alzheimer's disease. Curr. Pharm. Des. 18, 755–767.
Funke, S.A., van Groen, T., Kadish, I., Bartnik, D., Nagel-Steger, L., Brener, O., Sehl, T., Batra-Safferling, R., Moriscot, C., Schoehn, G., Horn, A.H., Muller-Schiffmann, A., Korth, C., Sticht, H., Willbold, D., 2010. Oral treatment with the d-enantiomeric peptide D3 improves the pathology and behavior of Alzheimer's disease transgenic mice. ACS Chem. Neurosci. 1, 639–648.
Funke, S.A., Willbold, D., 2009. Mirror image phage display—a method to generate D-peptide ligands for use in diagnostic or therapeutical applications. Mol. BioSyst. 5, 783–786.
Gomez-Orellana, I., 2005. Strategies to improve oral drug availability. Expert Opin. Drug Deliv. 2, 419–433.
Guengerich, F.P., 2001. Common and uncommon cytochrome P450 reactions related to metabolism and chemical toxicity. Chem. Res. Toxicol. 14, 611–650.
Hamman, J.H., Enslin, G.M., Kotzé, A.F., 2005. Oral delivery of peptide drugs: barriers and developments. BioDrugs 19, 165–177.
Hardy, J.A., Higgins, G.A., 1992. Alzheimer's disease: the amyloid cascade hypothesis. Science 256, 184–185.
Huang, Y., Mucke, L., 2012. Alzheimer mechanisms and therapeutic strategies. Cell 148, 1204–1222.
Jancova, P., Anzenbacher, P., Anzenbacherova, E., 2010. Phase II drug metabolizing enzymes. Biomed. Pap. Med. Fac. Univ. Palacky Olomouc Czech Repub. 154, 103–116.
Jiang, N., Leithold, L.H., Post, J., Ziehm, T., Mauler, J., Gremer, L., Cremer, M., Schartmann, E., Shah, N.J., Kutzsche, J., Langen, K.J., Breitkreutz, J., Willbold, D., Willuweit, A., 2015. Preclinical pharmacokinetic studies of the tritium labelled D-enantiomeric peptide D3 developed for the treatment of Alzheimer s disease. PLoS One 10, e0128553.
Keil, B., 1992. Specificity of Proteolysis. Springer-Verlag, Berlin-Heidelberg-New York.
Kumar, J., Sim, V., 2014. D-Amino acid-based peptide inhibitors as early or preventative therapy in Alzheimer disease. Prion 8, 119–124.
Lambert, M.P., Barlow, A.K., Chromy, B.A., Edwards, C., Freed, R., Liosatos, M., Morgan, T.E., Rozovsky, I., Trommer, B., Viola, K.L., Wals, P., Zhang, C., Finch, C.E., Krafft, G.A., Klein, W.L., 1998. Diffusible, nonfibrillar ligands derived from Abeta1-42 are potent central nervous system neurotoxins. Proc. Natl. Acad. Sci. U. S. A. 95, 6448–6453.
Lien, S., Lowman, H.B., 2003. Therapeutic peptides. Trends Biotechnol. 21, 556–562.
Lipscomb, W.N., 1970. Structure and mechanism in the enzymatic activity of carboxypeptidase A and relations to chemical sequence. Acc. Chem. Res. 3, 81–89.
Liu, H., Funke, A., Willbold, D., 2010. Transport of Alzheimer disease amyloid-β-binding D-amino acid peptides across an in vitro blood–brain barrier model. Rejuvenation Res. 13, 210–213.
Lu, A.Y., 1976. Liver microsomal drug-metabolizing enzyme system: functional components and their properties. Fed. Proc. 35, 2460–2463.
Miller, S.M., Simon, R.J., Ng, S., Zuckermann, R.N., Kerr, J.M., Moos, W.H., 1995. Comparison of the proteolytic susceptibilities of homologous L-amino acid, D-amino acid, and *N*-substituted clycine peptide and peptoid oligomers. Drug Dev. Res. 35, 20–32.
Poduslo, J.F., Curran, G.L., Kumar, A., Frangione, B., Soto, C., 1998. Beta-sheet breaker peptide inhibitor of Alzheimer's amyloidogenesis with increased blood-brain barrier permeability and resistance to proteolytic degradation in plasma. J. Neurobiol. 39, 371–382.
Prince, M., Comas-Herrera, A., Knapp, M., Guerchet, M., Karagiannidou, M., 2016. World Alzheimer Report. 2016. pp. 140.
Sato, A.K., Viswanathan, M., Kent, R.B., Wood, C.R., 2006. Therapeutic peptides: technological advances driving peptides into development. Curr. Opin. Biotechnol. 17, 638–642.
Schumacher, T.N., Mayr, L.M., Minor, D.L.J., Milhollen, M.A., Burgess, M.W., Kim, P.S., 1996. Identification of D-peptide ligands through mirror-image phage display. Science 271, 1854–1857.
Selkoe, D.J., Hardy, J., 2016. The amyloid hypothesis of Alzheimer's disease at 25 years. EMBO Mol. Med. 8, 595–608.
Soto, C., Kindy, M.S., Baumann, M., Frangione, B., 1996. Inhibition of Alzheimer's amyloidosis by peptides that prevent beta-sheet conformation. Biochem. Biophys. Res. Commun. 226, 672–680.
Sun, N., Funke, S.A., Willbold, D., 2012. A survey of peptides with effective therapeutic potential in Alzheimer's disease rodent models or in human clinical studies. Mini-Rev. Med. Chem. 12, 388–398.
Tugyi, R., Uray, K., Ivan, D., Fellinger, E., Perkins, A., Hudecz, F., 2005. Partial D-amino acid substitution: improved enzymatic stability and preserved Aβ recognition of a MUC2 epitope peptide. Proc. Natl. Acad. Sci. U. S. A. 102, 413–418.
U.S. Food and Drug Administration, 2008. Guidance for industry safety testing of drug metabolites. In: U.S. Department of Health and Human Services.
van Groen, T., Kadish, I., Funke, A., Bartnik, D., Willbold, D., 2012. Treatment with Aβ42 binding D-amino acid peptides reduce amyloid deposition and inflammation in APP/PS1 double transgenic mice. Adv. Protein Chem. Struct. Biol. 88, 133–152.
van Groen, T., Kadish, I., Funke, S.A., Bartnik, D., Willbold, D., 2013. Treatment with D3 removes amyloid deposits, reduces inflammation, and improves cognition in aged AbetaPP/PS1 double transgenic mice. J. Alzheimers Dis. 34, 609–620.
van Groen, T., Wiesehan, K., Funke, S.A., Kadish, I., Nagel-Steger, L., Willbold, D., 2008. Reduction of Alzheimer's disease amyloid plaque load in transgenic mice by D3, a D-enantiomeric peptide identified by mirror image phage display. ChemMedChem 3, 1848–1852.
Van Regenmortel, M.H., Muller, S., 1998. D-Peptides as immunogens and diagnostic reagents. Curr. Opin. Biotechnol. 9, 377–382.
Walsh, D.M., Klyubin, I., Fadeeva, J.V., Cullen, W.K., Anwyl, R., Wolfe, M.S., Rowan, M.J., Selkoe, D.J., 2002. Naturally secreted oligomers of amyloid beta protein potently inhibit hippocampal long-term potentiation in vivo. Nature 416, 535–539.
Wang, J., Yadav, V., Smart, A.L., Tajiri, S., Basit, A.W., 2015. Toward oral delivery of biopharmaceuticals: an assessment of the gastrointestinal stability of 17 peptide drugs. Mol. Pharm. 12, 966–973.
Werle, M., Bernkop-Schnurch, A., 2006. Strategies to improve plasma half life time of peptide and protein drugs. Amino Acids 30, 351–367.
Wiesehan, K., Willbold, D., 2003. Mirror-image phage display: aiming at the mirror. Chembiochem 4, 811–815 (a European journal of chemical biology).

3.3 Enzymatic resistance and investigation of potential human-specific metabolites of the amyloid-β oligomer eliminating all-D-enantiomeric peptide RD2

Elfgen A, Hupert M, Bochinsky K, Tusche M, González de San Román Martin E, Gering I, Sacchi S, Pollegioni L, Huesgen PF, Hartmann R, Santiago-Schübel B, Kutzsche J and Willbold D

In Peer-Review bei Chemical Science.

Enzymatic resistance and investigation of potential human-specific metabolites of the amyloid-β oligomer eliminating all-D-enantiomeric peptide RD2

Anne Elfgen[1], Michelle Hupert[2], Kevin Bochinsky[1], Markus Tusche[1], Estibaliz González de San Román Martin[2], Ian Gering[1], Silvia Sacchi[3,4], Loredano Pollegioni[3,4], Pitter F. Huesgen[2], Rudolf Hartmann[1], Beatrix Santiago-Schübel[2], Janine Kutzsche[1], Dieter Willbold[1,5]

[1]*Institute of Complex Systems, Structural Biochemistry (ICS-6), Research Center Jülich, 52428 Jülich, Germany*

[2]*Central Institute for Engineering, Electronics and Analytics (ZEA-3), Research Center Jülich, 52428 Jülich, Germany*

[3]*Dipartimento di Biotecnologie e Scienze della Vita, Università dell'Insubria, 21100 Varese, Italy*

[4]*The Protein Factory Research Center, Università dell'Insubria and Politecnico di Milano, 20100 Milano, Italy*

[5]*Institut für Physikalische Biologie, Heinrich-Heine-Universität Düsseldorf, 40225 Düsseldorf, Germany*

Abstract

Alzheimer's disease (AD) is a neurodegenerative disorder leading to dementia. Aggregation of the amyloid-β peptide (Aβ) plays an important role in the disease, with Aβ oligomers representing the most toxic species. Previously, we have developed the Aβ oligomer eliminating therapeutic compound RD2 consisting solely of D-enantiomeric amino acid residues. RD2 has been described to have an oral bioavailability of more than 75% and to improve cognition in transgenic Alzheimer's disease mouse models after oral administration. In the present study, we further examined the stability of RD2 in simulated gastrointestinal fluids, blood plasma and liver microsomes. In addition, we have examined, whether RD2 is a substrate for the human D-amino acid oxidase (hDAAO). Furthermore, metabolite profiles of RD2 incubated in human, rodent and non-rodent liver microsomes were compared across species to search for human-specific metabolites that might possibly constitute a threat when applying the compound in humans. RD2 was remarkably resistant against metabolization in all investigated media and not converted by hDAAO. Moreover, RD2 did not influence the activity of any of the tested enzymes. In conclusion, the high stability and the absence of relevant human-specific metabolites support RD2 to be safe for oral administration in humans.

1. Introduction

Alzheimer's disease (AD) is a progressive neurodegenerative disorder and the most common form of dementia. Currently more than 20 million people worldwide are affected by AD and the number of patients increases continuously (Reitz and Mayeux 2014, Alzheimer's Association 2016). AD is an amyloid related disorder associated with misfolding and self-assembly of the amyloid-β peptide (Aβ) leading to characteristic neuritic extracellular amyloid plaques, tau aggregates and loss of neurons in the brain (Hardy and Higgins 1992, Selkoe and Hardy 2016). Although utterly important, preventive or curative treatments are not yet available (Karran et al. 2011). An attractive approach for AD drug development is the intervention in the Aβ self-assembly process (Karran et al. 2011, Funke and Willbold 2012, Sun et al. 2012). As Aβ oligomers are the most neurotoxic Aβ species currently known (Lambert et al. 1998, Walsh et al. 2002, DaRocha-Souto et al. 2011, Benilova et al. 2012), our strategy is to target and eliminate them directly (van Groen et al. 2017). We have developed the Aβ oligomer eliminating D-peptide RD2, which improved cognition of AD transgenic mice after oral treatment (Kutzsche et al. 2017). Its oral bioavailability has been described to be surprisingly high with a terminal half-life of approx. 60 h (Leithold et al. 2016). These promising results for oral application are probably based on its structure constituted solely of D-enantiomeric amino acid residues. It has previously been shown that the integration of D-amino acids into peptides enhances their proteolytic stability (Miller et al. 1995, Soto et al. 1996, Poduslo et al. 1998, Findeis et al. 1999, Elmquist and Langel 2003, Tugyi et al. 2005, Werle and Bernkop-Schnurch 2006, Wang et al. 2015). Furthermore, for RD2's lead compound D3, the superior resistance of all-D-enantiomeric peptides against metabolization by proteases and cytochrome P450 (CYP) enzymes contained in the gastrointestinal tract, blood and liver has recently been shown in a thorough study (Elfgen et al. 2017).

In this study, we determined if the advanced D-peptide RD2 is also highly resistant against metabolization by these enzymes. Moreover, we investigated possible inhibitory effects of RD2 on these enzymes, including a detailed study of CYP isoforms inhibition. Additionally, activity and inhibition tests were performed with an enzyme specialized to metabolize D-enantiomeric amino acids, the human D-amino acid oxidase (hDAAO), which is mainly expressed in kidney, liver and brain (D'Aniello et al. 1993, Ohide et al. 2011, Sacchi et al. 2012, Yamanaka et al. 2012). These experiments help to predict the availability of the unmetabolized compound after oral administration. Furthermore, it has previously been shown in preclinical toxicology studies, mandatory for the application of a phase I study in humans, that orally administered RD2 does not cause toxic effects up to high doses

(complete study will be published elsewhere). Based on these findings, metabolite profiles of RD2 incubated in human liver microsomes were compared with metabolite profiles of RD2 incubated in liver microsomes of other species to identify potential human-specific metabolites and thus to forecast the safety for administration in humans (Iverson 2016).

2. Material & Methods

2.1 Peptides

The D-peptide RD2 (sequence: ptlhthnrrrrr, CBL Patras, Patras, Greece) consists of 12 D-enantiomeric amino acid residues with its C-terminus being amidated. The mirror image of RD2, L-RD2 (sequence: PTLHTHNRRRRR, peptides & elephants, Potsdam, Germany), has the identical amino acid sequence but with all amino acid residues in L-configuration, also with its C-terminus being amidated. RD2 and L-RD2 have a molecular mass of 1.599 kDa. The peptide KLVFFRRRRRR (peptides & elephants, Potsdam, Germany) consists of 11 L-enantiomeric amino acid residues with its C-terminus being amidated. It has a molecular mass of 1.589 kDa.

2.2 Media simulating the gastrointestinal tract, blood and liver

The preparation of the media was performed as described before in Elfgen et al. (2017). Preparation of simulated gastric and intestinal fluid (SGF & SIF) was done according to the European Pharmacopoeia 7.0. Plasma samples were obtained from human blood of a volunteer female donor. Pooled human liver microsomes were purchased from Sekisui XenoTech (Kansas City, USA; H1000, Lot: 0710494 and 1210270; H1500, Lot: 1210079), from Sigma-Aldrich (St. Louis, USA; M0692, Lot: SLBL1433V; M0567, Lot: SLBR2706V and SLBN7300V) and from Gibco, Thermo Fisher Scientific (Waltham, USA; HMMCPL, Lot: PL050; HMMCPM, Lot: PL039). Pooled Sprague Dawley rat liver microsomes were purchased from Sigma-Aldrich (St. Louis, USA; M9066, Lot: SLBN0707V) and from Gibco, Thermo Fisher Scientific (Waltham, USA; RTMCPL, Lot: RT053). Pooled cynomolgus monkey liver microsomes were purchased from Gibco, Thermo Fisher Scientific (Waltham, USA; MKMCPL, Lot: MK062) and from Sekisui XenoTech (Kansas City, USA; P2000, Lot: 1210334). The liver microsomes were diluted in an NADPH regenerating system (NRS).

2.3 Incubation of peptides in different media and sample preparation for analysis

For the stability tests, 150 µM RD2 or L-RD2 was incubated in SGF, SIF, human plasma and human liver microsomes in triplicate at 37 °C with slight shaking for different time periods. To prevent microbial contaminations in long-term plasma incubations, 0.1% sodium azide was added to the solutions. Microsomal long-term activity was examined by incubating microsomes without peptide for up to 24 h and adding L-RD2 after 8 and 24 h. The ability to degrade L-RD2 served as indicator for their activity. For the comparison of RD2 metabolite profiles across species, 150 µM RD2 was incubated in human, rat and cynomolgus liver microsomes at 37 °C for 2 and 24 h. The peptides were extracted by precipitating the proteins with trichloroacetic acid (TCA) and subsequent centrifugation, as described previously in Elfgen et al. (2017). Peptides immediately extracted from the media and precipitated media without peptides served as controls.

To investigate the chemical reaction by which HSM-3 is generated, 150 µM RD2 was incubated in water with and without 30 mM formaldehyde at 37 °C for 24 h. Subsequently, the samples were treated with TCA.

The samples were analyzed by reversed phase high performance liquid chromatography (RP-HPLC) (see 2.8) or ultra high performance liquid chromatography electrospray ionization quadrupole time-of-flight mass spectrometry (UHPLC-ESI-QTOF-MS) (see 2.9).

2.4 Inhibition assay with enzymes contained in SGF, SIF, human blood plasma and human liver microsomes

To investigate whether RD2 acts as potential inhibitor for the enzymes contained in SGF, SIF, human blood plasma and human liver microsomes, an exemplary L-peptide, KLVFFRRRRRR, was incubated in these media with and without RD2 and the potential inhibition of the L-peptide's degradation was monitored. For this purpose, 150 µM of the L-peptide with or without 150 µM RD2 was incubated in SGF, SIF, human plasma and liver microsomes and both peptides were extracted from the media immediately or after 5 min (SGF, SIF) or 30 min (plasma, liver microsomes) with the method mentioned under point 2.3. Time dependent compound degradation or modification was followed by RP-HPLC (see 2.8).

Additionally, the potential of RD2 to inhibit the main cytochrome P450 (CYP) isoforms contained in human liver microsomes (CYP1A, CYP2C9, CYP2C19, CYP2D6, CYP3A4) was investigated in detail. The experiments were performed by Cyprotex. 0.1, 0.25, 1.0, 2.5, 10.0 and 25.0 µM RD2 in DMSO (final DMSO concentration: 0.25 to 0.3%) was

incubated in human liver microsomes with 1 mM NADPH in the presence of CYP isoform-specific probe substrates at 37 °C for different time periods. Selective CYP isoform inhibitors were screened alongside RD2 as a positive control. The reactions were terminated by methanol and the generated metabolites were monitored by LC-MS/MS or fluorescence. Table 1 lists the microsome concentration, the CYP isoform-specific substrate, inhibitor and the generated metabolite as well as the incubation time used in the respective assays. All assays were performed sevenfold. For CYP1A, aliquots of the termination solutions were transferred to the relevant wells of clear bottomed 96-well plates and the formation of the metabolite was monitored by fluorescence (excitation: 535 nm; emission: 595 nm). For all other substrates, the termination plates were centrifuged at 2,500 rpm and 4 °C for 30 min and aliquots of the supernatants were combined and transferred to fresh 96-well plates. Formic acid in deionized water (final concentration 0.1%) containing internal standard was added to the supernatants prior to cassette analysis by LC-MS/MS. A decrease in the formation of the metabolite compared to the vehicle control was used to calculate the IC_{50} values.

Table 1: Conditions for the different CYP isoform-specific inhibition assays

CYP isoform	Microsome concentration [mg/mL]	Specific substrate	Specific inhibitor	Incubation time [min]	Generated metabolite
CYP1A	0.25	0.5 µM ethoxyresorufin	Max. 3 µM alpha-naphthoflavone	5	resorufin
CYP2C9	1	120 µM tolbutamide	Max. 10 µM sulphaphenazole	60	4-hydroxy-tolbutamide
CYP2C19	0.5	25 µM mephenytoin	Max. 50 µM tranylcypromine	60	4-hydroxy-mephenytoin
CYP2D6	0.5	5 µM dextromethorphan	Max. 3 µM quinidine	5	dextrorphan
CYP3A4	0.1	2.5 µM midazolam	Max. 3 µM ketoconazole	5	1-hydroxy-midazolam

2.5 Enzyme assays with the human D-amino acid oxidase (hDAAO)

For hDAAO activity and inhibition assays, the tested substances were incubated with 0.17 U/mL recombinant hDAAO, 0.1 U/mL horseradish peroxidase (Roche, Switzerland) and 4 µM flavin adenine dinucleotide (FAD) in 50 mM sodium phosphate buffer (pH 7.4). 35 µM Amplex UltraRed reagent (Invitrogen, Thermo Fisher Scientific, Waltham, USA) was added and the fluorescence signal was measured after 30 min (excitation: 535 nm; emission: 590 nm) in endpoint mode. The Amplex UltraRed reagent is a fluorogenic substrate for horseradish peroxidase that reacts with the hydrogen peroxide produced by the oxidative deamination of D-amino acids to build Amplex UltroxRed, a fluorescent reaction product, which served as indicator for hDAAO activity (Terry-Lorenzo et al. 2014). All enzymatic assays were conducted at room temperature in 96-well plate format using an automated liquid-handler system (epMotion 5075; Eppendorf, Hamburg, Germany). Recombinant hDAAO was overexpressed in *E. coli* and purified as previously reported (Molla et al. 2006). The final hDAAO preparation had a specific activity of ~15 U/mg protein on D-alanine.

2.5.1 hDAAO activity assay

To investigate whether RD2 acts as substrate for hDAAO, the enzyme was incubated with 2.9 mM RD2, horseradish peroxidase and FAD for up to 6 h and the fluorescence signal of the Amplex UltroxRed reagent was measured (sample values). Positive control measurements using 0.2 mM D-alanine as substrate were performed in parallel. Additionally, negative control measurements without substrates were performed. The relative emission at 590 nm was determined by subtracting control measurements to sample values.

2.5.2 hDAAO inhibition assay

To examined whether RD2 inhibits hDAAO activity, the enzyme was incubated with 7.5 mM D-serine alone and together with 0 to 625 µM RD2 or sodium benzoate (a known hDAAO inhibitor) (Molla et al. 2006), horseradish peroxidase and FAD for 30 min and the fluorescence signal of Amplex UltroxRed was recorded. hDAAO residual activity in the presence of different concentrations of RD2 or sodium benzoate was expressed relatively to the values recorded in the absence of ligands (set as 100% activity). The data were fit to a four-parameter equation to determine the curve top, bottom, IC_{50} and Hill slope.

2.6 Cell viability assay

Rat PC12 (pheochromocytoma) cells (Leibniz Institute DSMZ, Braunschweig, Germany) were cultivated in Dulbecco's Modified Eagle Medium (DMEM) supplemented with 10% fetal bovine serum, 5% horse serum and 1% penicillin-streptomycin. 10,000 cells per well were seeded on collagen A-coated 96-well plates (Thermo Fisher Scientific, Waltham, USA) and incubated in a 95% humidified atmosphere with 5% CO_2 at 37 °C for 24 h. Samples with untreated RD2 and RD2 or HSM-3 purified from human liver microsomes (see 2.8) in 10 mM sodium phosphate buffer (pH 7.4) were prepared. Buffer without peptides and Triton X-100 (cytotoxic compound) served as controls. The samples were added to the PC12 cells in quadruple and incubated in 95% humidified atmosphere with 5% CO_2 at 37 °C for 24 h. Final concentrations were 2 µM untreated RD2, purified RD2, purified HSM-3 and 0.125% Triton X-100. Cell viability was then measured using the Cell Proliferation Kit I (MTT) (Roche, Basel, Switzerland) according to the manufacturer's instruction. The final absorbance of the formazan product was determined as the absorbance at 570 nm subtracted by the absorbance at 660 nm. All results were normalized to cells that were treated with buffer only. The experiments were performed in triplicate.

2.7 Detection of formaldehyde in liver microsomes by derivatization with 2,4-DNPH

For derivatization of formaldehyde contained in each liver microsome batch, microsome stock solutions were mixed with 42% acetonitrile and derivatized with 0.023% (*w/v*) 2,4-dinitrophenylhydrazone (2,4-DNPH) (AppliChem, Darmstadt, Germany) diluted in 100% phosphoric acid for 3 min with slight shaking. The samples were centrifuged at 10,000 *g* and 4 °C for 5 min and the supernatant containing the derivatives was immediately analyzed by RP-HPLC (see 2.8). During the entire analysis period, background measurements of 2,4-DNPH derivatives in water were performed as formaldehyde is also contained in the atmosphere.

2.8 RP-HPLC

The RP-HPLC system (Agilent Technologies, Santa Clara, USA; 1200 series) consisted of a manual injector, quaternary pump, a thermostatted column compartment and a variable wavelength detector. Chromatography was performed with a C18 column (Agilent Technologies, Santa Clara, USA; ZORBAX 300SB-C18 5 µm, 4.6 x 250 mm) at 25 °C and 214 nm with a flow rate of 1 mL/min. The sample injection volume was 20 µl.

Chromatograms were recorded and analyzed with the Agilent software ChemStation (G2175BA; B03.01).

For sample analysis from stability tests (see 2.3), mobile phases were acetonitrile (A) and water (B) each supplemented with 0.15% trifluoroacetic acid (TFA) (*v/v*). The samples were measured isocratically at 10% solvent A for 30 min. This run conditions allowed us to detect smallest chemical changes including the differentiation between the original compound and a deamidated version (Fig. S1). RD2 and L-RD2 can potentially be deamidated at two sites, the C-terminus and the asparagine at position seven. Peak areas of the unmetabolized peptides after different incubation times were normalized to the peptides' peak areas after direct extraction from the media. Normalized peak areas of each measurement in triplicate were averaged. Data are presented as mean ± SD. A chromatographic metabolite profile of L-RD2 in SIF was recorded with the same mobile phases but using a gradient from 0 to 30% solvent A in 30 min.

For analysis of the inhibition assay with enzymes contained in SGF, SIF, plasma and liver microsomes (see 2.4), RD2, KLVFFRRRRRR and remaining media components were separated using the mobile phases acetonitrile (A) and water (B) each supplemented with 0.15% TFA and a gradient from 0 to 50% solvent A in 15 min.

For the comparison of RD2 metabolite profiles across species (see 2.3), mobile phases were acetonitrile (A) and water (B) each supplemented with 0.1% TFA. The gradient ran from 0 to 100% solvent A and is described in detail in table S1. The chromatographic RD2 metabolite profiles were screened for potential human-specific metabolites. RD2 and the major RD2 metabolite present after 24 h of incubation in human liver microsome batches 7 and 8, HSM-3, were purified by RP-HPLC. Mobile phases were acetonitrile (A) and water (B) each supplemented with 0.15% TFA. The samples were separated isocratically at 10% solvent A for 30 min. RD2 as well as HSM-3 were collected and the samples were freeze-dried subsequently. The amount of the purified HSM-3 was calculated based on a calibration curve of 10 to 100 µM RD2 extracted from human liver microsomes.

The formaldehyde derivatization experiments (see 2.7) were performed with a column temperature of 28 °C and a detection wavelength of 360 nm. 3 µg/mL aldehyde- and ketone-2,4-DNPH standard (CRM47651; Sigma-Aldrich, St. Louis, USA) in 50% acetonitrile was used to establish RP-HPLC conditions for separation of the formaldehyde-2,4-DNPH derivative from other ketone and aldehyde derivatives as well as unreacted 2,4-DNPH (Table S2). Mobile phases were acetonitrile (A) and water (B).

2.9 UHPLC-ESI-QTOF-MS

The UHPLC system (Agilent Technologies, Santa Clara, USA; 1290 Infinity series) consisted of a binary pump system, an autosampler, a thermostatted column compartment and a 6250 accurate-mass QTOF-MS with an electrospray ionization (ESI) interface with a resolution of 20.000. Chromatographic separation was performed on an Acquity UPLC BEH C18 column (2.1 x 100 mm, 1.7 µm particle size; Waters, Milford, USA). Column temperature was kept at 50 °C. Flow rate was 500 µL/min. Mobile phases were acetonitrile (A) and water (B) each supplemented with 0.025% heptafluorobutyric acid (HFBA) (*v/v*) and 1% formic acid (*v/v*). Sample injection volume was 20 µL. Detection was performed with the QTOF mass detector in the ESI positive ionization mode. The mass range was set to *m/z* 100 to 1000. MassHunter software LC-MS Data Acquisition B.05.01 (Agilent Technologies, Santa Clara, CA, USA) was used to control the instrument and data acquisition.

For mass determination of a metabolite generated on incubation of L-RD2 in human liver microsomes (see 2.3), a UHPLC gradient described in table S3 was used, which allowed the separation of RD2 from one-fold deamidated RD2 and the remaining plasma components after extraction.

For determination of HSM-3's molecular mass, samples containing purified RD2 or purified HSM-3 (see 2.8) were diluted 1:50 in a solution composed of 85% water, 15% acetonitrile and 0.1% formic acid (*v/v/v*). The end-concentration of RD2 and HSM-3 was approx. 1 µM. Samples of RD2 incubated in water with and without formaldehyde (see 2.3) were also diluted 1:50 in this solution. The UHPLC gradient used is described in table S4.

2.10 ESI-FTICR-MS

To determine the accurate molecular mass and molecular formula of HSM-3, a sample containing approx. 1 mM extracted RD2 and HSM-3 each (see 2.3 for incubation and extraction conditions) was diluted 1:20 in a solution composed of 85% water, 15% acetonitrile and 0.1% formic acid (*v/v/v*) and measured with electrospray ionization Fourier transform ion cyclotron resonance mass spectrometry (ESI-FTICR-MS). Analyses were performed using a hybrid linear ion trap FTICR mass spectrometer LTQ-FT (Thermo Fisher Scientific, Waltham, USA) equipped with a 7 T superconducting magnet by infusion. The mass spectrometer was first tuned and calibrated in the positive mode following the standard optimization procedure for all voltages and settings. Mass spectra

were recorded in full scan from 200 to 1000 Da with a resolution of 100.000 at *m/z* 400. All data were processed using the Xcalibur software version 2.1.

2.11 MALDI-MS

To test whether HSM-3 contains a free primary or secondary amine, a sample containing purified HSM-3 and RD2 (see 2.8) as well as a sample with purified HSM-3 and RD2 incubated with 20 mM sodium cyanoborohydride ($NaBH_3CN$) and 20 mM ^{13}C- and D-labeled formaldehyde ($^{13}CD_2O$) at 37 °C for 3 h were analyzed by matrix-assisted laser desorption/ionization mass spectrometry (MALDI-MS). For this purpose, 1 µL of the samples was mixed with 9 µL 5 mg/mL α-cyano-4-hydroxycinnamic acid (CHCA) matrix in 50% acetonitrile with 0.1% TFA. 1 µL of this solution was spotted onto a stainless steel MALDI target (Thermo Fisher Scientific, Waltham, USA) and air-dried. Analysis was performed using a LTQ-Orbitrap XL hybrid mass spectrometer (Thermo Fisher Scientific, Waltham, USA) equipped with MALDI source (Thermo Fisher Scientific, Waltham, USA). The instrument was externally calibrated using commercial peptide standard mixtures (ProteoMass calibration kit, Sigma Aldrich, St. Louis, USA). Data were acquired in positive ion mode using the Xcalibur software v2.3 (Thermo Fisher Scientific, Waltham, USA) in a mass range from *m/z* 800 to *m/z* 2000.

2.12 NMR spectroscopy

Approx. 30 µg purified RD2 and 60 µg purified HSM-3 (see 2.8) were separately dissolved in 200 µl D_2O corresponding to a sample concentration of approx. 95 µM and 190 µM, respectively. All nuclear magnetic resonance (NMR) experiments were performed at 25 °C on a Bruker AVANCE III 750 MHz spectrometer equipped with a 5 mm triple-resonance (^1H-^{13}C/^{15}N-D) TCI-cryoprobe with shielded z-gradient using 3 mm NMR-tubes. ^1H and ^{13}C resonance assignment of RD2 and the structure elucidation of the metabolite HSM-3 was achieved by two-dimensional experiments using the standard Bruker pulse-sequences HH-TOCSY, HH-ROESY, HC-HSQC and HC-HMBC.

3. Results

3.1 RD2 is remarkably resistant against enzymatic metabolization in media simulating the gastrointestinal tract, blood and liver

To investigate RD2's resistance against enzymatic degradation, RD2 was incubated in media simulating the gastrointestinal tract, blood and liver and the unmetabolized peptide was quantified by RP-HPLC. RD2's L-enantiomeric mirror image, L-RD2, served as comparative substance.

In simulated gastric and intestinal fluid (SGF and SIF), RD2 remained stable (≥ 97 ± 2.2%) for 24 h (Fig. 1 A & B). In contrast, L-RD2 was degraded by 23 ± 3.5% within the same time in SGF and was even completely metabolized within a few seconds in SIF. To confirm that L-RD2 is immediately metabolized in SIF, a chromatographic metabolite profile was recorded after incubation in SIF for a few seconds (Fig. S2).

In human plasma, L-RD2 was metabolized more than 90 times faster than RD2 (Fig. 1 C). In detail, 87 ± 2.9% of RD2 was degraded within 20 days, while 92 ± 3.5% of L-RD2 was already degraded within one day.

In human liver microsomes, only 33 ± 2.7% of RD2 was metabolized within 24 h, while L-RD2 was almost completely degraded within 30 min (87 ± 0.5%), (Fig. 1 D). A proportion of L-RD2 was increasingly metabolized to the one-fold deamidated species at one of the two possible deamidation sites within the peptide, as determined by UHPLC-ESI-QTOF-MS (Fig. S3). L-RD2 showed a mass at *m/z* of 533.6471^{3+}, which is consistent with the predicted *m/z* of the three-charged ion of L-RD2 and corresponds to a monoisotopic mass of 1597.931 Da. The one-fold deamidated peptide was detected with a mass at *m/z* of 533.9752^{3+} corresponding to a monoisotopic mass of 1598.898 Da and the expected mass shift of +1 Da versus the amidated form. In contrast to L-RD2, RD2 was not deamidated in human liver microsomes. Microsomal activity was ensured during the whole experiment (Fig. S4).

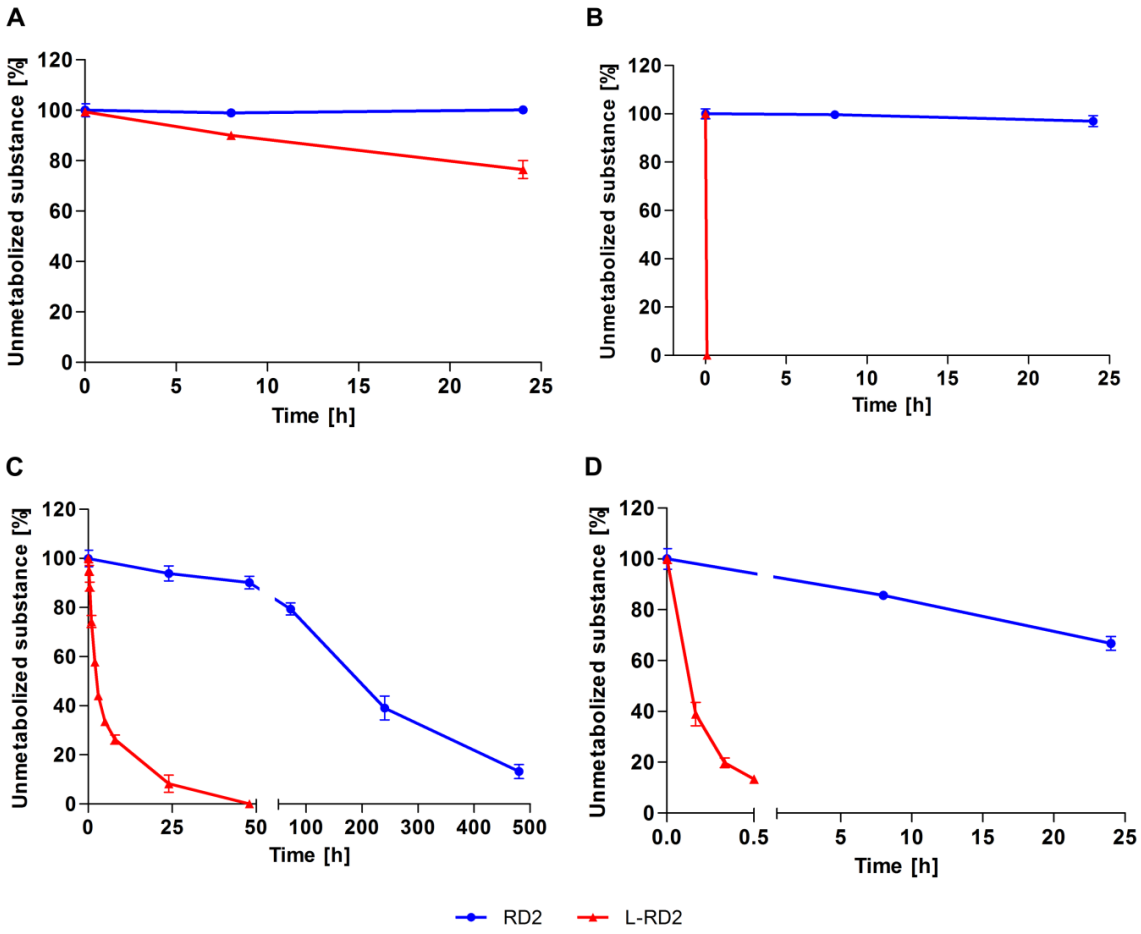

Figure 1: Stability of RD2 and L-RD2 in SGF, SIF, human plasma and human liver microsomes. RD2 and L-RD2 were incubated in SGF, SIF, human plasma and human liver microsomes. In SGF **(A)** and SIF **(B)**, RD2 remained stable for 24 h. In contrast, L-RD2 was degraded by 23 ± 3.5% within the same time in SGF and was even completely metabolized within a few seconds in SIF. Human plasma **(C)** and human liver microsomes **(D)** metabolized L-RD2 several hundred times faster than RD2. Peak areas of the unmetabolized peptides after different incubation times were normalized to the peptides' peak areas after direct extraction from the media. Data are presented as mean ± SD (n = 3).

3.2 RD2 does not inhibit proteases or CYP enzymes involved in peptide metabolization

To investigate whether the high long-term stability of RD2 in SGF, SIF, human plasma and human liver microsomes is due to its ability to act as an inhibitor of one or more enzymatic activities, the influence of RD2 on the degradation of an L-peptide (KLVFFRRRRRR) was examined. The results showed that the degradation of the L-peptide was not influenced by co-incubation with RD2 in any media (Fig. 2). As proof for the rapid degradation of the L-peptide in SIF and not a failure of the extraction method, a metabolite profile of directly extracted L-peptide from SIF with and without enzymes was recorded (Fig. S5).

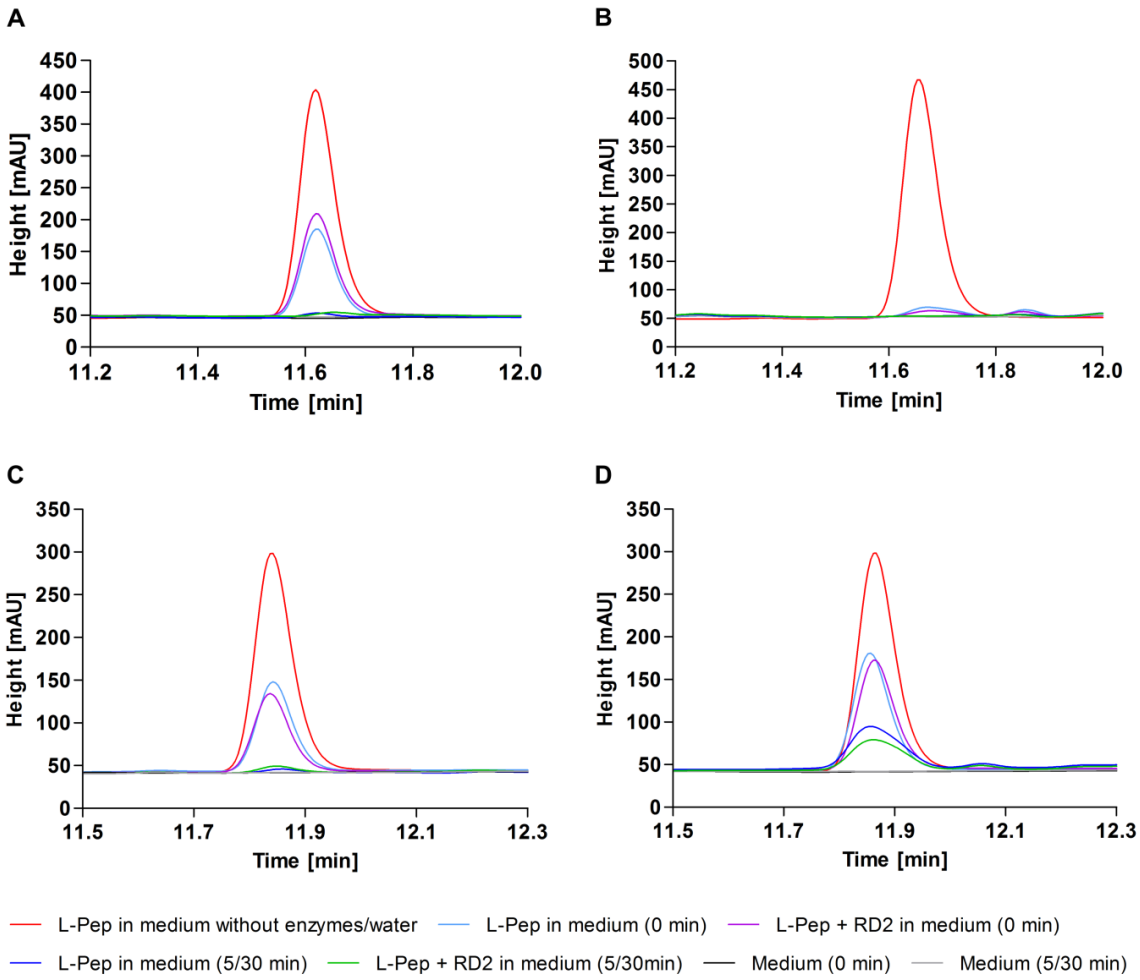

Figure 2: RD2 as potential inhibitor of enzymes contained in SGF, SIF, plasma and liver microsomes. Potential inhibition of the degradation of the L-peptide KLVFFRRRRRR (L-Pep) by RD2 was investigated in SGF **(A)**, SIF **(B)**, human plasma **(C)** and human liver microsomes **(D)** after immediate extraction and incubation for 5 min (SGF, SIF) or 30 min (plasma, liver microsomes). The L-peptide in SGF and SIF without enzymes or in water as well as SGF, SIF, plasma and liver microsomes without peptides served as controls. RD2 did not influence the degradation of the L-peptide in any of the media.

Moreover, we looked into detail at the potential of RD2 to inhibit the main CYP isoforms contained in human liver microsomes (CYP1A, CYP2C9, CYP2C19, CYP2D6, CYP3A4) using isoform-specific probe substrates and monitoring generated specific metabolites. Selective CYP isoform inhibitors were screened alongside RD2 as a positive control. RD2 did not inhibit any of the five CYP isoforms over the concentration range tested (0 to 25 µM) (Table S5). All of the specific inhibitors behaved as expected in the assays (Table S6) (Bourrie et al. 1996, Taavitsainen et al. 2001).

3.3 RD2 is not a substrate or inhibitor for the human D-amino acid oxidase (hDAAO)

First, it was investigated whether RD2 acts as substrate for hDAAO. For this purpose, the enzyme was incubated with 2.9 mM RD2 for up to 6 h and its activity was detected by means of a sensitive, fluorogenic reagent. No change in fluorescence emission was detected in this condition (Fig. 3 A). Control measurements using 0.2 mM D-alanine as substrate were performed in parallel as a positive control. In this case, the recorded emission at 590 nm increased to 61125 ± 2120 AU upon a 2 h incubation (Fig. 3 A). These observations indicate that RD2 does not act as a substrate for hDAAO.

Additionally, we examined whether RD2 acts as a hDAAO inhibitor. The enzyme was incubated with 7.5 mM D-serine alone or in the presence of RD2 or sodium benzoate (a known hDAAO inhibitor (Molla et al. 2006)) in concentrations of up to 625 µM. Enzyme activity was detected by means of a sensitive, fluorogenic reagent. While hDAAO was expectedly inactivated by sodium benzoate (a 92.8 ± 0.1% decrease in the activity was determined at 625 µM sodium benzoate with an estimated IC_{50} of 7.07 µM), RD2 only slightly affected hDAAO activity (which appeared to be decreased by 9.3 ± 2.1% at 625 µM RD2) (Fig. 3 B). Thus, RD2 does not act as an effective hDAAO inhibitor.

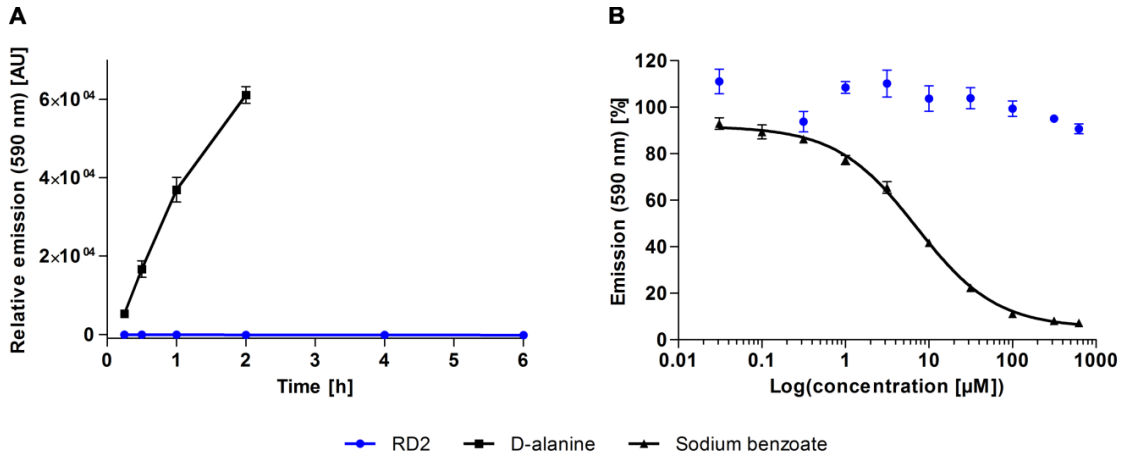

Figure 3: RD2 as potential substrate or inhibitor for hDAAO. The emission of a sensitive, fluorogenic reagent at 590 nm was monitored as indication for enzymatic activity. **A)** hDAAO was incubated with RD2 or D-alanine. No change in relative emission was detected within 6 h of incubation with RD2, while a substantial increase was observed upon incubation with D-alanine within 2 h. AU: arbitrary unit. **B)** hDAAO was incubated with D-serine alone or together with RD2 or sodium benzoate, a known hDAAO inhibitor. hDAAO activity was decreased by 92.8 ± 0.1% on incubation with 625 µM sodium benzoate, while the same concentration of RD2 only slightly affected the enzyme activity (decrease by 9.3 ± 2.1%). The IC_{50} of sodium benzoate was determined as 7.07 µM with a four-parameter fit.

3.4 Identification of potential human-specific RD2 metabolites from liver microsomes

As preclinical toxicology studies with rat and cynomolguses showed that orally administered RD2 does not cause toxic effects up to high doses (complete study will be published elsewhere), RD2 was incubated *in vitro* in human (n = 8), rat (n = 2) and cynomolgus (n = 2) liver microsomes for 0, 2 and 24 h and chromatographic metabolite profiles were recorded to search for potential human-specific metabolites and hence to predict the safety for administration in humans. In six of the eight human liver microsome batches, RD2 was metabolized only slightly (human samples 1 - 6), while two of them showed a remarkably higher extent of RD2 metabolization (human samples 7 & 8).

After 2 h of incubation, which is usually the maximum incubation time for more unstable substances (Wu and McKown 2004, Jia and Liu 2007), RD2 appeared to be unmetabolized in the human samples 1 - 6 and in all rat and cynomolgus samples. To promote the metabolic degradation and increase the chance of detecting emerging metabolites, RD2 was incubated for 24 h. After extension of the incubation time, the intensity of the RD2 peak was decreased by 21 ± 7% in the human samples 1 - 6, by 17 ± 4% in the rat samples and by 9 ± 2% in the cynomolgus samples (Fig. 4). In all samples, the same small metabolite emerged after 24 h, whose peak area represented less than 2% of the parent compound at time point zero (incubated for only a few seconds) (Fig. 4). Consequently, this metabolite was not human-specific. Only in batch no. 5, two minor potentially human-specific metabolites (HSM-1 & HSM-2) were generated. These metabolites represented only 3 to 5% of the parent compound (Fig. 5 A) and were thus irrelevant according to FDA guidelines (U.S. Food and Drug Administration 2008).

In the human samples 7 & 8, the RD2 peak was already slightly reduced after 2 h of incubation and a minor potentially human-specific metabolite (HSM-3) of 1 or 5% relative to the parent compound could be detected (Fig. S6). After 24 h of incubation, RD2 was metabolized by 48 or 69% and the same metabolite was detected representing 31 or 52% of the parent compound (Fig. 5 B). This metabolite was not detected, neither in the other six human samples, nor in the rat and the cynomolgus samples, as verified by LC-MS.

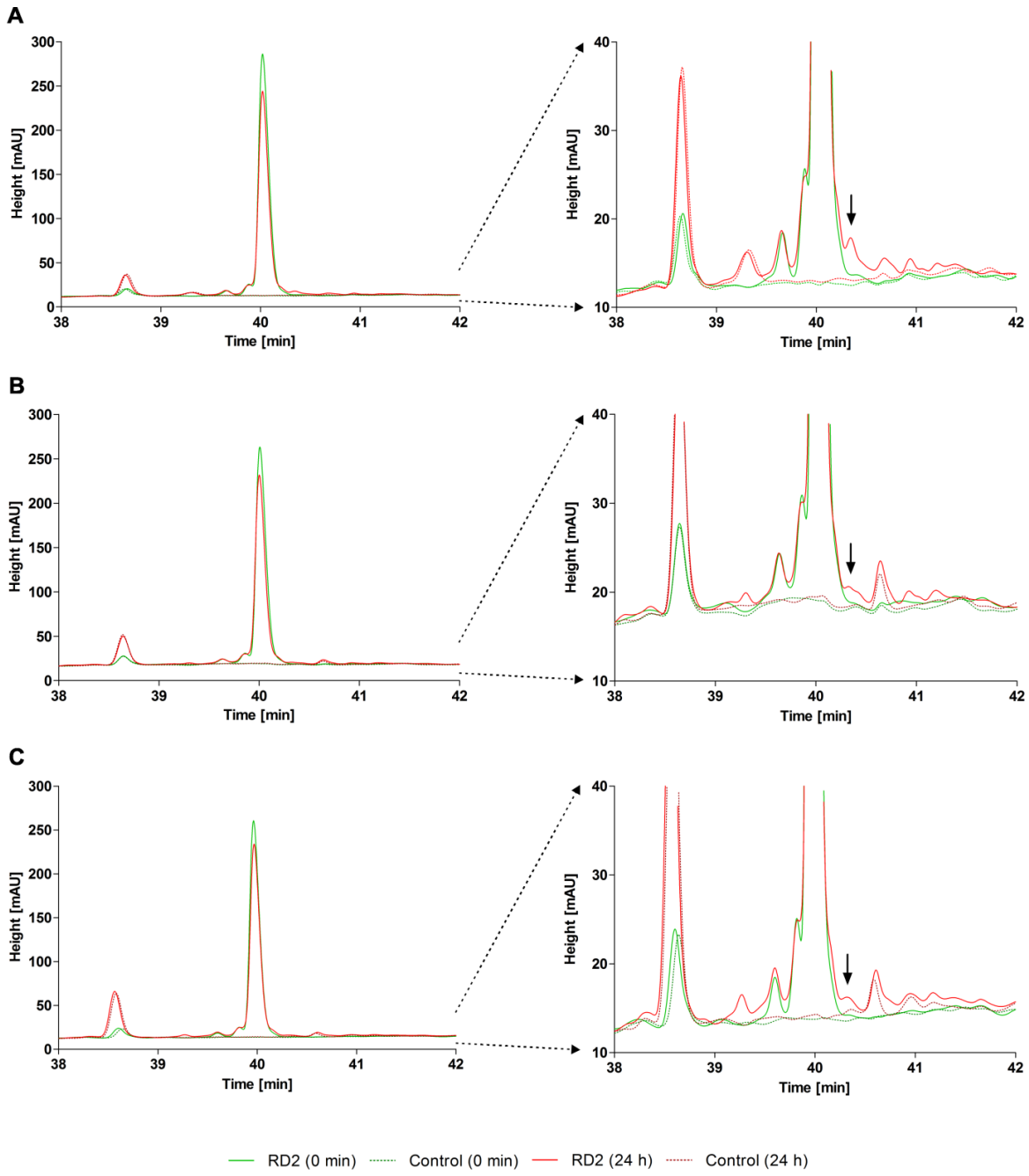

Figure 4: Metabolite profiles of RD2 incubated in human, rat and cynomolgus liver microsomes showing non-human-specific metabolites. RD2 was incubated in human, rat and cynomolgus liver microsomes for 0 and 24 h and chromatograms were recorded to search for potential human-specific metabolites. Incubated liver microsomes without RD2 served as controls. Only the relevant parts of the chromatogram are shown. Left: section of the chromatogram including the RD2 peak. Right: amplified section of the y-axis to focus on small metabolite peaks. In the human samples, only one metabolite with a peak area of less than 2% in comparison to the parent compound peak area appeared **(A)**. This metabolite (see arrows) was also present in rat **(B)** and cynomolgus **(C)** samples.

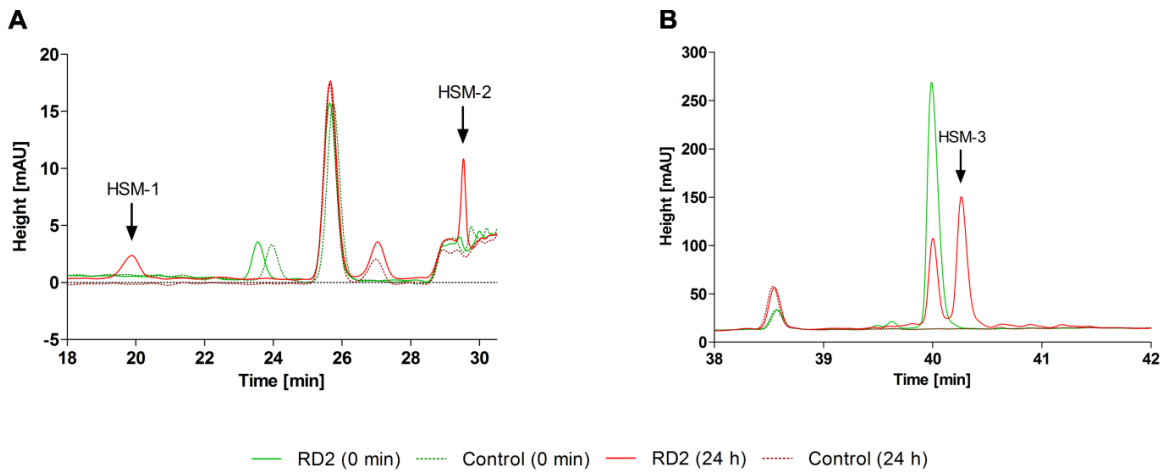

Figure 5: Metabolite profiles of RD2 incubated in human liver microsomes showing potential human-specific metabolites. RD2 was incubated in human, rat and cynomolgus liver microsomes for 0 and 24 h and chromatograms were recorded. Incubated liver microsomes without RD2 served as controls. Only the relevant parts of the chromatograms from the human samples are shown. Two minor potentially human-specific metabolites (HSM-1 & HSM-2) appeared in batch no. 5, which represented 3 to 5% of the parent compound **(A)**. One major potentially human-specific metabolite (HSM-3), only detected in the human samples 7 & 8, represented 31 or 52% of the parent compound **(B)**.

3.5 HSM-3 results from formaldehyde contamination and is not cytotoxic

The major potentially human-specific RD2 metabolite found upon incubation in liver microsomes, HSM-3, (Fig. 5 B) was identified by UHPLC-ESI-QTOF-MS, ESI-FTICR-MS, MALDI-MS and NMR spectroscopy and a toxicity test was performed.

Samples containing the purified RD2 or the purified HSM-3 were analyzed with UHPLC-ESI-QTOF-MS. RD2 showed a mass at *m/z* of 533.6482^{3+}, which is consistent with the predicted *m/z* of the three-charged ion of RD2 and corresponds to a monoisotopic mass of 1597.931 Da (Fig. S7). HSM-3 showed a mass at *m/z* of 537.6485^{3+}. This corresponds to a monoisotopic mass of 1609.933 Da. Consequentely, HSM-3 has a mass shift of +12 Da versus RD2.

Determination of the molecular formula of HSM-3 was performed with ESI-FTICR-MS. This measurement enables the calculation of corresponding molecular formulae based on accurate mass determination. A sample containing extracted but not purified RD2 and HSM-3 was analyzed. The measured mass of RD2 at *m/z* of 533.64914^{3+} could be attributed to the molecular composition of $[\mathbf{C_{65}}H_{118}O_{15}N_{33}]^{3+}$ with a deviation of 0.59 ppm (Fig. 6). For HSM-3, an accurate mass at *m/z* of 537.64915^{3+} was determined and assigned to the corresponding molecular formula of $[\mathbf{C_{66}}H_{118}O_{15}N_{33}]^{3+}$ with a deviation of 0.49 ppm. No other reasonable molecular formulae within the specified range

(deviation < 2 ppm) were found. From this it can be concluded that the difference of 12 Da between RD2 and the metabolite HSM-3 resulted in the net addition of one carbon atom.

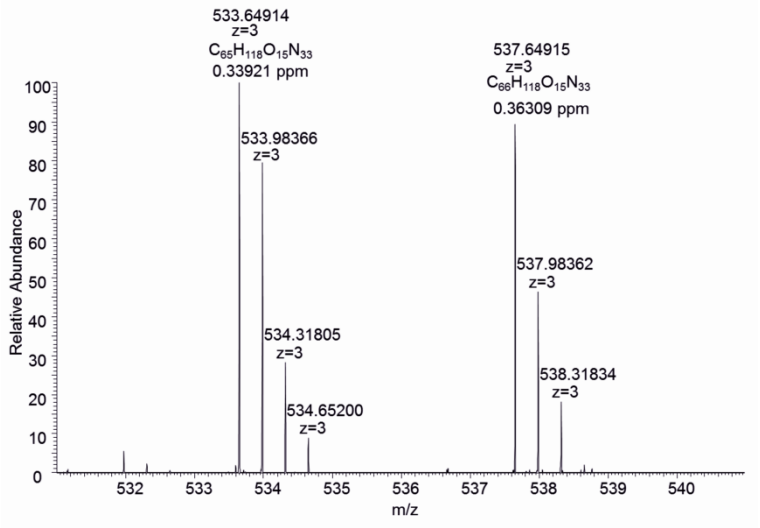

Figure 6: ESI-FTICR-MS analysis of RD2 and HSM-3. RD2 has a mass at *m/z* of 533.64914^{3+} and a molecular furmula of $[C_{65}H_{118}O_{15}N_{33}]^{3+}$. HSM-3 has a mass at *m/z* of 537.64915^{3+} and a molecular formula of $[C_{66}H_{118}O_{15}N_{33}]^{3+}$.

To determine the structural difference between RD2 and HSM-3, HH-TOCSY and HC-HSQC spectra were measured from each compound and signal assignment was done for protons and carbons (Table S7). By comparing the chemical shifts from both compounds, it was obvious that the proline ring was metabolized. The proline α-proton of HSM-3 shifted by 0.6 ppm upfield and the chemical shift difference from the δ-protons spread up to 0.4 ppm. The HH-ROESY spectrum of HSM-3 showed correlation signals from an additional CH_2-group (δ_H 4.45 ppm, 4.35 ppm) to the α- and δ-protons of the proline ring and to the β-proton of the neighboring threonine. To validate these correlations, a HC-HMBC experiment was measured. Proton correlation signals from the additional CH_2-group to the Cα- (64.65 ppm), Cδ- (55.00 ppm) and C=O (177.60 ppm) proline carbons and also correlations from the threonine-Hα to the CH_2-carbon (δ_c 67.51 ppm) were visible. The chemical shift information together with the correlation experiments confirmed a methylene bridge between the free amino group of the N-terminal proline and the nitrogen of the peptide bond to the second amino acid residue threonine generating a 4-imidazolidinone ring. Figure 7 shows the chemical structure of the N-terminal modification of HSM-3.

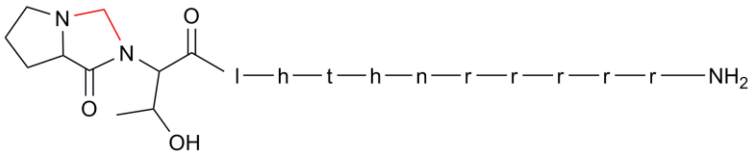

Figure 7: Chemical structure of the N-terminal modification of HSM-3. In comparison to RD2, HSM-3 contains an additional methylene bridge between the secondary amine of proline and the nitrogen of the peptide bond to threonine (red) generating a 4-imidazolidinone ring.

The modification of RD2's N-terminus detected by NMR spectroscopy was confirmed by high resolution MALDI-MS experiments. Reductive methylation of RD2 ($[M+H]^+$ 1598.933) and HSM-3 ($[M+H]^+$ 1610.933) with ^{13}C- and D-labeled formaldehyde ($^{13}CD_2O$) and sodium cyanoborohydride resulted in a conversion of RD2 to a $^{13}CD_2H$-methylated form with a mass shift of +17.033, whereas the HSM-3 peak remained unchanged (Fig. S8). This indicates that the N-terminal proline residue of RD2 is modified in HSM-3 and no longer a secondary amine. Moreover, this also indicates that the modification in HSM-3 is not a Schiff base.

The addition of only one carbon atom may be indicative of a formaldehyde reaction (Metz et al. 2004). To test our theory, RD2 was incubated for 24 h with or without 30 mM formaldehyde in water and the samples were analyzed by UHPLC-ESI-QTOF-MS. Indeed, on incubation without formaldehyde, only RD2 could be detected, whereas on incubation with formaldehyde, HSM-3 was generated (Fig. S9). Furthermore, it could be proven by 2,4-DNPH derivatization experiments with subsequent HPLC analysis that liver microsome batches generating the metabolite contained formaldehyde, whereas microsome batches not generating the metabolite did not or substantially less (Table S8).

Although it was clear that HSM-3 was only formed due to formaldehyde contamination of two of the eight human liver microsome batches, we have investigated its cytotoxic potential in an MTT cell viability assay with rat PC12 cells. 2 µM RD2 or HSM-3 purified from human liver microsomes as well as untreated RD2, which served as control for the purification step, were added to the cells and cell viability was analyzed after 24 h. Buffer without peptides and Triton X-100 (cytotoxic compound) served as controls. Neither HSM-3 (98.8 ± 2.7% cell viability) nor untreated RD2 (99.2 ± 3.5% cell viability) or the purified RD2 (93.4 ± 5.5% cell viability) showed any cell toxicity (Fig. 8). In the presence of 0.125% Triton X-100, the cell viability was reduced to 14.4 ± 1.2%.

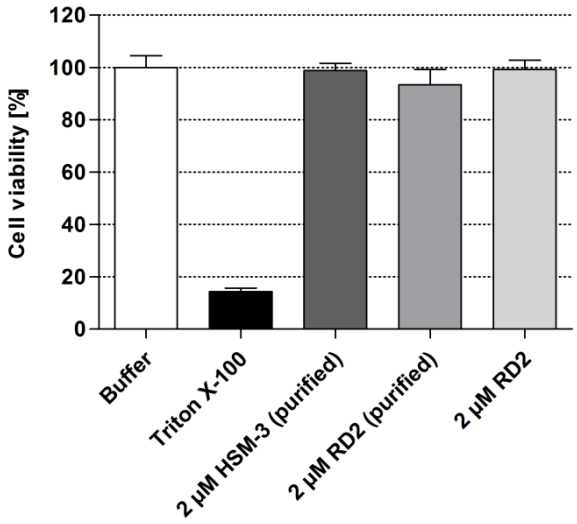

Figure 8: Cell viability test with HSM-3 and RD2. An MTT cell viability test with HSM-3 and RD2 purified from human liver microsomes as well as the untreated RD2 on rat PC12 cells was performed. Neither 2 µM HSM-3 nor the untreated or the purified RD2 showed any cell toxicity. A cytotoxic concentration of Triton X-100 (0.125%) was used as control.

Furthermore, high resolution MALDI-MS and UHPLC-ESI-QTOF-MS analysis of a sample of purified HSM-3 stored in solution at low temperatures revealed the presence not only of HSM-3 but also of RD2. This indicates that HSM-3 was instable and reacted back to RD2.

4. Discussion

Planning oral administration of a compound implies preliminary stability testing particularly in the gastrointestinal tract as well as in blood and liver. Although compounds are increasingly metabolized upon oral administration compared to any other administration route, like intravenous or subcutaneous injection, oral administration is still the preferred administration route as it offers several advantages like low invasiveness, good patient compliance and comparatively low costs.

In this study, we demonstrate that the all-D-enantiomeric peptide RD2 is suitable for oral application as it is remarkably resistant against metabolization in simulated gastric and intestinal fluid (SGF & SIF), human plasma and human liver microsomes. Although RD2 and L-RD2 have several potential cleavage sites for proteases contained in these media (Folk 1956, Christianson and Lipscomb 1989, Keil 1992, Lipscomb 1970), the D-amino acid peptide bonds are less recognized. Hence, one could assume that orally administered RD2 would pass the gastrointestinal tract unmetabolized without protective

formulation. This could also partially explain RD2's long terminal half-life in blood observed previously (Leithold et al. 2016).

Furthermore, we demonstrate that RD2 is not a substrate for the human D-amino acid oxidase, an enzyme expressed in kidney, liver and brain specialized to metabolize D-amino acids (D'Aniello et al. 1993, Ohide et al. 2011, Sacchi et al. 2012, Yamanaka et al. 2012).

Additional experiments to investigate RD2's potential to inhibit enzymes contained in the investigated media were performed, as compounds that inhibit these enzymes may cause a toxic accumulation of other substrates. Here, we demonstrate that RD2 does not act as inhibitor neither for the DAAO nor for any of the peptide metabolizing enzymes contained in SGF, SIF, plasma or liver microsomes.

As the liver plays a major role in oral drug metabolism, it is clearly mandatory to examine the compound's safety by screening for possible metabolites generated in the liver. Metabolites generated from metabolic biotransformation processes of phase I need particular safety evaluation. For *in vitro* assessment, usually liver microsomes are used containing phase I enzymes like the protein family cytochrome P450 (Lu 1976). To assess reasonable expectations concerning metabolite induced adverse side effects in humans treated with RD2, chromatographic metabolite profiles of RD2 incubated in human, rat and cynomolgus liver microsomes were compared. We investigated the compound's metabolism in eight different human liver microsome batches and in two different rat or cynomolgus liver microsome batches each, obtained from three different vendors in total to reveal inter-batch differences. After 24 h of incubation, three potentially human-specific metabolites were found. The two minor metabolites HSM-1 and HSM-2, found in only one of the human liver microsome batches, represented 3 to 5% of the parent compound. Additionally, the major metabolite HSM-3 present in two of the human liver microsome batches represented 31 to 52% of the parent compound. According to current guidance (U.S. Food and Drug Administration 2008), we did not consider HSM-1 and HSM-2 for safety assessment but characterized HSM-3 in detail. HSM-3 was identified as RD2 with the insertion of a methylene bridge between the secondary amine of proline at position 1 and the nitrogen of the peptide bond to threonine at position 2. As described analogously in the literature (Mathews et al. 1989, Heck et al. 2001, Metz et al. 2004) the 4-imidazolidinone ring with a mass increment of 12 Da was also formed by means of a Schiff-base intermediate after adding formaldehyde to RD2 in water. As liver microsome batches generating HSM-3 were shown to contain substantially more formaldehyde than batches not generating the metabolite, we concluded that HSM-3 is generated by reaction

with formaldehyde from contaminated microsome preparations. Moreover, the metabolite was non-toxic and instable and reacted back to the unmodified RD2, a process also described previously (Rasmussen and Bundgaard 1991).

The inter-batch differences including the identification of batches with formaldehyde contaminations revealed in the present metabolite study emphasize the importance of carefully investigating differences in metabolite formation in various liver microsomes batches.

Conclusion

In summary, we developed an all-D-enantiomeric peptide, which is a promising drug candidate for the oral treatment of Alzheimer's disease as it is therapeutically active *in vivo* after oral administration (Kutzsche et al. 2017, van Groen et al. 2017), has a high oral bioavailability (Leithold et al. 2016) and is highly resistant against metabolization in the gastrointestinal tract, blood and liver as well as metabolization by the hDAAO. This guarantees a high availability for absorption by the intestine even without protective formulation, increases the systemic availability, presumably contributes to the long terminal half-life of RD2 in the blood described previously (Leithold et al. 2016) and prolongs the duration of effectiveness. A high stability is advantageous as it is also accompanied by a low rate of metabolite generation and allows for a safe oral administration of the drug candidate.

Acknowledgment

This work was funded by the Portfolio Technology and Medicine, the Portfolio Drug Research and the "Helmholtz-Validierungsfond" of the "Impuls- und Vernetzungsfond der Helmholtzgemeinschaft" and by the Technology Transfer Department of the Forschungszentrum Jülich. The authors acknowledge the "Institut für Biochemie und Molekularbiologie" of the "Rheinische Friedrich-Wilhelms-Universität Bonn" for their supporting mass spectrometric experiments and thank the entire research group of the ICS-6, especially Dr. Christian Zafiu, for helpful discussions relating to this project.

References

Alzheimer's Association (2016). "2016 Alzheimer's Disease Facts and Figures". *Alzheimer's & Dementia* 12(4)

Benilova I, Karran E and De Strooper B (2012). "The toxic Abeta oligomer and Alzheimer's disease: an emperor in need of clothes". *Nat Neurosci* 15(3): 349-357

Bourrie M, Meunier V, Berger Y and Fabre G (1996). "Cytochrome P450 isoform inhibitors as a tool for the investigation of metabolic reactions catalyzed by human liver microsomes". *J Pharmacol Exp Ther* 277(1): 321-332

Christianson DW and Lipscomb WN (1989). "Carboxypeptidase A". *Acc. Chem. Res.* 22: 62-69

D'Aniello A, D'Onofrio G, Pischetola M, D'Aniello G, Vetere A, Petrucelli L and Fisher GH (1993). "Biological Role of D-Amino Acid Oxidase and D-Aspartate Oxidase. Effects of D-amino acids.". *J Biol Chem* 268(36): 26941-26949

DaRocha-Souto B, Scotton TC, Coma M, Serrano-Pozo A, Hashimoto T, Sereno L, Rodriguez M, Sanchez B, Hyman BT and Gomez-Isla T (2011). "Brain oligomeric beta-amyloid but not total amyloid plaque burden correlates with neuronal loss and astrocyte inflammatory response in amyloid precursor protein/tau transgenic mice". *J. Neuropathol. Exp. Neurol.* 70(5): 360-376

Elfgen A, Santiago-Schubel B, Gremer L, Kutzsche J and Willbold D (2017). "Surprisingly high stability of the Abeta oligomer eliminating all-d-enantiomeric peptide D3 in media simulating the route of orally administered drugs". *Eur J Pharm Sci* 107: 203-207

Elmquist A and Langel U (2003). "In vitro Uptake and Stability Study of pVEC and Its All-D Analog". *Biol Chem* 384: 387–393

Findeis MA, Musso GM, Arico-Muendel CC, Benjamin HW, Hundal AM, Lee JJ, Chin J, Kelley M, Wakefield J, Hayward NJ and Molineaux SM (1999). "Modified-peptide inhibitors of amyloid beta-peptide polymerization". *Biochem* 38(21): 6791-6800

Folk JE (1956). "A New Pancreatic Carboxypeptidase". *J. Am. Chem. Soc.* 78(14): 3541–3542

Funke A and Willbold D (2012). "Peptides for Therapy and Diagnosis of Alzheimer's Disease". *Curr Pharm Des* 18: 755-767

Hardy JA and Higgins GA (1992). "Alzheimer's Disease: The Amyloid Cascade Hypothesis". *Science* 256(5054): 184-185

Heck AJ, Bonnici PJ, Breukink E, Morris D and Wills M (2001). "Modification and inhibition of vancomycin group antibiotics by formaldehyde and acetaldehyde". *Chemistry* 7(4): 910-916

Iverson SL (2016). "Metabolite Safety in Drug Development". *John Wiley & Sons*

Jia L and Liu X (2007). "The Conduct of Drug Metabolism Studies Considered Good Practice (II). In Vitro Experiments.". *Curr Drug Metab.* 8(8): 822–829

Karran E, Mercken M and De Strooper B (2011). "The amyloid cascade hypothesis for Alzheimer's disease: an appraisal for the development of therapeutics". *Nat Rev Drug Discov* 10(9): 698-712

Keil B (1992). "Specificity of proteolysis.". Berlin-Heidelberg-New York, *Springer-Verlag*

Kutzsche J, Schemmert S, Tusche M, Neddens J, Rabl R, Jurgens D, Brener O, Willuweit A, Hutter-Paier B and Willbold D (2017). "Large-Scale Oral Treatment Study with the Four Most Promising D3-Derivatives for the Treatment of Alzheimer's Disease". *Molecules* 22(10)

Lambert MP, Barlow AK, Chromy BA, Edwards C, Freed R, Liosatos M, Morgan TE, Rozovsky I, Trommer B, Viola KL, Wals P, Zhang C, Finch CE, Krafft GA and Klein WL (1998). "Diffusible, nonfibrillar ligands derived from Abeta1-42 are potent central nervous system neurotoxins.". *Proc. Natl. Acad. Sci. U. S. A.* 95(11): 6448-6453

Leithold LH, Jiang N, Post J, Ziehm T, Schartmann E, Kutzsche J, Shah NJ, Breitkreutz J, Langen KJ, Willuweit A and Willbold D (2016). "Pharmacokinetic Properties of a Novel D-Peptide Developed to be Therapeutically Active Against Toxic beta-Amyloid Oligomers". *Pharm Res* 33(2): 328-336

Lipscomb WN (1970). "Structure and Mechanism in the Enzymatic Activity of Carboxypeptidase A and Relations to Chemical Sequence.". *Acc. Chem. Res.* 3(3): 81-89

Lu AY (1976). "Liver microsomal drug-metabolizing enzyme system: functional components and their properties". *Fed Proc* 35(13): 2460-2463

Mathews WR, Runge TA, Haroldsen PE and Gaskell SJ (1989). "Characterization of impurities in a synthetic renin substrate peptide by fast-atom bombardment mass spectrometry and hybrid tandem mass spectrometry". *Rapid Commun Mass Spectrom* 3(9): 314-319

Metz B, Kersten GF, Hoogerhout P, Brugghe HF, Timmermans HA, de Jong A, Meiring H, ten Hove J, Hennink WE, Crommelin DJ and Jiskoot W (2004). "Identification of formaldehyde-induced modifications in proteins: reactions with model peptides". *J Biol Chem* 279(8): 6235-6243

Miller SM, Simon RJ, Ng S, Zuckermann RN, Kerr JM and Moos WH (1995). "Comparison of the Proteolytic Susceptibilities of Homologous L-Amino Acid, D-Amino Acid, and N-Substituted Clycine Peptide and Peptoid Oligomers". *Drug Dev Res* 35: 20-32

Molla G, Sacchi S, Bernasconi M, Pilone MS, Fukui K and Polegioni L (2006). "Characterization of human D-amino acid oxidase". *FEBS Lett* 580(9): 2358-2364

Ohide H, Miyoshi Y, Maruyama R, Hamase K and Konno R (2011). "D-Amino acid metabolism in mammals: biosynthesis, degradation and analytical aspects of the metabolic study". *J Chromatogr B Analyt Technol Biomed Life Sci* 879(29): 3162-3168

Poduslo JF, Curran GL, Kumar A, Frangione B and Soto C (1998). "Beta-sheet breaker peptide inhibitor of Alzheimer's amyloidogenesis with increased blood-brain barrier permeability and resistance to proteolytic degradation in plasma". *J Neurobiol* 39(3): 371-382

Rasmussen GJ and Bundgaard H (1991). "Prodrugs of peptides. 15. 4-Imidazolidinone prodrug derivatives of enkephalins to prevent aminopeptidase-catalyzed metabolism in plasma and absorptive mucosae". *Int. J. Pharm.* 76: 113-122

Reitz C and Mayeux R (2014). "Alzheimer disease: epidemiology, diagnostic criteria, risk factors and biomarkers". *Biochem Pharmacol* 88(4): 640-651

Sacchi S, Caldinelli L, Cappelletti P, Pollegioni L and Molla G (2012). "Structure-function relationships in human D-amino acid oxidase". *Amino Acids* 43(5): 1833-1850

Selkoe DJ and Hardy J (2016). "The amyloid hypothesis of Alzheimer's disease at 25 years". *EMBO Mol Med* 8(6): 595-608

Soto C, Kindy MS, Baumann M and Frangione B (1996). "Inhibition of Alzheimer's amyloidosis by peptides that prevent beta-sheet conformation.". *Biochem Biophys Res Commun* 226(3): 672-680

Sun N, Funke SA and Willbold D (2012). "A survey of peptides with effective therapeutic potential in Alzheimer's disease rodent models or in human clinical studies.". *Mini-Rev Med Chem* 12(5): 388-398

Taavitsainen P, Juvonen R and Pelkonen O (2001). "In vitro inhibition of cytochrome P450 enzymes in human liver microsomes by a potent CYP2A6 inhibitor, trans-2-phenylcyclopropylamine (tranylcypromine), and its nonamine analog, cyclopropylbenzene". *Drug Metab Dispos* 29(3): 217-222

Terry-Lorenzo RT, Chun LE, Brown SP, Heffernan ML, Fang QK, Orsini MA, Pollegioni L, Hardy LW, Spear KL and Large TH (2014). "Novel human D-amino acid oxidase inhibitors stabilize an active-site lid-open conformation". *Biosci Rep* 34(4)

Tugyi R, Uray K, Ivan D, Fellinger E, Perkins A and Hudecz F (2005). "Partial D-amino acid substitution: Improved enzymatic stability and preserved Ab recognition of a MUC2 epitope peptide". *Proc Natl Acad Sci U S A* 102(2): 413-418

U.S. Food and Drug Administration (2008). Guidance for Industry Safety Testing of Drug Metabolites. U.S. Department of Health and Human Services.

van Groen T, Schemmert S, Brener O, Gremer L, Ziehm T, Tusche M, Nagel-Steger L, Kadish I, Schartmann E, Elfgen A, Jürgens D, Willuweit A, Kutzsche J and Willbold D (2017). "The Aβ oligomer eliminating D-enantiomeric peptide RD2 improves cognition without changing plaque pathology". *Sci Rep* 7(1): 16275

Walsh DM, Klyubin I, Fadeeva JV, Cullen WK, Anwyl R, Wolfe MS, Rowan MJ and Selkoe DJ (2002). "Naturally secreted oligomers of amyloid beta protein potently inhibit hippocampal long-term potentiation in vivo.". *Nature* 416(6880): 535-539

Wang J, Yadav V, Smart AL, Tajiri S and Basit AW (2015). "Toward oral delivery of biopharmaceuticals: an assessment of the gastrointestinal stability of 17 peptide drugs". *Mol Pharm* 12(3): 966-973

Werle M and Bernkop-Schnurch A (2006). "Strategies to improve plasma half life time of peptide and protein drugs". *Amino Acids* 30(4): 351-367

Wu WN and McKown LA (2004). "In Vitro Drug Metabolite Profiling Using Hepatic S9 and Human Liver Microsomes.". *Optimization in Drug Discovery. In Vitro Methods.* Z. Yan and G. W. Caldwell. Humana Press Inc., Totowa, NJ, Humana Press**:** 163-184.

Yamanaka M, Miyoshi Y, Ohide H, Hamase K and Konno R (2012). "D-Amino acids in the brain and mutant rodents lacking D-amino-acid oxidase activity". *Amino Acids* 43(5): 1811-1821

Supplement

1. Figures

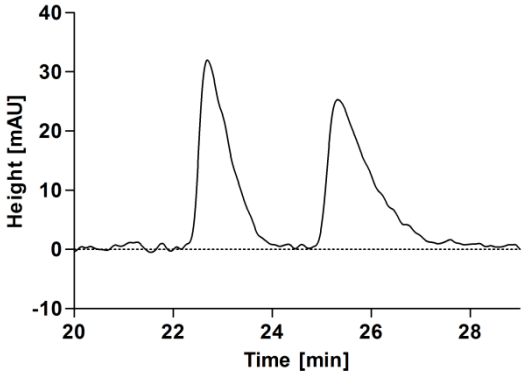

Figure S1: RP-HPLC chromatogram of separated amidated RD2 and one-fold deamidated RD2. Amidated RD2 (retention time: 22.7 min) and one-fold deamidated RD2 (retention time: 25.4) in water were separated by RP-HPLC.

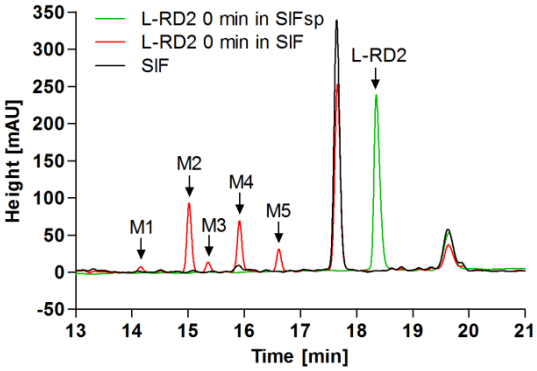

Figure S2: Metabolite profile of L-RD2 in simulated intestinal fluid (SIF). A chromatographic metabolite profile of L-RD2 was recorded after incubation in SIF for a few seconds and was compared to the profile of L-RD2 in SIF sine pancreas powder (SIFsp). L-RD2 could not be detected but several metabolites occurred (M1-5).

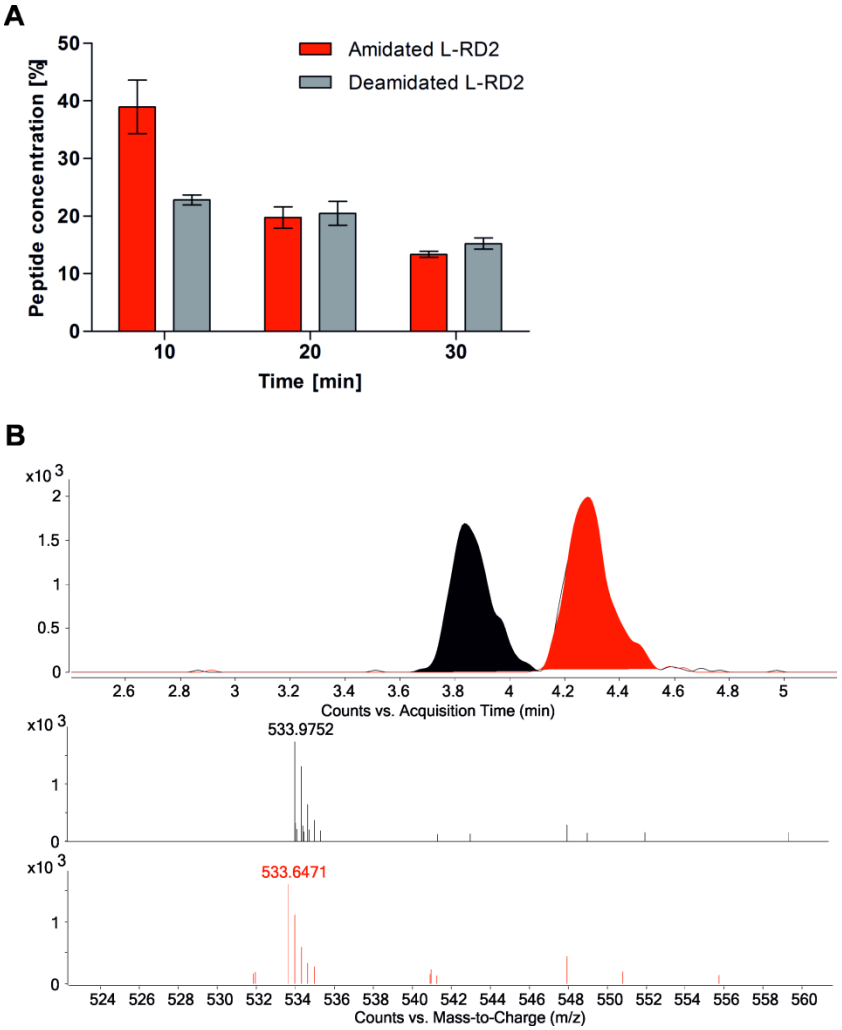

Figure S3: One-fold deamidation of L-RD2 in human liver microsomes. L-RD2 was incubated in human liver microsomes for up to 30 min. During this time, L-RD2 was metabolized increasingly to the one-fold deamidated form. **A)** RP-HPLC analysis: peak areas of the unmetabolized L-RD2 and the one-fold deamidated L-RD2 after different incubation times were normalized to L-RD2's peak areas after direct extraction from microsomes. Data are presented as mean ± SD (n = 3). **B)** UHPLC-ESI-QTOF-MS analysis of a sample with L-RD2 incubated for 10 min: extracted ion chromatogram of amidated (red) and one-fold deamidated L-RD2 (black). One-fold deamidated L-RD2 has a mass at *m/z* of 533.9756^{3+} and amidated L-RD2 has a mass at *m/z* of 533.6470^{3+}.

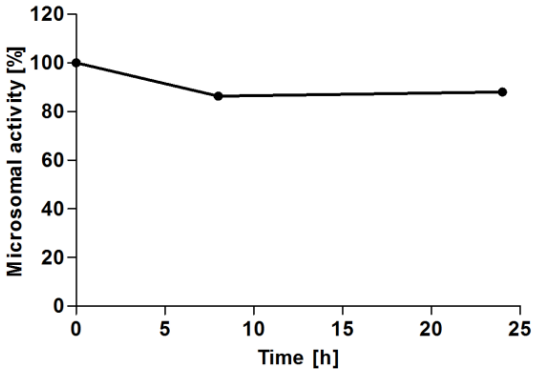

Figure S4: Microsomal activity. Microsomal long-term activity was examined by incubating microsomes without peptide for up to 24 h and examining their activity by their ability to degrade L-RD2, which was added after 8 and 24 h. The microsomes remained active during the whole experiment. Peak areas of the unmetabolized peptides after different incubation times were normalized to the peptides' peak areas after direct extraction from microsomes. Data are presented as mean ± SD (n = 3).

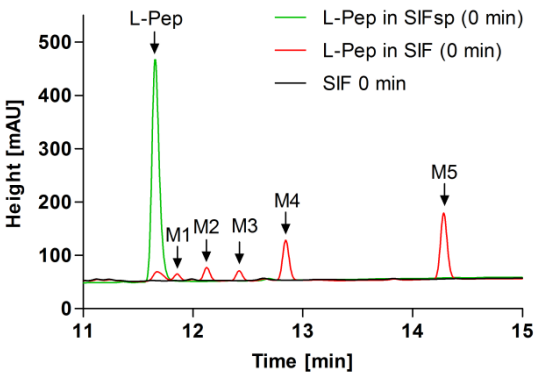

Figure S5: Metabolite profile of KLVFFRRRRRR (L-Pep) in simulated intestinal fluid (SIF). A chromatographic metabolite profile of L-Pep was recorded after incubation in SIF for a few seconds and was compared to the profile of L-Pep in SIF sine pancreas powder (SIFsp). L-Pep could not be detected, but several metabolites occurred (M1-5).

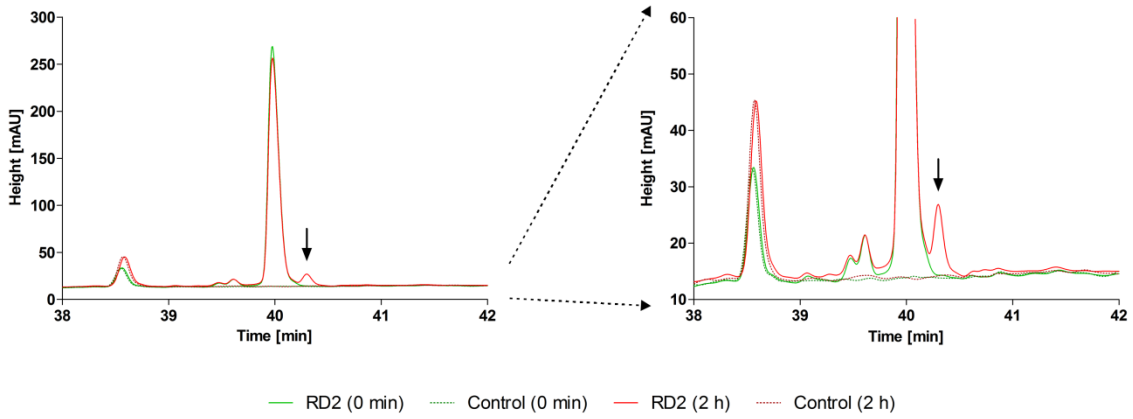

Figure S6: Metabolite profile of RD2 2 h incubated in human liver microsomes showing a potentially human-specific metabolite. RD2 was incubated in human liver microsomes for 0 and 2 h and chromatograms were recorded to search for potential human-specific metabolites. Incubated liver microsomes without RD2 served as controls. Only the relevant parts of the chromatogram are shown. One metabolite (HSM-3; arrow), only present in the human samples 7 & 8, represented 1 or 5% of the parent compound.

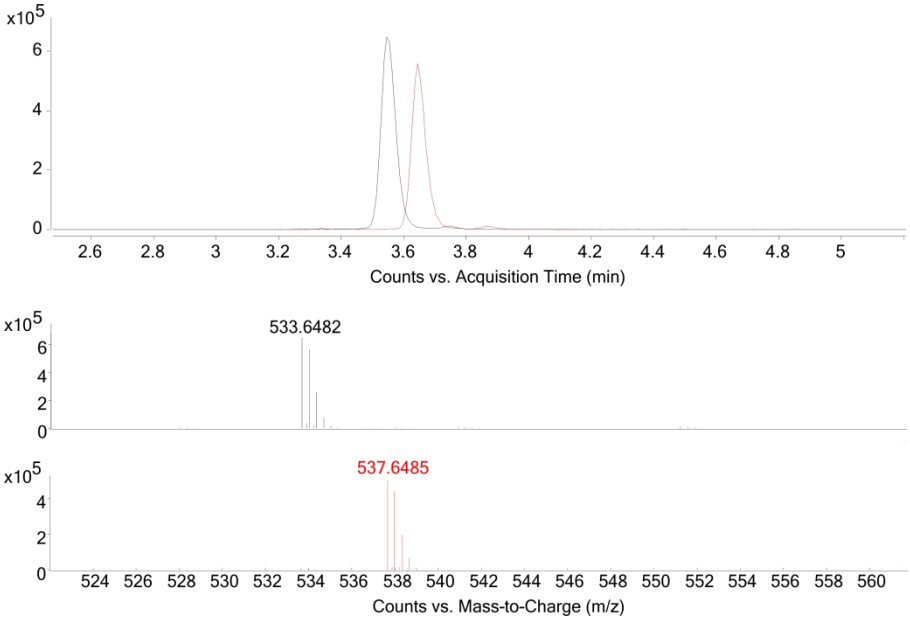

Figure S7: UHPLC-ESI-QTOF-MS analysis of RD2 and HSM-3 extracted from human liver microsomes. Overlay of RD2's (black) and HSM-3's (red) extracted ion chromatograms. RD2 has a mass at *m/z* of 533.6482^{3+} and HSM-3 has a mass at *m/z* of 537.6485^{3+}.

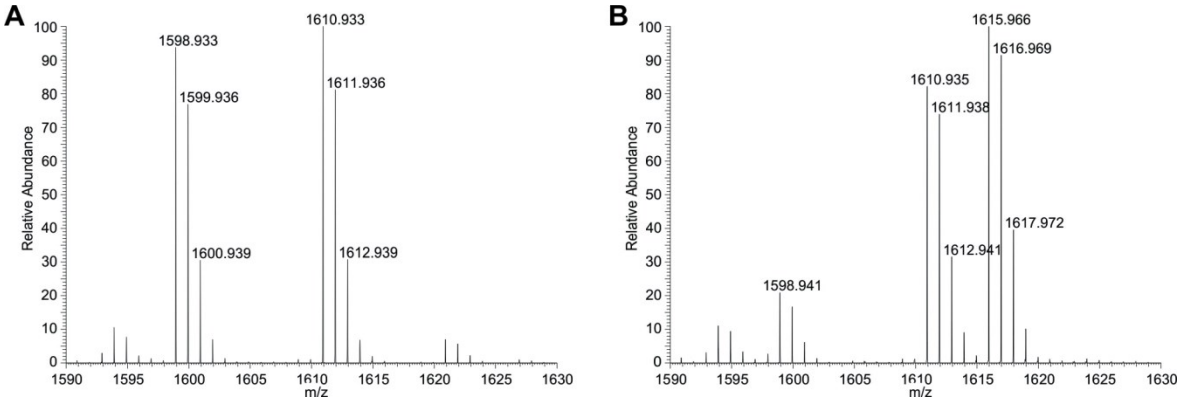

Figure S8: MALDI-MS analysis of HSM-3 and RD2. A) Analysis of the purified HSM-3 and RD2 by high resolution MALDI-MS showed a peak at *m/z* 1598.933, consistent with the predicted *m/z* of single-charged ion of RD2, and a second major peak with a mass shift of +12.000 at *m/z* 1610.933, which corresponds to HSM-3's mass. **B)** Addition of ^{13}C- and D-labeled formaldehyde ($^{13}CD_2O$) with sodium cyanoborohydride yielded a mass shift of +17.033 in the case of RD2 but not HSM-3.

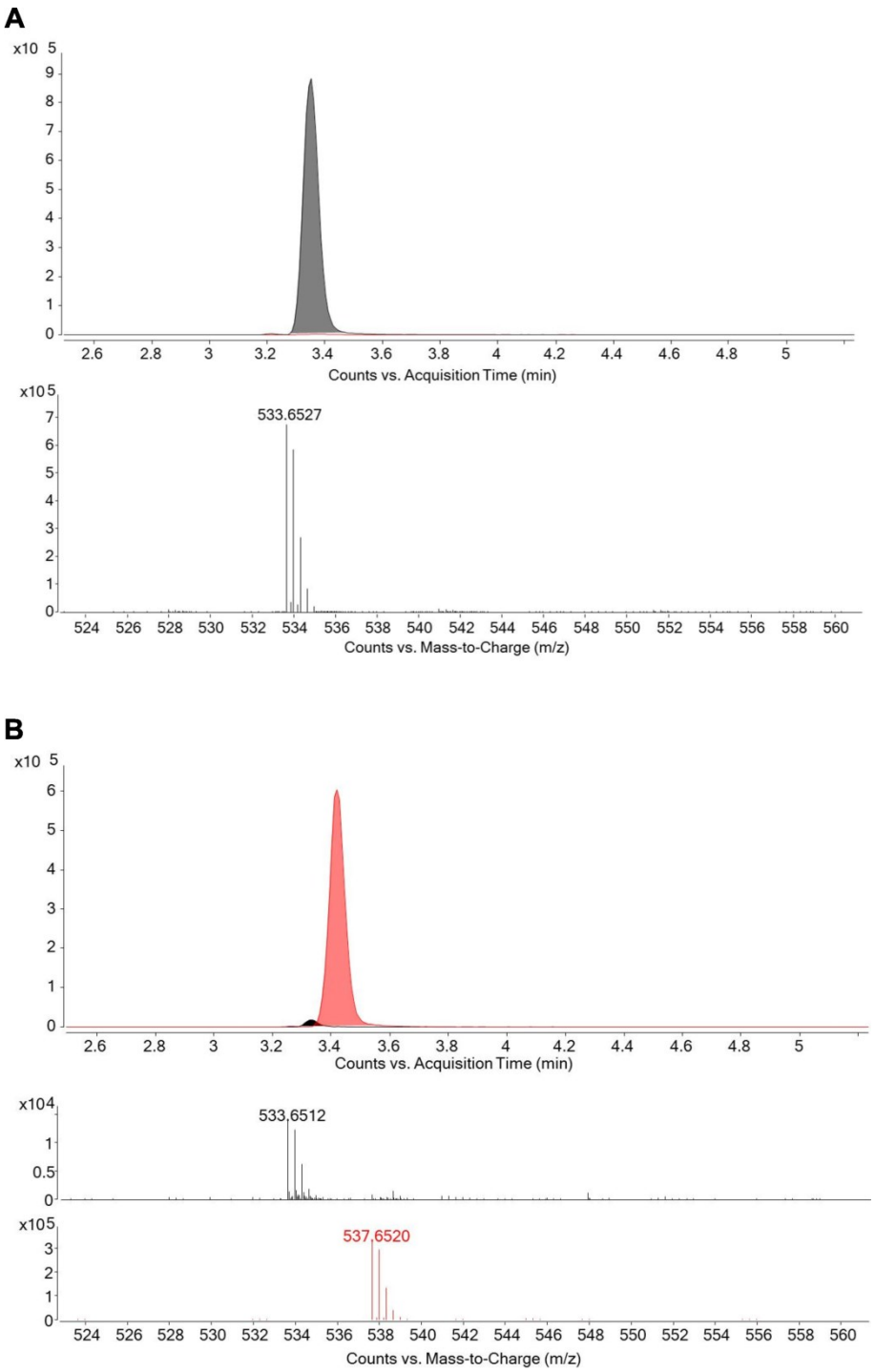

Figure S9: Reaction of RD2 with formaldehyde in water. RD2 was incubated for 24 h without **(A)** and with **(B)** 30 mM formaldehyde in water. The samples were analyzed by UHPLC-ESI-QTOF-MS. Without formaldehyde, only RD2 (black) was detected (*m/z* of 533.6527^{3+}). Under addition of formaldehyde, HSM-3 (red) was generated (*m/z* of 537.6520^{3+}).

2. Tables

Table S1: HPLC gradient used for the generation of metabolite profiles. Mobile phase A: acetonitrile with 0.1% TFA. Mobile phase B: water with 0.1% TFA.

Step	Time [min]	Mobile phase A [%]	Mobile phase B [%]
1	0	1	99
2	24	1	99
3	43	20	80
4	63	100	0

Table S2: HPLC gradient used for the separation of aldehyde- and ketone-2,4-dinitrophenylhydrazone derivatives. Mobile phase A: acetonitrile. Mobile phase B: water.

Step	Time [min]	Mobile phase A [%]	Mobile phase B [%]
1	0	32	68
2	10	32	68
3	15	46	54
4	20	46	54
5	25	60	40
6	32	80	20

Table S3: UHPLC gradient used for the separation of RD2 or L-RD2 and a one-fold deamidated peptide form. Mobile phase A: acetonitrile with 0.025% HFBA and 1% formic acid. Mobile phase B: water with 0.025% HFBA and 1% formic acid.

Step	Time [min]	Mobile phase A [%]	Mobile phase B [%]
1	0.0	10	90
2	0.5	10	90
3	0.6	17	83
4	6.0	17	83
5	6.6	95	5
6	8.0	95	5
7	8.1	10	90
8	10.0	10	90

Table S4: UHPLC gradient used for the analysis of RD2 and HSM-3. Mobile phase A: acetonitrile with 0.025% HFBA and 1% formic acid. Mobile phase B: water with 0.025% HFBA and 1% formic acid.

Step	Time [min]	Mobile phase A [%]	Mobile phase B [%]
1	0.0	10	90
2	2.0	10	90
3	2.1	22	78
4	2.6	22	78
5	6.0	25	75
6	6.1	95	5
7	8.0	95	5
8	8.1	10	90
9	10.0	10	90

Table S5: Inhibition of different CYP isoforms by RD2 in different concentrations.

	Inhibition [%]						
RD2 conc.	**0 µM**	**0.1 µM**	**0.25 µM**	**1 µM**	**2.5 µM**	**10 µM**	**25 µM**
CYP1A	0	0.906	6.18	9.42	1.34	-0.842	-0.198
CYP2C9	0	5.32	6.15	-0.871	0.607	-7.38	-26.8
CYP2C19	0	5.14	7.64	2.47	2.54	-5.77	-45.5
CYP2D6	0	7.58	1.33	0.671	3.53	-5.90	-9.57
CYP3A4	0	1.49	-0.223	5.77	1.71	-3.08	-12.0

Table S6: Inhibition of different CYP isoforms by CYP isoform-specific inhibitors. Determination of IC_{50} ± SD.

CYP isoform	Specific inhibitor	IC_{50} [µM]	SD [µM]
CYP1A	Alpha-naphthoflavone	0.0781	0.0204
CYP2C9	Sulfaphenazole	0.368	0.0589
CYP2C19	Tranylcypromine	10.7	0.654
CYP2D6	Quinidine	0.0451	0.00584
CYP3A4	Ketoconazole	0.0515	0.00381

Table S7: Signal assignment for protons and carbons after measurement of HH-TOCSY and HC-HSQC spectra of RD2 and HSM-3. RD2 und HSM-3 were measured in D_2O at 25 °C and 750 MHz.

		RD2			HSM-3		
		δ^1H [ppm]		**δ^{13}C [ppm]**	**δ^1H [ppm]**		**δ^{13}C [ppm]**
Pro	α	4.39		59.55	3.67		64.65
	β	2.40	1.96	29.84	1.99	1.80	27.10
	γ	1.98	1.94	23.61	1.67	1.62	24.50
	δ	3.37	3.33	46.51	3.03	2.54	55.00
	CO			169.83			177.60
N-CH_2-N					4.45	4.35	67.51
Thr	α	4.24		59.46	4.19		60.83
	β	3.99		66.94	4.03		64.52
	γ	1.07		18.80	0.99		19.38
	CO			171.07			
Leu	α	4.27		52.20	4.16		52.22
	β	1.51	1.41	39.85	1.40	1.31	39.48
	γ	1.47		24.25	1.36		24.32
	δ	0.82		21.90	0.73		21.94
	δ		0.76	20.79		0.66	20.60
	CO			174.08			
His	α	4.67		52.70	4.42		54.06
	β	3.11	3.03	26.96	2.95	2.92	
	CO			172.16			
	γC			129.85			
	δCH	7.09		117.00			
	εCH	8.22		134.38			
Thr	α	4.21		58.97	4.08		59.24
	β	4.08		66.94	4.01		66.78
	γ	1.07		18.80	0.95		18.64
	CO			171.50			
His	α	4.61		53.00	4.49		53.72
	β	3.12	3.04	27.28	2.90	2.87	
	CO			171.88			
	γC			130.28			
	δCH	7.06		116.92			
	εCH	8.11		134.55			
Asn	α	4.60		50.52	4.49		50.58
	β	2.73	2.66	36.02	2.66	2.59	35.73
	CO			172.35			
	γCO			174.07			
5x Arg*	α	4.24		53.30	4.15		53.30
	β	1.77	1.70	28.20	1.69	1.61	28.20
	γ	1.57		24.40	1.48		24.40
	δ	3.13		40.50	3.04		40.50
	CO			173.40			

*All Arginine resonances were broad signals and not resolved.

Table S8: Peak areas of formaldehyde-2,4-dinitrophenylhydrazone (2,4-DNPH) in different human liver microsome batches. Batches 7 & 8 were measured twice, batches 1 - 6 once each. The background was measured three times and did not change during analysis period.

	Human liver microsome batch #			Background
	1 - 6	**7**	**8**	
Formaldehyde-2,4-DNPH peak area ± SD [mAU*s]	13.7 ± 2.2	71.7 ± 0.2	106.5 ± 1.5	8.3 ± 1.5

3.4 Development and validation of an UHPLC-ESI-QTOF-MS method for quantification of the highly hydrophilic amyloid-β oligomer eliminating all-D-enantiomeric peptide RD2 in mouse plasma

Hupert M*, Elfgen A*, Schartmann E, Schemmert S, Buscher B, Kutzsche J, Willbold D and Santiago-Schübel B (*Geteilte Erstautorenschaft)

Journal of Chromatography B 2018, 1073:123-129

DOI: 10.1016/j.jchromb.2017.12.009

http://www.sciencedirect.com/science/article/pii/S1570023217316562?via%3Dihub

Journal of Chromatography B 1073 (2018) 123–129

Contents lists available at ScienceDirect

Journal of Chromatography B

journal homepage: www.elsevier.com/locate/jchromb

Development and validation of an UHPLC-ESI-QTOF-MS method for quantification of the highly hydrophilic amyloid-β oligomer eliminating all-D-enantiomeric peptide RD2 in mouse plasma

Michelle Hupert[a,1], Anne Elfgen[b,1], Elena Schartmann[b], Sarah Schemmert[b], Brigitte Buscher[c], Janine Kutzsche[b], Dieter Willbold[b,d,*], Beatrix Santiago-Schübel[a,*]

[a] Forschungszentrum Jülich GmbH, Central Institute for Engineering, Analytics (ZEA-3), Jülich, Germany
[b] Forschungszentrum Jülich GmbH, Institute of Complex Systems, Structural Biochemistry (ICS-6), Jülich, Germany
[c] Triskelion B.V., Zeist, The Netherlands
[d] Institut für Physikalische Biologie, Heinrich-Heine-Universität Düsseldorf, Düsseldorf, Germany

ARTICLE INFO

Keywords:
UHPLC-ESI-QTOF-MS
Mouse plasma
D-peptide
Amyloid-β peptide
Therapeutic compound
Alzheimer's disease

ABSTRACT

During preclinical drug development, a method for quantification of unlabeled compounds in blood plasma samples from treatment or pharmacokinetic studies in mice is required. In the current work, a rapid, specific, sensitive and validated liquid chromatography mass-spectrometric UHPLC-ESI-QTOF-MS method was developed for the quantification of the therapeutic compound RD2 in mouse plasma. RD2 is an all-D-enantiomeric peptide developed for the treatment of Alzheimer's disease, a progressive neurodegenerative disease finally leading to dementia. Due to RD2's highly hydrophilic properties, the sample preparation and the chromatographic separation and quantification were very challenging. The chromatographic separation of RD2 and its internal standard were accomplished on an Acquity UPLC BEH C18 column (2.1 × 100 mm, 1.7 µm particle size) within 6.5 min at 50 °C with a flow rate of 0.5 mL/min. Mobile phases consisted of water and acetonitrile with 1% formic acid and 0.025% heptafluorobutyric acid, respectively. Ions were generated by electrospray ionization (ESI) in the positive mode and the peptide was quantified by QTOF-MS. The developed extraction method for RD2 from mouse plasma revealed complete recovery. The linearity of the calibration curve was in the range of 5.3 ng/mL to 265 ng/mL ($r^2 > 0.999$) with a lower limit of detection (LLOD) of 2.65 ng/mL and a lower limit of quantification (LLOQ) of 5.3 ng/mL. The intra-day and inter-day accuracy and precision of RD2 in plasma ranged from −0.54% to 2.21% and from 1.97% to 8.18%, respectively. Moreover, no matrix effects were observed and RD2 remained stable in extracted mouse plasma at different conditions. Using this validated bioanalytical method, plasma samples of unlabeled RD2 or placebo treated mice were analyzed. The herein developed UHPLC-ESI-QTOF-MS method is a suitable tool for the quantitative analysis of unlabeled RD2 in plasma samples of treated mice.

1. Introduction

RD2 is an all-D-enantiomeric peptide specifically and directly targeting amyloid β peptide (Aβ) oligomers, which play a major role in the pathogenesis of Alzheimer's disease (AD), a progressive neurodegenerative disease leading to loss of memory [1]. The neuropathological cause for the development of AD is the aggregation of monomeric Aβ into Aβ oligomers and fibrils followed by the deposition of characteristic senile plaques accompanied by neuronal degeneration [2,3]. However, not the insoluble senile plaques but the soluble Aβ oligomers are currently widely believed to be the most toxic species triggering AD pathology [4–6]. The compound RD2 consists of 12 D-enantiomeric amino acid residues and has an amidated C-terminus (sequence: ptlhthnrrrrr-NH_2). It is the rationally rearranged sequence of the lead compound D3, which was previously selected by mirror image phage display against monomeric Aβ [7]. The rearrangement resulted in enhanced Aβ oligomer elimination [8,9]. *In vitro* assays also revealed that RD2 inhibits Aβ fibril formation efficiently [9]. In studies with AD transgenic mice, RD2 reduced the AD pathology in the mice's brains and showed improvement of cognition [9]. A pharmacokinetic study with the radiolabeled compound (^{3}H-RD2) revealed that RD2 has a high oral bioavailability, long blood circulation and an efficient blood brain

* Corresponding authors.
[1] These authors contributed equally to this work.

https://doi.org/10.1016/j.jchromb.2017.12.009
Received 22 September 2017; Received in revised form 30 November 2017; Accepted 6 December 2017
Available online 08 December 2017
1570-0232/

barrier permeability [10]. In these studies, it could be shown via thin layer chromatography with auto-radiographic detection that ^{3}H-RD2 remains stable after incubation in different body fluids and tissues. However, it is desirable to monitor RD2 levels also without any radioactive label in order to follow for example long-term treatment studies. Thus, as a first step, a suitable extraction method for the highly hydrophilic, arginine-rich RD2 from blood plasma followed by a rapid, sensitive and validated method for quantitative analysis of unlabeled RD2 via LC–MS has been developed for pharmacokinetic or treatment studies in this work. All validation parameters were carried out on the Guideline on bioanalytical method validation of the European Medicines Agency [11]. Using the validated method, plasma samples of RD2 or placebo treated mice were then analyzed as proof of concept.

2. Material and methods

2.1. Chemicals and reagents

UPLC-grade acetonitrile (ACN) was purchased from VWR (Langenfeld, Germany), UPLC-grade water from Merck (Darmstadt, Germany), heptafluorobutyric acid (HFBA) in LC-grade from Sigma Aldrich (Taufkirchen, Germany), formic acid (FA) in UPLC–MS grade from Biosolve (Valkenswaard, Netherlands) and trichloroacetic acid (TCA) from Sigma-Aldrich (Taufkirchen, Germany). Low binding Eppendorf tubes (Eppendorf, Hamburg, Germany) and auto-sampler vials (Agilent, Santa Clara, USA) were used because of the sticky characteristic of the peptides. Blank pooled blood plasma from healthy CD-1 mice (Innovative Grade US Origin Mouse Plasma – CD-1) was purchased from Dunn Labortechnik GmbH (Asbach, Germany). K3-EDTA served as anti-coagulator.

2.2. Peptides

The all-D-enantiomeric peptide RD2 consists of 12 amino acid residues each in D-configuration and has an amidated C-terminus (ptlhthnrrrrr-NH_2). RD2 has a monoisotopic mass of 1597.914 Da. The peptide was purchased from CBL Patras (Patras, Greece). The RD2 concentration was corrected for purity (92.3%), water content (3.7%), residual trifluoroacetic acid (TFA) (0.15%) and acetate content (25.5%). The internal standard (ISTD) has the same sequence as RD2 but with a substitution of leucine against valine at position three. It has a monoisotopic mass of 1583.898 Da. The ISTD was purchased from Peptides & Elephants GmbH (Potsdam, Germany) with a purity of 99.8%.

2.3. Stock solutions, calibration curve and quality control (QC) samples preparation

Calibration stock solutions of RD2 and ISTD were separately prepared in a water/ACN/FA (85/15/0.1%) mixture at a final concentration of 1.0 mg/mL, respectively. Dilution of 1:100 of the stock solutions in the same water/ACN/FA mixture resulted in the working solutions (10 µg/mL). Appropriate volumes of RD2 working solutions were diluted in blank mouse plasma samples to prepare the calibration standards and the QC standards. For the calibration curve, 5.30, 13.25, 26.5, 53, 132.5 and 265 ng/mL RD2 was prepared dissolving an appropriate volume of RD2 working solution. 33 ng/mL ISTD was added to correct the loss of analytes during sample preparation. For the extraction of RD2 and the ISTD, 3% TCA were added while vortexing the solution for 10 s. Precipitated proteins were removed by centrifugation at 14,000 *g* for 5 min at 4 °C. The supernatants containing the peptides were transferred to a low binding autosampler vial and stored at −20 °C. Blank plasma samples were prepared using water instead of RD2 working solution and ISTD. In addition, low quality control (LQC, 21.2 ng/mL), medium quality control (MQC, 106 ng/mL) and high quality control (HQC, 212 ng/mL) samples were prepared in the same manner. Furthermore, a quality control sample in water/ACN/FA (50 ng/mL) was prepared (QC-P) to check the performance of the method and the instrument before every series of measurements. The coefficient of determination (r^2) was used to evaluate the linearity of the calibration curve. The calibration standards were always prepared in triplicate and each extract was analyzed three times.

2.4. Chromatographic and mass spectrometry conditions

An Agilent UHPLC-ESI-QTOF-MS system was used for separation of RD2 from the ISTD and the remaining plasma components. The UHPLC (Agilent 1290 Infinity series) system consisted of a binary pump system, an autosampler, a thermostatted column compartment and a 6250 accurate-mass QTOF-MS with an electrospray ionization (ESI) interface with a resolution of 20,000. Chromatographic separation was performed on an Acquity UPLC BEH C18 column (2.1 × 100 mm, 1.7 µm particle size; Waters, Milford, USA). Column temperature was kept at 50 °C. Flow rate was 500 µL/min. The mobile phase consisted of solvent A, which was 0.025% HFBA and 1% FA in water, and solvent B, which was 0.025% HFBA and 1% FA in ACN. Sample injection volume was 20 µL. At the beginning of the run was an isocratic step of 5% B (0–2 min) followed by an increase to 22% B within 0.1 min, which was held for 0.5 min. The gradient increased from 22% to 25% B (2.6–6.5 min) in which RD2 eluted separately from the ISTD and other extracted plasma products from the column. Afterwards, the gradient increased rapidly within 0.7 min to 95% B and was held for cleaning with 95% B for 2 min. The gradient returned to 5% B within 0.1 min and equilibrated the system until 11 min. Detection was performed with the QTOF mass detector in the ESI positive ionization mode. The nebulizer pressure was set to 20 psi and the drying gas flow was set to 11 L/min. A fragmentation voltage of 215 V, a skimmer voltage of 68 V and an octopole voltage of 750 V were used. The mass range was set to m/z 500–600 and data acquisition rate was two spectra. Source temperature was set to 300 °C. MassHunter software LC–MS Data Acquisition B.05.01 (Agilent Technologies, Santa Clara, USA) was used to control the instrument and data acquisition. To correct the loss of analytes during sample preparation, quantification of RD2 was carried out with the ISTD. The first isotope of the three times loaded species RD2 ($(M+H^+)^{3+} = 533.649$) and ISTD ($(M+H^+)^{3+} = 528.977$) ± 8 ppm was extracted using the MassHunter software Quantitative Analysis for QTOF B.05.02 (Agilent Technologies, Santa Clara, USA). The correct isotopic ratio of RD2 and ISTD was a requirement for the identification and quantification of RD2. The advantage of this quantification method, which relies on the correct monoisotopic mass/isotopic ratio of RD2 compared to the quantification using a multiple reaction monitoring (MRM) mode, is the identification of possible metabolites of RD2 with only small modification, e.g., deamidation. We know from other studies that deamidation of RD2 sometimes occurs. In the case of deamidation of RD2, the isotope distribution ratio will be shifted to the second isotope. With an MRM method, this modification would not be detectable.

2.5. Method validation

All validation parameters were carried out on the Guideline on bioanalytical method validation of the European Medicines Agency [11].

2.5.1. Selectivity

For investigation of the method selectivity, six different blank mouse plasma matrix samples were exposed to the same extraction procedures as described before. The samples were tested for any interference peaks at retention time of RD2 or ISTD matching the chromatogram with RD2 and the ISTD spiked plasma. The assay is assured to be selective if the peak responses of tested samples were limited to ≤ 20% of the peak response of LLOQ and ≤ 5% of the ISTD.

2.5.2. Linearity, sensitivity and carry-over

Linearity and sensitivity of the suggested procedure were assessed on the basis of three individually prepared calibration curves. The calibration samples were freshly prepared and extracted with the described method. Statistical least square method was applied for the analysis of the resulting data. The % deviation for each calibrator should be ≤ 15% and for the LLOQ ≤ 20%. At least 75% of the calibration standards must fulfill this criterion. LLOQ and LLOD were calculated as a signal/noise ratio of 10 (LLOQ) or 3 (LLOD) comparing measured signals from standards of low concentrations of RD2 with those of blank samples.

Carry-over was assessed by injecting three blank plasma samples after highest calibration standard (265 ng/mL). The area response of blank samples must not exceed 20% of LLOQ and 5% of ISTD.

2.5.3. Accuracy and precision studies

Intra-day accuracy studies were carried out with the LQC, MQC and HQC samples. All samples were measured six times within one day. Additionally inter-day measurements were done in the same way in three successive days. For expression accuracy and precision of the method, the percentages error (% error) and the percentages relative standard deviation (% RSD) were used. The accuracy was determined as follows: % error = [(average measured concentration-expected concentration)/expected concentration] × 100, whereas the precision was determined as follows: % RSD = (standard deviation/average measured concentration) × 100. The acceptance criterion for accuracy was ≤ 15% of the actual values and precision should be ≤ 15%, except for LLOQ (≤ 20%) for both parameters.

2.5.4. Recovery and matrix effect

The extraction recovery was evaluated by comparing the concentrations of the extracted QC samples with the equal concentrations of RD2 spiked to plasma after extraction. Therefore, six lots of plasma were pre-treated and the extracts were spiked with RD2 concentrations corresponding to the QC samples.

The percentage of matrix effect was calculated by comparing the peak area of RD2 or ISTD spiked into blank plasma to the peak area of equal amounts of RD2 or ISTD in water/ACN/FA. The matrix factor (MF) of both RD2 and ISTD was calculated and the ISTD normalized MF was also determined. If MF is = 1, then there is no matrix effect. An MF < 1 means ion suppression and an MF > 1 means ion enhancement effects.

2.5.5. Reproducibility, performance and robustness

The QC-P sample was tested on every measurement day for one month. To show the variation within the days, the peak areas of RD2 were documented in a control chart.

2.5.6. Stability and dilution integrity

For assessing the RD2 stability in plasma matrix, the QC samples were used to perform the stability studies under different conditions. The samples were measured immediately after preparation, after 24 h at room temperature and after 72 h in the autosampler at 15 °C to assess the bench top and autosampler stability. Additionally, RD2 in plasma was measured after two weeks in the freezer (−20 °C). Moreover, the stability of the samples during three freeze-thaw-cycles was examined.

Furthermore, dilution integrity of RD2 samples was evaluated to confirm the integrity of concentrated RD2 samples that need a dilution step. Therefore, a 530 ng/mL RD2 solution was spiked into blank plasma or into water/ACN/FA to attain a concentration of two times of highest calibration standard. Then, the samples were five- or tenfold diluted with blank plasma or water/ACN/FA. Three replicates of each dilution were evaluated and the integrity of the samples was accepted when the deviation laid below 15% of the nominal values.

2.6. Applicability of the validated method for analysis of samples from a preclinical treatment study

2.6.1. Animals

Old male double transgenic APPswe/PS1ΔE9 mice [12] were purchased from The Jackson Laboratory (Sacramento, USA) and bred in-house. Water and food were available *ad libitum*. Housing rooms were maintained on a 12/12 h light–dark cycle (7:00 a.m.–7:00 p.m.) with a temperature of 22 °C and approx. 54% humidity. All animal experiments were performed in accordance with the German Law on the protection of animals and were approved by the local ethics committee (LANUV, North-Rhine-Westphalia, Germany, AZ84-02.04.2011.A359).

2.6.2. Treatment and blood collection

Treatment with RD2 or placebo was performed via intraperitoneal micro-osmotic pumps (type no. 1004) purchased from Alzet Osmotic Pumps (Cupertino, USA). The pumps were primed with 0.9% sodium chloride for 24 h at room temperature before filling with RD2 dissolved in 0.9% sodium chloride (n = 3) or 0.9% sodium chloride without peptide (placebo; n = 3). The pumps were implanted as described before [13]. In brief, for the implantation, the mice were anaesthetized intraperitoneally with 100 mg/kg ketamine (Bela-Pharm, Vechta, Germany) and 5 mg/kg medetomidine (Alfavet, Neumuenster, Germany). The skin and the muscle layer below the skin were cut in the midline and the pump was inserted into the abdominal cavity. Afterwards, the wound was sutured. The mice were treated with 40 mg/kg/day RD2 or placebo for 28 days. Subsequently, the mice were anaesthetized intraperitoneally with 100 mg/kg ketamine and 0.3 mg/kg medetomidine for blood collection via cardiac puncture. About 50 µL of 100 U/mL heparin (BD, Franklin Lakes, NJ, USA) served as anti-coagulator in the syringe.

The blood samples were centrifuged at 3,000 *g* and 4 °C for 10 min to obtain the cell free plasma. The plasma samples were frozen and stored at −20 °C.

2.6.3. Sample preparation and peptide extraction

Three RD2 and three placebo treated mice were analyzed in triplicates. The peptides were extracted from the plasma samples by the method described above. The supernatant containing the peptides RD2 and ISTD were stored at −20 °C. The samples were quantitatively analyzed in triplicate using the described method. If necessary, the samples were diluted in water/ACN/FA.

3. Results and discussion

3.1. Chromatographic separation and mass spectrometry

High resolution instruments have the ability to determine accurate mass and isotopic distribution and therefore enable high selectivity and specificity. In ESI, peptides are charged by excess of positive ions such as NH_4^+. The number of charges of each peptide depends on the experimental conditions but much more on protonable functional groups of the amino acid residues (e.g., amino groups in lysine, arginine and histidine). In addition, peptides show characteristic isotopic patterns depending on the functional groups of their amino acid composition. These two parameters were used for identification and quantification of RD2. RD2, which contains five arginine residues, has a monoisotopic mass of 1597.914 Da and was detected with two to four charges, in which > 95% was in the charge of three with a *m/z* of 533.649 $(M+H^+)^{3+}$ at all concentration levels of the calibration samples. The ISTD with a mass of 1583.898 Da was also detected > 95% via the threefold charged state with a *m/z* of 528.977 $(M+H^+)^{3+}$. As a consequence, the threefold charged state was used for quantification. The accuracy for confirmation of the extracted masses of RD2 and ISTD was within ± 8 ppm mass error showing high mass accuracy for the components' identification. The experimentally obtained isotopic pattern

was in close agreement with the theoretical isotopic pattern of RD2 and ISTD. Several parameters of mass spectrometry were optimized to obtain the highest stabilized mass response.

In addition, chromatographic conditions were adjusted. RD2 is very polar and hence difficult to chromatograph without ion pairing. We tried different additives, such as formic acid and TFA in different concentrations, but finally the combination of 1% formic acid and 0.025% HFBA improved the chromatography significantly. A run time of 7 min was capable for a good separation of ISTD (retention time: 3.5 min) and RD2 (retention time: 3.7 min) (Fig. 1).

3.2. Method validation

3.2.1. Selectivity

The developed method is specific as no interference from components of the extracted mouse plasma matrix was observed at the retention time of ISTD or RD2. ISTD and RD2 were well separated under the optimized chromatographic conditions with retention times at 3.5 min and 3.7 min, respectively (Fig. 1A).

3.2.2. Linearity, sensitivity and carry-over

The suggested method was sensitive and reliable for quantifying RD2 in mouse plasma. The linear regression analysis for the results was carried out using the least square method. The calibration curve showed linearity of RD2 concentrations between 5.3 ng/mL and 265 ng/mL with a correlation coefficient (r^2) > 0.999 in mouse plasma. The calibration curve of RD2 in plasma has a regression equation of $y = 1.01\,x–0.14$. The precision (RSD) of each concentration point did not exceed 7% and varied between 0.44% and 6.13%. Accuracy ranged from −4.34% to 4.79% (Table 1). The high r^2 value was indicative for the good linearity and the values of standard deviation were indicative for the significant validity of the calibration points.

Table 1
Back-calculated RD2 concentration of the calibration standards in mouse plasma.

Nominal concentration [ng/mL]	Mean [ng/mL]	Standard deviation [ng/mL]	Precision [%]	Accuracy [%]
5.30	5.07	0.18	3.60	−4.34
13.25	13.24	0.81	6.10	−0.08
26.5	27.77	0.72	2.59	4.79
53	53.22	3.26	6.13	0.42
132.5	132.72	0.58	0.44	0.55
265	269.10	16.36	6.08	1.55

No carry-over effect for RD2 or ISTD was observed in three blank plasma samples measured directly after the highest calibration standard. The peak area of blank mouse plasma revealed less than 4% of the peak area of the lowest RD2 calibration standard and less than 5% of the ISTD peak area.

The analytical measurement range started with 5.3 ng/mL as the lower limit of quantification (LLOQ). The calibration standard at 2.65 ng/mL was still detectable but was not in the linear range for quantification any more. Therefore, the lower limit of detection (LLOD) was set to 2.65 ng/mL.

3.2.3. Accuracy and precision studies

The developed method was confirmed to be reproducible using intra- and inter-day precision and accuracy of the QC samples. For expressing precision and accuracy, % RSD and % error were used. The

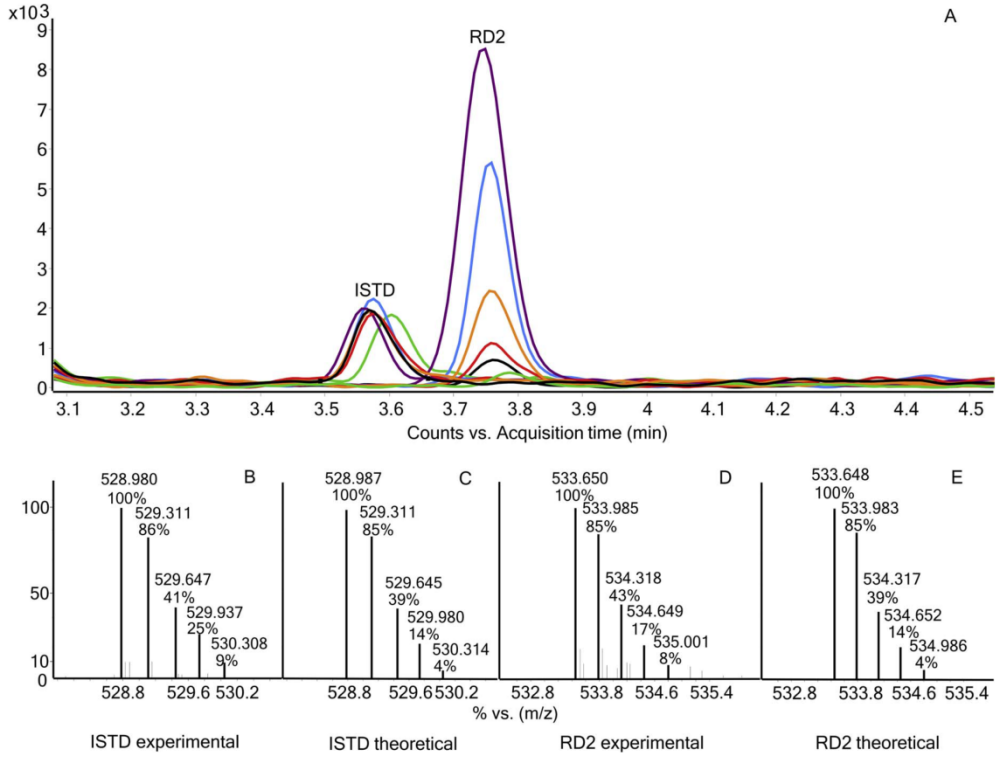

Fig. 1. Chromatographic separation and isotopic ratios of RD2 and the internal standard (ISTD). Extracted ion chromatogram (EIC) of RD2 (5.3–265 ng/mL) and ISTD (33 ng/mL) (A). Experimental (B, D) and theoretical (C, E) isotopic intensity distribution of the 3^+ charge peptide ion cluster of RD2 (D, E) and ISTD (B, C).

Table 2
Intra-day and inter-day precision and accuracy values of RD2 in mouse plasma.

	LQC [21.2 ng/mL]		MQC [106 ng/mL]		HQC [212 ng/mL]	
	Intra-day	Inter-day	Intra-day	Inter-day	Intra-day	Inter-day
Mean [ng/mL]	21.2	21.1	106.2	108.3	211.4	211.6
Standard deviation [ng/mL]	1.74	1.41	5.95	4.02	4.17	5.73
Precision [%]	8.18	6.69	5.60	3.71	1.97	2.71
Accuracy [%]	−0.24	−0.54	0.22	2.21	−0.29	−0.18

Table 3
Extraction recovery of QC samples of RD2 in mouse plasma (n = 6).

	RD2 extracted from mouse plasma			RD2 spiked to blank mouse plasma extract		
Nominal concentration [ng/mL]	21.2	106.0	212	21.2	106.0	212
Mean [ng/mL]	21.2	106.2	211.3	22.5	112.6	210.7
Recovery [%]	99.8	100.2	99.7	106.2	105.8	99.4
Standard deviation [ng/mL]	1.74	5.95	4.17	2.54	6.21	4.05
Precision [%]	8.18	5.60	1.97	11.24	5.52	1.92
Accuracy [%]	−0.24	2.83	−0.29	6.18	5.75	−0.61

values laid in the suitable range following the Guideline on bioanalytical method validation of the European Medicines Agency (2011) (Table 2).

3.2.4. Extraction recovery and matrix effect

Sample preparation for LC–MS of peptides is a critical step since peptides can undergo undesired phenomena such as adsorption to surfaces, degradation, variable recoveries or loss during transferring or drying steps. To minimize these issues, the use of a fast, simple technique such as protein precipitation with an organic solvent is preferred. To optimize the extraction of RD2 out of plasma, we used several organic solvents (ACN, methanol) and acids (HCOOH, TCA) in different ratios (varying concentrations). Finally, the extraction with 3% TCA showed best recoveries. In addition, the use of Low binding Eppendorf vials was indispensable because of the sticky character of the RD2 peptide.

Table 3 summarizes the extraction recoveries of the QC samples of RD2 in mouse plasma. The extraction recovery of RD2 was determined comparing the calculated concentration of RD2 extracted from plasma and extracted plasma spiked with corresponding amounts of RD2. The extraction efficiency was determined for the three QC samples with 99.8% (LQC), 100.2% (MQC) and 99.7% (HQC), respectively. Theoretically, the recovery rate cannot be above 100%. Due to the precision of the measurement, which was determined to be 7.1% (see 3.2.5), however, the calculations can ultimately lead to recovery rates slightly above 100%.

Table 5
Determination of RD2 in mouse plasma of intraperitoneally treated mice.

Mouse	RD2 treated			Placebo treated
	1	2	3	4–6
Mean [ng/mL]	1157.6	1554.3	1804.6	< LLOD
Standard deviation [ng/mL]	57.31	53.30	50.01	
Precision [%]	4.95	3.43	2.77	

For evaluation of the matrix effect, the peak area of RD2 or ISTD spiked into blank plasma was compared to the peak area of equal amounts of RD2 or ISTD in water/ACN/FA. The peak areas of RD2 and ISTD in water/ACN/FA and plasma samples showed that plasma has a maximal influence of 9% on the ionization of RD2 and 7% on the ionization of ISTD. The ISTD normalized MF values were 1.03 (LQC), 0.95

Table 4
RD2 stability and dilution integrity of RD2 in mouse plasma (n = 6).

	Nominal concentration [ng/mL]	Mean [ng/mL]	Recovery [%]	Precision [%]	Accuracy [%]
After extraction, 0 min	21.2	21.6	101.9	2.8	1.9
	106.0	107.7	101.5	3.6	1.5
	212.0	217.8	102.7	5.0	2.7
Room temp., after 24 h	21.2	21.4	100.9	8.3	0.9
	106.0	109.3	103.1	3.7	3.1
	212	211.0	99.5	2.8	−0.5
−20 °C, after 2 weeks	21.2	20.3	95.7	6.7	−4.2
	106.0	110.5	104.2	9.1	4.2
	212	202.1	95.3	1.7	−4.7
15 °C, 72 h	21.2	19.2	90.7	4.9	−9.3
	106.0	107.1	101.0	2.1	1.0
	212	210.7	99.4	2.0	−0.6
Three freeze-thaw-cycles	21.2	20.7	97.6	8.9	−2.4
	106.0	110.1	103.9	3.5	3.9
	212	210.4	99.3	2.5	−0.7
Dilution integrity	106.0 in plasma	114.8	108.3	4.0	8.3
	53.0 in plasma	55.4	104.6	4.6	4.6
	106.0 in water/ACN/FA	114.0	107.6	4.6	7.6
	53.0 in water/ACN/FA	55.1	104.0	3.9	4.0

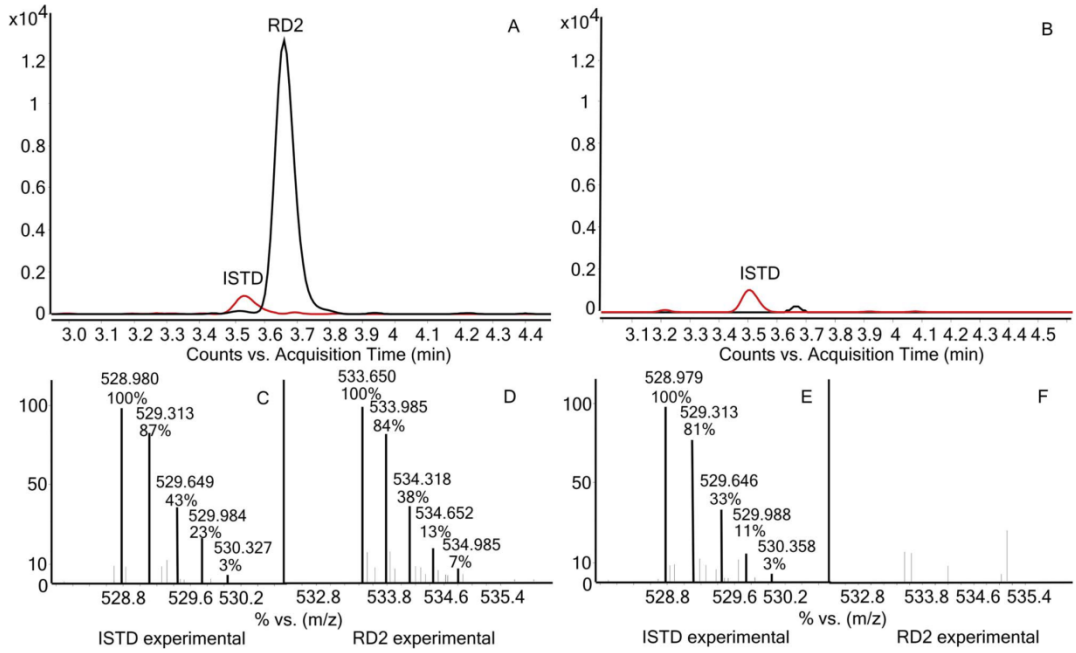

Fig. 2. Extracted ion chromatogram (EIC) of RD2 (black) and ISTD (red) of samples from RD2 treated mouse 2 (A) and placebo treated mouse 6 (B). Experimental distribution of the 3+ charged peptide ion cluster of ISTD (C, E) and RD2 (D, F). (For interpretation of the references to colour in this figure legend, the reader is referred to the web version of this article.)

(MQC) and 1.01 (HQC) respectively. This confirms matrix independency of this assay due to co-eluting matrix components.

3.2.5. Reproducibility, performance and robustness

The system is reproducible and robust. This was demonstrated by determination of the mean area of the QC-P standard over one month, which showed a precision of 7.1%.

3.2.6. Stability and dilution integrity

QC samples of RD2 were used to perform the stability studies under different conditions. The results of the stability studies are shown in Table 4. No loss of RD2 was observed during the storage at the tested conditions.

For evaluation of dilution integrity of RD2 samples, the mean recovery % and the precision % for the 1/5 and 1/10 dilution samples in plasma and in water/ACN/FA were determined. The recovery was within 104% and 108% and the precision was < 4.6%.

3.3. Applicability of the validated method for analysis of samples from a preclinical treatment study

To determine the applicability of the method for future treatment or pharmacokinetic studies, we analyzed plasma samples from mice after intraperitoneal treatment with 40 mg/kg/day unlabeled RD2 or with placebo (Table 5). Every mouse plasma sample was extracted in triplicate. The samples from the RD2 treated mice yielded ISTD and RD2 well separated with retention times at 3.5 and 3.7 min, respectively (Fig. 2A). The correct isotopic ratios of ISTD and RD2 were detected (Fig. 2C, D, E). In addition, no interferences from components of the extracted mouse plasma matrix were observed at the retention time of RD2 in placebo treated mice (Fig. 2F) substantiating the selectivity of the method.

Plasma of RD2 treated mice revealed an RD2 concentration of 1157.6, 1554.3 and 1804.6 ng/mL with a precision of 4.95%, 3.34% and 2.77%, respectively. As expected, RD2 has not been found in placebo treated mice (Table 5). From these results, we can conclude that the validated analytical method is reliable and suitable for the quantification of RD2 in plasma of treated mice.

4. Conclusion

Here, we describe the development and evaluation of a rapid UHPLC-ESI-QTOF-MS method for quantification of the highly hydrophilic, arginine-rich all-D-enantiomeric peptide RD2 in mouse plasma. The applied method showed a linearity range for RD2 spiked in plasma between 5.3 and 265 ng/mL with an LLOD of 2.65 ng/mL. The analysis was performed within 6.5 min with low solvent consumption. Quantifying several RD2 samples within one day as well as spread over various days demonstrated the accuracy, precision and reproducibility of the procedure. The developed method was successfully applied for the quantification of RD2 in intraperitoneally treated mice. These results provide a meaningful basis to evaluate preclinical or clinical applications of RD2.

Declaration of interest

The authors declare no competing financial or personal interests.

Acknowledgements

This work was funded by the Portfolio Technology and Medicine, the Portfolio Drug Research and the “Helmholtz-Validierungsfond” of the “Impuls- und Vernetzungsfond der Helmholtzgemeinschaft” and by the Technology Transfer Department of the Forschungszentrum Jülich.

References

[1] Alzheimer's Association, Alzheimer's disease facts and figures, Alzheimer's Dementia 12 (2016) (2016).

[2] J.A. Hardy, G.A. Higgins, Alzheimer's disease: the amyloid cascade hypothesis, Science 256 (1992) 184–185.
[3] D.J. Selkoe, J. Hardy, The amyloid hypothesis of Alzheimer's disease at 25 years, EMBO Mol. Med. 8 (2016) 595–608.
[4] S.T. Ferreira, W.L. Klein, The Abeta oligomer hypothesis for synapse failure and memory loss in Alzheimer's disease, Neurobiol. Learn. Mem. 96 (2011) 529–543.
[5] M.E. Larson, S.E. Lesne, Soluble Abeta oligomer production and toxicity, J. Neurochem. 120 (Suppl. 1) (2012) 125–139.
[6] I. Benilova, E. Karran, B. De Strooper, The toxic Abeta oligomer and Alzheimer's disease: an emperor in need of clothes, Nat. Neurosci. 15 (2012) 349–357.
[7] S.A. Funke, D. Willbold, Mirror image phage display–a method to generate D-peptide ligands for use in diagnostic or therapeutical applications, Mol. Biosyst. 5 (2009) 783–786.
[8] O.O. Olubiyi, D. Frenzel, D. Bartnik, J.M. Glück, O. Brener, L. Nagel-Steger, S.A. Funke, D. Willbold, B. Strodel, Amyloid aggregation inhibitory mechanism of arginine-rich D-peptides, Curr. Med. Chem. 21 (2014) 1448–1457.
[9] T. van Groen, S. Schemmert, O. Brener, L. Gremer, T. Ziehm, M. Tusche, L. Nagel-Steger, I. Kadish, E. Schartmann, A. Elfgen, D. Jürgens, A. Willuweit, J. Kutzsche, D. Willbold, The Aβ oligomer eliminating D-enantiomeric peptide RD2 improves cognition without changing plaque pathology, Sci. Rep. 7 (2017) 16275, http://dx.doi.org/10.1038/s41598-017-16565-1.
[10] L.H. Leithold, N. Jiang, J. Post, T. Ziehm, E. Schartmann, J. Kutzsche, N.J. Shah, J. Breitkreutz, K.J. Langen, A. Willuweit, D. Willbold, Pharmacokinetic properties of a novel D-peptide developed to be therapeutically active against toxic beta-amyloid oligomers, Pharm. Res. 33 (2016) 328–336.
[11] European Medicines Agency, Guideline on Validation of Bioanalytical Methods, Committee for Medicinal Products for Human Use, London, 2011.
[12] J.L. Jankowsky, H.H. Slunt, T. Ratovitski, N.A. Jenkins, N.G. Copeland, D.R. Borchelt, Co-expression of multiple transgenes in mouse CNS a comparison of strategies, Biomol. Eng. 17 (2001) 157–165.
[13] Alzet Osmotic Pumps, Intraperitoneal Implantation: Alzet Surgical Instuction Sheet, Alzet Osmotic Pumps, 2017.

4 Weitere Ergebnisse

4.1 Material & Methoden

4.1.1 Peptide

Das D-Peptid RD2 (Sequenz: ptlhthnrrrrr) besteht aus 12 D-enantiomeren Aminosäureresten mit einem amidierten C-Terminus und besitzt ein Molekulargewicht von 1598,9 Da. RD2 wurde von der Firma CBL Patras (Patras, Griechenland) synthetisiert. Der interne Standard für RD2 besitzt die gleiche Sequenz wie RD2 mit einem Aminosäure-Austausch an Position 3 – Leucin gegen Valin (Sequenz: ptvhthnrrrrr). Das Peptid hat ein Molekulargewicht von 1586,0 Da und wurde von der Firma Peptides & Elephants (Potsdam, Deutschland) synthetisiert. Bei den beiden Folsäure-RD2-Konjugaten Fol(G-t)-RD2 und Fol(p)-RD2 wurde Folsäure an RD2 gekoppelt. Bei Fol(G-t)-RD2 wurde die α- bzw. γ-Carboxygruppe der Folsäure über einen Glycin-Linker mit der Hydroxygruppe des Threonins an Position 2 der RD2-Sequenz gekoppelt. Das Peptid hat ein Molekulargewicht von 2080,6 Da. Bei Fol(p)-RD2 wurde die α- bzw. γ-Carboxygruppe der Folsäure über das sekundäre Amin des N-terminalen Prolins von RD2 gekoppelt. Das Peptid besitzt ein Molekulargewicht von 2023,3 Da. Beide Konjugate liegen aufgrund der alternativen Kopplungsmöglichkeiten über die beiden Carboxygruppen der Folsäure in je zwei verschiedenen Isomeren vor. Abbildung 4.1 zeigt die Strukturformeln der beiden Folsäure-RD2-Konjugate in α- und γ-Isomerie. Die Konjugate wurden von der Firma Peptides & Elephants (Potsdam, Deutschland) synthetisiert.

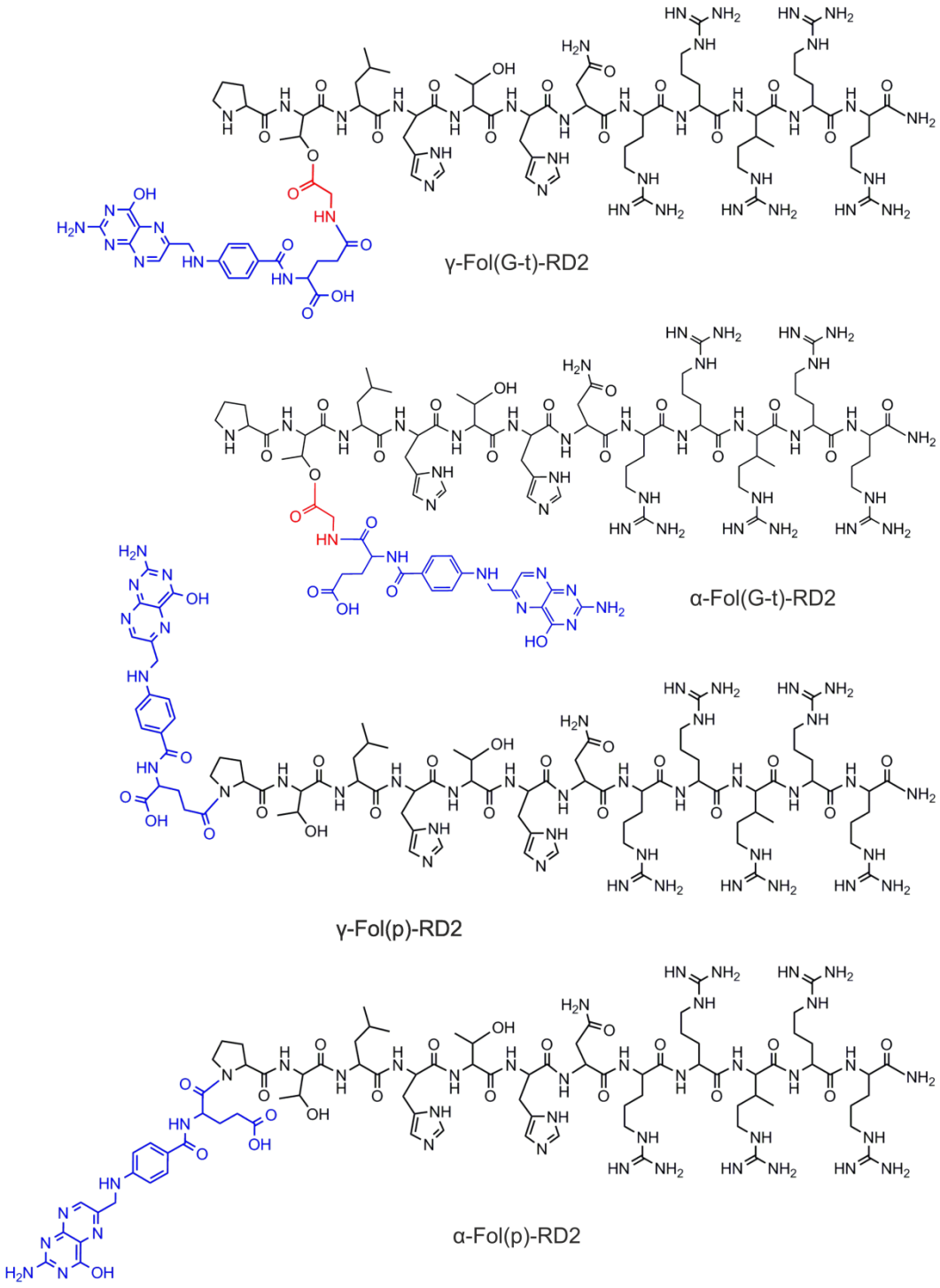

Abbildung 4.1: Strukturformeln der Folsäure-RD2-Konjugate Fol(G-t)-RD2 und Fol(p)-RD2. Strukturformeln der Folsäure-RD2-Konjugate Fol(G-t)-RD2 und Fol(p)-RD2 jeweils mit Darstellung des α- und des γ-Isomers. RD2: schwarz; Folsäure: blau; Glycin-Linker: rot.

4.1.2 Zellviabilitätstest der Folsäure-RD2-Konjugate und RD2

Zur Untersuchung der Zytotoxizität von Fol(G-t)-RD2, Fol(p)-RD2 und RD2 sowie deren Einfluss auf das zytotoxische Potential von $A\beta_{1-42}$ wurde ein MTT (3-(4,5-Dimethylthiazol-2-yl)-2,5-diphenyltetrazoliumbromid)-Zellviabilitätstest durchgeführt.

Phäochromozytom-Zellen (PC12) aus der Ratte (Leibniz-Institut DSMZ, Braunschweig, Deutschland) wurden in Dulbecco's Modified Eagle Medium (DMEM), ergänzt mit 10 % fötalem Kälberserum, 5 % Pferdeserum und 1 % Penicillin-Streptomycin, inkubiert. Es wurden 10.000 Zellen je Well auf Collagen A-beschichteten 96-Well-Platten (Gibco, Life Technology, Carlsberg, USA) in einem Volumen von 100 µL je Vertiefung ausgesät und bei 95 %-iger Luftfeuchtigkeit und 5 % CO_2 für 24 h bei 37 °C inkubiert. Die Proben wurden am Versuchstag nach folgendem Schema frisch angesetzt: Fol(G-t)-RD2, Fol(p)-RD2 bzw. RD2 wurden in 10 mM Natriumphosphatpuffer (pH 7,4) zu 255 µM gelöst. 51 µM $A\beta_{1-42}$ wurden bei 21 °C unter leichtem Schütteln für 4,5 h in 10 mM Natriumphosphatpuffer (pH 7,4) inkubiert, um zytotoxische Aβ-Oligomere zu erhalten. Anschließend wurden 255 µM Fol(G-t)-RD2, Fol(p)-RD2 bzw. RD2 hinzugefügt und für weitere 40 min ohne Schütteln inkubiert. Inkubiertes $A\beta_{1-42}$ sowie Puffer ohne Zugabe von Peptiden dienten als Positiv- und Negativkontrollen. 5 µl der Proben wurden in Fünffachbestimmung zu den Zellen gegeben und bei 37 °C und 5 % CO_2 für 24 h inkubiert. Die finalen Konzentrationen betrugen 5 µM Peptide und 1 µM $A\beta_{1-42}$. Der MTT-Zellviabilitätstest wurde nach Herstellerangaben durchgeführt (Cell Proliferation Kit I (MTT); Roche, Basel, Schweiz). Der Versuch wurde für Fol(G-t)-RD2 und RD2 insgesamt dreimal und für Fol(p)-RD2 einmal durchgeführt. Der arithmetische Mittelwert aller Messungen wurde kalkuliert. Die Ergebnisse sind als prozentuale MTT-Reduktion bezogen auf die Extinktion der Kontrollzellen ohne Probenzugabe dargestellt. Normalverteilte Daten wurden mit einer einfaktoriellen Varianzanalyse (ANOVA; engl. *analysis of variance*) mit einem Tukey-Post-hoc-Test analysiert.

4.1.3 Inkubation der Folsäure-RD2-Konjugate in künstlichem Magen- und Darmsaft, humanem Blutplasma und humanen Lebermikrosomen sowie Probenaufbereitung für die Analyse

Künstlicher Magen- und Darmsaft wurden gemäß des Europäischen Arzneibuchs 7.0 hergestellt. Zur Herstellung des künstlichen Magensafts (SGF; engl. *simulated gastric fluid*) wurde destilliertes Wasser mit 80 mM Salzsäure angesäuert und anschließend 2 mg/mL Natriumchlorid sowie 3,2 mg/mL Pepsin aus dem Schweinemagen (Carl Roth,

Karlsruhe, Deutschland; EC-Nr. 3.4.23.1; CAS-Nr. 9001-75-6; Best.-Nr. 0230.1; ≥ 0,5 Einheiten/mg Ph. Eur.) hinzugefügt. Der finale pH-Wert lag bei 1. Künstlicher Darmsaft (SIF; engl. *simulated intestinal fluid*) wurde hergestellt, indem eine 0,2 M Kaliumdihydrogenphosphat-Lösung mit 15,4 mM Natriumhydroxid versetzt und 10 mg/mL Pankreas-Pulver aus dem Schweinepankreas (Sigma-Aldrich, St. Louis, USA; CAS-Nr. 8049-47-6; Best.-Nr. P7545; 8x USP) hinzugefügt wurde. Der finale pH-Wert lag bei 6,8.

Die humanen Blutplasmaproben stammten von einer freiwilligen weiblichen Spenderin. K_3- Ethylendiamintetraacetat (EDTA) diente als Gerinnungshemmer. Die Blutproben wurden bei 3.000 *g* und 4 °C für 10 min zentrifugiert, um das zellfreie Plasma zu erhalten.

Gepoolte humane Lebermikrosomen (Sekisui XenoTech, Kansas City, USA; Best.-Nr. H1000, Charge 0710494) wurden in einem Nicotinamidadenindinukleotidphosphat (NADPH)-regenerierenden System (NRS) zu einer finalen Konzentration von 4,8 mg/mL verdünnt. Das NRS diente der permanenten Aktivierung der Enzyme der Cytochrom P450 Enzymfamilie (CYP). Es bestand aus 1,3 mM $NADP^+$, 3,3 mM Glukose-6-Phosphat, 0,4 Einheiten/mL Glukose-6-Phosphat-Dehydrogenase und 3,3 mM Magnesiumchlorid in 100 mM Kaliumphosphatpuffer (pH 7,4).

150 µM der Folsäure-RD2-Konjugate wurden in SGF, SIF, humanem Blutplasma und humanen Lebermikrosomen bei 37 °C unter leichtem Schütteln in Dreifachansätzen inkubiert. Als Referenzwert für das unmetabolisierte Konjugat zum Zeitpunkt Null wurden die Peptide zu den Medien gegeben und die Inkubation direkt beendet. Darüber hinaus wurden die Peptide in destilliertem Wasser für 0 und 24 h inkubiert, um den Einfluss einer möglichen Instabilität bei 37 °C berücksichtigen zu können. Die Inkubation wurde gestoppt, indem die Proteine mit 3 % *(w/v)* Trichloressigsäure (TCA; engl. *trichloroacetic acid*) gefällt wurden. Für die Extraktion der Folsäure-RD2-Konjugate sowie deren Spaltprodukte wurden die Proben bei 14.000 *g* und 4 °C für 5 min zentrifugiert. Der Überstand, der die Peptide enthielt, wurde abgenommen und bis zur Analyse bei -80 °C gelagert. Präzipitiertes Medium ohne Peptide diente als Kontrolle.

4.1.4 Intravenöse Injektion der Folsäure-RD2-Konjugate und Probenaufbereitung für die Analyse

Jeweils drei männlichen Wildtyp-C57BL/6J-Mäusen (12 Wochen) wurde intravenös (i.v.) Fol(G-t)-RD2 oder Fol(p)-RD2 verabreicht. Dabei wurde die applizierte Konzentration der Folsäure-RD2-Konjugate so angepasst, dass sie einer RD2-Konzentration von 3,3 mg/kg entsprach. Das heißt, es wurden 4,29 mg/kg Fol(G-t)-RD2 sowie 4,19 mg/kg Fol(p)-RD2

verabreicht. Die Konjugate wurden zur i.v. Injektion in 0,9 %-iger Natriumchlorid-Lösung gelöst. Die i.v. Injektion erfolgte in die Schwanzvene. 60 min nach Applikation wurden die Mäuse mit Isofluran anästhesiert und mit einer Heparin-enthaltenden Spritze Blutproben mittels Herzpunktion entnommen. Anschließend wurden die Mäuse finalisiert. Das Blut wurde bei 3.000 *g* und 4 °C für 5 min zentrifugiert, um zellfreies Plasma zu erhalten. Die Proben wurden bis zur Analyse bei -20 °C gelagert.

Für die Quantifizierung von RD2 wurde interner Standard (Endkonzentration: 16,7 ng/mL) zu den entnommenen Plasmaproben hinzugefügt. Plasma unbehandelter Mäuse sowie die eingesetzten Stammlösungen mit und ohne internen Standard dienten als Kontrolle. Alle Proben wurden wie zuvor beschrieben präzipitiert und die Folsäure-RD2-Konjugate, deren Spaltprodukte sowie der interne Standard extrahiert. Die Plasmaproben der behandelten Mäuse wurden jeweils dreimal extrahiert. Der Überstand wurde abgenommen und bis zur Analyse bei -80 °C gelagert.

4.1.5 Quantifizierung der Folsäure-RD2-Konjugate und RD2 mittels RP-HPLC

Die Stabilität der Folsäure-RD2-Konjugate in künstlichem Magen- und Darmsaft, humanem Plasma und humanen Lebermikrosomen (siehe Punkt 4.1.3) wurde mittels Umkehrphasen- Hochleistungsflüssigkeitschromatographie (RP-HPLC; engl. *reversed-phase high-performance liquid chromatography*) ermittelt. Das HPLC-System (Agilent Technologies, Santa Clara, USA; 1200-Serie) bestand aus einem manuellen Injektor, einer quartären Pumpe, einem temperierbaren Säulenofen und einem variablen Wellenlängen-Detektor. Die Chromatographie erfolgte mit einer C18-Säule (Agilent Technologies, Santa Clara, USA; ZORBAX 300SB-C18 5 µm, 4,6 x 250 mm) bei 25 °C und 214 nm mit einer Flussrate von 1 mL/min. Das Injektionsvolumen der Proben betrug 20 µL. Die mobilen Phasen bestanden aus (A) Acetonitril mit 0,15 % (*v/v*) Trifluoressigsäure (TFA; engl. *trifluoroacetic acid*) und (B) destilliertem Wasser mit 0,15 % TFA. Die Laufbedingungen wurden so etabliert, dass die beiden Isomere der Folsäure-RD2-Konjugate voneinander, von abgespaltenem RD2 und von den extrahierten Bestandteilen des Mediums getrennt wurden. Die Laufbedingungen für Fol(G-t)-RD2 und Fol(p)-RD2 sind in Tabelle 4.1 gelistet. Die Chromatogramme wurden mit der Agilent Software ChemStation (G2175BA, B03.01) aufgenommen und analysiert. Die Summe der Peakflächen der beiden unmetabolisierten Konjugat-Isomere nach verschiedenen Inkubationszeiten wurde auf die Summe der Peakflächen der beiden Konjugat-Isomere nach sofortiger Extraktion normiert. Die Peakfläche des entstandenen RD2s wurde auf die RD2-Peakfläche normiert, die detektiert wird, wenn RD2 in gleicher molarer Konzentration

wie die Folsäure-RD2-Konjugate zum Zeitpunkt Null vorliegt. Normierte Peakflächen jeder Dreifachmessung wurden gemittelt und die Daten als Mittelwert ± Standardabweichung angegeben.

Tabelle 4.1: RP-HPLC-Laufbedingungen für die Trennung der beiden Isomere der Folsäure-RD2-Konjugate sowie RD2.

Mobile Phase A: Acetonitril mit 0,15 % TFA. Mobile Phase B: Wasser mit 0,15 % TFA.

	Fol(G-t)-RD2			Fol(p)-RD2		
Schritt	**Zeit [min]**	**Mobile Phase A [%]**	**Mobile Phase B [%]**	**Zeit [min]**	**Mobile Phase A [%]**	**Mobile Phase B [%]**
1	0	10	90	0	10	90
2	11	10	90	11	10	90
3	19	14	86	21	15	85
4	33	14	86	40	15	85

4.1.6 Massenbestimmung der Folsäure-RD2-Konjugate und deren Metaboliten mittels UHPLC-ESI-QTOF-MS

Ein Teil der Proben des *in vitro* inkubierten Fol(G-t)-RD2s (siehe Punkt 4.1.3) wurde zusätzlich zur Analyse mittels RP-HPLC (siehe Punkt 4.1.5) auch mittels Ultra-Hochleistungsflüssigkeitschromatographie Elektrospray-Ionisation Quadrupol-Flugzeitmassenspektrometrie (UHPLC-ESI-QTOF-MS; engl. *ultra high-performance liquid chromatography electrospray ionization quadrupole time-of-flight mass spectrometry*) gemessen, um über die Identität der Peptide, die bei der HPLC-Analyse lediglich als Peaks im Chromatogramm auftauchten, eine präzise Aussage treffen zu können. Dazu wurden die Proben 1:50 in einem Wasser/Acetonitril/Ameisensäure-Gemisch (85/15/0,1 % (*v/v*)) verdünnt. Darüber hinaus wurden die murinen Plasmaproben der *in vivo* metabolisierten Folsäure-RD2-Konjugate (siehe Punkt 4.1.4) mit dieser Methode analysiert. Unterschiede in der Ionisierungsstärke von Fol(G-t)-RD2 und RD2 wurden ermittelt, indem die Peakflächen gleicher Peptid-Konzentrationen in einem Wasser/Acetonitril/Ameisensäure-Gemisch (85/15/0,1 % (*v/v*)) miteinander verglichen wurden.

Es wurde ein Agilent UHPLC-ESI-QTOF-MS-System verwendet. Das UPLC-System (Agilent 1290 Infinity Serie) bestand aus einem Autosampler, einer binären Pumpe und einem temperierbaren Säulenofen. Über eine ESI-Schnittstelle war daran ein QTOF-MS (Agilent Q-TOF 6250) gekoppelt. Dieses Massenspektrometer hat eine Auflösung von

20000. Die Chromatographie erfolgte mit einer C18-Säule (Waters, Milford, USA; Acquity UPLC BEH C18 1,7 µm, 2,1 x 100 mm) bei 50 °C und einer Flussrate von 500 µL/min. Das Injektionsvolumen der Proben betrug 20 µL. Die mobilen Phasen bestanden aus (A) Acetonitril mit 0,025 % (*v/v*) Heptafluorbuttersäure (HFBA; engl. *heptafluorobutyric acid*) und 1 % Ameisensäure sowie (B) destilliertem Wasser mit 0,025 % (*v/v*) HFBA und 1 % Ameisensäure. Die Laufbedingungen für Fol(G-t)-RD2 und Fol(p)-RD2 sind in Tabelle 4.2 gelistet. Die Detektion erfolgte mit einem QTOF-Detektor im ESI-positivem Ionisierungsmodus in einem Massenbereich von *m/z* 100 bis 1000. Die Instrumentenkontrolle und Datenauswertung erfolgte mit der MassHunter-Software LC-MS Data Acquisition B.05.01 (Agilent Technologies, Palo Alto, USA).

Tabelle 4.2: UHPLC-Laufbedingungen für die Detektion der Folsäure-RD2-Konjugate und ihrer Metaboliten.
Mobile Phase A: Acetonitril mit 0,025 % HFBA und 1 % Ameisensäure. Mobile Phase B: Wasser mit 0,025 % HFBA und 1 % Ameisensäure.

Schritt	Zeit [min]	Mobile Phase A [%]	Mobile Phase B [%]
1	0,0	5	95
2	2,0	5	95
3	2,1	22	78
4	5,0	25	75

4.2 Ergebnisse

4.2.1 Die beiden Folsäure-RD2-Konjugate besitzen kein zytotoxisches Potential und können die $A\beta_{1-42}$-induzierte Zytotoxizität reduzieren

Um zu zeigen, dass Fol(G-t)-RD2 und Fol(p)-RD2 kein zytotoxisches Potential besitzen und die $A\beta_{1-42}$-induzierte Zytotoxizität reduzieren, wie es bereits für unkonjugiertes RD2 gezeigt werden konnte, wurde ein MTT-Zellviabilitätstest mit PC12-Zellen durchgeführt. Der Test wurde zusätzlich mit RD2 durchgeführt, um einen direkten Vergleichswert zu erhalten. Die Inkubation mit den Zellen erfolgte zum einen mit 5 µM Fol(G-t)-RD2, Fol(p)-RD2 bzw. RD2 und zum anderen mit 1 µM aggregiertem $A\beta_{1-42}$, das mit und ohne 5 µM Fol(G-t)-RD2, Fol(p)-RD2 bzw. RD2 vorinkubiert wurde. Puffer ohne Peptide diente als Referenzwert für hundertprozentige Zellviabilität.

Die Ergebnisse zeigten, dass die Zellviabilität unter Zugabe von Fol(G-t)-RD2, Fol(p)-RD2 bzw. RD2 gegenüber der Puffer-Kontrolle nicht signifikant verändert wurde und somit die

Peptide kein zytotoxisches Potential besitzen (Abb. 4.2). Darüber hinaus konnten Fol(G-t)-RD2, Fol(p)-RD2 und RD2 die Zytotoxizität des aggregierten $A\beta_{1-42}$ (Zellviabilität = 36 ± 3 %) signifikant reduzieren (Zellviabilität nach Inkubation mit Fol(G-t)-RD2 = 55 ± 16 %, mit Fol(p)-RD2 = 48 ± 17 % und mit RD2 = 64 ± 19 %).

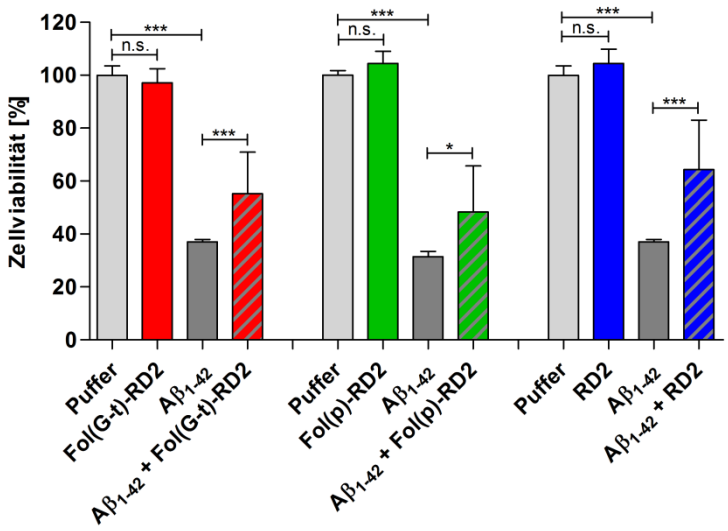

Abbildung 4.2: Zellviabilitätstest mit Fol(G-t)-RD2, Fol(p)-RD2, RD2 und Aβ1-42.
Das zytotoxische Potential von Fol(G-t)-RD2, Fol(p)-RD2 und RD2 sowie deren Einfluss auf die $A\beta_{1-42}$-induzierte Zytotoxizität wurde mithilfe eines MTT-Zellviabilitätstests mit PC12-Zellen untersucht. Es wurden zum einen 5 µM Fol(G-t)-RD2, Fol(p)-RD2 bzw. RD2 und zum anderen 1 µM aggregiertes $A\beta_{1-42}$, vorinkubiert mit und ohne 5 µM Fol(G-t)-RD2, Fol(p)-RD2 bzw. RD2, eingesetzt. Die Extinktion unter Zugabe der Peptide wurde auf die Extinktion ohne Zugabe der Peptide (Puffer) normiert. Fol(G-t)-RD2, Fol(p)-RD2 und RD2 wirkten nicht zytotoxisch und konnten den negativen Einfluss des aggregierten $A\beta_{1-42}$ auf die Zellviabilität signifikant reduzieren. Die Daten sind dargestellt als Mittelwert ± Standardabweichung. Statistik: einfaktorielle ANOVA mit Tukey-Post-hoc-Test; *: $p \leq 0{,}05$; ***: $p \leq 0{,}001$; n.s.: nicht signifikant.

4.2.2 Analyse der Proben zur in vitro- und in vivo-Metabolisierung der beiden Folsäure-RD2-Konjugate mittels RP-HPLC und LC-MS

Für die Analyse der *in vitro*-Metabolisierung der beiden Folsäure-RD2-Konjugate mittels RP-HPLC wurden die beiden Isomere der Konjugate voneinander und von abgespaltenem RD2 sowie den extrahierten Bestandteilen der Medien getrennt. Abbildung 4.3 zeigt einen Ausschnitt der Chromatogramme zur Trennung der Peptide in Wasser. Die Trennung der Isomere erforderte isokratische Laufbedingungen, wodurch die Peakschärfe verringert wurde. Bei den Fol(G-t)-RD2-Isomeren deuteten sich zudem

Doppelspitzen an, die durch cis/trans-Isomere des N-terminalen Prolins bedingt sein könnten. Die Isomere der Folsäure-RD2-Konjugate wurden getrennt, damit mögliche Stabilitätsunterschiede zwischen den Isomeren festgestellt werden konnten.

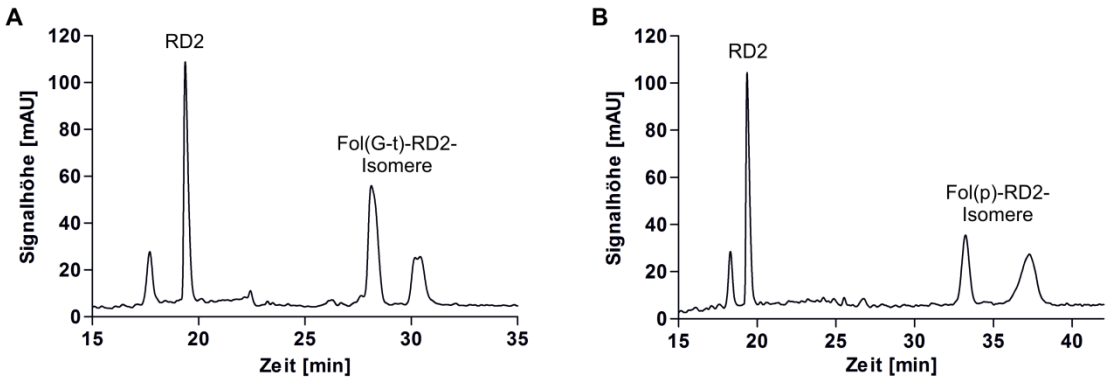

Abbildung 4.3: Chromatogramme der mittels RP-HPLC getrennten Fol(G-t)-RD2- bzw. Fol(p)-RD2-Isomere und RD2 in Wasser.

100 µM RD2 sowie 100 µM Fol(G-t)-RD2 **(A)** bzw. Fol(p)-RD2 **(B)** in Wasser wurden mittels RP-HPLC getrennt und analysiert. Die chromatographischen Bedingungen wurden so gewählt, dass die beiden Isomere des Fol(G-t)-RD2s und des Fol(p)-RD2s voneinander getrennt wurden.

Zur Bestimmung der Extraktionsqualität der Folsäure-RD2-Konjugate und des RD2s aus künstlichem Magen- (SGF) und Darmsaft (SIF), Plasma und Lebermikrosomen wurde die Peakfläche der Peptide nach Extraktion aus den Medien mit der Peakfläche der Peptide in Wasser verglichen. Tabelle 4.3 zeigt eine Übersicht der Ergebnisse. Die Extraktion erfolgte durch Proteinpräzipitation mittels TCA und anschließender Zentrifugation, da sich diese Methode in der Vergangenheit für die Extraktion von RD2 aus allen Medien bewährt hatte. Da die Metabolisierung zu RD2 im Fokus dieser Studie stand und nur eine Aussage über die Möglichkeit einer Folsäure-Abspaltung und keine Quantifizierung erfolgen sollte, war eine etwas geringere Extraktionsqualität der Folsäure-RD2-Konjugate aus manchen Medien vertretbar.

Tabelle 4.3: Extraktionsqualität der Folsäure-RD2-Konjugate und des RD2s aus SGF, SIF, Plasma und Lebermikrosomen.

	Fol(G-t)-RD2	Fol(p)-RD2	RD2
	Extraktionsqualität [%]		
SGF	94	99	86
SIF	80	85	87
Plasma	67	72	92
Lebermikrosomen	85	72	83

Um die Identität von Fol(G-t)-RD2, Fol(p)-RD2 und RD2 zu bestätigen und potentielle weitere Metaboliten zu identifizieren, wurden Messungen mittels LC-MS durchgeführt. Darüber hinaus wurde bei den *in vivo*-Versuchen RD2 mithilfe eines internen Standards quantifiziert. Die monoisotopische Masse von Fol(G-t)-RD2 betrug 2079,06 Da, von Fol(p)-RD2 2021,05 Da, von RD2 mit verbliebenem Glycin-Linker (G-RD2) 1651,90 Da, von RD2 1597,91 Da und vom internen Standard 1583,90 Da. RD2 wurde ausschließlich mit *m/z* $533{,}64^{3+}$, G-RD2 mit *m/z* $551{,}63^{3+}$ und der interne Standard mit *m/z* $528{,}98^{3+}$ detektiert, was jeweils dem dreifachen Ladungszustand $(M+3H)^{3+}$ der Peptide entspricht. Fol(G-t)-RD2 und Fol(p)-RD2 wurden in der dreifach (*m/z* $693{,}69^{3+}$ und *m/z* $674{,}69^{3+}$) sowie vierfach (*m/z* $520{,}52^{4+}$ und *m/z* $506{,}26^{4+}$) geladenen Spezies detektiert. Dies wurde bei der Bestimmung der Ionisierungseffizienz mit einbezogen. Die Ionisierungseffizienz wurde durch Vergleich der Peakflächen der einzelnen Komponenten in Wasser ermittelt. Bei gleichen Konzentrationen ionisiert RD2 um den Faktor 2,9 bzw. 6,4 besser als Fol(G-t)-RD2 bzw. Fol(p)-RD2. Bei G-RD2, für das keine Referenz vorlag, konnte davon ausgegangen werden, dass es sich ähnlich wie RD2 verhielt. Idealerweise sollte die Ionisierungseffizienz aufgrund möglicher Matrixeffekte in allen Medien untersucht werden. Für eine qualitative Überprüfung der Metabolisierung ohne Quantifizierung war der berechnete Faktor für Wasser jedoch ausreichend.

4.2.3 Fol(G-t)-RD2 wird in vitro bevorzugt in Plasma metabolisiert, während Fol(p)-RD2 unverändert bleibt

Um zu überprüfen, ob die beiden Folsäure-RD2-Konjugate Fol(G-t)-RD2 und Fol(p)-RD2 im Gastrointestinaltrakt stabil bleiben, im Blut oder der Leber aber zum unkonjugierten Wirkstoff, sprich RD2 ohne Ligand, metabolisiert werden, wurden die Peptide in SGF, SIF, humanem Blutplasma und humanen Lebermikrosomen inkubiert. Unmetabolisiertes

Folsäure-RD2-Konjugat sowie abgespaltenes RD2 wurden per RP-HPLC detektiert. Im Folgenden ist immer der prozentuale Anteil der Summe der beiden unmetabolisierten Konjugat-Isomere angegeben. In den Abbildungen 4.4 bis 4.6 werden die Isomere dennoch getrennt voneinander dargestellt, um mögliche Unterschiede im Metabolisierungsverhalten aufzuzeigen.

In SGF blieb Fol(G-t)-RD2 über 24 h fast vollständig stabil (82,0 ± 4,2 %). Dabei wurde das Konjugat nur zu 5,5 ± 0,8 % zu RD2 abgebaut (Abb. 4.4 A). Vergleicht man dieses Ergebnis mit der Stabilität von Fol(G-t)-RD2 in Wasser (fast vollständige Stabilität und Bildung von < 5 % RD2) (Abb. 4.6 A), lässt sich daraus schlussfolgern, dass der Abbau von Fol(G-t)-RD2 in SGF nicht enzymatisch bedingt ist. In SIF wurde Fol(G-t)-RD2 nach 2 h zu 16,9 ± 3,0 %, nach 8 h zu 40,3 ± 2,1 % und nach 24 h zu 67,3 ± 1,4 % metabolisiert, wobei bis zu 41,1 ± 2,9 % RD2 nach 24 h entstanden sind (Abb. 4.4 B). In Plasma wurde das Konjugat schneller zu RD2 metabolisiert, sodass bereits nach 8 h 77,0 ± 1,6 % des Konjugats abgebaut waren und 47,7 ± 1,8 % RD2 entstanden sind (Abb. 4.4 C). Auch in den Lebermikrosomen wurde die Folsäure von RD2 zunehmend abgespalten, sodass nach 24 h nur noch 32,5 ± 0,8 % des Konjugats detektiert werden konnten und 24,3 ± 1,2 % RD2 entstanden sind (Abb. 4.4 D). In SGF, Plasma und Lebermikrosomen konnte kein Unterschied im Metabolisierungsverhalten zwischen den Konjugat-Isomeren festgestellt werden. In SIF zeigten sich geringe Unterschiede bei der Metabolisierungsgeschwindigkeit, die sich aber nach 24 h wieder relativierten.

Die Wiederfindungsrate für verbliebenes Fol(G-t)-RD2 addiert mit abgespaltenem RD2 lag nie bei 100 %. Betrachtet man die Stabilität des unkonjugierten RD2s in diesen Medien (Elfgen et al. 2018), kann man davon ausgehen, dass das in SGF und SIF entstandene RD2 in der untersuchten Zeitspanne nicht weiter abgebaut wurde, während für Plasma und Lebermikrosomen davon ausgegangen werden muss, dass ein geringer Anteil des abgespaltenen RD2s während der weiteren Inkubation wiederrum metabolisiert wurde. Darüber hinaus konnte durch eine Probenanalyse mittels LC-MS gezeigt werden, dass nicht nur RD2, sondern auch kleine Mengen G-RD2 gebildet wurden (Tabelle 4.4).

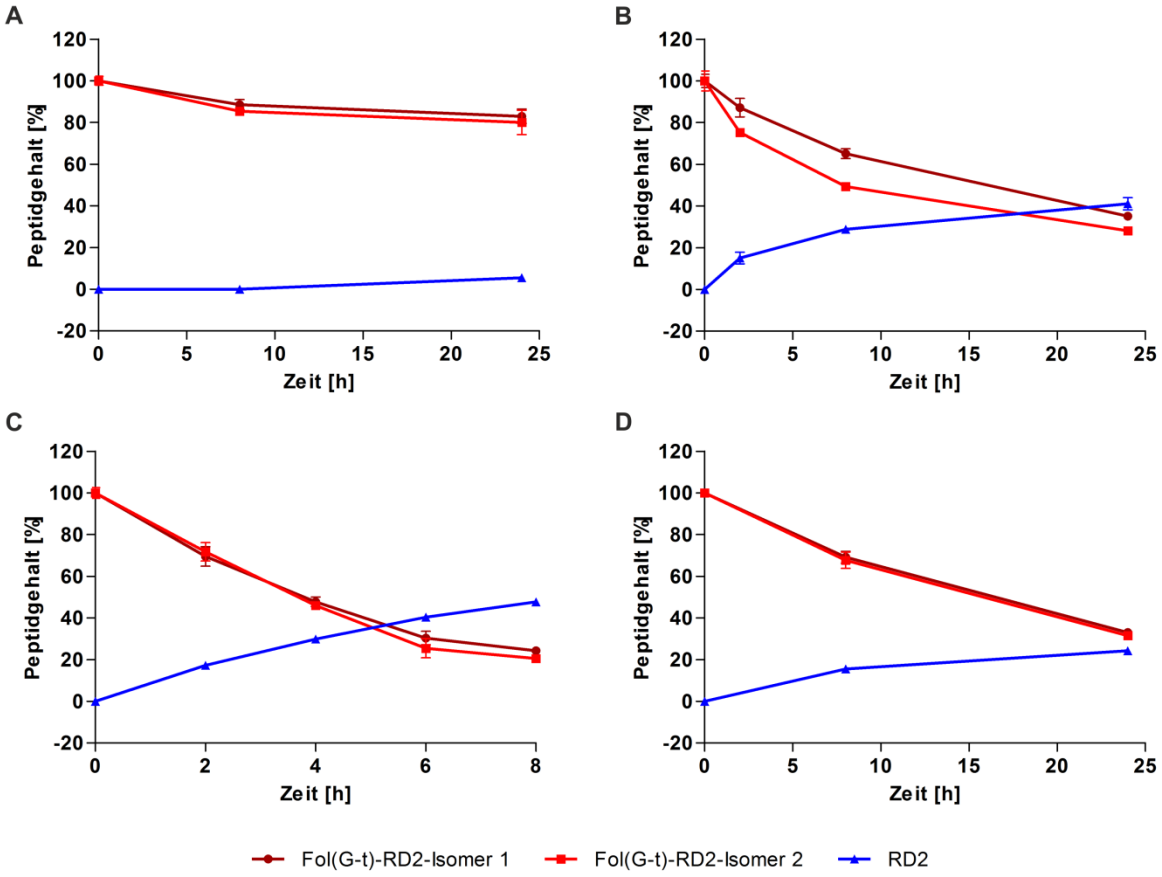

Abbildung 4.4: Stabilität von Fol(G-t)-RD2 in SGF, SIF, Plasma und Lebermikrosomen.
Fol(G-t)-RD2 wurde in SGF **(A),** SIF **(B)**, Plasma **(C)** und Lebermikrosomen **(D)** inkubiert und die Metabolisierung zu RD2 mittels RP-HPLC analysiert. Die beiden Isomere konnten getrennt werden und werden hier als Isomer 1 und 2 bezeichnet. Fol(G-t)-RD2 blieb in SGF fast vollständig stabil, während es in SIF, Plasma und Lebermikrosomen zunehmend zu RD2 metabolisiert wurde. Am schnellsten wurde dabei Fol(G-t)-RD2 in Plasma abgebaut. Die Daten sind dargestellt als Mittelwert ± Standardabweichung (n = 3).

Tabelle 4.4: Ungefähres molares Mengenverhältnis des Fol(G-t)-RD2s zu RD2 und zu G-RD2 in SGF, SIF, Plasma und Lebermikrosomen.
Die 2,9-fach stärkere Ionisierung von RD2 und G-RD2 gegenüber Fol(G-t)-RD2 wurde mit in die Berechnungen einbezogen.

	Mengenverhältnis	
	Fol(G-t)-RD2 / RD2	**Fol(G-t)-RD2 / G-RD2**
SGF, 24 h	25,3	1589,6
SIF, 8 h	2,8	224,9
Plasma, 8 h	0,5	34,0
Lebermikrosomen, 24 h	1,9	13,3

Das zweite Folsäure-RD2-Konjugat, Fol(p)-RD2, blieb hingegen in SGF, SIF und Lebermikrosomen über 24 h und in Plasma sogar über 3 Tage fast vollständig stabil (88,8 %, 88,3 %, 82,8 % bzw. 82,7 %) und wurde nicht zu RD2 metabolisiert (Abb. 4.5). In Wasser ohne Zusatz von Enzymen blieb das Konjugat über 24 h vollständig stabil (Abb. 4.6 B). In keinem der Medien gab es einen Unterschied im Metabolisierungsverhalten der beiden Konjugat-Isomere.

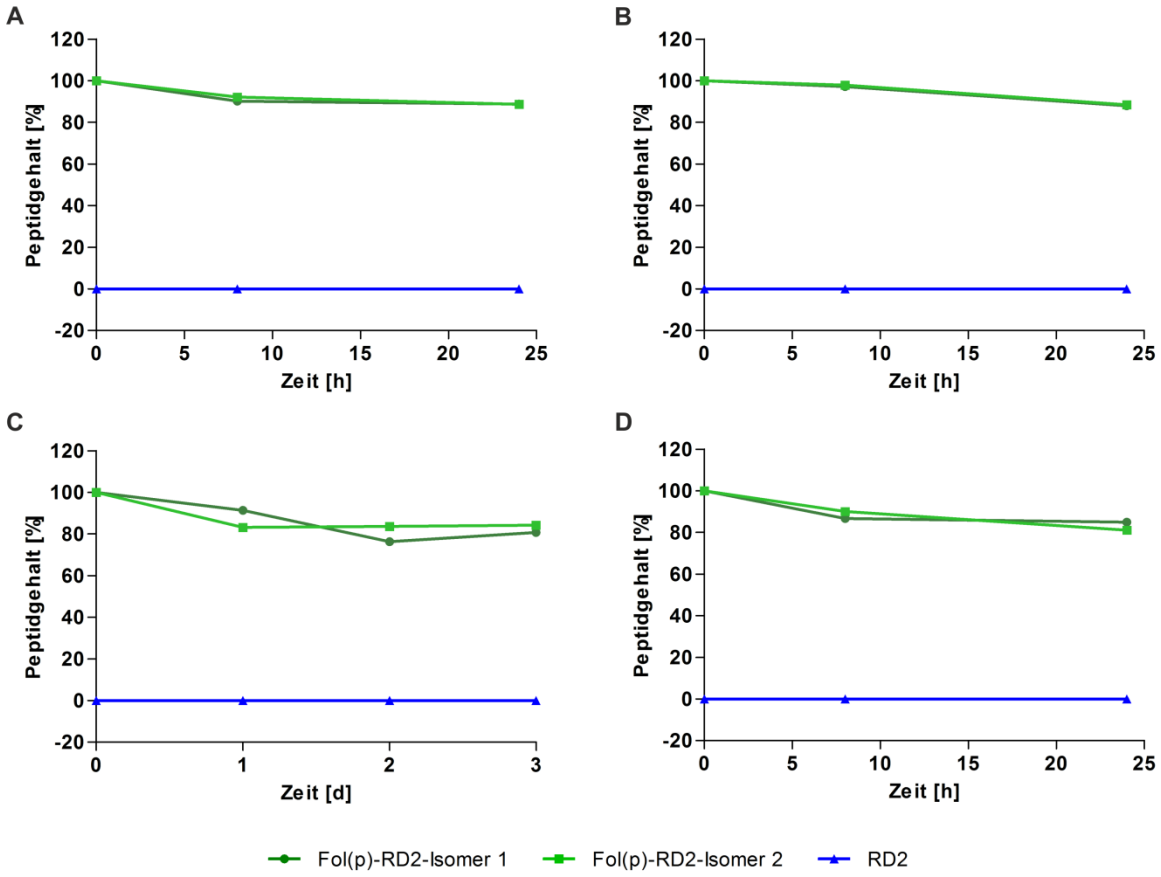

Abbildung 4.5: Stabilität von Fol(p)-RD2 in SGF, SIF, Plasma und Lebermikrosomen.
Fol(p)-RD2 wurde in SGF **(A),** SIF **(B)**, Plasma **(C)** und Lebermikrosomen **(D)** inkubiert und die Metabolisierung zu RD2 mittels RP-HPLC analysiert. Die beiden Isomere konnten getrennt werden und werden hier als Isomer 1 und 2 bezeichnet. Fol(p)-RD2 blieb in allen Medien über die gemessene Zeit fast vollständig stabil. Es wurde kein RD2 abgespalten. Die Daten stellen Einfachbestimmungen dar.

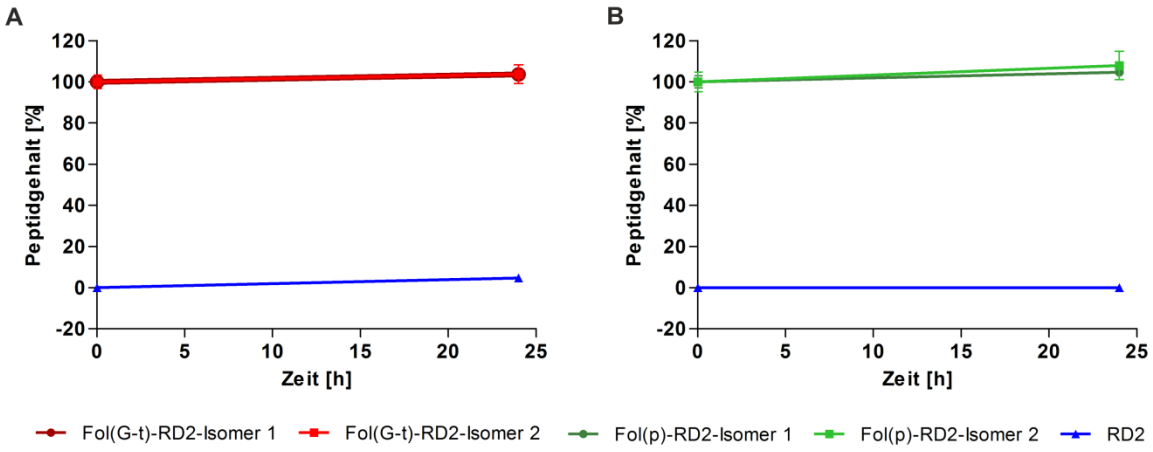

Abbildung 4.6: Stabilität von Fol(G-t)-RD2 und Fol(p)-RD2 in Wasser.
Fol(G-t)-RD2 und Fol(p)-RD2 wurden 0 und 24 h in destilliertem Wasser bei 37 °C inkubiert und die Metabolisierung mittels RP-HPLC analysiert. Die beiden Isomere konnten getrennt werden und werden hier als Isomer 1 und 2 bezeichnet. **(A)** Fol(G-t)-RD2 blieb über 24 h fast vollständig stabil. Es wurden nur geringe Mengen (< 5 %) RD2 gebildet. **(B)** Fol(p)-RD2 blieb vollständig stabil. Die Daten sind dargestellt als Mittelwert ± Standardabweichung (n = 3).

4.2.4 Fol(G-t)-RD2 wird im Gegensatz zu Fol(p)-RD2 nach i.v. Injektion in vivo zu RD2 metabolisiert

Die Metabolisierung der beiden Folsäure-RD2-Konjugate zum unkonjugierten Wirkstoff RD2 wurde zusätzlich *in vivo* in Mäusen untersucht. Dazu wurden beide Konjugate i.v. verabreicht (4,29 mg/kg Fol(G-t)-RD2 bzw. 4,19 mg/kg Fol(p)-RD2; entspricht 3,3 mg/kg bzgl. der molaren RD2-Konzentration) und die Konjugate sowie deren Metaboliten im Blutplasma 60 min nach Applikation mittels LC-MS nachgewiesen. Bezogen auf die ermittelten Konzentrationen des vor der Extraktion hinzugefügten internen Standards wurde die RD2-Konzentration bestimmt.

Nach Injektion von Fol(p)-RD2 konnte ausschließlich Fol(p)-RD2 im Plasma detektiert werden, was bedeutet, dass Fol(p)-RD2 innerhalb von 60 min nicht zu RD2 metabolisiert wurde.

Für Fol(G-t)-RD2 konnte eine Metabolisierung zu RD2 und Metaboliten mit monoisotopischen Massen von 1903,03 Da und 1783,99 Da, aber keine Metabolisierung zu G-RD2, nachgewiesen werden. Fol(G-t)-RD2 wurde allerdings innerhalb von 60 min nicht vollständig metabolisiert. Das Verhältnis von Fol(G-t)-RD2 zu RD2 lag bei ca. 9:1 (Ionisierungsfaktoren der Peptide mit einberechnet). Durch den internen Standard konnte

die Menge des nach 60 min im Plasma enthaltenen RD2s auf 27,6 ± 5,8 ng/mL bestimmt werden (Tabelle 4.5).

Tabelle 4.5: Detektion von Fol(G-t)-RD2 und dessen Metaboliten in Maus-Plasma 60 min nach i.v. Injektion von 4,29 mg/kg Fol(G-t)-RD2.

Die Proben wurden jeweils dreimal extrahiert, mittels LC-MS analysiert und die Peakflächen kalkuliert. Das Mengenverhältnis zwischen Fol(G-t)-RD2 und RD2 ist die Peakfläche von Fol(G-t)-RD2 dividiert durch die Peakfläche von RD2. Die Quantifizierung des abgespaltenen RD2s erfolgte mithilfe des internen Standards.

	Maus 1			**Maus 2**			**Maus 3**		
	Peakflächen								
Fol(G-t)-RD2	33800	52502	50500	26500	48564	52862	18600	40372	44595
RD2	8700	17507	14606	8300	16224	18602	6200	19280	17004
1903,03 Da	26000	53040	47761	19700	41225	43644	19000	50314	52278
1783,99 Da	10600	14400	14319	7800	12495	13496	6400	14224	14165
Interner Standard	4400	9328	7916	6800	9882	9306	3900	10021	9507
	Kalkulierte Mengenverhältnisse und Konzentrationen								
Mengenverhältnis Fol(G-t)-RD2 / RD2	11,3	8,7	10,0	9,3	8,7	8,2	8,7	6,1	7,6
RD2-Konz. [ng/mL]	37	29	25	19	26	30	20	33	29

Fol(G-t)-RD2 hat eine Masse von 2079,06 Da und die Summenformel $C_{86}H_{136}N_{41}O_{21}$. Die beiden zusätzlich detektierten Massen (1903,03 Da und 1783,99 Da) entsprechen den Summenformeln $C_{79}H_{130}N_{36}O_{20}$ und $C_{72}H_{125}N_{35}O_{19}$ (kalkuliert mit http://www.chemcalc.org/mf_finder). Die Massendifferenz zu Fol(G-t)-RD2 beträgt somit -176,03 Da und -295,07 Da. Diese Differenz entspricht den Summenformeln $C_7H_6N_5O$ und $C_{14}H_{11}N_6O_2$ (kalkuliert mit http://www.chemcalc.org/mf_finder). Abbildung 4.7 zeigt potentielle Bruchstellen in der Folsäure-Einheit von Fol(G-t)-RD2, die mit den Differenzen der Massen und der Summenformeln übereinstimmen. Eine endgültige Bestätigung der Ergebnisse mittels MS/MS-Fragmentierungen der beiden Metaboliten steht noch aus.

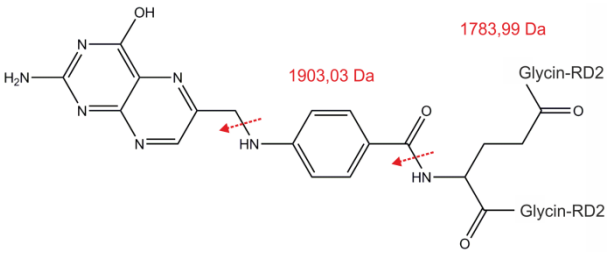

Abbildung 4.7: Potentielle Schnittstellen zweier Fol(G-t)-RD2-Metaboliten.

Die Massen der Fol(G-t)-RD2-Metaboliten betragen 1903,03 Da bzw. 1783,99 Da und ihre Summenformeln lauten $C_{79}H_{130}N_{36}O_{20}$ und $C_{72}H_{125}N_{35}O_{19}$. Diese Ergebnisse passen zu den eingezeichneten potentiellen Schnittstellen im Folsäure-Molekül. Die Bindungsstellen des Folsäure-Moleküls zu Glycin-RD2 beider Fol(G-t)-RD2-Isomere sind eingezeichnet.

5 Diskussion

AD ist eine neurodegenerative Erkrankung, die durch eine progressive Abnahme kognitiver Funktionen charakterisiert ist und für die bislang noch kein präventives oder kuratives Medikament zugelassen ist. Die meisten krankheitsmodifizierenden therapeutischen Strategien sind gegen Aβ gerichtet (Folch et al. 2016, Godyn et al. 2016), dessen Aggregation nach heutigem Kenntnisstand die Grundlage für die Entstehung und Progression der AD bildet (Selkoe and Hardy 2016). Eine vielversprechende Strategie ist dabei, den Fokus auf die Eliminierung von Aβ-Oligomeren zu legen, die den vermeintlich neurotoxischsten Aβ-Aggregationszustand darstellen (Lue et al. 1999, McLean et al. 1999, Ferreira and Klein 2011, Benilova et al. 2012, Larson and Lesne 2012). Auf diesem Therapieansatz basieren die beiden D-enantiomeren Peptide D3 und RD2.

5.1 *In vitro*- und *in vivo*-Effizienz von RD2

Die Wirksamkeit von D3 für die AD-Therapie konnte bereits in zahlreichen Studien *in vitro* und *in vivo* erfolgreich gezeigt werden (van Groen et al. 2008, van Groen et al. 2009, Funke et al. 2010, Funke et al. 2012, van Groen et al. 2012, van Groen et al. 2013, Olubiyi et al. 2014, Brener et al. 2015, Klein et al. 2017). Die Wirksamkeit des rational umstrukturierten D3-Derivats RD2 wurde hingegen erst kürzlich detailliert dargelegt (van Groen et al. 2017). Die Untersuchungen zeigten, dass RD2 nicht toxisch auf Zellen wirkte und sogar die Aβ-induzierte Zytotoxizität verringerte. RD2 hatte eine ähnliche Affinität zu Aβ-Monomeren wie D3 (K_d im mikromolaren Bereich), zeigte im Vergleich zu D3 jedoch eine effizientere Eliminierung von Aβ-Oligomeren. Darüber hinaus konnten kognitive Defizite transgener AD-Mäuse durch intraperitoneale Behandlung mit RD2 verbessert werden.

Um den Einfluss von RD2 auf die durch Aβ-Nuklei beschleunigte Aggregation von Aβ-Monomeren zu untersuchen, wurde ein Fluoreszenz-basierter Assay etabliert und durchgeführt, bei dem die Aβ-Aggregationskinetik verfolgt werden kann. Dabei wurde die Aggregation von Aβ-Monomeren ohne und mit Aβ-Nuklei, die entweder mit oder ohne RD2 vorinkubiert wurden, analysiert. Es zeigte sich, dass RD2 den katalytischen Effekt der Aβ-Nuklei auf die Aβ-Aggregation signifikant verringert. Die Menge letztendlich gebildeter Fibrillen wurde allerdings nicht durch die Vorbehandlung der Nuklei mit RD2 beeinflusst. Das lässt darauf schließen, dass der beobachtete Effekt auf die Nuklei tatsächlich durch eine Reduzierung des katalytischen Potentials der Nuklei durch die Vorbehandlung mit RD2 und nicht durch verbliebenes freies RD2 verursacht wurde,

welches die gesamte Fibrillenbildung reduzieren würde, wie in einem Aggregationsassay ohne Nuklei gezeigt wurde.

Die Ergebnisse der *in vitro*- und *in vivo*-Studien lassen darauf schließen, dass RD2 ein vielversprechender krankheitsmodifizierender Wirkstoffkandidat für die Behandlung der AD darstellt.

5.2 Metabolisierung der D-Peptide D3 und RD2 und Bildung potentieller human-spezifischer Metaboliten

Im Rahmen dieser Arbeit wurden *in vitro* Untersuchungen zur Metabolisierung der beiden D-enantiomeren Peptide D3 und RD2 durchgeführt. Eine hohe Stabilität ist besonders wichtig, wenn Peptide oral verabreicht werden sollen, da bei dieser Applikationsform Wirkstoffe zahlreichen Metabolisierungseinflüssen ausgesetzt sind. Zunächst wurde eine Studie zur D3- und RD2-Stabilität sowie ihrer L-enantiomeren Äquivalente, L-D3 und L-RD2, in humanem künstlichen Magen- und Darmsaft (SGF und SIF) sowie Plasma und Lebermikrosomen durchgeführt. Eine solch ausführliche Stabilitätsstudie zwischen Enantiomeren der gleichen Aminosäuresequenz wurde zuvor noch nicht publiziert, vor allem nicht in künstlichem Magen- und Darmsaft. Hierbei zeigte sich, dass sowohl D3 als auch RD2 in allen untersuchten Medien wesentlich stabiler waren als ihre L-enantiomeren Äquivalente. In SGF und SIF blieben D3 und RD2 über 24 h vollständig stabil (89 und 100 %), während L-D3 und L-RD2 in SGF in der gleichen Zeit zu 70 bzw. 23 % und in SIF sogar innerhalb weniger Sekunden vollständig metabolisiert wurden. In Plasma wurden die D-Peptide über 20 Tage zu 70-90 % metabolisiert, während die L-Peptide bereits nach 2 h (L-D3) bzw. 2 Tagen (L-RD2) gänzlich abgebaut waren. Auch in Lebermikrosomen wurden die L-Peptide mehrere hundert Male schneller metabolisiert als die D-Peptide.

Obwohl D3 und RD2 genauso wie ihre L-enantiomeren Äquivalente mehrere potentielle Schnittstellen für Proteasen besitzen, die in den untersuchten Medien enthalten waren, wurden die Peptidbindungen bei den D-Peptiden nicht oder weniger erkannt. Daraus lässt sich schlussfolgern, dass oral verabreichtes D3 oder RD2 den Gastrointestinaltrakt auch ohne Protease-protektive Formulierung vollständig passieren würde. Dies spiegelt sich auch in pharmakokinetischen Studien wider, bei denen die D-Peptide ohne Formulierung (also nur in Lösung) oral verabreicht wurden und sie dennoch eine orale Bioverfügbarkeit von 60-80 % besaßen (Jiang et al. 2015, Leithold et al. 2016). Die hohe Resistenz gegenüber proteolytischem Abbau trägt darüber hinaus zu den langen Halbwertszeiten im Blut von über 40-60 h bei (Jiang et al. 2015, Leithold et al. 2016), wodurch eine lange

systemische Verfügbarkeit für den Transport zum Gehirn, dem Zielorgan der Wirkstoffe, ermöglicht wird. Obwohl die Leber das Organ ist, in dem die meisten Wirkstoffe am stärksten metabolisiert werden, sind D3 und RD2 bemerkenswert stabil gegenüber metabolischen Biotransformationsprozessen durch CYP-Enzyme, die häufig eine Hydroxylierung des Substrats bewirken (Lu 1976, Guengerich 2001).

Im menschlichen Organismus gibt es allerdings ein Enzym, das die oxidative Desaminierung speziell basischer und neutraler D-Aminosäurereste katalysiert, die D-Aminosäureoxidase (DAAO) (D'Aniello et al. 1993, Ohide et al. 2011, Yamanaka et al. 2012). Interessanterweise stellte RD2 auch kein Substrat für die DAAO dar, was darauf schließen lässt, dass die DAAO nur einzelne D-enantiomere Aminosäurereste, aber keine D-Peptide metabolisiert.

Des Weiteren zeigte sich, dass RD2 keinen Einfluss auf die Aktivität der DAAO und der in SGF, SIF, Plasma und Lebermikrosomen an der Peptid-Metabolisierung beteiligten Enzyme nimmt. Diese Untersuchungen sind von besonderer Bedeutung, da z.B. Substanzen, die die Enzymaktivität inhibieren, eine toxische Akkumulation anderer Substrate verursachen könnten.

In der Leber stattfindende metabolische Biotransformationsprozesse können zu einer Veränderung der physikochemischen Wirkstoff-Eigenschaften führen, wodurch deren Wirkung und Aufnahme in die Zielorgane verändert werden können und sie infolgedessen einen unerwünschten oder gar toxischen Effekt auf den Organismus haben könnten. Metaboliten, die während der sogenannten Phase I-Reaktionen gebildet werden, gelten als pharmakologisch reaktiver als Phase II-Metaboliten (U.S. Food and Drug Administration 2008). Daher ist es besonders wichtig den Phase I-Metabolismus eines Wirkstoffkandidaten zu untersuchen, was *in vitro* häufig mithilfe von Lebermikrosomen gemacht wird, die Phase I-Enzyme (hauptsächlich CYP-Enzyme) enthalten.

In einer Toxikologie-Studie mit Ratten und Affen, die oral mit RD2 in hohen Konzentrationen behandelt wurden, konnte gezeigt werden, dass RD2 in diesen Spezies keine unerwünschten Arzneimittelwirkungen hervorruft (unveröffentlichte Daten). Das bedeutet, dass in diesen Spezies möglicherweise auftretende Metaboliten keine toxische Wirkung besitzen. Vergleicht man die in Lebermikrosomen von Ratten und Affen gebildeten Metaboliten mit Metaboliten, die in humanen Lebermikrosomen entstehen, kann eine erste Einschätzung zur Wirkstoffsicherheit im Menschen gegeben werden.

In den insgesamt acht untersuchten verschiedenen Chargen humaner Lebermikrosomen wurden drei potentiell human-spezifische Metaboliten (HSM-1, -2 und -3) gefunden, von

denen HSM-1 und HSM-2 unter 5 % bezüglich der ursprünglich eingesetzten RD2-Konzentration ausmachten. HSM-3 hingegen stellte mit 30-50 % einen häufiger vorkommenden Metaboliten dar. Da der Anteil von HSM-1 und HSM-2 unter der von der FDA (amerikanische Lebens- und Arzneimittelbehörde; engl. *Food and Drug Administration*) angegebenen Grenze von 10 % lag, ab der ein Metabolit für eine genauere Sicherheitsbeurteilung in Betracht gezogen werden sollte (U.S. Food and Drug Administration 2008), wurden HSM-1 und HSM-2 nicht weiter untersucht. Der größere Metabolit, HSM-3, wurde hingegen detailliert analysiert. Die Struktur des Metaboliten HSM-3, die mittels Kernspinresonanz-Spektroskopie aufgeklärt werden konnte, entspricht RD2 mit einer Methylenbrücke zwischen Prolin (Position 1) und der Peptidbindung zu Threonin (Position 2). Diese Reaktion wird durch Formaldehyd induziert, dessen Konzentration in den Lebermikrosomen-Chargen, in denen HSM-3 gebildet wird, erhöht war. Die Modifizierung erwies sich als recht instabil und war reversibel zu RD2. Des Weiteren konnte in einem Zellviabilitätstest gezeigt werden, dass HSM-3 nicht zytotoxisch ist.

Aufgrund der Tatsache, dass die wenigen Metaboliten entweder in geringer Konzentration vorlagen oder nicht zytotoxisch und reversibel zu RD2 waren, ist nicht davon auszugehen, dass durch eine orale RD2-Applikation und der damit verbundenen Leberpassage unerwünschte Arzneimittelwirkungen im Menschen hervorgerufen werden.

5.3 Systemische Metabolisierung von RD2-Prodrugs, entwickelt zur Erhöhung der oralen Bioverfügbarkeit von RD2

Die Wirkstoff-Konjugation mit Liganden, die eine Rezeptor-vermittelte Endozytose induzieren, ist eine häufig angewandte Methode, um große Moleküle in Zellen zu transportieren. Zu diesen speziellen Liganden zählt die Folsäure, die spezifisch für sogenannte Folat-Rezeptoren ist (Kamen and Capdevila 1986, Leamon and Low 1991, Zhao et al. 2011). Da die Folat-Rezeptoren u.a. im Darmepithel im Bereich des Colons und Rektums exprimiert werden (Holm et al. 1994, Parker et al. 2005), werden Folsäure-konjugierte Wirkstoffe zur Erhöhung der oralen Bioverfügbarkeit entwickelt. Es konnte bereits gezeigt werden, dass die Aufnahme oral verabreichter Liposomen bzw. Nanopartikel durch die Konjugation mit Folsäure erhöht werden kann (Anderson et al. 2001, Roger et al. 2012).

Im Rahmen dieser Arbeit wurden zwei Folsäure-RD2-Konjugate zur Erhöhung der oralen Bioverfügbarkeit von RD2 entwickelt und ihre Metabolisierung zum unkonjugierten

Wirkstoff in künstlichem Magen- und Darmsaft, humanem Blutplasma und humanen Lebermikrosomen untersucht. Obwohl die orale Bioverfügbarkeit von RD2 mit 80 % schon außerordentlich hoch ist, würde eine weitere Steigerung der oralen Bioverfügbarkeit die Wirksamkeit des Wirkstoffs bei gleicher Dosierung möglicherweise steigern können bzw. eine geringere Dosierung erlauben. Darüber hinaus wird durch die Untersuchungen der Folsäure-RD2-Konjugate eine Optimierungsvariante für weitere Peptide mit geringerer oraler Bioverfügbarkeit geschaffen.

Die Folsäure-RD2-Konjugate wurden so entworfen, dass sie im Idealfall im Gastrointestinaltrakt stabil sind und die Folsäure erst in den Darmepithelzellen oder im Blut und in der Leber von RD2 abgespalten wird. Somit soll sichergestellt werden, dass RD2 seine unveränderte Wirksamkeit behält. Die beiden Folsäure-RD2-Konjugate wurden mit unterschiedlich stabilen Bindungen zwischen Ligand und Wirkstoff entworfen. Fol(p)-RD2 wurde so entworfen, dass die Folsäure direkt über das N-terminale Prolin von RD2 gekoppelt ist. Fol(G-t)-RD2 wurde hingegen so entworfen, dass die Folsäure über einen Glycin-Linker mit dem Threonin an Position 2 der RD2-Sequenz gekoppelt ist. Beide Konjugate liegen aufgrund der alternativen Kopplungsmöglichkeiten über die beiden Carboxygruppen der Folsäure als zwei verschiedene Isomere vor. Dabei wird vermutet, dass die Folsäure-Bindung an den Rezeptor höher ist, wenn der Ligand über die γ-Carboxygruppe gekoppelt wird (Leamon et al. 1993, Wang et al. 1996).

Beide Folsäure-RD2-Konjugate blieben in künstlichem Magensaft über 24 h fast vollständig stabil. Bei Fol(G-t)-RD2 wurden dabei geringe Mengen RD2 abgespalten, die jedoch in gleichem Maße in Wasser ohne Enzym-Zusatz gebildet wurden und somit nicht auf einen proteolytischen Abbau zurückzuführen sind. In künstlichem Darmsaft zeigte Fol(p)-RD2 ebenfalls eine sehr hohe Stabilität und keine RD2-Abspaltung. Im Gegensatz dazu wurde Fol(G-t)-RD2 nach 2 h zu 17 % abgebaut, wobei zunehmend RD2 gebildet wurde. Da die Verweildauer von Partikeln im Dünndarm bei 1 bis 3 h liegt (Dressman et al. 1998), kann also davon ausgegangen werden, dass Fol(G-t)-RD2 den Dünndarm nahezu vollständig unmetabolisiert Richtung Colon passieren würde. Im Colon selbst sind die beiden Konjugate hauptsächlich bakteriellem und enzymatischem Abbau durch Exoenzyme ausgesetzt, wobei die Verweildauer im Colon Stunden bis Tage betragen kann (Dressman et al. 1998), sodass dort ausreichend Zeit für die Aufnahme gewährleistet ist.

Untersuchungen zur Stabilität des Fol(G-t)-RD2s in humanem Blutplasma und humanen Lebermikrosomen zeigten, dass das Konjugat hauptsächlich zu unverändertem RD2 ohne Glycin-Linker metabolisiert wurde. Nach i.v. Injektion von Fol(G-t)-RD2 in Mäusen wurde

im Plasma aber nicht nur unverändertes RD2, sondern auch Metaboliten mit Massen von 1903,03 Da und 1783,99 Da, detektiert. Im Gegensatz dazu erfolgte bei Fol(p)-RD2 *in vitro* und *in vivo* keine Abspaltung der Folsäure.

Für beide Folsäure-RD2-Konjugate konnte gezeigt werden, dass sie die Zellviabilität nicht beeinträchtigen und das zytotoxische Potential von $A\beta_{1-42}$ reduzieren können, so wie bereits für RD2 beschrieben. Die Abspaltung der Folsäure wird als unkritisch eingestuft, da es laut Bundesinstitut für Risikobewertung zwar Hinweise aus Tierstudien darauf gibt, dass 60-90 mg/kg synthetische Folsäure i.v. verabreicht neurotoxisch oder epileptogen wirken könnten, jedoch aus Humanstudien keine Hinweise für eine solche Neurotoxizität durch Folsäureeinnahmen bestehen. Eine zusätzliche mäßige Folsäure-Zufuhr kann in manchen Fällen, besonders in der Schwangerschaft, sogar gesundheitsförderlich sein (Bundesinstitut für Risikobewertung 2005).

Die Versuche zeigen, dass Fol(G-t)-RD2 potentiell als Prodrug geeignet sein könnte, da es eine hohe Stabilität im Gastrointestinaltrakt aufweist und der Ligand nach systemischer Aufnahme vom Wirkstoff abgespalten werden kann, sodass durch unverändertes RD2 die bekannte Wirksamkeit gewährleistet wäre. Im Gegensatz dazu ist die Folsäure bei Fol(p)-RD2 so stabil gebunden, dass im gesamten Organismus voraussichtlich keine Abspaltung erfolgen würde, sodass dieses Konjugat nicht als Prodrug geeignet zu sein scheint.

5.4 Entwicklung und Validierung einer Methode zur Quantifizierung unmarkierten RD2s in Mausplasma

Diverse therapeutische und pharmakokinetische Studien in Mäusen wurden in der Vergangenheit mit radioaktiv- oder fluoreszenzmarkiertem D3 bzw. RD2 durchgeführt. Obwohl die Probenanalyse sehr sensitiv ist und in vielen Flüssigkeiten und Geweben erfolgen kann, ist es dennoch wünschenswert, unmarkierte Wirkstoffe für solche Studien zu verwenden und mittels Flüssigchromatographie mit Massenspektrometrie-Kopplung (LC-MS) zu quantifizieren. Diese Methode bietet den Vorteil, dass die Eigenschaften des Wirkstoffs nicht verändert werden und der Wirkstoff nicht nur über die Markierung detektiert wird, sondern über eine präzise Bestimmung der Masse, wodurch kleinste Wirkstoff-Veränderungen erkannt werden können.

Aus diesem Grund wurde eine LC-MS-Methode etabliert, um unmarkiertes RD2 in Maus-Plasmaproben zu quantifizieren. Die dafür entwickelte Extraktionsmethode ermöglichte

eine vollständige Rückgewinnung des sehr hydrophilen RD2s aus Plasma. Zur Quantifizierung des extrahierten RD2s wurde eine sensitive, stabile und effiziente UHPLC-ESI-QTOF-MS-Methode entwickelt und nach Vorgaben der „*Guideline on bioanalytical method validation of the European Medicines Agency*“ (European Medicines Agency 2011) validiert. Die Methode erlaubte die Trennung und Quantifizierung von RD2 und dem internen Standard innerhalb von 7 min und wies einen Linearitätsbereich bei Konzentrationen zwischen 5,3 und 265 ng/mL auf. Unter Verwendung der validierten Methode wurden Plasmaproben intraperitoneal mit RD2 bzw. Placebo behandelter Mäuse analysiert. Die Ergebnisse zeigten, dass die validierte Methode für die Evaluierung präklinischer oder klinischer Anwendungen von unmarkiertem RD2 geeignet ist.

5.5 Fazit und Ausblick

Mit den D-Peptiden D3 und RD2 wurden potentielle krankheitsmodulierende Wirkstoffkandidaten gegen die AD entwickelt, die *in vitro* toxische Aβ-Oligomere eliminieren und somit auch in den Aggregationsprozess eingreifen. Der Aggregationsprozess wird durch primäre und sekundäre Nukleationsmechanismen beschleunigt, welche durch D3 (Klein et al. 2017) und RD2 inhibiert werden können. Des Weiteren verringern D3 (van Groen et al. 2008) und RD2 *in vitro* die Aβ-induzierte Zytotoxizität. Behandlungsstudien mit transgenen AD-Mäusen belegen, dass die kognitiven Defizite durch D3 (van Groen et al. 2008, Funke et al. 2010, van Groen et al. 2012, van Groen et al. 2013) und RD2 verbessert werden konnten.

Weiterhin weisen mehrere Studien darauf hin, dass die Peptide für eine orale Applikation geeignet sind. Sie besitzen eine hohe orale Bioverfügbarkeit (Jiang et al. 2015, Leithold et al. 2016) und sind äußerst resistent gegenüber einer Metabolisierung. Eine hohe Stabilität erhöht die Verfügbarkeit im Gastrointestinaltrakt und im gesamten Körper, wirkt sich positiv auf die Halbwertszeit im Blut aus (Jiang et al. 2015, Leithold et al. 2016) und verlängert somit auch die Wirkdauer. In Behandlungsstudien mit transgenen AD-Mäusen konnte inzwischen gezeigt werden, dass D3 und RD2 selbst nach oraler Applikation therapeutisch aktiv sind (Funke et al. 2010, Kutzsche et al. 2017). Ein weiterer wichtiger Vorteil der oralen Behandlung mit D-Peptiden ist der Sicherheitsaspekt. Für RD2 konnte bereits gezeigt werden, dass es in anderen Spezies selbst in hohen Konzentrationen keine unerwünschten Arzneimittelwirkungen hervorruft (unveröffentlichte Daten). Der Vergleich zwischen den in Lebermikrosomen dieser Spezies gebildeten Metaboliten und den in humanen Lebermikrosomen gebildeten Metaboliten lässt darüber hinaus vermuten,

dass auch im Menschen voraussichtlich keine Leber-generierten toxischen Metaboliten gebildet werden.

Wenn die orale Bioverfügbarkeit von RD2 weiter gesteigert werden kann, dient dies einer höheren therapeutischen Wirksamkeit bzw. einer geringeren Dosierungsmöglichkeit. Eine möglichst geringe Dosierung sollte immer angestrebt werden, da so ein geringeres Risiko für das Auftreten potenzieller unerwünschter Arzneimittelwirkungen gewährleistet wird und zudem weniger Kosten für die Wirkstoffsynthese aufgebracht werden müssen, die v.a. bei D-Peptiden nicht zu vernachlässigen sind. Um die orale Bioverfügbarkeit von RD2 weiter zu erhöhen, wurden zwei Folsäure-RD2-Konjugate entwickelt. Fol(G-t)-RD2 stellt nach eingehenden Untersuchungen ein vielversprechendes Prodrug dar, das den Gastrointestinaltrakt voraussichtlich unverändert passieren und erst im restlichen Körper zum unkonjugierten Wirkstoff metabolisiert werden würde. Zukünftig sollen eine Absorptionsstudie mit Fol(G-t)-RD2 im Zellmodell (humane epitheliale kolorektale Tumorzellen) sowie eine pharmakokinetische Studie mit oral verabreichtem Fol(G-t)-RD2 in Mäusen klären, ob die Konjugation mit Folsäure zu einer Erhöhung der oralen Bioverfügbarkeit des RD2s beiträgt. Anschließend soll in Behandlungsstudien an Mäusen untersucht werden, inwiefern die RD2-Dosis durch Gabe des Konjugats reduziert werden kann, ohne dass die therapeutische Wirksamkeit verringert wird. Die Quantifizierung von RD2 in Maus-Plasma kann dabei durch die im Rahmen dieser Arbeit entwickelte und validierte Methode erfolgen.

Referenzen

Adessi C, Frossard MJ, Boissard C, Fraga S, Bieler S, Ruckle T, Vilbois F, Robinson SM, Mutter M, Banks WA and Soto C (2003). "Pharmacological profiles of peptide drug candidates for the treatment of Alzheimer's disease". *J Biol Chem* 278(16): 13905-13911

Adessi C and Soto C (2002). "Converting a peptide into a drug: strategies to improve stability and bioavailability". *Curr Med Chem* 9(9): 963-978

Alberdi E, Sanchez-Gomez MV, Cavaliere F, Perez-Samartin A, Zugaza JL, Trullas R, Domercq M and Matute C (2010). "Amyloid beta oligomers induce Ca2+ dysregulation and neuronal death through activation of ionotropic glutamate receptors". *Cell Calcium* 47(3): 264-272

Alzheimer's Association (2016). "2016 Alzheimer's Disease Facts and Figures". *Alzheimer's & Dementia* 12(4)

Alzheimer's Association. (2017a). "Brain Tour." from https://www.alz.org/braintour/healthy_vs_alzheimers.asp.

Alzheimer's Association. (2017b). "Alzheimer's & Dementia." from https://www.alz.org/dementia/types-of-dementia.asp.

Alzheimer A (1907). "Ueber eine eigenartige Erkrankung der Hirnrinde". *Allgemeine Zeitschrift für Psychiatrie und psychisch-gerichtliche Medizin* 64: 146-148

Anderson KE, Eliot LA, Stevenson BR and Rogers JA (2001). "Formulation and evaluation of a folic acid receptor-targeted oral vancomycin liposomal dosage form". *Pharm Res* 18(3): 316-322

Arosio P, Knowles TP and Linse S (2015). "On the lag phase in amyloid fibril formation". *Phys Chem Chem Phys* 17(12): 7606-7618

Avramopoulos D (2009). "Genetics of Alzheimer's disease: recent advances". *Genome Med* 1(3): 34

Bailey JA, Maloney B, Ge YW and Lahiri DK (2011). "Functional activity of the novel Alzheimer's amyloid beta-peptide interacting domain (AbetaID) in the APP and BACE1 promoter sequences and implications in activating apoptotic genes and in amyloidogenesis". *Gene* 488(1-2): 13-22

Ballard C, Gauthier S, Corbett A, Brayne C, Aarsland D and Jones E (2011). "Alzheimer's disease". *Lancet* 377(9770): 1019-1031

Barrow CJ and Zagorski MG (1991). "Solution structures of beta peptide and its constituent fragments: relation to amyloid deposition". *Science* 253(5016): 179-182

Bartus RT (2000). "On neurodegenerative diseases, models, and treatment strategies: lessons learned and lessons forgotten a generation following the cholinergic hypothesis". *Exp Neurol* 163(2): 495-529

Bartus RT, Dean RL, 3rd, Beer B and Lippa AS (1982). "The cholinergic hypothesis of geriatric memory dysfunction". *Science* 217(4558): 408-414

Baumgart M, Snyder HM, Carrillo MC, Fazio S, Kim H and Johns H (2015). "Summary of the evidence on modifiable risk factors for cognitive decline and dementia: A population-based perspective". *Alzheimers Dement* 11(6): 718-726

Bekris LM, Yu CE, Bird TD and Tsuang DW (2010). "Genetics of Alzheimer disease". *J Geriatr Psychiatry Neurol* 23(4): 213-227

Benet LZ (1978). "Effect of route of administration and distribution on drug action". *J Pharmacokinet Biopharm* 6(6): 559-585

Benilova I, Karran E and De Strooper B (2012). "The toxic Abeta oligomer and Alzheimer's disease: an emperor in need of clothes". *Nat Neurosci* 15(3): 349-357

Birks J (2006). "Cholinesterase inhibitors for Alzheimer's disease". *Cochrane Database Syst Rev*(1): CD005593

Brener O, Dunkelmann T, Gremer L, van Groen T, Mirecka EA, Kadish I, Willuweit A, Kutzsche J, Jurgens D, Rudolph S, Tusche M, Bongen P, Pietruszka J, Oesterhelt F, Langen KJ, Demuth HU, Janssen A, Hoyer W, Funke SA, Nagel-Steger L and Willbold D (2015). "QIAD assay for quantitating a compound's efficacy in elimination of toxic Abeta oligomers". *Sci Rep* 5: 13222

Bundesinstitut für Risikobewertung (2005). Folsäureversorgung der deutschen Bevölkerung, Weißenborn A, Burger M, Mensink GBM, Klemm C, Sichert-Hellert W, Kersting M, Przyrembel H.

Burrell MM (1993). "Enzymes of Molecular Biology". *Methods in Molecular Biology*. M. M. Burrell. Totowa, New Jersey, Humana Press.

Bush AI (2002). "Metal complexing agents as therapies for Alzheimer's disease". *Neurobiol Aging* 23(6): 1031-1038

Butterfield DA (2002). "Amyloid beta-peptide (1-42)-induced oxidative stress and neurotoxicity: implications for neurodegeneration in Alzheimer's disease brain. A review". *Free Radic Res* 36(12): 1307-1313

Caccamo A, Oddo S, Sugarman MC, Akbari Y and LaFerla FM (2005). "Age- and region-dependent alterations in Abeta-degrading enzymes: implications for Abeta-induced disorders". *Neurobiol Aging* 26(5): 645-654

Camenisch G, Alsenz J, van de Waterbeemd H and Folkers G (1998). "Estimation of permeability by passive diffusion through Caco-2 cell monolayers using the drugs' lipophilicity and molecular weight". *Eur J Pharm Sci* 6(4): 317-324

Chalifour RJ, McLaughlin RW, Lavoie L, Morissette C, Tremblay N, Boule M, Sarazin P, Stea D, Lacombe D, Tremblay P and Gervais F (2003). "Stereoselective interactions of peptide inhibitors with the beta-amyloid peptide". *J Biol Chem* 278(37): 34874-34881

Citron M (2010). "Alzheimer's disease: strategies for disease modification". *Nat Rev Drug Discov* 9(5): 387-398

Cohen SI, Linse S, Luheshi LM, Hellstrand E, White DA, Rajah L, Otzen DE, Vendruscolo M, Dobson CM and Knowles TP (2013). "Proliferation of amyloid-beta42 aggregates occurs through a secondary nucleation mechanism". *Proc Natl Acad Sci U S A* 110(24): 9758-9763

Coleman MD (2010). "Human Drug Metabolism: An Introduction". *John Wiley & Sons, Ltd.*

Corder EH, Saunders AM, Strittmatter WJ, Schmechel DE, Gaskell PC, Small GW, Roses AD, Haines JL and Pericak-Vance MA (1993). "Gene dose of apolipoprotein E type 4 allele and the risk of Alzheimer's disease in late onset families". *Science* 261(5123): 921-923

D'Aniello A, D'Onofrio G, Pischetola M, D'Aniello G, Vetere A, Petrucelli L and Fisher GH (1993). "Biological Role of D-Amino Acid Oxidase and D-Aspartate Oxidase. Effects of D-amino acids.". *J Biol Chem* 268(36): 26941-26949

da Rocha MD, Viegas FP, Campos HC, Nicastro PC, Fossaluzza PC, Fraga CA, Barreiro EJ and Viegas C, Jr. (2011). "The role of natural products in the discovery of new drug candidates for the treatment of neurodegenerative disorders II: Alzheimer's disease". *CNS Neurol Disord Drug Targets* 10(2): 251-270

Danho W, Swistok J, Khan W, Chu XJ, Cheung A, Fry D, Sun H, Kurylko G, Rumennik L, Cefalu J, Cefalu G and Nunn P (2009). "Opportunities and challenges of developing peptide drugs in the pharmaceutical industry". *Adv Exp Med Biol* 611: 467-469

Danysz W and Parsons CG (2012). "Alzheimer's disease, beta-amyloid, glutamate, NMDA receptors and memantine - searching for the connections". *Br J Pharmacol* 167(2): 324-352

De Felice FG, Wu D, Lambert MP, Fernandez SJ, Velasco PT, Lacor PN, Bigio EH, Jerecic J, Acton PJ, Shughrue PJ, Chen-Dodson E, Kinney GG and Klein WL (2008). "Alzheimer's disease-type neuronal tau hyperphosphorylation induced by A beta oligomers.". *Neurobiol Aging* 29(9): 1334-1347

De Genst E, Messer A and Dobson CM (2014). "Antibodies and protein misfolding: From structural research tools to therapeutic strategies". *Biochim Biophys Acta* 1844(11): 1907-1919

de la Monte SM (1989). "Quantitation of cerebral atrophy in preclinical and end-stage Alzheimer's disease". *Ann Neurol* 25(5): 450-459

De Strooper B (2010). "Proteases and proteolysis in Alzheimer disease: a multifactorial view on the disease process". *Physiol Rev* 90(2): 465-494

Deane R, Du Yan S, Submamaryan RK, LaRue B, Jovanovic S, Hogg E, Welch D, Manness L, Lin C, Yu J, Zhu H, Ghiso J, Frangione B, Stern A, Schmidt AM, Armstrong DL, Arnold B, Liliensiek B, Nawroth P, Hofman F, Kindy M, Stern D and Zlokovic B (2003). "RAGE mediates amyloid-beta peptide transport across the blood-brain barrier and accumulation in brain". *Nat Med* 9(7): 907-913

Deane R, Wu Z, Sagare A, Davis J, Du Yan S, Hamm K, Xu F, Parisi M, LaRue B, Hu HW, Spijkers P, Guo H, Song X, Lenting PJ, Van Nostrand WE and Zlokovic BV (2004). "LRP/amyloid beta-peptide interaction mediates differential brain efflux of Abeta isoforms". *Neuron* 43(3): 333-344

Derreumaux P (2013). "Alzheimer's Disease: Insights into Low Molecular Weight and Cytotoxic Aggregates from In Vitro and Computer Experiments. Molecular Basis of Amyloid-Beta Protein Aggregation and Fibril Formation.". *Imperial College Press*

Dressman JB, Amidon GL, Reppas C and Shah VP (1998). "Dissolution Testing as a Prognostic Tool for Oral Drug Absorption. Immeadiate Release Dosage Forms.". *Pharm Res* 15(1): 11-22

El-Agnaf OM, Mahil DS, Patel BP and Austen BM (2000). "Oligomerization and toxicity of beta-amyloid-42 implicated in Alzheimer's disease". *Biochem Biophys Res Commun* 273(3): 1003-1007

El-Kattan A and Varma M (2012). Oral Absorption, Intestinal Metabolism and Human Oral Bioavailability. Topics on Drug Metabolism. J. Paxton, InTech.

Elfgen A, Hupert M, Bochinsky K, Tusche M, González de San Román Martin E, Gering I, Sacchi S, Pollegioni L, Huesgen PF, Hartmann R, Santiago-Schübel B, Kutzsche J and Willbold D (2018). "Enzymatic resistance and investigation of human-specific metabolites of the amyloid-β oligomer eliminating all-D-enantiomeric peptide compound RD2". *Chem Sci (in peer review)*

Elmquist A and Langel U (2003). "In vitro Uptake and Stability Study of pVEC and Its All-D Analog". *Biol Chem* 384: 387–393

European Medicines Agency (2011). Guideline on Validation of Bioanalytical Methods. London, Committee for Medicinal Products for Human Use.

Ferreira ST and Klein WL (2011). "The Abeta oligomer hypothesis for synapse failure and memory loss in Alzheimer's disease". *Neurobiol Learn Mem* 96(4): 529-543

Ferri CP, Prince M, Brayne C, Brodaty H, Fratiglioni L, Ganguli M, Hall K, Hasegawa K, Hendrie H, Huang Y, Jorm A, Mathers C, Menezes PR, Rimmer E, Scazufca M and Alzheimer's Disease I (2005). "Global prevalence of dementia: a Delphi consensus study". *Lancet* 366(9503): 2112-2117

Findeis MA, Musso GM, Arico-Muendel CC, Benjamin HW, Hundal AM, Lee JJ, Chin J, Kelley M, Wakefield J, Hayward NJ and Molineaux SM (1999). "Modified-peptide inhibitors of amyloid beta-peptide polymerization". *Biochem* 38(21): 6791-6800

Finder VH and Glockshuber R (2007). "Amyloid-beta aggregation". *Neurodegener Dis* 4(1): 13-27

Folch J, Petrov D, Ettcheto M, Abad S, Sanchez-Lopez E, Garcia ML, Olloquequi J, Beas-Zarate C, Auladell C and Camins A (2016). "Current Research Therapeutic Strategies for Alzheimer's Disease Treatment". *Neural Plast* 2016: 8501693

Food and Agriculture Organization of the United Nations and World Health Organization (2001). Human Vitamin and Mineral Requirements. F. R. Food and Nutrition Division.

Funke A and Willbold D (2012). "Peptides for Therapy and Diagnosis of Alzheimer's Disease". *Curr Pharm Des* 18: 755-767

Funke SA, Liu H, Sehl T, Bartnik D, Brener O, Nagel-Steger L, Wiesehan K and Willbold D (2012). "Identification and characterization of an abeta oligomer precipitating peptide that may be useful to explore gene therapeutic approaches to Alzheimer disease". *Rejuvenation Res* 15(2): 144-147

Funke SA, van Groen T, Kadish I, Bartnik D, Nagel-Steger L, Brener O, Sehl T, Batra-Safferling R, Moriscot C, Schoehn G, Horn AH, Muller-Schiffmann A, Korth C, Sticht H and Willbold D (2010). "Oral treatment with the d-enantiomeric peptide D3 improves the

pathology and behavior of Alzheimer's Disease transgenic mice". *ACS Chem Neurosci* 1(9): 639-648

Funke SA and Willbold D (2009). "Mirror image phage display--a method to generate D-peptide ligands for use in diagnostic or therapeutical applications". *Mol. Biosyst.* 5(8): 783-786

Ghezzi L, Scarpini E and Galimberti D (2013). "Disease-modifying drugs in Alzheimer's disease". *Drug Des Devel Ther* 7: 1471-1478

Giuffrida ML, Caraci F, Pignataro B, Cataldo S, De Bona P, Bruno V, Molinaro G, Pappalardo G, Messina A, Palmigiano A, Garozzo D, Nicoletti F, Rizzarelli E and Copani A (2009). "Beta-amyloid monomers are neuroprotective". *J Neurosci* 29(34): 10582-10587

Glenner GG and Wong CW (1984). "Alzheimer's disease: initial report of the purification and characterization of a novel cerebrovascular amyloid protein". *Biochem Biophys Res Commun* 120(3): 885-890

Godyn J, Jonczyk J, Panek D and Malawska B (2016). "Therapeutic strategies for Alzheimer's disease in clinical trials". *Pharmacol Rep* 68(1): 127-138

Golde TE, Koo EH, Felsenstein KM, Osborne BA and Miele L (2013). "gamma-Secretase inhibitors and modulators". *Biochim Biophys Acta* 1828(12): 2898-2907

Gomez-Orellana I (2005). "Strategies to improve oral drug availability". *Expert Opin Drug Delivery* 2(3): 419-433

Grundke-Iqbal I, Iqbal K, Tung YC, Quinlan M, Wisniewski HM and Binder LI (1986). "Abnormal phosphorylation of the microtubule-associated protein tau (tau) in Alzheimer cytoskeletal pathology". *Proc Natl Acad Sci U S A* 83(13): 4913-4917

Guengerich FP (2001). "Common and Uncommon Cytochrome P450 Reactions Related to Metabolism and Chemical Toxicity". *Chem Res Toxicol* 14(6): 611-650

Gunn AP, Masters CL and Cherny RA (2010). "Pyroglutamate-Abeta: role in the natural history of Alzheimer's disease". *Int J Biochem Cell Biol* 42(12): 1915-1918

Haapasalo A and Kovacs DM (2011). "The many substrates of presenilin/gamma-secretase". *J Alzheimers Dis* 25(1): 3-28

Hamley IW (2012). "The amyloid beta peptide: a chemist's perspective. Role in Alzheimer's and fibrillization". *Chem Rev* 112(10): 5147-5192

Hamman JH, Enslin GM and Kotzé AF (2005). "Oral delivery of peptide drugs: barriers and developments.". *BioDrugs* 19(3): 165-177

Han HK and Amidon GL (2000). "Targeted prodrug design to optimize drug delivery". *AAPS PharmSci* 2(1): E6

Hardy J, Duff K, Hardy KG, Perez-Tur J and Hutton M (1998). "Genetic dissection of Alzheimer's disease and related dementias: amyloid and its relationship to tau". *Nat Neurosci* 1(5): 355-358

Hardy J and Selkoe DJ (2002). "The amyloid hypothesis of Alzheimer's disease: progress and problems on the road to therapeutics". *Science* 297(5580): 353-356

Hardy JA and Higgins GA (1992). "Alzheimer's Disease: The Amyloid Cascade Hypothesis". *Science* 256(5054): 184-185

Harigaya Y, Saido TC, Eckman CB, Prada CM, Shoji M and Younkin SG (2000). "Amyloid beta protein starting pyroglutamate at position 3 is a major component of the amyloid deposits in the Alzheimer's disease brain". *Biochem Biophys Res Commun* 276(2): 422-427

Harman D (2006). "Alzheimer's disease pathogenesis: role of aging". *Ann N Y Acad Sci* 1067: 454-460

Hashimoto M, Takada K, Kiso Y and Muranishi S (1989). "Synthesis of palmitoyl derivatives of insulin and their biological activities". *Pharm Res* 6(2): 171-176

Hashizume M, Douen T, Murakami M, Yamamoto A, Takada K and Muranishi S (1992). "Improvement of large intestinal absorption of insulin by chemical modification with palmitic acid in rats". *J Pharm Pharmacol* 44(7): 555-559

Hebert LE, Bienias JL, Aggarwal NT, Wilson RS, Bennett DA, Shah RC and Evans DA (2010). "Change in risk of Alzheimer disease over time". *Neurology* 75(9): 786-791

Hebert LE, Weuve J, Scherr PA and Evans DA (2013). "Alzheimer disease in the United States (2010–2050) estimated using the 2010 census". *Neurology* 80(19): 1778-1783

Hetenyi C, Szabo Z, Klement E, Datki Z, Kortvelyesi T, Zarandi M and Penke B (2002). "Pentapeptide amides interfere with the aggregation of beta-amyloid peptide of Alzheimer's disease". *Biochem Biophys Res Commun* 292(4): 931-936

Higuchi M, Iwata N and Saido TC (2005). "Understanding molecular mechanisms of proteolysis in Alzheimer's disease: progress toward therapeutic interventions". *Biochim Biophys Acta* 1751(1): 60-67

Hilgenbrink AR and Low PS (2005). "Folate receptor-mediated drug targeting: from therapeutics to diagnostics". *J Pharm Sci* 94(10): 2135-2146

Hippius H and Neundörfer G (2003). "The discovery of Alzheimer’s disease". *Dialogues Clin Neurosci* 5(1): 101–108

Holm J, Hansen SI, Hoier-Madsen M, Sondergaard K and Bzorek M (1994). "The high-affinity folate receptor of normal and malignant human colonic mucosa". *APMIS* 102(11): 828-836

Huang Y and Mucke L (2012). "Alzheimer mechanisms and therapeutic strategies". *Cell* 148(6): 1204-1222

Hynd MR, Scott HL and Dodd PR (2004). "Glutamate-mediated excitotoxicity and neurodegeneration in Alzheimer's disease". *Neurochem Int* 45(5): 583-595

Iadecola C (2004). "Neurovascular regulation in the normal brain and in Alzheimer's disease". *Nat Rev Neurosci* 5(5): 347-360

Imbimbo BP (2008). "Therapeutic potential of gamma-secretase inhibitors and modulators". *Curr Top Med Chem* 8(1): 54-61

Institute of Medicine (2015). "Cognitive Aging: Progress in Understanding and Opportunities for Action". Washington (DC), *The National Academies Press*

Itagaki S, McGeer PL, Akiyama H, Zhu S and Selkoe D (1989). "Relationship of microglia and astrocytes to amyloid deposits of Alzheimer disease". *J Neuroimmunol* 24(3): 173-182

Jancova P, Anzenbacher P and Anzenbacherova E (2010). "Phase II Drug Metabolizing Enzymes.". *Biomed Pap Med Fac Univ Palacky Olomouc Czech Repub* 154(2): 103-116

Jančová P and Šiller M (2012). Phase II Drug Metabolism. Topics on Drug Metabolism. P. J, InTech.

Jarrett JT and Lansbury PT, Jr. (1993). "Seeding "one-dimensional crystallization" of amyloid: a pathogenic mechanism in Alzheimer's disease and scrapie?". *Cell* 73(6): 1055-1058

Jawhar S, Wirths O and Bayer TA (2011). "Pyroglutamate amyloid-beta (Abeta): a hatchet man in Alzheimer disease". *J Biol Chem* 286(45): 38825-38832

Jia Q, Deng Y and Qing H (2014). "Potential therapeutic strategies for Alzheimer's disease targeting or beyond beta-amyloid: insights from clinical trials". *Biomed Res Int* 2014: 837157

Jiang N, Frenzel D, Schartmann E, van Groen T, Kadish I, Shah NJ, Langen KJ, Willbold D and Willuweit A (2016). "Blood-brain barrier penetration of an Abeta-targeted, arginine-rich, d-enantiomeric peptide". *Biochim Biophys Acta* 1858(11): 2717-2724

Jiang N, Leithold LH, Post J, Ziehm T, Mauler J, Gremer L, Cremer M, Schartmann E, Shah NJ, Kutzsche J, Langen KJ, Breitkreutz J, Willbold D and Willuweit A (2015). "Preclinical Pharmacokinetic Studies of the Tritium Labelled D-Enantiomeric Peptide D3 Developed for the Treatment of Alzheimer s Disease". *PLoS One* 10(6): e0128553

Jin M, Shepardson N, Yang T, Chen G, Walsh D and Selkoe DJ (2011). "Soluble amyloid beta-protein dimers isolated from Alzheimer cortex directly induce Tau hyperphosphorylation and neuritic degeneration". *Proc Natl Acad Sci U S A* 108(14): 5819-5824

Kamen BA and Capdevila A (1986). "Receptor-mediated folate accumulation is regulated by the cellular folate content". *Proc Natl Acad Sci U S A* 83(16): 5983-5987

Kang J, Lemaire HG, Unterbeck A, Salbaum JM, Masters CL, Grzeschik KH, Multhaup G, Beyreuther K and Muller-Hill B (1987). "The precursor of Alzheimer's disease amyloid A4 protein resembles a cell-surface receptor". *Nature* 325(6106): 733-736

Keil B (1992). "Specificity of proteolysis.". Berlin-Heidelberg-New York, *Springer-Verlag*

King ME, Kan HM, Baas PW, Erisir A, Glabe CG and Bloom GS (2006). "Tau-dependent microtubule disassembly initiated by prefibrillar beta-amyloid". *J Cell Biol* 175(4): 541-546

Klein AN, Ziehm T, van Groen T, Kadish I, Elfgen A, Tusche M, Thomaier M, Reiss K, Brener O, Gremer L, Kutzsche J and Willbold D (2017). "Optimization of d-Peptides for Abeta Monomer Binding Specificity Enhances Their Potential to Eliminate Toxic Abeta Oligomers". *ACS Chem Neurosci*

Kril JJ, Hodges J and Halliday G (2004). "Relationship between hippocampal volume and CA1 neuron loss in brains of humans with and without Alzheimer's disease". *Neurosci Lett* 361(1-3): 9-12

Krysmann MJ, Castelletto V, Kelarakis A, Hamley IW, Hule RA and Pochan DJ (2008). "Self-assembly and hydrogelation of an amyloid peptide fragment". *Biochem* 47(16): 4597-4605

Kumar J and Sim V (2014). "D-amino acid-based peptide inhibitors as early or preventative therapy in Alzheimer disease". *Prion* 8(1): 119-124

Kuo YM, Emmerling MR, Vigo-Pelfrey C, Kasunic TC, Kirkpatrick JB, Murdoch GH, Ball MJ and Roher AE (1996). "Water-soluble Abeta (N-40, N-42) oligomers in normal and Alzheimer disease brains". *J Biol Chem* 271(8): 4077-4081

Kutzsche J, Schemmert S, Tusche M, Neddens J, Rabl R, Jurgens D, Brener O, Willuweit A, Hutter-Paier B and Willbold D (2017). "Large-Scale Oral Treatment Study with the Four Most Promising D3-Derivatives for the Treatment of Alzheimer's Disease". *Molecules* 22(10)

LaFerla FM, Green KN and Oddo S (2007). "Intracellular amyloid-beta in Alzheimer's disease". *Nat Rev Neurosci* 8(7): 499-509

Larson ME and Lesne SE (2012). "Soluble Abeta oligomer production and toxicity". *J Neurochem* 120: 125-139

Leamon CP (2008). "Folate-targeted drug strategies for the treatment of cancer". *Curr Opin Investig Drugs* 9(12): 1277-1286

Leamon CP and Low PS (1991). "Delivery of macromolecules into living cells: a method that exploits folate receptor endocytosis". *Proc Natl Acad Sci U S A* 88(13): 5572-5576

Leamon CP, Pastan I and Low PS (1993). "Cytotoxicity of folate-Pseudomonas exotoxin conjugates toward tumor cells. Contribution of translocation domain". *J Biol Chem* 268(33): 24847-24854

Leithold LH, Jiang N, Post J, Ziehm T, Schartmann E, Kutzsche J, Shah NJ, Breitkreutz J, Langen KJ, Willuweit A and Willbold D (2016). "Pharmacokinetic Properties of a Novel D-Peptide Developed to be Therapeutically Active Against Toxic beta-Amyloid Oligomers". *Pharm Res* 33(2): 328-336

Lien S and Lowman HB (2003). "Therapeutic peptides". *Trends Biotechnol* 21(12): 556-562

Liu H, Funke A and Willbold D (2010). "Transport of Alzheimer Disease Amyloid-b-Binding d-Amino Acid Peptides across an In Vitro Blood–Brain Barrier Model". *Rejuvenation Res* 13(2-3): 210-213

Lu AY (1976). "Liver microsomal drug-metabolizing enzyme system: functional components and their properties". *Fed Proc* 35(13): 2460-2463

Lue LF, Kuo YM, Roher AE, Brachova L, Shen Y, Sue L, Beach T, Kurth JH, Rydel RE and Rogers J (1999). "Soluble amyloid beta peptide concentration as a predictor of synaptic change in Alzheimer's disease". *Am J Pathol* 155(3): 853-862

Lukiw WJ (2012). "Amyloid beta (Abeta) peptide modulators and other current treatment strategies for Alzheimer's disease (AD)". *Expert Opin Emerg Drugs*

Mahalakshmi R and Balaram P (2006). "The Use of D-Amino Acids in Peptide Design". *D-Amino Acids: A New Frontier in Amino Acid and Protein Research*, Nova Science Publishers, Inc.

Matharu B, El-Agnaf O, Razvi A and Austen BM (2010). "Development of retro-inverso peptides as anti-aggregation drugs for beta-amyloid in Alzheimer's disease". *Peptides* 31(10): 1866-1872

McLean CA, Cherny RA, Fraser FW, Fuller SJ, Smith MJ, Beyreuther K, Bush AI and Masters CL (1999). "Soluble pool of Abeta amyloid as a determinant of severity of neurodegeneration in Alzheimer's disease". *Ann Neurol* 46(6): 860-866

McShane R, Areosa Sastre A and Minakaran N (2006). "Memantine for dementia". *Cochrane Database Syst Rev*(2): CD003154

Meraz-Rios MA, Toral-Rios D, Franco-Bocanegra D, Villeda-Hernandez J and Campos-Pena V (2013). "Inflammatory process in Alzheimer's Disease". *Front Integr Neurosci* 7: 59

Miller SM, Simon RJ, Ng S, Zuckermann RN, Kerr JM and Moos WH (1995). "Comparison of the Proteolytic Susceptibilities of Homologous L-Amino Acid, D-Amino Acid, and N-Substituted Clycine Peptide and Peptoid Oligomers". *Drug Dev Res* 35: 20-32

Morishita M and Peppas NA (2006). "Is the oral route possible for peptide and protein drug delivery?". *Drug Discov Today* 11(19-20): 905-910

Mullard A (2012). "Sting of Alzheimer's failures offset by upcoming prevention trials". *Nat Rev Drug Discov* 11(9): 657-660

Muller-Hill B and Beyreuther K (1989). "Molecular biology of Alzheimer's disease". *Annu Rev Biochem* 58: 287-307

Murphy MP and LeVine H, 3rd (2010). "Alzheimer's disease and the amyloid-beta peptide". *J Alzheimers Dis* 19(1): 311-323

Nalivaeva NN, Belyaev ND, Zhuravin IA and Turner AJ (2012). "The Alzheimer's amyloid-degrading peptidase, neprilysin: can we control it?". *Int J Alzheimers Dis* 2012: 383796

O'Brien RJ and Wong PC (2011). "Amyloid precursor protein processing and Alzheimer's disease". *Annu Rev Neurosci* 34: 185-204

Oddo S, Caccamo A, Tran L, Lambert MP, Glabe CG, Klein WL and LaFerla FM (2006). "Temporal profile of amyloid-beta (Abeta) oligomerization in an in vivo model of Alzheimer disease. A link between Abeta and tau pathology". *J Biol Chem* 281(3): 1599-1604

Ohide H, Miyoshi Y, Maruyama R, Hamase K and Konno R (2011). "D-Amino acid metabolism in mammals: biosynthesis, degradation and analytical aspects of the metabolic study". *J Chromatogr B Analyt Technol Biomed Life Sci* 879(29): 3162-3168

Olubiyi OO, Frenzel D, Bartnik D, Glück JM, Brener O, Nagel-Steger L, Funke SA, Willbold D and Strodel B (2014). "Amyloid aggregation inhibitory mechanism of arginine-rich D-peptides.". *Curr Med Chem* 21(12): 1448-1457

Olubiyi OO and Strodel B (2012). "Structures of the amyloid beta-peptides Abeta1-40 and Abeta1-42 as influenced by pH and a D-peptide". *J Phys Chem B* 116(10): 3280-3291

Panza F, Seripa D, Solfrizzi V, Imbimbo BP, Lozupone M, Leo A, Sardone R, Gagliardi G, Lofano L, Creanza BC, Bisceglia P, Daniele A, Bellomo A, Greco A and Logroscino G (2016). "Emerging drugs to reduce abnormal beta-amyloid protein in Alzheimer's disease patients". *Expert Opin Emerg Drugs* 21(4): 377-391

Parker N, Turk MJ, Westrick E, Lewis JD, Low PS and Leamon CP (2005). "Folate receptor expression in carcinomas and normal tissues determined by a quantitative radioligand binding assay". *Anal Biochem* 338(2): 284-293

Pauletti GM, Gangwar S, Siahaan TJ, Aube J and Borchardt RT (1997). "Improvement of oral peptide bioavailability: Peptidomimetics and prodrug strategies". *Adv Drug Deliv Rev* 27(2-3): 235-256

Perl DP (2010). "Neuropathology of Alzheimer's disease". *Mt Sinai J Med* 77(1): 32-42

Perry EK (1986). "The cholinergic hypothesis - ten years on". *Br Med Bull* 42(1): 63-69

Peters I, Igbavboa U, Schutt T, Haidari S, Hartig U, Rosello X, Bottner S, Copanaki E, Deller T, Kogel D, Wood WG, Muller WE and Eckert GP (2009). "The interaction of beta-amyloid protein with cellular membranes stimulates its own production". *Biochim Biophys Acta* 1788(5): 964-972

Pivovarova O, Hohn A, Grune T, Pfeiffer AF and Rudovich N (2016). "Insulin-degrading enzyme: new therapeutic target for diabetes and Alzheimer's disease?". *Ann Med* 48(8): 614-624

Poduslo JF, Curran GL, Kumar A, Frangione B and Soto C (1998). "Beta-sheet breaker peptide inhibitor of Alzheimer's amyloidogenesis with increased blood-brain barrier permeability and resistance to proteolytic degradation in plasma". *J Neurobiol* 39(3): 371-382

Pollack SJ, Sadler, II, Hawtin SR, Tailor VJ and Shearman MS (1995). "Sulfonated dyes attenuate the toxic effects of beta-amyloid in a structure-specific fashion". *Neurosci Lett* 197(3): 211-214

Porat Y, Abramowitz A and Gazit E (2006). "Inhibition of amyloid fibril formation by polyphenols: structural similarity and aromatic interactions as a common inhibition mechanism". *Chem Biol Drug Des* 67(1): 27-37

Postina R (2012). "Activation of alpha-secretase cleavage". *J Neurochem* 120: 46-54

Prince M, Comas-Herrera A, Knapp M, Guerchet M and Karagiannidou M (2016). World Alzheimer Report 2016**:** 140.

Quist A, Doudevski I, Lin H, Azimova R, Ng D, Frangione B, Kagan B, Ghiso J and Lal R (2005). "Amyloid ion channels: a common structural link for protein-misfolding disease". *Proc Natl Acad Sci U S A* 102(30): 10427-10432

Re F, Airoldi C, Zona C, Masserini M, La Ferla B, Quattrocchi N and Nicotra F (2010). "Beta amyloid aggregation inhibitors: small molecules as candidate drugs for therapy of Alzheimer's disease". *Curr Med Chem* 17(27): 2990-3006

Renukuntla J, Vadlapudi AD, Patel A, Boddu SH and Mitra AK (2013). "Approaches for enhancing oral bioavailability of peptides and proteins". *Int J Pharm* 447(1-2): 75-93

Roger E, Kalscheuer S, Kirtane A, Guru BR, Grill AE, Whittum-Hudson J and Panyam J (2012). "Folic acid functionalized nanoparticles for enhanced oral drug delivery". *Mol Pharm* 9(7): 2103-2110

Rubas W, Cromwell ME, Shahrokh Z, Villagran J, Nguyen TN, Wellton M, Nguyen TH and Mrsny RJ (1996). "Flux measurements across Caco-2 monolayers may predict transport in human large intestinal tissue". *J Pharm Sci* 85(2): 165-169

Rubio-Aliaga I and Daniel H (2008). "Peptide transporters and their roles in physiological processes and drug disposition". *Xenobiotica* 38(7-8): 1022-1042

Russell-Jones GJ (2004). "Use of targeting agents to increase uptake and localization of drugs to the intestinal epithelium". *J Drug Target* 12(2): 113-123

Sadowski M, Pankiewicz J, Scholtzova H, Ripellino JA, Li Y, Schmidt SD, Mathews PM, Fryer JD, Holtzman DM, Sigurdsson EM and Wisniewski T (2004). "A Synthetic Peptide Blocking the Apolipoprotein E/β-Amyloid Binding Mitigates β-Amyloid Toxicity and Fibril Formation in Vitro and Reduces β-Amyloid Plaques in Transgenic Mice". *Am J Pathol* 165(3): 937-948

Sagare A, Deane R, Bell RD, Johnson B, Hamm K, Pendu R, Marky A, Lenting PJ, Wu Z, Zarcone T, Goate A, Mayo K, Perlmutter D, Coma M, Zhong Z and Zlokovic BV (2007). "Clearance of amyloid-beta by circulating lipoprotein receptors". *Nat Med* 13(9): 1029-1031

Saido TC, Iwatsubo T, Mann DM, Shimada H, Ihara Y and Kawashima S (1995). "Dominant and differential deposition of distinct beta-amyloid peptide species, A beta N3(pE), in senile plaques". *Neuron* 14(2): 457-466

Sato AK, Viswanathan M, Kent RB and Wood CR (2006). "Therapeutic peptides: technological advances driving peptides into development". *Curr Opin Biotechnol* 17(6): 638-642

Saunders AM, Strittmatter WJ, Schmechel D, George-Hyslop PH, Pericak-Vance MA, Joo SH, Rosi BL, Gusella JF, Crapper-MacLachlan DR and Alberts MJ (1993). "Association of apolipoprotein E allele epsilon 4 with late-onset familial and sporadic Alzheimer's disease.". *Neurology* 43(8): 1467-1472

Savonenko AV, Melnikova T, Laird FM, Stewart KA, Price DL and Wong PC (2008). "Alteration of BACE1-dependent NRG1/ErbB4 signaling and schizophrenia-like phenotypes in BACE1-null mice". *Proc Natl Acad Sci U S A* 105(14): 5585-5590

Schumacher TN, Mayr LM, Minor DLJ, Milhollen MA, Burgess MW and Kim PS (1996). "Identification of D-Peptide Ligands Through Mirror-image Phage Display". *Science* 271(5257): 1854-1857

Selkoe DJ (2001). "Clearing the brain's amyloid cobwebs". *Neuron* 32(2): 177-180

Selkoe DJ and Hardy J (2016). "The amyloid hypothesis of Alzheimer's disease at 25 years". *EMBO Mol Med* 8(6): 595-608

Serrano-Pozo A, Frosch MP, Masliah E and Hyman BT (2011). "Neuropathological alterations in Alzheimer disease". *Cold Spring Harb Perspect Med* 1(1): a006189

Smart AL, Gaisford S and Basit AW (2014). "Oral peptide and protein delivery: intestinal obstacles and commercial prospects". *Expert Opin Drug Deliv* 11(8): 1323-1335

Soscia SJ, Kirby JE, Washicosky KJ, Tucker SM, Ingelsson M, Hyman B, Burton MA, Goldstein LE, Duong S, Tanzi RE and Moir RD (2010). "The Alzheimer's disease-associated amyloid beta-protein is an antimicrobial peptide". *PLoS One* 5(3): e9505

Soto C and Estrada L (2005). "Amyloid inhibitors and beta-sheet breakers". *Subcell Biochem* 38: 351-364

Soto C, Kindy MS, Baumann M and Frangione B (1996). "Inhibition of Alzheimer's amyloidosis by peptides that prevent beta-sheet conformation.". *Biochem Biophys Res Commun* 226(3): 672-680

Sun N, Funke SA and Willbold D (2012). "A survey of peptides with effective therapeutic potential in Alzheimer's disease rodent models or in human clinical studies.". *Mini-Rev Med Chem* 12(5): 388-398

Sunde M, Serpell LC, Bartlam M, Fraser PE, Pepys MB and Blake CC (1997). "Common core structure of amyloid fibrils by synchrotron X-ray diffraction". *J Mol Biol* 273(3): 729-739

Swaan PW (1998). "Recent advances in intestinal macromolecular drug delivery via receptor-mediated transport pathways". *Pharm Res* 15(6): 826-834

Szegedi V, Fulop L, Farkas T, Rozsa E, Robotka H, Kis Z, Penke Z, Horvath S, Molnar Z, Datki Z, Soos K, Toldi J, Budai D, Zarandi M and Penke B (2005). "Pentapeptides derived from Abeta 1-42 protect neurons from the modulatory effect of Abeta fibrils--an in vitro and in vivo electrophysiological study". *Neurobiol Dis* 18(3): 499-508

Tan Y, Zhang Q, Wong SG and Hua Q (2016). "Anti-Alzheimer Therapeutic Drugs Targeting gamma-Secretase". *Curr Top Med Chem* 16(5): 549-557

Tanzi RE, Moir RD and Wagner SL (2004). "Clearance of Alzheimer's Abeta peptide: the many roads to perdition". *Neuron* 43(5): 605-608

Taylor M, Moore S, Mayes J, Parkin E, Beeg M, Canovi M, Gobbi M, Mann DM and Allsop D (2010). "Development of a proteolytically stable retro-inverso peptide inhibitor of beta-amyloid oligomerization as a potential novel treatment for Alzheimer's disease". *Biochemistry* 49(15): 3261-3272

Tekirian TL, Yang AY, Glabe C and Geddes JW (1999). "Toxicity of pyroglutaminated amyloid beta-peptides 3(pE)-40 and -42 is similar to that of A beta1-40 and -42". *J Neurochem* 73(4): 1584-1589

Terry RD, Gonatas NK and Weiss M (1964). "Ultrastructural Studies in Alzheimer's Presenile Dementia". *Am J Pathol* 44: 269-297

Texido L, Martin-Satue M, Alberdi E, Solsona C and Matute C (2011). "Amyloid beta peptide oligomers directly activate NMDA receptors". *Cell Calcium* 49(3): 184-190

Tugyi R, Uray K, Ivan D, Fellinger E, Perkins A and Hudecz F (2005). "Partial D-amino acid substitution: Improved enzymatic stability and preserved Ab recognition of a MUC2 epitope peptide". *Proc Natl Acad Sci U S A* 102(2): 413-418

U.S. Food and Drug Administration (2008). Guidance for Industry Safety Testing of Drug Metabolites. U.S. Department of Health and Human Services.

van Groen T, Kadish I, Funke A, Bartnik D and Willbold D (2012). "Treatment with Aβ42 binding D-amino acid peptides reduce amyloid deposition and inflammation in APP/PS1 double transgenic mice". *Adv Protein Chem Struct Biol* 88: 133-152

van Groen T, Kadish I, Funke SA, Bartnik D and Willbold D (2013). "Treatment with D3 removes amyloid deposits, reduces inflammation, and improves cognition in aged AbetaPP/PS1 double transgenic mice". *J Alzheimers Dis* 34(3): 609-620

van Groen T, Kadish I, Wiesehan K, Funke SA and Willbold D (2009). "In vitro and in vivo staining characteristics of small, fluorescent, Abeta42-binding D-enantiomeric peptides in transgenic AD mouse models". *ChemMedChem* 4(2): 276-282

van Groen T, Schemmert S, Brener O, Gremer L, Ziehm T, Tusche M, Nagel-Steger L, Kadish I, Schartmann E, Elfgen A, Jürgens D, Willuweit A, Kutzsche J and Willbold D (2017). "The Aβ oligomer eliminating D-enantiomeric peptide RD2 improves cognition without changing plaque pathology". *Sci Rep* 7(1): 16275

van Groen T, Wiesehan K, Funke SA, Kadish I, Nagel-Steger L and Willbold D (2008). "Reduction of Alzheimer's disease amyloid plaque load in transgenic mice by D3, A D-enantiomeric peptide identified by mirror image phage display". *ChemMedChem* 3(12): 1848-1852

Van Regenmortel MH and Muller S (1998). "D-peptides as immunogens and diagnostic reagents". *Curr Opin Biotechnol* 9(4): 377-382

Vanderah T and Gould D (2015). "Nolte's The Human Brain: An Introduction to its Functional Anatomy". *Elsevier*

Vassar R (2014). "BACE1 inhibitor drugs in clinical trials for Alzheimer's disease". *Alzheimers Res Ther* 6(9): 89

Walsh DM, Klyubin I, Fadeeva JV, Rowan MJ and Selkoe DJ (2002). "Amyloid-beta oligomers: their production, toxicity and therapeutic inhibition". *Biochem Soc Trans* 30(4): 552-557

Walsh DM, Lomakin A, Benedek GB, Condron MM and Teplow DB (1997). "Amyloid beta-protein fibrillogenesis. Detection of a protofibrillar intermediate". *J Biol Chem* 272(35): 22364-22372

Wang DS, Iwata N, Hama E, Saido TC and Dickson DW (2003). "Oxidized neprilysin in aging and Alzheimer's disease brains". *Biochem Biophys Res Commun* 310(1): 236-241

Wang J, Chow D, Heiati H and Shen WC (2003). "Reversible lipidization for the oral delivery of salmon calcitonin". *J Control Release* 88(3): 369-380

Wang J, Yadav V, Smart AL, Tajiri S and Basit AW (2015). "Toward oral delivery of biopharmaceuticals: an assessment of the gastrointestinal stability of 17 peptide drugs". *Mol Pharm* 12(3): 966-973

Wang S, Lee RJ, Mathias CJ, Green MA and Low PS (1996). "Synthesis, purification, and tumor cell uptake of 67Ga-deferoxamine--folate, a potential radiopharmaceutical for tumor imaging". *Bioconjug Chem* 7(1): 56-62

Werle M and Bernkop-Schnurch A (2006). "Strategies to improve plasma half life time of peptide and protein drugs". *Amino Acids* 30(4): 351-367

Weuve J, Hebert LE, Scherr PA and Evans DA (2014). "Deaths in the United States among persons with Alzheimer's disease (2010-2050)". *Alzheimers Dement* 10(2): e40-46

Wiesehan K and Willbold D (2003). "Mirror-image phage display: aiming at the mirror". *ChemBioChem* 4(9): 811-815

Wolfe MS (2002). "Therapeutic strategies for Alzheimer's disease". *Nat Rev Drug Discov* 1(11): 859-866

Yamanaka M, Miyoshi Y, Ohide H, Hamase K and Konno R (2012). "D-Amino acids in the brain and mutant rodents lacking D-amino-acid oxidase activity". *Amino Acids* 43(5): 1811-1821

Yan R and Vassar R (2014). "Targeting the beta secretase BACE1 for Alzheimer's disease therapy". *Lancet Neurol* 13(3): 319-329

Yan SD, Zhu H, Zhu A, Golabek A, Du H, Roher A, Yu J, Soto C, Schmidt AM, Stern D and Kindy M (2000). "Receptor-dependent cell stress and amyloid accumulation in systemic amyloidosis". *Nat Med* 6(6): 643-651

Youssef I, Florent-Bechard S, Malaplate-Armand C, Koziel V, Bihain B, Olivier JL, Leininger-Muller B, Kriem B, Oster T and Pillot T (2008). "N-truncated amyloid-beta oligomers induce learning impairment and neuronal apoptosis". *Neurobiol Aging* 29(9): 1319-1333

Zhang L and Bulaj G (2012). "Converting peptides into drug leads by lipidation". *Curr Med Chem* 19(11): 1602-1618

Zhang S, Iwata K, Lachenmann MJ, Peng JW, Li S, Stimson ER, Lu Y, Felix AM, Maggio JE and Lee JP (2000). "The Alzheimer's peptide a beta adopts a collapsed coil structure in water". *J Struct Biol* 130(2-3): 130-141

Zhao R, Diop-Bove N, Visentin M and Goldman ID (2011). "Mechanisms of membrane transport of folates into cells and across epithelia". *Annu Rev Nutr* 31: 177-201

Zhao R, Matherly LH and Goldman ID (2009). "Membrane transporters and folate homeostasis: intestinal absorption and transport into systemic compartments and tissues". *Expert Rev Mol Med* 11: e4

Zlokovic BV (2004). "Clearing amyloid through the blood-brain barrier". *J Neurochem* 89(4): 807-811

Danksagung

In erster Linie gilt mein besonderer Dank Prof. Dieter Willbold für die Möglichkeit, meine Dissertation am ICS-6 anfertigen zu können. Du hast jederzeit beste Voraussetzungen für eine erfolgreiche Forschung geschaffen und mich permanent gefördert. Außerdem schätze ich es sehr, dass Du mir die Teilnahme an mehreren Konferenzen ermöglicht hast.

Ein weiterer Dank geht an Prof. Henrike Heise für die Übernahme des Koreferats.

Darüber hinaus möchte ich Janine Kutzsche für die gute Betreuung, hilfreichen Diskussionen und permanente Hilfsbereitschaft danken. Die Zusammenarbeit mit Dir hat mir sehr viel Spaß gemacht und mich stets motiviert.

Weiterhin danke ich meiner gesamten Arbeitsgruppe für die hilfsbereite und freundliche Zusammenarbeit. Ein besonderer Dank geht dabei an Tamar, Elena, Sarah und Markus. Es hat sehr viel Spaß mit euch gemacht und ich habe die Zeit sehr genossen. Ihr habt mir jederzeit bei Problemen geholfen, ein offenes Ohr gehabt und mich immer wieder zum Lachen gebracht.

An dieser Stelle möchte ich mich auch bei allen übrigen Mitarbeiterinnen und Mitarbeitern des ICS-6 für das angenehme Arbeitsklima, die gute Zusammenarbeit und die anregenden Diskussionen bedanken. Auch den ehemaligen Kolleginnen und Kollegen, insbesondere Antonia und Franziska, möchte ich danken.

Ein herzlicher Dank gilt meiner Familie und Johannes, die mir immer ihre Unterstützung und ihr großes Interesse entgegengebracht haben. Danke, dass ihr immer an mich geglaubt habt, und für eure Geduld und Motivation in schwierigeren Zeiten.

Eidesstattliche Erklärung

Ich versichere an Eides statt, dass die Dissertation von mir selbständig und ohne unzulässige fremde Hilfe unter Beachtung der „Grundsätze zur Sicherung guter wissenschaftlicher Praxis an der Heinrich-Heine-Universität Düsseldorf“ erstellt worden ist und ich Zitate deutlich kenntlich gemacht habe.

Ferner erkläre ich, dass ich in keinem anderen Dissertationsverfahren mit oder ohne Erfolg versucht habe, diese Dissertation einzureichen.

Jülich,

Liste der Publikationen

Elfgen A, Santiago-Schübel B, Gremer L, Kutzsche J and Willbold D (2017). "Surprisingly high stability of the Abeta oligomer eliminating all-D-enantiomeric peptide D3 in media simulating the route of orally administered drugs". Eur J Pharm Sci 107: 203-207

Elfgen A, Hupert M, Bochinsky K, Tusche M, González de San Román Martin E, Gering I, Sacchi S, Pollegioni L, Huesgen PF, Hartmann R, Santiago-Schübel B, Kutzsche J and Willbold D (2017). "Enzymatic resistance and investigation of potential human-specific metabolites of the amyloid-β oligomer eliminating all-D-enantiomeric peptide RD2". Chem Sci (in Peer-Review)

Hupert M*, Elfgen A*, Schartmann E, Schemmert S, Buscher B, Kutzsche J, Willbold D and Santiago-Schübel B (2018). "Development and validation of an UHPLC-ESI-QTOF-MS method for quantification of the highly hydrophilic amyloid-β oligomer eliminating all-D-enantiomeric peptide RD2 in mouse plasma". J Chromatogr B 1073: 123-129
*Geteilte Erstautorenschaft

van Groen T, Schemmert S, Brener O, Gremer L, Ziehm T, Tusche M, Nagel-Steger L, Kadish I, Schartmann E, Elfgen A, Jürgens D, Willuweit A, Kutzsche J and Willbold D (2017). "The Aβ oligomer eliminating D-enantiomeric peptide RD2 improves cognition without changing plaque pathology". Sci Rep 7(1): 16275

Klein AN, Ziehm T, van Groen T, Kadish I, Elfgen A, Tusche M, Thomaier M, Reiss K, Brener O, Gremer L, Kutzsche J and Willbold D (2017). "Optimization of D-Peptides for Abeta Monomer Binding Specificity Enhances Their Potential to Eliminate Toxic Abeta Oligomers". ACS Chem Neurosci 8(9): 1889-1900

Rudolph S, Klein AN, Tusche M, Schlosser C, Elfgen A, Brener O, Teunissen C, Gremer L, Funke SA, Kutzsche J and Willbold D (2016). "Competitive Mirror Image Phage Display Derived Peptide Modulates Amyloid Beta Aggregation and Toxicity". PLoS One 11(2): e0147470
"Correction: Competitive Mirror Image Phage Display Derived Peptide Modulates Amyloid Beta Aggregation and Toxicity". PLoS One 11(7): e0159470

Liste der Posterpräsentationen

Elfgen A, Hupert M, Bochinsky K, Tusche M, González de San Román Martin E, Gering I, Sacchi S, Pollegioni L, Huesgen PF, Hartmann R, Santiago-Schübel B, Kutzsche J, Willbold D. "Enzymatic resistance and investigation of potential human-specific metabolites of the amyloid-β oligomer eliminating all-D-enantiomeric peptide compound Pri-002". Düsseldorf-Jülich Symposium on Neurodegenerative Diseases: Formation, aggregation and propagation of amyloids 2017, Düsseldorf, Deutschland.

Elfgen A, Santiago-Schübel B, Sacchi S, Pollegioni L, Kutzsche J, Willbold D. "Surprisingly high resistance of the Aβ oligomer eliminating all-D-enantiomeric peptide Pri-002 against metabolisation by enzymes involved in the biotransformation of orally administered drugs". Alzheimer's Association International Conference (AAIC) 2017, London, England.

Elfgen A, Kutzsche J, Willbold D. "High resistance of small all-D-enantiomeric peptides against metabolic degradation and modifications". Alzheimer's Association International Conference (AAIC) 2016, Toronto, Kanada.

Druckgenehmigungen

Surprisingly high stability of the Abeta oligomer eliminating all-D-enantiomeric peptide D3 in media simulating the route of orally administered drugs

Elfgen A, Santiago-Schübel B, Gremer L, Kutzsche J, Willbold D

European Journal of Pharmaceutical Sciences 2017, 107, 203-207

DOI: 10.1016/j.ejps.2017.07.015

http://www.sciencedirect.com/science/article/pii/S0928098717304141?via%3Dihub

Development and validation of an UHPLC-ESI-QTOF-MS method for quantification of the highly hydrophilic amyloid-β oligomer eliminating all-D-enantiomeric peptide RD2 in mouse plasma

Hupert M*, Elfgen A*, Schartmann E, Schemmert S, Buscher B, Kutzsche J, Willbold D and Santiago-Schübel B (*Geteilte Erstautorenschaft)

Journal of Chromatography B 2018, 1073:123-129

DOI: 10.1016/j.jchromb.2017.12.009

http://www.sciencedirect.com/science/article/pii/S1570023217316562?via%3Dihub